

**Component-Based Dynamic Modelling of  
Energy Entities and Energy  
Management Strategies for a Smart  
Home Area Power Network (HAPN)**

**Komponentenbasierte dynamische  
Modellierung von Energiesystemen und  
Energiemanagement-Strategien für ein  
intelligentes Stromnetz im Heimbereich**

Dissertation  
zur Erlangung des Grades  
des Doktors der Ingenieurwissenschaften  
der Naturwissenschaftlich-Technischen Fakultät  
der Universität des Saarlandes

von

Daud Mustafa Minhas

Saarbrücken

2023

**Tag des Kolloquiums:** 5.Juli.2023  
**Dekan:** Prof. Dr. Ludger Santen  
**Berichterstatter:** Prof. Dr.-Ing. Georg Frey  
Prof. Dr.-Ing. Stefan Seelecke  
**Akad. Mitglied:** Dr.-Ing. Idriss El Azhari  
**Vorsitz:** Prof. Dr.-Ing. Michael Vielhaber

“In the name of Allah, Most Gracious, Most Merciful,  
there is no power and strength except with Allah.”

The present work is respectfully dedicated to my loved ones, including my family and friends. I am deeply grateful for their unwavering support, encouragement, and compassionate care throughout my endeavors. Special recognition goes to my parents for their boundless kindness and my beloved spouse for her constant love and support. May Allah bless and safeguard them always.

Daud Mustafa Minhas



---

# Abstract

**English:** The motivation of this work is to present an energy cost reduction concept in a home area power network (HAPN) with intelligent generation and flexible load demands. This study endeavors to address the energy management system (EMS) and layout-design challenges faced by HAPN through a systematic design approach. The growing demand for electricity has become a significant burden on traditional power networks, prompting power engineers to seek ways to improve their efficiency. One such solution is to integrate dispersed generation sources, such as photovoltaic (PV) and storage systems, with an appropriate control mechanism at the distribution level. In recent years, there has been a significant increase in interest in the installation of PV-Battery systems, due to their potential to reduce carbon emissions and lower energy costs. This research proposes an optimal economic power dispatch strategy using Model Predictive Control (MPC) to enhance the overall performance of HAPN. A hybrid AC/DC microgrid concept is proposed to address the control choices made by the appliance scheduling and hybrid switching approaches based on a linear programming optimization framework. The suggested optimization criteria improve consumer satisfaction, minimize grid disconnections, and lower overall energy costs by deploying inexpensive clean energy generation and control. Various examples from actual case study demonstrate the use of the established EMS and design methodology.

**German:** Die Motivation dieser Arbeit besteht darin, ein Konzept zur Senkung der Energiekosten in einem Heimnetzwerk (HAPN) mit intelligenter Erzeugung und flexiblen Lastanforderungen vorzustellen. Im Rahmen dieser Forschungsarbeit wird ein Entwurf für ein HAPN entwickelt, indem das Energiemanagementsystem (EMS) und der Entwurf des Layouts auf der Grundlage des Systemmodells und der betrieblichen Anforderungen gelöst werden. Die steigende Nachfrage nach Elektrizität ist für traditionelle Stromnetze kostspielig und infrastrukturintensiv. Daher konzentrieren sich Energietechniker darauf, die Effizienz der derzeitigen Netze zu erhöhen. Dies kann durch die Integration verteilter Erzeugungsanlagen (z. B. Photovoltaik (PV), Speicher) mit einem geeigneten Kontrollmechanismus für das Energiemanagement auf der Verteilungsseite erreicht werden. Darüber hinaus hat das Interesse an der Installation von PV-Batterie-basierten Systemen aufgrund der Reduzierung der  $CO_2$ -Emissionen und der Senkung der Energiekosten erheblich zugenommen. Es wird eine optimale wirtschaftliche Strategie für den Energieeinsatz unter Verwendung einer modellprädiktiven Steuerung (MPC) entwickelt. Es wird zudem ein hybrides AC/DC-Microgrid-Konzept vorgeschlagen, um die Steuerungsentscheidungen, die von den Ansätzen der Geräteplanung und der hybriden Umschaltung getroffen werden, auf der Grundlage eines linearen Programmierungsoptimierungsrahmens zu berücksichtigen. Die vorgeschlagenen Optimierungskriterien verbessern die Zufriedenheit der Verbraucher, minimieren Netzabschaltungen und senken die Gesamtenergiekosten durch den Einsatz von kostengünstiger und sauberer Energieerzeugung. Verschiedene Beispiele aus einer Fallstudie demonstrieren den Einsatz des entwickelten EMS und der Entwurfsmethodik.



---

# Acknowledgment

The completion of this thesis would not have been possible without the guidance and support of my doctoral advisor, Professor Dr.-Ing. Georg Frey. I am deeply grateful to him for granting me the opportunity to work as part of his team at the Chair of Automation and Energy Systems at Saarland University. His consistent encouragement, accessibility, and insightful suggestions were instrumental in shaping this work, and I am deeply thankful for his unwavering support throughout my academic journey.

I would also like to thank my institute colleagues who have assisted me directly or indirectly throughout the research.





# Contents

|  |           |
|--|-----------|
| <b>Abstract</b>  | <b>ii</b> |
| <b>Acknowledgment</b>  | <b>ii</b> |
| <b>1 Introduction</b>  | <b>12</b> |
| 1.1 Background . . . . .   | 12        |
| 1.2 Motivation . . . . .   | 14        |
| 1.3 Problem Definition . . . . .   | 15        |
| 1.4 Research Objectives . . . . .  | 16        |
| 1.4.1 Benefits to The Society . . . . .  | 18        |
| 1.5 Research Strategy . . . . .  | 19        |
| 1.6 Thesis Contribution . . . . .  | 20        |
| 1.7 Outline of The Book . . . . .  | 22        |
| 1.8 List of Publications . . . . .   | 24        |
| <b>2 State of the Art Work</b>   | <b>26</b> |
| 2.1 Evolution of Smart Grid . . . . .  | 26        |
| 2.1.1 Traditional Power System . . . . .   | 26        |
| 2.1.2 The Intelligent Power Grids . . . . .  | 27        |
| 2.1.3 The Term “Microgrid” . . . . .   | 27        |
| 2.1.4 Distributed Smart Power Systems . . . . .  | 29        |
| 2.2 Components and Microgrid Layouts . . . . .   | 30        |
| 2.2.1 Technologies for Renewable and Non-Renewable Distributed<br>Generation . . . . . | 30        |
| 2.2.2 Technologies for Energy Storage . . . . .  | 31        |
| 2.2.3 Types of Microgrids . . . . .  | 34        |
| 2.2.4 Microgrid Configurations . . . . .   | 37        |
| 2.3 Microgrid Control Architecture . . . . .   | 38        |
| 2.3.1 Microgrid Local Control . . . . .  | 39        |
| 2.3.2 Microgrid Internal Control . . . . .   | 41        |
| 2.3.3 Microgrid Upstream Control . . . . .   | 42        |
| 2.3.4 Master Slave Control . . . . .   | 43        |
| 2.3.5 Centralized Control . . . . .  | 43        |
| 2.4 Microgrid Communication Network . . . . .  | 44        |
| 2.4.1 Microgrid Communication Layers and Technologies . . . . .                        | 45        |
| 2.5 Optimal Design and Operations Strategies for Microgrids . . . . .                  | 46        |
| 2.5.1 Importance of Forecasting in Microgrids . . . . .                                | 46        |
| 2.5.2 Stochastic Optimization Strategies . . . . .                                     | 47        |
| 2.6 Conclusion . . . . .   | 50        |

|          |   |            |
|----------|---|------------|
| <b>3</b> | <b>Components Based System Modeling</b>   | <b>51</b>  |
| 3.1      | Modelling Energy Supply Entities (ESEs) . . . . .                                 | 51         |
| 3.1.1    | Solar Energy . . . . .  | 51         |
| 3.1.2    | PV Panel Analytical Model . . . . .   | 55         |
| 3.1.3    | Grid Tie-line Model . . . . .   | 58         |
| 3.1.4    | Diesel Generator Model . . . . .  | 59         |
| 3.2      | Modelling Energy Storage devices (ESDs) . . . . .                                 | 61         |
| 3.2.1    | Battery Dynamics . . . . .  | 63         |
| 3.2.2    | Battery Operation and Degradation Cost Model . . . . .                            | 64         |
| 3.3      | Modelling Home Energy Appliances . . . . .  | 66         |
| 3.3.1    | Traditional Appliances . . . . .  | 66         |
| 3.3.2    | Smart Appliances . . . . .  | 67         |
| 3.3.3    | Case Study Example . . . . .  | 69         |
| 3.4      | Modelling ESEs Energy Pricing Scheme . . . . .                                    | 72         |
| 3.4.1    | Utility Grid Energy Price . . . . .   | 72         |
| 3.4.2    | Inverter's Distributed Energy Cost . . . . .                                      | 73         |
| 3.5      | Modelling Optimization Problem . . . . .  | 74         |
| 3.5.1    | Model Predictive Control . . . . .  | 75         |
| 3.5.2    | Microgrid optimal operation . . . . .   | 75         |
| 3.5.3    | Optimization Algorithms . . . . .   | 76         |
| 3.6      | Conclusion . . . . .  | 78         |
| <b>4</b> | <b>Home Area Power Network Design Framework and Power Scheduling Algorithms</b>   | <b>79</b>  |
| 4.1      | Critical Analysis of Optimization Strategies . . . . .                            | 79         |
| 4.2      | Home Area Power Network Design and Scheduling Strategies . . . . .                | 81         |
| 4.2.1    | Home Area Power Network Architecture . . . . .                                    | 82         |
| 4.2.2    | Battery Capacity Loss Model . . . . .   | 83         |
| 4.2.3    | Energy Supply Entities Cost Modeling . . . . .                                    | 84         |
| 4.3      | Rule-based Energy Scheduling Scheme . . . . .                                     | 84         |
| 4.3.1    | Algorithms and Implementation . . . . .   | 85         |
| 4.3.2    | Evaluation Indices . . . . .  | 93         |
| 4.4      | A Case Study . . . . .  | 94         |
| 4.4.1    | Data Preparation . . . . .  | 95         |
| 4.4.2    | Comparative Analysis of Power Scheduling Scenarios . . . . .                      | 95         |
| 4.5      | Conclusion . . . . .  | 112        |
| <b>5</b> | <b>Time-Triggered Model Predictive Optimal Distributed Control for AC/DC HAPN</b> | <b>113</b> |
| 5.1      | Communication Based Scheduling Policy for HAPN . . . . .                          | 113        |
| 5.2      | Hybrid AC/DC Home Area Power Network . . . . .                                    | 117        |
| 5.2.1    | HAPN Architecture . . . . .   | 117        |
| 5.2.2    | Model Dynamics for Energy Entities . . . . .                                      | 119        |
| 5.2.3    | Entities Operating Cost Model . . . . .   | 120        |
| 5.3      | Multi-Stage Power Scheduling and Energy Sharing Control . . . . .                 | 121        |
| 5.3.1    | Rolling-Horizon Based Optimal Power Scheduling . . . . .                          | 122        |
| 5.3.2    | Distributed Coordinated Control for Energy Balancing . . . . .                    | 124        |
| 5.3.3    | Robust Power Tracking Control . . . . .   | 124        |

|          |   |            |
|----------|---|------------|
| 5.4      | A Case Study Based Performance Validation . . . . .   | 126        |
| 5.4.1    | Comparison Study for Power Scheduling Scenarios . . . . .   | 126        |
| 5.4.2    | Communication Link Performance Parameters and Experimental Setup . . . . .  | 131        |
| 5.4.3    | Power Sharing During Communication Failure and Load Uncertainties . . . . .   | 133        |
| 5.5      | Conclusion . . . . .  | 134        |
| <b>6</b> | <b>Co-scheduling of Energy Supply Entities with Flexible Smart Load Demands: A Case Study of Demand Side Management</b> | <b>136</b> |
| 6.1      | Critical Analysis of Demand Side Management Techniques . . . . .  | 136        |
| 6.2      | Analytical Modeling of Home Area Power Network and the Attached Power Devices . . . . .                                 | 138        |
| 6.2.1    | Energy Usage Cost Formulations . . . . .  | 139        |
| 6.2.2    | HAPN Component Level Constraints . . . . .  | 142        |
| 6.2.3    | HAPN System Level Constraints . . . . .   | 145        |
| 6.3      | Demand Side Management Problem Formulation and Optimization Strategy . . . . .  | 146        |
| 6.3.1    | Co-scheduling Optimization Algorithm . . . . .  | 147        |
| 6.4      | Numerical Analysis of DSM Technique . . . . .   | 150        |
| 6.4.1    | Load Demand Prediction Module . . . . .   | 151        |
| 6.4.2    | Energy Supply Entities Utilization . . . . .  | 152        |
| 6.4.3    | Activation of Smart Load Devices . . . . .  | 154        |
| 6.4.4    | Incorporation of Energy Storage Devices . . . . .   | 157        |
| 6.4.5    | Power Mix in a Single HAPN . . . . .  | 158        |
| 6.4.6    | Computational Results . . . . .   | 160        |
| 6.5      | Conclusion . . . . .  | 161        |
| <b>7</b> | <b>Thesis Summary and Future Challenges</b>   | <b>162</b> |
| 7.1      | Future Prospective . . . . .  | 164        |

# List of Figures

|      |   |    |
|------|---|----|
| 1.1  | Futuristic power network. . . . .   | 14 |
| 2.1  | Conventional grid. . . . .  | 27 |
| 2.2  | Smart grid. . . . .   | 28 |
| 2.3  | Microgrid illustration. . . . .   | 28 |
| 2.4  | Comparison of energy storage technologies based on power and energy densities [47]. . . . . | 34 |
| 2.5  | Microgrid layout. . . . .   | 35 |
| 2.6  | Picogrid layout. . . . .  | 38 |
| 2.7  | Nanogrid layout. . . . .  | 39 |
| 2.8  | Microgrid layout. . . . .   | 40 |
| 2.9  | Microgrid layers [47]. . . . .  | 41 |
| 2.10 | Microgrid control architecture. . . . .   | 41 |
| 2.11 | Microgrid communication Standards and Technologies [47]. . . . .                            | 46 |
| 3.1  | The solar height and azimuth [25]. . . . .  | 52 |
| 3.2  | Sky conditions. . . . .   | 52 |
| 3.3  | Weather measuring location [1] . . . . .  | 53 |
| 3.4  | Solar radiation components falling on a slanted PV-module [19]. . . . .                     | 53 |
| 3.5  | Correlations and histograms of solar beam irradiation patterns. . . . .                     | 54 |
| 3.6  | Correlations and histograms of solar diffuse irradiation patterns. . . . .                  | 54 |
| 3.7  | Correlations and histograms of solar reflected irradiation patterns. . . . .                | 55 |
| 3.8  | (a) PV array structure. (b) PV schematic model. . . . .                                     | 55 |
| 3.9  | PV distribution on daily, weekly, and monthly basis. . . . .                                | 56 |
| 3.10 | PV predicted values and forecasting error rates. . . . .                                    | 58 |
| 3.11 | Diesel generator efficiency characteristics. . . . .  | 59 |
| 3.12 | ESDs model. . . . .   | 62 |
| 3.13 | Storage life cycle degradation and the induced cost with the increasing DoD. . . . .        | 65 |
| 3.14 | Home electrical appliances classification. . . . .  | 66 |
| 3.15 | ETP model and thermal behaviour of a TCL device . . . . .                                   | 68 |
| 3.16 | Electricity demand model architecture [165]. . . . .  | 70 |
| 3.17 | Energy pricing scheme model. . . . .  | 73 |
| 3.18 | Predictive control strategy. . . . .  | 75 |
| 3.19 | Illustration of a hierarchical multi-layer structure for MGs control system. . . . .        | 76 |
| 4.1  | Proposed dynamic scheduling scheme. . . . .   | 81 |
| 4.2  | HAPN architecture. . . . .  | 82 |
| 4.3  | Flowchart of the conventional rule-based scheduling scheme (Conv-EG). . . . .               | 87 |
| 4.4  | Flowchart of the conventional rule-based scheduling scheme (Conv-PEG). . . . .              | 87 |
| 4.5  | Flowchart of the mixed integer rule-based scheduling scheme. . . . .                        | 89 |

---

|      |  |     |
|------|--|-----|
| 4.6  | Case I flow chart. . . . .   | 90  |
| 4.7  | Case II flow chart. . . . .  | 91  |
| 4.8  | Case III flow chart. . . . .   | 91  |
| 4.9  | Case IV flow chart. . . . .  | 92  |
| 4.10 | Case V flow chart. . . . .   | 92  |
| 4.11 | Case VI flow chart. . . . .  | 93  |
| 4.12 | Predicted load demands. . . . .  | 96  |
| 4.13 | Predicted PV power. . . . .  | 96  |
| 4.14 | EV (dis)charge rates and SOC. . . . .  | 97  |
| 4.15 | Driving indicator and EV power dissipation. . . . .  | 97  |
| 4.16 | Discharging indicator and EV discharge rates. . . . .  | 98  |
| 4.17 | Charging indicator and EV charge rates. . . . .  | 98  |
| 4.18 | EV battery capacity loss. . . . .  | 99  |
| 4.19 | a) Electricity prices. b) Power mix by various ESEs. . . . .                                       | 99  |
| 4.20 | a) ESEs utilization factor (UF). b) Energy shares. . . . .   | 100 |
| 4.21 | Total load demands and the scheduling power. . . . .   | 100 |
| 4.22 | Seasonal comparison of PV power generation. . . . .  | 100 |
| 4.23 | Seasonal comparison of users' load demands. . . . .  | 101 |
| 4.24 | Seasonal comparison of driving indicator and EV power dissipation. . . . .                         | 101 |
| 4.25 | Seasonal comparison of EV battery discharge indicator and their<br>power rates. . . . .            | 102 |
| 4.26 | Seasonal comparison of EV battery charging rates and the indicators. . . . .                       | 102 |
| 4.27 | Seasonal comparison of EV (dis)charge rates and their SOC. . . . .                                 | 103 |
| 4.28 | Seasonal comparison of power mix. . . . .  | 103 |
| 4.29 | Seasonal comparison of energy shares. . . . .  | 104 |
| 4.30 | Seasonal comparison of battery capacity loss. . . . .  | 105 |
| 4.31 | a) ESEs utilization factor (UF) and penetration level. b) Energy<br>shares for whole year. . . . . | 106 |
| 4.32 | Yearly battery capacity loss. . . . .  | 106 |
| 4.33 | Comparative power utilization. . . . .   | 107 |
| 4.34 | Total energy cost. . . . .   | 107 |
| 4.35 | Total grid energy cost. . . . .  | 108 |
| 4.36 | Total EV storage utilization cost. . . . .   | 108 |
| 4.37 | Histogram of EV storage SOC. . . . .   | 109 |
| 4.38 | Histogram of EV storage charge rates. . . . .  | 109 |
| 4.39 | Annual accumulative charge and discharge energy for EV storage. . . . .                            | 109 |
| 4.40 | Total EV storage loss. . . . .   | 110 |
| 4.41 | Comparison of total capacity loss. . . . .   | 110 |
| 4.42 | Comparison of various capacity losses among different schemes. . . . .                             | 110 |
| 4.43 | Hourly mean total loss increment for Scheme 1 (Conv-EG). . . . .                                   | 111 |
| 4.44 | Hourly mean total loss increment for Scheme 2 (Conv-PEG). . . . .                                  | 112 |
| 4.45 | Hourly mean total loss increment for Scheme 3 (MP-iEMS). . . . .                                   | 112 |
| 5.1  | Proposed control strategy and system model. . . . .  | 115 |
| 5.2  | HAPN architecture (Scheduler perspective). . . . .   | 117 |
| 5.3  | Energy management system Architecture. . . . .   | 122 |
| 5.4  | HAPN components architecture (Primary robust control perspective). . . . .                         | 125 |
| 5.5  | AC/DC bus (w/o losses) Vs AC/DC bus (with losses). . . . .   | 127 |

|      |  |     |
|------|--|-----|
| 5.6  | Hybrid AC/DC bus with losses. . . . .  | 128 |
| 5.7  | Frequency spectrum and data symbols output . . . . .   | 132 |
| 5.8  | Master slave communication experimental setup. . . . .   | 133 |
| 5.9  | Time-triggered communication setup between nodes. . . . .  | 133 |
| 5.10 | Real-time HAPN operation. . . . .  | 134 |
| 6.1  | Home area power network system model . . . . .   | 139 |
| 6.2  | The multi-objective optimization problem for HEMS. . . . .   | 148 |
| 6.3  | House occupants and their energy demands. . . . .  | 152 |
| 6.4  | Day-ahead predicted price. . . . .   | 152 |
| 6.5  | Predicted room temperature. . . . .  | 153 |
| 6.6  | Electric grid power outage signal. . . . .   | 153 |
| 6.7  | Grid power utilization. . . . .  | 153 |
| 6.8  | Diesel generator power production. . . . .   | 154 |
| 6.9  | Power procured from the PV. . . . .  | 154 |
| 6.10 | Power elastic load demands. . . . .  | 155 |
| 6.11 | a) Power profile of WM. b) Phase indicator. . . . .  | 155 |
| 6.12 | a) Power profile of DW. b) Phase indicator. . . . .  | 156 |
| 6.13 | a) Temperature profile and on/off status of a refrigerator. b) Power<br>profile of a refrigerator. . . . . | 156 |
| 6.14 | a) Temperature profile and on/off status of a freezer. b) Power profile<br>of a freezer. . . . .           | 157 |
| 6.15 | a) Predicted DT demands. b) Scheduled DT demands. c) DT de-<br>mands queue backlog. . . . .                | 157 |
| 6.16 | a) ESDs (dis)charging rates. b) SoCs of HB and EV storages. . . . .  | 158 |
| 6.17 | a) Changing electricity prices. b) Scheduling various ESEs. . . . .  | 159 |
| 6.18 | a) ESEs utilization factor (UF). b) Energy shares. . . . .   | 159 |
| 6.19 | a) SLDs satisfaction level (SL). b) Load shares. . . . .   | 159 |
| 6.20 | Total load demands and the scheduling power. . . . .   | 160 |
| 6.21 | Pre and post scheduling load demands. . . . .  | 160 |

# List of Tables

|     |   |     |
|-----|---|-----|
| 2.1 | Comparison of conventional and renewable technologies. . . . .  | 31  |
| 2.2 | Comparison of energy storage technologies [47, 191] . . . . .   | 32  |
| 2.3 | Comparison of battery energy storage technologies [47] . . . . .  | 32  |
| 3.1 | Home appliances activities and classification. . . . .  | 71  |
| 3.2 | Dish washer parameters. . . . .   | 72  |
| 3.3 | Washing machine parameters. . . . .   | 72  |
| 4.1 | Objectives, limitations, and critical analysis of the past literature. . .  | 80  |
| 4.2 | System parameters. . . . .  | 94  |
| 4.3 | The simplified reduced-order battery model's coefficients. . . . .  | 95  |
| 4.4 | Seasonal comparison of ESEs utilization factor (UF) and penetration level (PL). . . . .   | 105 |
| 4.5 | Comparison of ESEs utilization factor (UF) and penetration level (PL) for various schemes. . . . .  | 106 |
| 5.1 | Critical analysis of past work. (Con, converter; P, active power; Q, reactive power; RT, real-time; DA, day-ahead.) . . . . .   | 116 |
| 5.2 | System parameters . . . . .   | 126 |
| 5.3 | Home appliances activities and classification. . . . .  | 129 |
| 5.4 | ESEs utilization factor and penetration level. . . . .  | 129 |
| 5.5 | Estimated aggregated energy cost for one day. . . . .   | 130 |
| 5.6 | Communication system parameters . . . . .   | 131 |
| 6.1 | Objectives and limitations in state of the art work. . . . .  | 137 |
| 6.2 | Critical analysis of past work. (PE, power elastic loads; ECL, electric controllable loads; TCL, thermal controllable loads; DT, delay tolerant load demands; Occ, occupancy behaviour; Ss, Self-sufficiency; Ps, pricing scheme; Cr, cost reduction; DA, day-ahead; Roll, rolling time horizon.) . . . . . | 138 |
| 6.3 | System parameters. (pred, predicted) . . . . .  | 150 |
| 6.4 | Cost parameters (cents/Watt). (pred, predicted) . . . . .   | 150 |
| 6.5 | Energy demands parameters. (pred, predicted) . . . . .  | 151 |





# Nomenclature

Abbreviations:

|             |                                       |
|-------------|---------------------------------------|
| <i>DE</i>   | Diesel engine generator.              |
| <i>PV</i>   | Photovoltaic generator.               |
| <i>ESEs</i> | Energy supply entities.               |
| <i>DSM</i>  | Demand side management.               |
| <i>RTP</i>  | Real time price.                      |
| <i>NGs</i>  | Nanogrids.                            |
| <i>EEs</i>  | Energy entities.                      |
| <i>EVs</i>  | Electric vehicles.                    |
| <i>OM</i>   | Operations and management.            |
| <i>ESSs</i> | Energy storage systems.               |
| <i>DGs</i>  | Distributed generations.              |
| <i>RESs</i> | Renewable energy sources.             |
| <i>PV2V</i> | PV to vehicle power transfer.         |
| <i>V2H</i>  | Vehicle to home.                      |
| <i>iEMS</i> | Intelligent energy management system. |
| <i>UF</i>   | Utilization factor.                   |
| <i>PL</i>   | Penetration level.                    |
| <i>AWGN</i> | Additive white gaussian noise.        |
| <i>DERs</i> | Distributed energy resources.         |
| <i>ESDs</i> | Energy storage devices.               |
| <i>GAS</i>  | Grid auxiliary storage.               |
| <i>HAPN</i> | Home area power network.              |
| <i>HEMS</i> | Home energy management system.        |
| <i>HBS</i>  | Home battery storage.                 |
| <i>IEDs</i> | Intelligent energy devices.           |

|                  |  |
|------------------|--|
| <i>MPC</i>       | Model predictive control.                              |
| <i>MPPT</i>      | Maximum power point tracking.                          |
| <i>MILP</i>      | Mixed integer linear programming.                      |
| <i>QAM</i>       | Quadrature amplitude modulation.                       |
| <i>SNR</i>       | Signal to noise ratio.                                 |
| <i>VSI</i>       | Voltage source inverter.                               |
| <i>MP – iEMS</i> | Model predictive intelligent energy management system. |
| <i>SOC</i>       | State of charge.                                       |
| <i>DOD</i>       | Depth of discharge.                                    |
| <i>WLAN</i>      | PV to vehicle power transfer.                          |
| <i>MIMO</i>      | Multiple input and multiple output.                    |
| <i>EVS</i>       | Electric vehicle storage.                              |
| <i>TA</i>        | Traditional appliances.                                |
| <i>CE</i>        | Consumer electronics.                                  |
| <i>CR</i>        | Cooking ranges.  |
| <i>WH</i>        | Water heater.  |
| <i>SA</i>        | Smart appliances.                                      |
| <i>PE</i>        | Power elastic appliances.                              |
| <i>TE</i>        | Time elastic appliances.                               |
| <i>TS</i>        | Time shiftable devices.                                |
| <i>DT</i>        | Delay tolerant devices.                                |
| <i>ECL</i>       | Electric controlled loads.                             |
| <i>TCL</i>       | Thermal controllable loads.                            |
| <i>WM</i>        | Washing machines.                                      |
| <i>CD</i>        | Clothes dryers.  |
| <i>WP</i>        | Water pumps.   |
| <i>AC</i>        | Air conditioners.                                      |
| <i>WC</i>        | Water coolers.   |
| <i>RF</i>        | Refrigerators.   |

|        |                                     |
|--------|-------------------------------------|
| $DR$   | Demand response.                    |
| $ToU$  | Time of use pricing.                |
| $DAP$  | Day-ahead pricing.                  |
| $CCP$  | Critical peak pricing.              |
| $IBR$  | Inclined block rates.               |
| $EEs$  | Energy entities.                    |
| $IoE$  | Internet of energy.                 |
| $DEs$  | Diesel engines.                     |
| $SLDs$ | Smart load demands.                 |
| $SGR$  | Self generation ratio.              |
| $NOCT$ | Nominal operative cell temperature. |

Sets and Indices:

|               |  |
|---------------|--|
| $A_{TA}$      | Set of traditional appliances.                                 |
| $A_{SA}$      | Set of smart appliances.                                       |
| $A_{PE}$      | Set of power elastic appliances.                               |
| $A_{TS}$      | Set of time shiftable appliances.                              |
| $A_{ECL}$     | Set of electric controllable loads.                            |
| $A_{TCL}$     | Set of thermal controllable loads.                             |
| $A_{DT}$      | Set of delay tolerant loads.                                   |
| $\mathcal{G}$ | Set of total generators attached to HAPN.                      |
| $\mathcal{D}$ | Set of total demands attached to HAPN.                         |
| $A_{EEs}$     | Set of all electric entities in HAPN.                          |
| $t$           | Index of low resolution time steps, $t \in \{1, \dots, T\}$ .  |
| $k$           | Index of high resolution time steps, $k \in \{1, \dots, K\}$ . |
| $a$           | Index of power elastic loads, $a \in \{1, \dots, A\}$ .        |
| $b$           | Index of ECL devices, $b \in \{1, \dots, B\}$ .                |
| $c$           | Index of TCL devices, $c \in \{1, \dots, C\}$ .                |
| $d$           | Index of power phase of ECL demand, $d \in \{1, \dots, D\}$ .  |
| $e$           | Index of DT loads, $e \in \{1, \dots, E\}$ .                   |

---

|                       |   |
|-----------------------|---|
| $f$                   | Index of traditional devices, $f \in \{1, \dots, F\}$ .   |
| $s$                   | Index of energy storage devices, $s \in \{1, \dots, S\}$ .                                      |
| $U$                   | Index of User's occupancy, $U \in \{1, \dots, n^u\}$ .  |
| $M$                   | Index of diesel generating units, $M \in \{1, \dots, m\}$ .                                     |
| $J$                   | Index of PV sub-arrays, $J \in \{1, \dots, j\}$ .   |
| Microgrid parameters: |   |
| $P_{g.ac}(t)$         | Grid supply power at the AC bus at anytime $t$ .  |
| $P_{g.av}(t)$         | Available grid power at anytime $t$ .   |
| $x_{g.ac}(t)$         | Grid Boolean operator at anytime $t$ .  |
| $P_{g.disp}(t)$       | Dispatchable grid power at anytime $t$ .  |
| $P_{ac.load}(t)$      | Desired load demands at anytime $t$ .   |
| $P_{pv.ac}(t)$        | Power provided by solar panels at AC bus at anytime $t$ .                                       |
| $P_{pv.disp}(t)$      | Dispatchable PV power at anytime $t$ .  |
| $P_{ac.b}(t)$         | Power utilized to to charge the storage devices using AC bus at anytime $t$ .                   |
| $x_{pv.ac}(t)$        | PV Boolean operator for supplying to AC bus at anytime $t$ .                                    |
| $\eta_{pv.con}$       | PV converter efficiency.  |
| $P_{b.av}(t)$         | Available supply from storage device at anytime $t$ .   |
| $P_{b.ac}(t)$         | Power supply from storage device to AC bus at anytime $t$ .                                     |
| $P_{ac.b}(t)$         | Power utilized to to charge the storage devices using AC bus at anytime $t$ .                   |
| $x_{b.ac}(t)$         | Storage device Boolean operator for supply power to AC bus at anytime $t$ .                     |
| $x_{ac.b}(t)$         | Storage device Boolean operator for supply power from AC bus to storage device at anytime $t$ . |
| $\bar{S}_{inv.ac}$    | inverter's maximum power handling capacity.   |
| $\eta_{inv}$          | Inverter efficiency.  |
| $P_{dc.inv}(t)$       | Power transfer from DC bus to inverter at anytime $t$ .   |
| $P_{inv.ac}(t)$       | Power transfer from inverter to AC bus at anytime $t$ .   |
| $P_{inv.loss}(t)$     | Inverter losses at anytime $t$ .  |
| $S_{g.disp}(t)$       | Dispatchable apparent power from utility grid at anytime $t$ .                                  |

- $S_{g.av}(t)$  Available apparent power from grid at anytime  $t$ .
- $\overline{S}_g$  Upper threshold of apparent power obtained from grid.
- $S_{g.ac}(t)$  Apparent power supplied by the utility company to the AC sub-grid at anytime  $t$ .
- $x_{g.dc}(t)$  Boolean operator for supply energy from Grid to DC sub-grid at anytime  $t$ .
- $P_{g.dc}(t)$  Power transfer from grid to DC sub-grid at anytime  $t$ .
- $x_{pv.dc}(t)$  Boolean operator for supply energy from PV to DC sub-grid at anytime  $t$ .
- $P_{pv.dc}(t)$  Power transfer from PV to DC bus at anytime  $t$ .
- $P_{b.dc}(t)$  Power supply from storage to DC sub-grid at anytime  $t$ .
- $x_{b.dc}(t)$  Boolean operator for supply energy from storage to DC sub-grid at anytime  $t$ .
- $P_{dc.b}(t)$  Power supply from DC sub-grid to storage at anytime  $t$ .
- $P_{dc}(t)$  Power available at DC sub-grid at anytime  $t$ .
- $P_{dc.inv}(t)$  Power transfer from DC bus to inverter at anytime  $t$ .
- $x_{dc.b}(t)$  Boolean operator for supply energy from DC sub-grid to storage at anytime  $t$ .
- $x_{dc.inv}(t)$  Boolean operator for supply energy from DC sub-grid towards inverter at anytime  $t$ .
- $S_{inv.ac}(t)$  Apparent power supply from inverter to AC sub-grid at anytime  $t$ .
- $S_{req.load}(t)$  Apparent power required by the home appliances at anytime  $t$ .
- $S_{ac.load}(t)$  Apparent power supplied to the home appliances at anytime  $t$ .
- $\mathbf{u}_{gas}(k)$  Control signal used to activate the auxiliary storage power at anytime  $k$ .
- $P_{gas}(k)$  Grid auxiliary storage power exchange at anytime  $k$ .
- $x_{gas}(k)$  Boolean operator to activate the auxiliary storage power at anytime  $k$ .
- $P_{de.ac}(t)$  Power supply from diesel generator to AC bus at anytime  $t$ .
- $x_{de.ac}(t)$  On-off status of DE unit (0/1).
- $z_{de}(t)$  Start-up status of DE unit (0/1).
- $v_{de}(t)$  Shut-down status of DE unit (0/1).
- $x_{b.dc}^{HBS}(t)$  Home battery storage discharging indicator at any time  $t$ .

---

|  |   |
|--|---|
| $x_{dc.b}^{HBS}(t)$                      | Home battery storage charging indicator at any time $t$ .                         |
| $x_{b,dc}^{EVS}(t)$                      | Electric vehicle storage discharging indicator at any time $t$ .                  |
| $x_{dc.b}^{EVS}(t)$                      | Electric vehicle storage discharging indicator at any time $t$ .                  |
| $TP_{b,dc/dc.b}^{EVS}(t)$                | User time preference for EVS charging/discharging at any time ( $t$ ).            |
| $TP_{b,d}^{ECL}(t)$                      | User time preference for supplying power to ECL load demand at any time ( $t$ ).  |
| $P_{ac.load}^{peak}(t)$                  | Demand response peak signal.  |
| $\underline{P}_{g.ac}$                   | Minimum grid supply power limit.  |
| $\overline{P}_{g.ac}$                    | Maximum grid supply power limit.  |
| $\overline{P}_{pv.dc}$                   | Maximum PV supply power limit.  |
| $\underline{P}_{de.ac}$                  | Minimum diesel generator supply power limit.                                      |
| $\overline{P}_{de.ac}$                   | Maximum diesel generator supply power limit.                                      |
| $\eta_{de}(t)$                           | electrical efficiency of a diesel generator at anytime $t$ .                      |
| $P_{de.disp}(t)$                         | Dispatchable power by the diesel generator at anytime $t$ .                       |
| $\overline{P}_a^{PE-}$                   | Maximum power requirement of a device of PE load demands.                         |
| $\overline{P}_{b,d}^{ECL}$               | Maximum power dissipated by ECL unit $b$ .  |
| $\underline{P}_{b,d}^{ECL}$              | Minimum power dissipated by ECL unit $b$ .  |
| $x_{b,d}^{ECL}(t)$                       | Status of device $b$ for its specific energy phase $d$ of ECL load demands (0/1). |
| $\underline{\tau}_{b,d}^{ECL}$           | Minimum time bound for each phase $d$ of ECL loads to run (0/1).                  |
| $\overline{\tau}_{b,d}^{ECL}$            | Maximum time bound for each phase $d$ of ECL loads to run (0/1).                  |
| $s_{b,d}^{ECL}(t)$                       | Power phase finishing indicator (0/1).  |
| $d_{b,d}^{ECL}(t)$                       | Inter-phase delay indicator (0/1).  |
| $\overline{D}_{b,d}/\underline{D}_{b,d}$ | Upper and lower limits of inter-phase delay ( $t$ ).                              |
| $x_c^{TCL}(t)$                           | Status of unit $c$ of TCL load demands (0/1).                                     |
| $\underline{P}_c^{TCL}$                  | Minimum power usage by the TCL unit.  |
| $\overline{P}_c^{TCL}$                   | Maximum power usage by the TCL unit.  |
| $\overline{T}_c^{TCL}$                   | User's set maximum temperature.   |
| $\underline{T}_c^{TCL}$                  | User's set minimum temperature.   |

|                              |   |
|------------------------------|---|
| $T_c^{TCL}(t)$               | User's set temperature.   |
| $T^{room}(t)$                | Room temperature.   |
| $R_c^{TCL}$                  | Equivalent thermal resistance.                                    |
| $C_c^{TCL}$                  | Equivalent heat rate.   |
| $\bar{P}_e^{DT}$             | Maximum power dissipation by DT device.                           |
| $\underline{P}_e^{DT}$       | Minimum power dissipation by DT device.                           |
| $L_a^{PE}(t)$                | Estimated power elastic load demand.                              |
| $Q_e^{DT}(t)$                | Load demands in a queue.  |
| $x_e^{DT}(t)$                | Status of unit $e$ of DT load demands (0/1).                      |
| $L_e^{DT}(t)$                | Load demands entering the queue.                                  |
| Solar generation parameters: |   |
| $P_{pv.av}(t)$               | Available energy from PV at anytime $t$ .                         |
| $\bar{P}_{pv}(t)$            | Maximum power produced by the photovoltaic array at anytime $t$ . |
| $P_{sa.j}(t)$                | PV $j^{th}$ subarray power.                                       |
| $P_m(t)$                     | Power generated by a single PV module.                            |
| $N_m$                        | Number of PV modules.   |
| $F_{sa.j}$                   | Electrical loss factor of PV sub-array $j$ (%).                   |
| $L_{m.j}$                    | Mismatch loss index of PV subarray $j$ .                          |
| $L_{dc.j}$                   | DC wiring loss index in PV subarray $j$ .                         |
| $\bar{P}_m$                  | Maximum power output of a PV module.                              |
| $G_{STC}$                    | Standard irradiance value ( $W/m^2$ ).                            |
| $G_T(t)$                     | Predicted irradiance ( $W/m^2$ ).                                 |
| $\alpha$                     | Temperature coefficient.  |
| $T_C(t)$                     | Ambient temperature $^{\circ}C$ .                                 |
| $FF(t)$                      | Fill factor (%)   |
| $V_{oc}^{pvcell}$            | Open circuit voltage of PV cell ( $V$ ).                          |
| $I_{sc}^{pvcell}$            | Short circuit current in PV cell ( $A$ ).                         |
| $I_{sc.stc}(t)$              | Normalized short circuit current of a PV module.                  |
| $FF_0$                       | Nominal fill factor of a PV module.                               |

---

|                                    |  |
|------------------------------------|--|
| $r_s(t)$                           | Normalized series resistance of a PV module.   |
| $v_{oc.stc}(t)$                    | Normalized open circuit voltage of a PV module.  |
| $R_s$                              | Series resistance of PV module.  |
| $V_t(t)$                           | Thermal voltage of a PV-cell.  |
| $n_d$                              | Diode ideality factor.   |
| $k_B$                              | Boltzmann's constant, equal to $1.38 \times 10^{-23}$ .                                    |
| $T_{a.k}(t)$                       | Ambient temperature in Kelvin.   |
| $e$                                | Charge of electron, i.e. $1.602 \times 10^{-19}$ .   |
| $K_i$                              | Temperature coefficient of the short circuit current of a PV module.                       |
| $K_v$                              | Temperature coefficient of the short circuit current of a PV module.                       |
| $G_B(t)$                           | Direct beam irradiance ( $W/m^2$ ).  |
| $G_D(t)$                           | Diffuse irradiance ( $W/m^2$ ).  |
| $G_R(t)$                           | Reflected irradiance ( $W/m^2$ ).  |
| Energy storage devices parameters: |  |
| $\bar{E}_b$                        | Maximum state of energy of the storage device.   |
| $\eta_{b.con}$                     | Battery and converter efficiency.  |
| $P_{b.dch}(t)$                     | Storage device discharge rate at anytime $t$ .   |
| $P_{b.ch}(t)$                      | Storage device charge rate at anytime $t$ .  |
| $\underline{E}_b$                  | Minimum state of energy of the storage device.   |
| $E_b$                              | State of energy of the storage device.   |
| $\underline{P}_{b.ch}$             | Minimum Storage device charge rate at anytime $t$ .  |
| $\bar{P}_{b.ch}$                   | Maximum Storage device charge rate at anytime $t$ .  |
| $\underline{P}_{b.dch}$            | Minimum Storage device discharge rate at anytime $t$ .                                     |
| $\bar{P}_{b.dch}$                  | Maximum Storage device discharge rate at anytime $t$ .                                     |
| $Q_{SEI}(t)$                       | Capacity loss of the storage device due to solid electrolyte interface (SEI) layer growth. |
| $Q_{AM}(t)$                        | Capacity loss of the storage device due to active material (AM) loss.                      |
| $M$                                | Ideal gas constant.  |
| $N$                                | Cell temperature.  |



|                       |   |
|-----------------------|---|
| $SOC(t)$              | State of charge of storage device at anytime $t$ .            |
| $\theta$              | Function of SOC.  |
| $k_{SEI}$             | Storage constant parameters.                                  |
| $E_{SEI}$             | Storage constant parameters.                                  |
| $\lambda$             | Storage constant parameters.                                  |
| $k_{AM}$              | Storage constant parameters.                                  |
| $E_{AM}$              | Storage constant parameters.                                  |
| $P_{b.loss}(t)$       | Storage power losses at anytime $t$ .                         |
| $\eta_b$              | Storage efficiency.   |
| $\eta_{con}$          | Converter efficiency.   |
| $P_{b.self}(t)$       | Self discharge power at anytime $t$ .                         |
| $L_f(t)$              | Life reduction for a storage device at anytime $t$ .          |
| $A_c$                 | Effective consumed power of a storage device at anytime $t$ . |
| $A_{total}$           | Total effective capacity of the storage device.               |
| $A'c(t)$              | Actual consumed power from the storage at anytime $t$ .       |
| $\lambda_{SOC}(t)$    | Storage's operational state of charge at anytime $t$ .        |
| $E_{gas}(k)$          | Available energy in grid auxiliary storage at anytime $k$ .   |
| $\overline{E}_{gas}$  | Upper threshold for energy stored in grid auxiliary storage.  |
| $\underline{E}_{gas}$ | Lower threshold for energy stored in grid auxiliary storage.  |
| $P_{gas.dch}(k)$      | Grid auxiliary battery discharge rate at anytime $k$ .        |
| $P_{gas.ch}(k)$       | Grid auxiliary battery charge rate at anytime $k$ .           |
| $E_{av.b}$            | Available capacity of the storage unit.                       |
| $V_b^{oc}$            | Open circuit voltage of battery cell.                         |
| $I_b$                 | Short circuit current in battery cell.                        |
| $R_b$                 | Internal resistance of a battery.                             |
| $P_b$                 | Battery output power.   |
| $\eta_{bcell}$        | Battery cell dis(charging) efficiency's.                      |
| $\eta_{bcell}^{ch}$   | Battery cell charging efficiency's.                           |
| $\eta_{bcell}^{dch}$  | Battery cell discharging efficiency's.                        |

|                                |   |
|--------------------------------|---|
| $P_{cell}$                     | Battery cell power.   |
| $P_{b.loss}(t)$                | Power loss in battery at any time $t$ .                                   |
| $\eta_b$                       | Overall battery efficiency.   |
| $N_{cycle,b}(t)$               | Number of (dis)charging cycles of ESD at any time $t$ .                   |
| Optimal operations parameters: |   |
| $C_{b,t}(t)$                   | Storage state's lifetime loss cost at anytime $t$ .                       |
| $C_{b,inv}$                    | Investment cost of the storage bank.                                      |
| $C_g(t)$                       | Dynamic grid pricing at anytime $t$ .                                     |
| $C_{inv.ac}(t)$                | Inverter power cost at anytime $t$ .                                      |
| $\varphi$                      | Per power unit operating cost of the battery at anytime $t$ .             |
| $\phi$                         | Per power unit operating cost of the photovoltaic system at anytime $t$ . |
| $K_{PV,UF}$                    | PV utilization factor.  |
| $K_{PV,PL}$                    | PV penetration level.   |
| $K_{PV,LF}$                    | PV loss factor.   |
| $K_{G,UF}$                     | Grid utilization factor.  |
| $K_{G,PL}$                     | Grid penetration level.   |
| $K_{G,LF}$                     | Grid loss factor.   |
| $K_{EV,UF}$                    | EV storage utilization factor.  |
| $C_G(t)$                       | Cost of energy obtained from Grid at time $t$ .                           |
| $K_{EV,PL}$                    | EV storage penetration level.   |
| $\varrho_t$                    | Per unit grid electricity price at anytime $t$ .                          |
| $K_{EV,LF}$                    | EV storage loss factor.   |
| $K_{I,LF}$                     | Inverter loss factor.   |
| $K_{SS}$                       | Degree of self-sufficiency.   |
| $C_{DE}(t)$                    | Cost for producing energy using Diesel generator.                         |
| $a_{de.ac}/b_{de.ac}$          | Diesel engine fuel coefficients.  |
| $\sigma^f$                     | Price for the fossil fuel.  |
| $C_{DE}^{su}(t)/\sigma^{su}$   | Start-up cost of diesel engine.   |
| $C_{DE}^{sd}(t)/\sigma^{sd}$   | Shut-down cost of diesel engine.  |

$C_{DE}^{om}(t)/\sigma^{om}$  Operation and maintenance cost of DE.

$C_{DE}^{CO_2}$  Cost for producing  $CO_2$  by the DE.

$\xi$  Penalty price for  $CO_2$ .

$C_b(t)$  Price per (dis)charging power unit from ESDs.

$IC_b$  Investment cost of a storage device.

$C_{PE}^{pen}(t)$  Penalty cost for curtailable PE loads.

$\zeta$  Penalty rate for PE load curtailment.

$C_{DT}^{del}(t)$  Cost associated with the loads in the queue.

$\delta$  Penalty rate for DT loads in the queue.

Power electronics parameters:

$Q_{gas}$  Reactive power exchanged by the grid auxiliary storage

$\omega$  Reference frequency for d-q reference frame transition.

$L$  Inductance.

$R$  Resistance.

Power load demands parameters:

$P_f^{TA^-}(t)$  Power dissipated by TA unit  $f$ .

$E^{TA}$  Energy requirement for TA load.

$E_a^{PE}$  Energy requirement of a PE unit  $a$ .

$P_a^{PE^-}(t)$  Power dissipated by PE unit  $a$ .

$E_{b,d}^{ECL}$  Energy requirement of a ECL device  $b$ .

$P_{b,d}^{ECL^-}(t)$  Power dissipated by ECL unit  $b$ .

$E_c^{TCL}$  Energy requirement of a TCL device  $c$ .

$P_c^{TCL^-}(t)$  Power dissipated by TCL unit  $c$ .

$E^{DT}$  Energy requirement of DT load demands.

$P_e^{DT^-}(t)$  Power dissipated by DT unit  $e$ .

---

# 1 Introduction

Electricity consumption has risen dramatically in recent years all around the world. This rise is attributed to the growth of the digital economy based on modern civilizations and robust industrialization. The present fossil fuel-based energy generating infrastructure may also be expanded to meet this need, so the increase in environmental pollution is inevitable. However, for environmental and economic reasons, it is critical to create hybrid energy systems that combine renewable energy sources (RESs) with conventional fossil fuels. To accomplish a successful energy transition, practical and low-cost solutions that permit socioeconomic growth in energy policy are required. These solutions can only be possible by revisiting the concept of modern energy grids, also known as “Smart Grids.” Which can generate and supply practically cheap, efficient, and clean electricity.

## 1.1 Background

Electric energy is now an essential home requirement and plays a significant part in driving one’s daily life. However, there are various issues that modern civilizations face regarding energy creation, supply, and consumption [23]. Existing electrical facilities, in particular, are ill-equipped to handle the energy supply volume. Long-distance transmission lines transporting power from major energy stations to clients incur significant line losses and impair grid efficiency. Similarly, environmental factors (e.g., heavy rain or wind) and equipment malfunctioning (e.g., equipment breakdown due to age) can significantly influence power outages and costly grid operations. Furthermore, as a result of coal and oil scarcity and the growing prevalence of pollution problems, energy regulations and consumer habits are being reviewed, particularly regarding sustainable power usage. Massive central power producers commonly employ fossil fuels, resulting in annual  $CO_2$  emissions of 30.8 billion tons [93]. It must be handled for the sake of future generations.

Furthermore, governments and large utilities in developing countries continue to overestimate the impact of power failures. In particular, long-term power outages are caused by inefficient and outdated electrification and a lack of local energy supplies. As a result, industrialists and local investors established small-scale local backup systems to meet their energy needs during grid outages [122]. However, these systems frequently rely on expensive and environmentally hazardous diesel and gas generators. Again, there is a significant environmental worry with using such a large number of fossil fuel generators, with each litre of diesel fuel emitting 2.6 kg of  $CO_2$  [59]. As a result, for a 5-hour daily power outage, a primary residential structure may require up to 5,000 gallons of fuel, which is a significant worry.

Another important aspect is that an estimated 1.2 billion people live without energy [7]. Most of these people live in rural or isolated places where power from the central grid is too expensive. Distributed generation (DG), however, is one method currently being investigated to alleviate the issues of supplying power to remote populations. However, DG comprises renewable energy sources (RESs) and has two key drawbacks that preclude extensive residential/commercial integration.

The first is its irregular power production considering photovoltaic modules, whose output power varies with the amount of irradiation coming from the sun throughout the day. This intermittent behaviour of RES might prevent customers from investing in new energy technologies since they anticipate immediate power. The second is the upfront cost of installing RESs and the long payback period [112].

Despite the current challenges, there is an increased need for clean and inexpensive energy that originates a new terminology of hybrid energy systems. The German Federal Government, for example, recognizes the importance of renewable energy by setting an expected goal of 2.5 GW of PV system deployments promoting the motto “Energiewende.” [33]. Renewable energy sources should be used to minimize the reliance on oil and reduce greenhouse gas emissions. An efficient energy management system (EMS) must be developed to maximize the output from RESs, reduce the energy loss during operations, and reduce the overall operational and maintenance costs [131]. As a result, efficient EMSs may provide inexpensive energy by increasing the system efficiency and lowering the system’s effective price. With RESs and battery costs steadily falling, societies will soon be supplied by the energy obtained from these sources in collaboration with old conventional energy generators, i.e., diesel generators or the central grid [122].

A complicated energy management situation arises from the necessity to investigate new ways of efficiently dispatching and distributing energy from various components depending on their availability and prices. For this purpose, the different energy supply and demand control strategies need to be investigated [62]. As energy suppliers, fossil fuel-based energy generators may be partly or entirely replaced by renewables and energy storage. Load control may help accomplish this aim at the energy receiver end. It will provide flexibility and influence consumption by reducing unneeded loads or changing its operations to a cheaper time of day. It may be possible to move some load demands from the time slot of high energy prices to alternative excessive energy production time slots with low prices. However, actual situations and operational settings must be utilized to assess the solutions’ practicality and efficacy [125].

The advent of cutting-edge advancements, including renewable energy generation, imaginative storage solutions, demand-side management, and demand response, is disrupting conventional modes of energy consumption and production. Consequently, it is possible to attain more energy-efficient electrical supply chains by optimizing energy supplies and consumption, reducing greenhouse gas emissions, and enhancing system stability [9]. At present, the crucial issue in power networks is their efficiency and the cost associated with electricity consumption.

The energy crises of the 1970s and 1980s served as a wake-up call to the world, highlighting the importance of energy optimization. The emergence of renewable energy production with varying time characteristics ushers in a new era of energy management research [53]. However, the traditional power grid struggles to accommodate the increasing load demands and the integration of renewable energy sources. Moreover, the expanding energy-producing capacity comes at a steep cost. To address this challenge, the concept of a smart grid has been proposed as a solution. It makes the power systems more sophisticated and facilitates the integration of renewable energy resources into the grid [131].

A novel hybrid AC/DC micro-grid design is presented in [123] within the context of an innovative grid platform that integrates the advantages of both AC and DC

grids, connected by multi-directional converters. The hybrid micro-grid optimizes load demands and generation through the evaluation of available renewable energy sources and conversion efficiencies, while operating within the constraints of power quality considerations [135].

In conclusion, consumers desire a consistent, cost-effective power supply with exceptional service quality, which can only be achieved through the reliance on renewable energy sources and the implementation of delay-tolerant load demands [115]. Figure 1.1 provides an initial outlook on the expected operational areas within this field, showcasing the central idea of a sophisticated grid that accommodates micro-generations, grid configurations, utility applications, and consumer load demands.

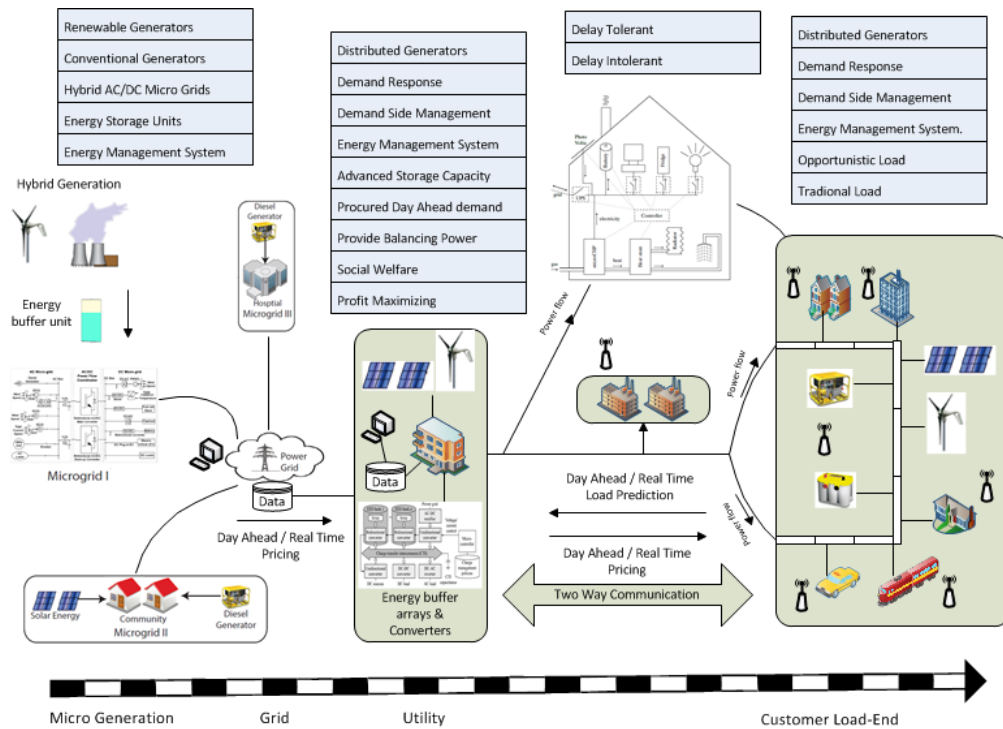


Figure 1.1: Futuristic power network.

## 1.2 Motivation

As a natural response to the renewable energy revolution, considerable changes are required in the existing power infrastructure. Smooth integration of RESs into the present electricity infrastructure requires overcoming many physical and computational constraints. Creative and comprehensive energy flow techniques are required to get an actual potential out of these newly integrated electrifying technologies.

The concept of “Microgrids” (MGs) is illustrated at the dawn of the twenty-first century to address the above challenges of integrating new technologies in old power networks. It has a promising solution for the upcoming challenges of energy transition from conventional to renewable sources idealizing the cost-efficient future power systems. MGs are small power distribution hubs with variable supply and controllable load demands. Besides, it has the advantage of generating electricity

near the point of consumption and can address the existing power system inefficiencies. The small distance transmission lines are therefore more efficient, and a micro power system is more reliable.

Smaller in power capacity than a central power generator, MGs are much more flexible in operating. Even though a regular power user may generate electricity from its own home or business, this makes it a viable option for customers in rural or remote areas. It may also minimize global carbon emissions by using renewable, carbon-neutral energy sources (e.g., wind and solar). The computational architectural modelling of microgrids is the fundamental motivation for this work. The prior research in this area falls into two categories: 1) Microgrid layout-design (component size) issue. 2) Design of customized energy management systems. Neither of these concerns can be fully addressed in isolation since each directly influences the other.

To the author's knowledge, no complete studies cover the above difficulties systematically. First, beginning with the basic system needs, providing in-depth energy management strategies. Then, demonstrating the optimal system operations to maximize the usage of the installed RESs and lessen the impact on environmental degradation by reducing the usage of diesel generators.

This thesis' study addresses the challenges associated with achieving the above motivations from a technological standpoint. A regulated power structure may strengthen the connection between power generation and consumption, reducing intermittency and increasing PV's financial viability. Hence, this work presents the different grid typologies, their layout designs, and most importantly, the control system strategies controlling the whole grid. A simple and appropriate energy management system (EMS) is a solution to these sophisticated, intelligent power networks. So that these can be controlled effectively and efficiently to achieve high sustainability, reliability, and dependability.

Unlike other previous works on microgrids, this work not only presents the detailed mathematical modelling of the main components of the systems but also provides case study-based solutions involving various grid typologies and architectural configurations. However, it also demonstrates different control scenarios and strategies for the energy flows in the power network. Nevertheless, further chapters discuss the relevant case studies where such growing concerns are worth exploring.

### 1.3 Problem Definition

This thesis is concerned with the notion of a smart grid, which consists of intelligent energy components and an optimum device control framework. As a result, this endeavour aims to create an efficient, independent, self-sufficient, and cost-effective micro-energy network.

The actual problems that need to be addressed while constructing an optimal solution for intelligent grids are as follows:

- Optimize generation operating cost at generation end.
- Reduce carbon emissions at generation end.
- Optimize power efficiency at generation end.

- Optimize production from renewable energy resources.
- Optimize the utilization of energy storage devices.
- Maximize grid utility profit.
- Optimize power flow in power network.
- Optimize energy utilization cost at consumer end.
- Coordinate demand side management and demand response.
- Increase Social welfare at consumer end by saving extra energy.
- Improve energy consumer experience by enhancing energy management system

Consequently, this book presents a concept of economical power operation through the implementation of a hybrid dual AC/DC micro-grid, aimed at reducing accumulated electricity costs. The concept is based on the modeling and scheduling of energy entities (EEs). It offers an innovative approach to automation, highlighting energy management and load balancing techniques. In this study, customer demands are differentiated under the category of AC and DC appliances. These demands are validated based on appliance scheduling problems with worst-case delay constraints. In addition, various cost regimes are introduced to differentiate the electricity cost for energy obtained from AC and DC power lines. To make the problem formulation more realistic, the micro-grid model with all of its parameters and a realistic pricing function model is introduced.

In this research work, optimal algorithms have been proposed to manage the sudden switching between AC-DC buses during load schedules. These proposed schemes offer an efficient strategy for switching between AC-DC buses. Additionally, the concept of creating queues to regulate demand buffers when electricity prices are high is also introduced. This approach results in optimal electricity pricing and system efficiency, and it has the potential to enhance grid sustainability while fostering high customer satisfaction. The algorithm operates in a highly dynamic environment, where renewable resources are uncertain, and load demands are highly diverse. The advanced control strategies proposed in this research work make the current power grid more intelligent.

## 1.4 Research Objectives

Small-scale renewable energy sources may reduce carbon emissions while relieving the strain on inefficient centralized electricity infrastructures. Despite these advantages, the intermittent nature and high cost of renewable energy make it difficult for individuals and small communities to embrace them. However, an EMS strategy to control a microgrid can minimize intermittency, making small-scale renewable energy more accessible to individuals and small communities. We will see whether combining many small grids into a microgrid further reduces intermittency's consequences.



This study focuses on system-level modelling, critical for effective EMS development. This study does not investigate the power electronics concept's grid operations. However, it targets the empirical-based scheduling problems with a discrete-time step of more than a minute. It saves excessive computing time, but complicated planning and operating scenarios are of no concern at the moment. The modelling method used here is unconcerned with precise modelling. Hence, this study does not examine voltage stability, power quality, or quick responsiveness problems.

Therefore, model-based development is employed here to characterize the progressive performance of each particular element of the power grid. In addition, a portion of this study illustrates a unique power management system (e.g., a rule-based) as a preliminary management approach already discussed in many research titles throughout the literature. But, eventually the author identifies the shortcomings that may be corrected to enhance the system's capability.

For this purpose, the following study goals were set:

1. The current literature has a flaw: it does not explicitly describe a microgrid as a power structure for residential power networks. Furthermore, how component-based modelling may enhance the energy management of microgrids and their different topologies must be compared to improve the outcomes.
2. There are numerous power grid configurations in the energy networks. The most well-known is a microgrid configuration, which integrates multiple small-scale power systems to form a community-level energy sharing grid. However, relatively little research has been conducted on small-scale power networks, often known as nanogrids or picogrids. In contrast to microgrids, a nanogrid provides a low-cost power arrangement. Because a nanogrid is limited to a single house, its technological goals, hardware, and software are usually different from those of a microgrid.
3. A nanogrid control technology that mitigates the adverse effects of solar intermittency shall be developed. The strategy should reduce the electricity used by users, boosting small-scale PV installations. A less expensive alternative to storage methods (for example, battery banks) should be found. The grid power consumption of the managed nanogrid should be reduced as compared to the uncontrolled nanogrid under various load and solar irradiance scenarios.
4. To illustrate the actual cost-saving and the natural power flow balancing in the nanogrid, the model should incorporate real-world data sets and operational constraints for conventional and renewable energy power sources. Furthermore, it should model the working behaviour of the load appliances to have further control over intelligent load demands.
5. Moreover, component-based empirical models of various energy entities could be an outstanding achievement of this work. It may reflect the energy losses in overall power flow calculations. In addition, the concept of hybrid AC/DC nanogrid is another advantage where this study addresses the efficiencies of both the grid and the energy entities. It may involve the inefficiency criteria of power converters. Besides, a set of controlled flexible energy supply sources and load demands are employed to increase system flexibility.

### 1.4.1 Benefits to The Society

This research work will significantly impact society through environmental and financial effects. Moreover, some countries face the challenging problem of power shortages due to inadequate power distribution management. It reflects a poor power quality issue due to old infrastructure resulting in high losses, resulting in deregulation of power delivery and the influx of high electricity prices. This work will help the Government authorities to make energy policies more effective.

### Environmental Analysis

By supporting scheduling tactics and integrating enormous data centres, this research will assist in enhancing the efficiency of power transmission and minimising power consumption at the consumer end. Similarly, instead of using coal and thermal power stations, we can build distributed generation infrastructure to reduce massive carbon emissions from conventional power stations. Furthermore, most of the World's population is in a power emergency condition, which is the short-term planning of installing coal and diesel power stations in large numbers. It negatively affects the environment. Instead of using a short-term policy of installing these power stations, the situation can be countered by improving our system efficiencies and reducing the losses through various energy control policies.

### Market Analysis

Moreover, the World market is wide open in the energy field for foreign and local investors. Especially in the sector of distributed generations and the demand side management. There is much potential to work for implementing distributed resources to improve efficiencies and effectively use renewable generations. The following agendas are in the fact sheet of the work plan of any country:

- Reduce carbon emissions.
- Save excess energy for an emergency.
- Restore and upgrade thermal and hydroelectric power plants.
- Encourage targeted public and private investments.
- Improve the energy industry's policies, governance, performance, and efficiency.
- Promote the sector's financial self-sufficiency through full-cost-based tariffs and other tools.
- Encourage energy-saving activities.
- Enhance electricity distribution businesses' performance.
- Providing funds to the government sector to close its environmentally concerned energy generation initiatives.

## 1.5 Research Strategy

This thesis investigates the home power network architecture, control, and connection to promote residential PV and electric vehicle-based storage adoption. The following research strategy is planned to establish the desired goals of this work.

- An initial literature review is necessary to develop the research within the home area power network (HAPN) domain and obtain information on this subject matter. It may aid in identifying the effective nanogrid power flow scheme, optimal control strategies, and gaps in the literature, allowing for improvements. Furthermore, because nanogrid research is constantly changing, it is vital to maintain the literature review up to date. Different modelling designs and control algorithms related to system optimization and stability problems have been studied as design and research problems. Various design algorithms for the same problem have been searched out. Most of the literature survey regarding basic applications of Smart Grid has been completed, which is more specified towards cost optimization problem and load balancing in smart grid.
- Early solution thoughts are mind mapped after identifying research gaps and understanding the problem. Then data related to the problem definition is collected and verified throughout various platforms. The required literature is collected mainly from different Journals (e.g., Springer, Elsevier, Wiley, etc.), Control Conferences and IEEE transactions. However, priority has been given to the IEEE transaction on Smart Grid to gather quality work in the field of Smart Grid. Information related to different mathematical models proposed by numerous researchers in the area of interest has been gathered. A few journals with good impact factors have been targeted for research publications. A comprehensive study of various tools/software, especially MATLAB for system modelling, algorithm designing, and the PYTHON for forecasting models, has been done. Furthermore, real-time data sets of energy generations and utilization are collected from various international energy databases, referred to in the literature in the following Chapters.
- Further, the concepts for developing effective and efficient nanogrid topology are investigated, and the model of the home power flow network is finalized. Then the problems of cost minimization and load balancing are investigated and refined into a pseudo-algorithm that tackles the critical solution. Finally, the pseudo algorithm is theoretically modelled before coding and simulating. Sufficient data has been analyzed before working on the solution strategy. The work has been divided into two main domains. One is cost optimization, and the other is system balancing (a stability problem). These two domains could merge at the end, but initially, these are analyzed at different paces. A study of dynamic local and global optimization algorithms is carried out for cost optimization problems. While for power network balancing, a model predictive control scheme is suggested. These algorithms have been chosen based on their applications in this research area. The application of some working algorithms has been discussed in the literature review in the coming chapter.

- A simulated comparative case study is conducted to evaluate the solution's impact. The study evaluates a household's grid power usage with and without the proposed solution. The outcome's success is judged by the household's reduced grid electricity consumption. In addition, various house appliance demands are simulated using temporal data. Weekly data for summer and winter is used to ensure that the predicted household load curve is not distorted. The optimal solution is developed through non-linear, dynamic, and intelligent algorithms and is compared with the traditional optimization solutions for performance analysis. The mathematical models of various elements are redesigned following the problem configuration and simulated on defined software to solve the problems discussed above. This work is incredibly advantageous to a complex problem-solving approach through empirical methods. Expected results are in favour of the social welfare program for energy consumers. It includes electricity cost minimization and quality of service on the consumer side. At the same time, profit maximization and power network stabilization are achieved on the generation and distribution side. Mainly, the utility or aggregator make such control decisions to handle both sides (generation and utilization) for optimization.
- Following the creation of the simulated test situations, an iterative approach of outcome analysis, reflection, and progression is developed. Although the analysis is satisfactory, there is always some space for improvement. The most effective ways for addressing the solution's flaws are chosen. After which, the solution is re-simulated and re-analyzed.

## 1.6 Thesis Contribution

This thesis develops a model-based energy optimum power grid design and a framework for controlling PV-based home area power network (HAPN). It considers dynamic real-time grid prices, battery lifespan degradation, and grid blackout models. This research focuses on creating an accurate nanogrid model that considers each component's practical limits. Moreover, various case studies are employed depending on the problem definition. A cost-effective model predictive controller is developed to enhance HAPN functioning. The load's reactive power usage is also included in the nanogrid operations to establish an actual cost saving. Finally, it estimates the natural line losses among different grid topologies.

Moreover, an excellent nanogrid design is necessary to enhance PV-system energy consumption and lower the grid's power generating costs. The developed technique employs an accurate model for battery longevity. A forecasting model is also used to assess the unpredictability of solar power generation. Finally, in addition to grid outages and real-time utility pricing signals, an accurate estimate of the Levelized cost of energy (LCOE) and a robust nanogrid architecture are considered. As a consequence, the following are the contributions of this thesis:

- This work examines the literature's broad energy nanogrid and microgrid definitions, addressing their strengths and faults, before defining a home power network structure.

- Most importantly, this book highlights distributed and uncertain flexibilities' in supply-side and demand-side management. It utilizes real-life yearly data sets of household demands, EV driving patterns, and EV battery (dis)charging patterns. It demonstrates the proposed system model's actual energy management capabilities.
- A detailed converter-based nanogrid model is presented. This model incorporates real-world data sets and operational constraints for conventional and renewable energy power sources. The model also takes into account the lifespan depreciation of the EV storage capacity.
- Analyze detailed PV and energy storage devices (ESDs) models to identify component inefficiencies and energy losses. ESDs model also gives the outlook of the storage device life cycle.
- The probability distribution approach is applied to model uncertainty in solar energy generation, users' load demands, and the commencement of grid outages.
- A better technique for calculating the LOCE considers the battery's state of charge, discharging current, and number of cycles.
- It incorporates a constraint-based mathematical model for different flexible smart load demands (SLDs) attributing the demand side management strategies.
- A substantially realistic PV-battery nanogrid model is utilized by including the actual functioning constraints of the grid components.
- A unique operating approach based on the cost-efficient model predictive control is presented to reduce overall nanogrid operating costs and properly balance power flow.
- Adding a reward and penalty component allows cheap activation of power elastic and delay-tolerant loads while considering user comfort.
- This thesis develops a novel nanogrid control method that employs conventional storage and adjustable load needs, such as thermostatically regulated loads. In addition, it tackles the challenge of cost reduction and handling power variations generated by integrated PV panels.
- A novel two-stage "min-max co-scheduling (MMCS)" optimization technique is proposed. It successfully handles the cost reduction and customer satisfaction optimization problems inside a single optimization framework. The models are solved using a mixed-integer linear programming (MILP) branch and bound approach and a computationally efficient mixed-integer rule-based sliding horizon dynamical method.
- A complex hybrid AC/DC nanogrid model is presented that incorporates real-world operational constraints for conventional and renewable energy sources. It also accounts for battery life loss and component-based power losses during DC-AC sub-grid energy exchange.

- A proportional power-sharing and a two-stage co-simulation framework is presented to build a multi-time scale energy management and control approach. On the other hand, the AC/DC hybrid nanogrid's dispatch may be optimized offline to lower total energy expenditures. Lastly, a real-time synchronized power sharing strategy is used to balance the power network.
- To lower the total operating expenses of the nanogrid, a MPC-based reactive optimum energy allocation approach is recommended. In addition, a unique approach is also adopted for supplying reactive energy from storage banks and photovoltaics.
- A robust local controller utilizes time-triggered communication to monitor the ideal data acquired from the scheduler. Nevertheless, a lossless connection between device-level control and actuators is envisioned.
- The suggested design includes secondary predictive control and main distributed robust control layers. It increases system predictability, redundancy and facilitates HAPN plug-and-play. The secondary control layer implements the HAPN analytical model, whereas the main control layer implements the HAPN physical model.
- A performance comparison is made with some previous works based on the inclusion of various types of losses and system topologies. Furthermore, the influence of the hierarchical control framework on the AC/DC hybrid HAPN's stability and economic operation is fully examined.
- A signal house simulation model is adopted to validate the optimal scheduling problem, utilizing real-time/day-ahead electricity price information for realistic outcomes.

## 1.7 Outline of The Book

The research work is classified into seven chapters, beginning with the introduction of the work stated in this chapter. This chapter outlines the background, motivation of the work, problem definition, research objectives, research strategy, and thesis organization. The remainder of the book is structured as follows:

- Chapter 2: Small-scale intelligent power networks are the center of discussion in this book. A comprehensive discussion on the formation of intelligent power networks is presented in this chapter. It begins with an overview of the evolution of intelligent grids providing insight into how the grids are transforming from traditional systems to intelligent smart grids. It also gives an insight into various grid topologies and configurations. Further, this chapter discusses the microgrid's main components and control architectures. In addition, a communication layer that helps in making the microgrid intelligent is also discussed in this chapter. In the end, some forecasting and optimization strategies are reviewed in the state of art literature work.
- Chapter 3: This chapter discusses in detail the analysis of various grid component models and proposes new analytical thinking regarding system modeling.

These components are divided into five main parts discussing energy supply entities, energy storage devices, energy consuming devices, energy pricing schemes, and grid optimization models. The analytical models of various grid components are integrated into a single control entity to form an intelligent energy management system for a small home area power network. Hence, this chapter presents an optimum design strategy for PV-storage-based microgrids. Which also introduces generic models for PV forecasting and solar generators, grid-tie lines, and fossil fuel generators. It also presents the models for evaluating the battery lifespan and classification of various load demands depending on their working phenomenon.

- Chapter 4: This chapter presents an introductory model of a small-scale home area power network (HAPN). It integrates an empirical battery degradation model into the power flow model of a nanogrid to demonstrate the actual behavior of storage devices in power networks. Cost optimal energy management system, is derived by introducing specific optimization algorithms. The proposed approach leverages a case study of real-life yearly data sets of household energy demands, EV driving patterns, and EV battery (dis)charging patterns to demonstrate the precise energy management capabilities of the suggested model and to illustrate the actual phenomenon of the scheduling algorithms. Simulation findings compare energy suppliers' penetration levels and usage factors on daily, monthly, and yearly basis. In addition, a daily, monthly, and annual capacity loss percentage is calculated with the system's battery life-cycle degradation model. Also, the algorithms match the power demands with the cheapest energy sources, ensuring customer comfort and reasonable expenses.
- Chapter 5: This chapter extends the work in previous module, where the nanogrid model is expanded to integrate the reactive power with active power model. Moreover, the model has been altered to explore more possibilities to work as a hybrid AC/DC nanaogrid. Here the DC and AC power flow can be controlled separately, and the grid efficiency parameters are explained in detail by introducing the inverter efficiency model. Besides, a new battery lifetime loss model is incorporated, which reflects its importance in the cost minimization operation of the energy management system. Furthermore, this chapter presents a co-simulated intelligent home energy management system (iHEMS) that integrates the robust rolling horizon-based predictive scheduling framework with the real-time power electronics-based control mechanism. Furthermore, this chapter also introduces a communication model using which the central scheduler sends time-triggered low-jitter wireless signals to the distributed device level local controller to execute the control law. Furthermore, a real-time, distributed, and robust control strategy is established by implementing a coordinated energy sharing mechanism that incorporates an auxiliary power source. Finally, the proposed model is evaluated through a comparison of various AC/DC models for home area power networks (HAPN).
- Chapter 6: This chapter emphasizes the power load demands extensively. It explains the component-based modeling of various home appliances and derives their energy requirement patterns. This chapter proposes a linearized

component-based model that incorporates energy inefficiencies, power phase modes of intelligent demands, and the energy storage deterioration phenomenon. It adopts a co-scheduling strategy in a small-scale energy nanogrid combining roof-top photovoltaics panels, backup diesel engine generators, energy storage devices, and intelligent load demands with grid electricity. The scheduling model uses mixed-integer linear programming (MILP) and a min-max optimization technique to lower daily energy expenses, maintain high consumer comfort, and promote home energy self-sufficiency. A numerical case study validates the suggested HAPN model. The applied technique leverages a cost-effective optimum balance of diverse energy entities in a HAPN showing real-world potential.

- Chapter 7: This final chapter provides a quick summary of the thesis’s significant contributions and summarizes the study’s primary views.

## 1.8 List of Publications

### Journal articles

1. Minhas, D.M.; Meiers, J.; Frey, G. Electric Vehicle Battery Storage Concentric Intelligent Home Energy Management System Using Real Life Data Sets. *Energies* 2022, 15, 1619.  
<https://doi.org/10.3390/en15051619>
2. D. M. Minhas and G. Frey, “Rolling Horizon Based Time-Triggered Distributed Control for AC/DC Home Area Power Network,” in *IEEE Transactions on Industry Applications*, vol. 57, no. 4, pp. 4021-4032, July-Aug. 2021,  
doi: 10.1109/TIA.2021.3074901.
3. D. M. Minhas and G. Frey, “Modeling and Optimizing Energy Supply and Demand in Home Area Power Network (HAPN),” in *IEEE Access*, vol. 8, pp. 2052-2072, 2020,  
doi: 10.1109/ACCESS.2019.2962660.

### Conference papers

1. D. M. Minhas and G. Frey, “Co-Simulation Strategy for Photovoltaic Power Prediction and Validation of Digital Twin,” 2023 IEEE International Conference on Environment and Electrical Engineering and 2020 IEEE Industrial and Commercial Power Systems Europe (EEEIC / I&CPS Europe), 2023, pp. 1-6.
2. D. M. Minhas, J. Meiers and G. Frey, “A Rule-based Expert System for Home Power Management Incorporating Real-Life Data Sets,” 2022 3rd International Conference on Smart Grid and Renewable Energy (SGRE), 2022, pp. 1-6,  
doi: 10.1109/SGRE53517.2022.9774212.
3. D. M. Minhas and G. Frey, “Stochastic Optimization Scheme to Schedule Energy Supply and Demands in an Islanded Microgrid,” *IECON 2020 The*



- 46th Annual Conference of the IEEE Industrial Electronics Society, 2020, pp. 1704-1709,  
doi: 10.1109/IECON43393.2020.9254749.
4. D. M. Minhas and G. Frey, "Two-Stage Multi-time Scale Energy Management & Control framework for Home Area Power Network," 2020 IEEE International Conference on Environment and Electrical Engineering and 2020 IEEE Industrial and Commercial Power Systems Europe (EEEIC / I&CPS Europe), 2020, pp. 1-6,  
doi: 10.1109/EEEIC/ICPSEurope49358.2020.9160519.
  5. D. M. Minhas and G. Frey, "Optimal Scheduling of Energy Supply Entities in Home Area Power Network," 2019 6th International Conference on Control, Decision and Information Technologies (CoDIT), 2019, pp. 732-737,  
doi: 10.1109/CoDIT.2019.8820673.
  6. D. M. Minhas, R. R. Khalid and G. Frey, "Real-time power balancing in photovoltaic-integrated smart micro-grid," IECON 2017 - 43rd Annual Conference of the IEEE Industrial Electronics Society, 2017, pp. 7469-7474,  
doi: 10.1109/IECON.2017.8217308.
  7. D. M. Minhas, R. R. Khalid and G. Frey, "Activation of electrical loads under electricity price uncertainty," 2017 IEEE International Conference on Smart Energy Grid Engineering (SEGE), 2017, pp. 373-378,  
doi: 10.1109/SEGE.2017.8052828.
  8. D. M. Minhas, R. R. Khalid and G. Frey, "Load control for supply-demand balancing under Renewable Energy forecasting," 2017 IEEE Second International Conference on DC Microgrids (ICDCM), 2017, pp. 365-370,  
doi: 10.1109/ICDCM.2017.8001071.
  9. D. M. Minhas, R. R. Khalid and G. Frey, "Short term load forecasting using hybrid adaptive fuzzy neural system: The performance evaluation," 2017 IEEE PES PowerAfrica, 2017, pp. 468-473,  
doi: 10.1109/PowerAfrica.2017.7991270.

---

## 2 State of the Art Work

Smart grids are gaining popularity because of the integration of new technologies like electric automobiles and renewables into conventional power systems. These technologies enhance the power network's efficiency, environmental impact, and economic growth of the sector. Aware of the ecological consequences of carbon-intensive conventional energy sources, authorities are progressively moving toward a more sustainable energy future. Furthermore, developing new technologies has prompted countries to seek more ecologically-friendly energy sources. Using sustainable energy resources (e.g., wind and solar) has replaced traditional carbon fuels that address the environmental challenges and the depletion of fossil fuel reserves. Furthermore, renewables cannot be regulated, and their unpredictability makes them difficult to incorporate. It makes it more challenging to balance energy production and consumption. These issues may be addressed by deploying power electronics devices, adopting the correct power network design, and controlling microgrids. Hence, coordination of sustainable energy resources and storage mechanisms is critical in this case.

### 2.1 Evolution of Smart Grid

#### 2.1.1 Traditional Power System

Traditional power systems are divided into generation, transmission, and delivery. Traditionally, electricity flows from generators to end-users. Large conventional generators like thermal power plants produce electricity transmitted to medium voltage substations through high voltage transmission lines. Finally, the distribution network delivers power to end-users. Transformers of various sizes are positioned between generators and transmission lines and between transmission and distribution regions to step voltage levels up or down. Traditional power systems are vertically integrated [62].

Power is generated centrally at enormous power facilities located far from end-users, as shown in Figure 2.1. This renders power systems subject to unforeseen occurrences like bad weather, accidents, and component failures, causing power outages when the system is not resilient enough. Demand is also not flexible in conventional power networks. In other words, centrally controlled power plants are solely accountable for balancing production and demand. This raises power prices, particularly during peak hours. Renewable energy sources, including wind and solar, have been distributively installed throughout the last decade. However, conventional power systems were not built to accommodate highly variable renewable energy sources, posing enormous hurdles [23]. For example, introducing dispersed generation at the distribution level may cause voltage changes and harmonic issues. In addition, the production of active power in the downstream network may significantly impact power flow in the upper network. Unlike existing power systems, where electricity flows in one direction from generation to distribution, future power systems may become bidirectional. Because the installed equipment was not intended for such

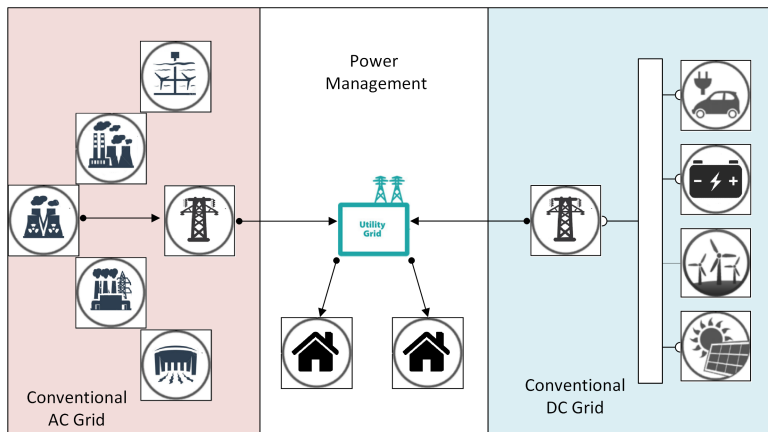


**Figure 2.1:** Conventional grid.

bidirectional flows, the upstream power flow might create protection and stability issues [126].

### 2.1.2 The Intelligent Power Grids

The term “intelligent grids” has been used by various research institutes, companies, and institutions. For example, the European Technology Platform for smart grids promotes intelligent integration, sustainability, low cost, and supply security [51]. Furthermore, these grids are power infrastructures that can automatically detect energy flow and respond to shortages and surpluses. Intelligent grids, when integrated with intelligent metering, may provide real-time user statistics for consumers and providers. As a result, customers may reduce their energy costs by using more energy during low-cost hours. An illustration of an intelligent grid is shown in Figure 2.2.

The intelligent grid may also sometimes be called a smart grid that helps integrate renewable energy in the conventional power network [183]. Both the sun and the wind do not always shine and blow. Grid managers can improve renewable energy integration while preserving power balance by combining energy demand data and weather forecasts. Smart grids include automation, monitoring, and more renewable energy integration. A bottom-up approach might help pave the way for efficient, intelligent grid implementation [137]. To construct efficient smart grids, one must ensure that each component is adaptive, reliable, and stable. This kind of network cell is called a microgrid, and is the domain of power systems where the efforts in this thesis are made.

### 2.1.3 The Term “Microgrid”

Energy production, transmission, and distribution occur at the “power grid” layer. Large-scale power facilities or renewable energy farms like wind or solar farms often produce electricity. The produced electricity is then sent to the loads through transmission lines. The second tier of the distribution network is the “utility service area,” which includes residential, industrial, and commercial areas. This second layer may consist of several microgrids. A microgrid is a remote system of feeders or electrical components. There may be a supervisory control system and distributed generating units, as shown in Figure 2.3. Demand side management schemes may

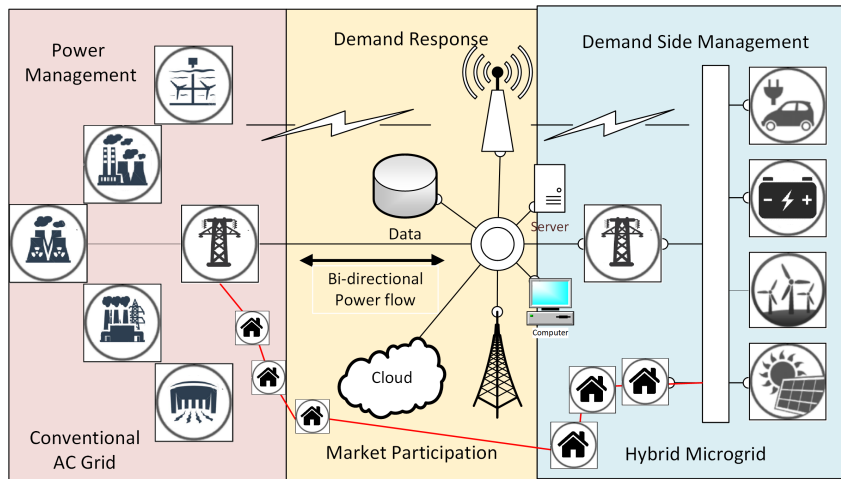


Figure 2.2: Smart grid.

be added to the primary control system. In the figure Nanogrids are coupled via a DC backbone. However it is not a necessary feature of Microgrids.

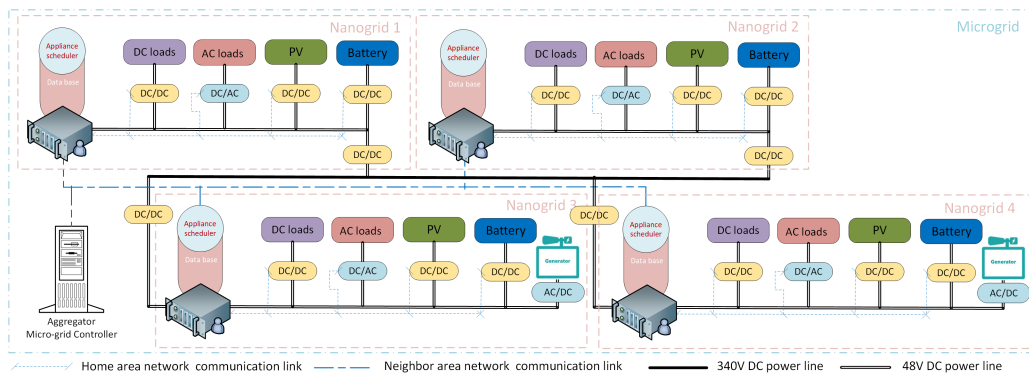


Figure 2.3: Microgrid illustration.

A microgrid is defined differently in various literature. However, the idea dates back over a decade. As per the U.S. Department of Energy, a microgrid is a collection of electrical loads, generators, and storage devices linked together by a single connection point to the main supply grid [184]. Whereas the four essential qualities that the microgrids should have include:

- A microgrid connects local generation, storage, and demand to a local distribution system. Local generation occurs at low voltages and is called micro-generation due to its small size.
- Second, a microgrid should have two modes of operation: grid-connected and emergency or islanded.
- Third, microgrids allow active distribution network operation. This architecture's management and coordination allow for micro-source integration.
- Fourth, microgrids may be multi-scale. A small microgrid is a dwelling with PV panels, power converters, and loads. A factory-sized microgrid can be a university campus or a neighborhood.

A microgrid is linked to the upstream primary power grid at a “point of common coupling.” This point serves as a link between a microgrid and an upstream grid. Microgrids outperform passive distribution networks in many ways. A battery storage mechanism makes them more resistant to failures, disruptions, and defects. They are more efficient since the electricity is produced at the point of usage. They are more eco-friendly because they enable more significant quantities of clean, renewable energy. Microgrids may also reduce the demand for polluting power facilities like coal-fired ones. Microgrids may give more flexibility due to better storage integration and supervisory control. Greater flexibility allows for additional renewable energy sources to be integrated. Microgrids are also less susceptible to disruptions or faults. They can do this because they are island capable. Control and protection schemes may activate this mode. Microgrids, unlike traditional power plants, have built-in modules. So they can be managed and maintained separately. Also, electrical components may be readily changed, improved, and standardized. Microgrids may be islanded during upstream electrical network outages. This action improves supply dependability and continuity. A robust energy management system keeps the microgrid from failing or going dark. Likewise, demand-side management aims to promote customer comfort and involvement in decision-making.

### 2.1.4 Distributed Smart Power Systems

In the subsequent decades, the passive distribution power network will transform into a more intelligent and controlled active distribution network. As a result, distribution networks will soon play a more significant part in electrical network operation, administration, and monitoring. The Independent Electricity System Operator (IESO) defines an active distribution network as a “control platform for shared energy resources including distributed generators, loads, and storage [77]. Using a flexible network structure, distribution system operators may control power flows. One of the essential features of such networks is bidirectional power flow. Decentralized decision-making and control replace centralized authority. The active management of the distribution network will allow power to flow bidirectionally from upstream to downstream and vice versa. Furthermore, voltage and frequency will be monitored by the generation or transmission side and the distribution network operators. Finally, there will be an increase in efficiency due to the active management [63, 124].

As previously stated, active networks may include tools for managing dispersed energy sources. Operators of distribution and transmission systems will need to work together to achieve this. New commercial auxiliary services and grid codes will also be required for distribution system operators. The lack of communication between transmission system operators and distributed generator owners or distribution system operators is now a concern in passive networks. Online and real-time information sharing is required for active networks to function effectively. A brief illustration of an operational power network is depicted in Figure 2.2

Active distribution networks may provide significant potential advantages when information sharing is allowed. First, their greater flexibility may enable incorporating distributed generation, demand side control, and energy storage. Second, changing the distribution network structure and management may allow new service options. Another possible advantage is that it can effectively match electricity production with customer demand. For example, demand-side management techniques

and forecasting methodologies may help accomplish this [39]. Furthermore, unlike passive networks, active networks may sustain stand-alone functioning due to decentralized creation and storage. The closeness of dispersed generators to demand sites also reduces transit losses. Finally, active networks may help the network by easing congestion and restoring service after faults, among other things [62, 127, 132].

Due to the significant unpredictability associated with renewable energy sources, rapid management and operation strategies must be adapted. In such harsh situations, power storage automation may aid system stabilization. Depending on the design scheme, these can store a lot of energy, which may be used for many hours or days. Power control and conversion devices link dispersed energy entities to the electricity grid. Electrical entities will also help stabilize the system. Active and reactive power can be controlled quickly, effectively addressing rapid phenomena like frequency and voltage variations.

## 2.2 Components and Microgrid Layouts

On the one hand, renewables like solar and wind have seen remarkable increases in their penetration rates. However, on the other hand, worldwide population expansion, industrialization, and other factors have increased overall energy consumption. In addition, new power grid-connected technology like electric automobiles may also increase the power demand. Energy storage technologies are also being incorporated into electrical networks to address the generation-consumption mismatch [93].

### 2.2.1 Technologies for Renewable and Non-Renewable Distributed Generation

The reciprocating engine, gas turbine, and microturbine are three frequently utilized distributed generations (DGs) based on non-renewable resources [110]. The reciprocating engine, which uses fuels such as diesel and gas, was one of the nineteenth century's most significant technological breakthroughs. These engines range from very small to quite big, for example, from 3 *kW* to 6 *MW* [5]. While gas turbine technology is one of the most advanced and mature. A gas turbine can be as large as a few megawatts. Whereas non-renewable DG is a micro turbine, a growing and promising technology that uses non-renewable resources such as natural gas [6].

The benefits of a reciprocating engine are low prices and flexible control over the input mechanical power. The negative is that they are ecologically unfavorable owing to emissions [162]. Furthermore, as previously stated, gas turbines have the potential to achieve high efficiency in combined heat and power (CHP) applications, making them more cost-effective. They have strong ramp-up capabilities, making them essential for black start applications and covering the picked load [50]. However, gas turbines are often too massive for tiny customers. Alternately, microturbines have the benefit of being compact and light. They feature an easy start-up and shutdown procedure and affordable maintenance expenses. The micro-turbine is currently in the early stages of development and is somewhat pricey. They are also ecologically friendly [150].

Wind turbines, solar photovoltaics, biomass power plants, hydro units, geothermal, ocean energy, and solar-thermal plants, on the other hand, may be used as microgrid distributed generators [55]. The geothermal and solar-thermal plants use

**Table 2.1:** Comparison of conventional and renewable technologies.

| Technologies   | Primary source | Output voltage | Installed capacity (kW) | Efficiency (%) | Pros  | Cons  |
|----------------|----------------|----------------|-------------------------|----------------|---|---|
| Non-renewables | Diesel/Gas     | AC             | 3-6000                  | 28-33          | Inexpensive installation<br>Flexible mechanical control   | Produce high emissions.   |
|                | Gas            | AC             | 0.5-30000               | 21-35          | It has high efficiency in combined heat and power (CHP) applications.<br>They have excellent ramp-up capabilities, making them indispensable for black start operations and compensate for the load spikes. | Too large for small consumers.  |
|                | Natural gas    | AC             | 30-1000                 | 20-30          | Compact and light.<br>Simple start-up and shutdown procedures<br>Low maintenance costs  | Development stage.<br>Pricey.   |
| Renewables     | Wind           | AC             | 0.1-9000                | 40-59          | Many sites have wind availability.<br>Power generation at all hours of the day and night<br>Mature technology   | Still pricey.<br>Stochasticity is high.                                       |
|                | Sun            | DC             | 0.01-5000               | 40-60          | Capacity for flexible installation.<br>Suitability for a variety of applications.   | Storage mechanism is needed.  |
|                | Biomass        | AC             | 100-20000               | 45-70          | Low environmental impact.<br>High availability.<br>Alcohol as well as other fuels generated by Biofuels are cost-effective and environmentally friendly.  | Still costly.<br>A total waste of energy on a rational level.                 |
|                | Water          | AC             | 5-1000000               | 66-95          | Environmentally and economically favorable.<br>Low initial investment and ongoing maintenance expenses.<br>It helps supply peak power and spin reserves.  | Energy expansion is difficult.<br>Impact on the environment.                  |
|                | Hot water      | AC             | 5000-100000             | 12-18          | Environmentally friendly on the outside.<br>Low operating expenses.   | Geo thermal locations are not available in the area of interest.              |
|                | Tidal waves    | AC             | 10-1000                 | n.a.           | Low operating expenses.<br>Grater concentration.<br>More consistent than PV and wind power.   | Lack of commercial projects.<br>Uncertain operating and maintenance expenses. |
|                | Sun & Water    | AC             | 1000-80000              | 17-25          | Simple and low-maintenance.<br>The operation costs almost nothing.<br>Advanced technology.  | Low energy density.<br>Limited scalability.                                   |

hot water to generate electricity. Concerning the installed capacity, over the last year, large-scale wind turbines up to 9 MW have been installed, and there is a continuing upscaling to reduce the cost. Wind turbines are also a developed technology that can generate power throughout the day. Also, the largest installed capacity of hydro units is now over 1 GW [18]. Hydro units can provide peak power and spinning reserve. Wind and solar photovoltaics have a theoretical efficiency of 40% depending on technology and operating point. On the other side, Geothermal and solar-thermal units have relatively low efficiency, for instance, between 10% and 20%. The critical advantage of wind and solar is that they are abundant in many locations. The output voltage of all these technologies except the solar photovoltaic is AC. Solar photovoltaic units have a flexible installed capacity and may be used for various applications, including off-grid and pumping [28].

### 2.2.2 Technologies for Energy Storage

There are several energy storage systems available today. In general, energy storage methods are divided into two types based on the form of the stored energy: direct energy storage and indirect energy storage [46]. The former store energy as electrical energy and do not need to be converted to another form. In contrast, indirect energy storage solutions need the conversion of electrical energy from/to mechanical or chemical energy. Table 2.2 depicts technologies of each kind.

Other than batteries, there are eight regularly used energy storage technologies: thermal energy storage, pumped hydro storage, compressed air energy storage, fly-wheel, fuel-cells, capacitors, supercapacitors, and superconducting magnetic energy storage. An overview of the properties of various energy storage systems is provided below, including electrical efficiency, installed capacity, energy density, capital expenses, life duration, and maturity [178, 193].

Superconducting magnetic energy storage (SMES) and ultra-capacitor energy storage (UCES) are two forms of electrical energy storage systems that are advanced variants of basic electrical components such as inductors and capacitors. These systems possess the capability to rapidly discharge substantial amounts of power, making them well-suited for power quality applications. Mechanical energy storage

**Table 2.2:** Comparison of energy storage technologies [47, 191]

| Storage technology       | Efficiency (%) | Capacity (MW) | Energy Density (Wh/kg) | Capital (\euro/kW) | Lifetime (Years) | Maturity      |
|--------------------------|----------------|---------------|------------------------|--------------------|------------------|---------------|
| Thermal energy storage   | 35-65          | 0-300         | 80-250                 | 140-220            | 5-40             | Developed     |
| Pumped hydro storage     | 75-80          | 100-6000      | 0.5-1.5                | 400-1500           | 40-60            | Mature        |
| Compressed air storage   | 50-89          | 3-800         | 30-60                  | 250-1500           | 20-60            | Developed     |
| Flywheel                 | 93-95          | 0-25          | 10-30                  | 250                | ~15              | Demonstration |
| Fuel-cells               | 20-50          | 0-50          | 800-10000              | 350-1100           | 5-15             | Developing    |
| Capacitors               | 60-65          | 9-0.05        | 0.05-5                 | 250                | >5               | Developed     |
| Super capacitor          | 90-95          | 0-0.3         | 2.5-15                 | 200                | >20              | Developing    |
| Superconducting magnetic | 95-98          | 0.1-10        | 0.5-5                  | 200                | >20              | Demonstration |

**Table 2.3:** Comparison of battery energy storage technologies [47]

| Battery Storage technology | Efficiency (%) | Capacity (MW) | Energy Density (Wh/kg) | Capital (\euro/kW) | Lifetime (Years) | Maturity      |
|----------------------------|----------------|---------------|------------------------|--------------------|------------------|---------------|
| Lead acid                  | 70-90          | 0-40          | 30-50                  | 200                | 5-15             | Mature        |
| Nickel cadmium             | 60-65          | 0-40          | 50-75                  | 250-900            | 10-20            | Commercial    |
| Sodium sulphur             | 80-90          | 0.05-8        | 150-240                | 400-1200           | 10-15            | Commercial    |
| Lithium ion                | 85-90          | 0-1           | 75-200                 | 250-500            | 5-15             | Demonstration |
| Flow batteries             | 75-85          | 0.3-15        | 10-50                  | 400-1100           | 5-15             | Developing    |

technologies, on the other hand, store energy in the form of kinetic or potential energy. Examples of such systems include pumped hydro energy storage (PHES), compressed air energy storage (CAES), and flywheel energy storage (FES).

Thermal energy storage has an electrical efficiency ranging from 35% to 65%, whereas compressed air energy storage has an electrical efficiency ranging from 75% to 80%. A flywheel's electrical efficiency ranges between 93% and 95%. The efficiency of a fuel cell is between 20% and 50%. Capacitors have an efficiency of roughly 60%, but supercapacitors and superconducting magnetic energy storage have more than 90% electrical efficiency [47, 60]. Pumped hydro storage has the highest installed capacity of up to 6 GW, while compressed air energy storage has a capacity of hundreds of MW. Thermal units with installed capacities of up to 300 MW are possible. The rest of the storage technologies would have a smaller installed capacity, according to [47, 60]. Except for thermal storage, fuel cells, and batteries, most energy storage methods would have a poor energy density. With high capital expenditures, fuel cells are one of the most costly methods of storage. Energy storage using pumped hydro and compressed air has the most extended lifetimes (up to 60 years), whereas capacitors have a lifespan of about five years. Pumped hydro is the most developed of these technologies in terms of maturity [180]. Flywheels and superconducting magnetic energy storage are being tested. In addition, thermal energy storage, compressed air energy storage, capacitors, fuel cells and supercapacitors are all being developed. Battery energy storage is better suited for microgrids and balancing solar energy. A comparison of various battery technologies is shown in Table 2.3. In comparison, it is helpful to understand the features of battery energy storage methods. Nickel-cadmium and lead-acid batteries have the lowest efficiency, but lithium-ion and sodium-sulfur batteries offer excellent round-trip electrical efficiency of up to 90 %. For large-scale grid applications, lead-acid and flow batteries are viable possibilities [163]. Many projects based on lithium-ion batteries have recently been completed, with installed capacities exceeding 1 MW [47]. Lead-acid



and nickel-cadmium batteries have a modest energy density, but sodium-sulfur and lithium-ion batteries have a high energy density of up to  $240 \text{ Wh/kg}$ . The energy density of flow batteries ranges from  $10 \text{ Wh/kg}$  to  $50 \text{ Wh/kg}$ . In general, battery technology capital costs are rapidly declining. The life of these batteries, of course, depends on the sort of services they give, which can range from 5 to 15 years depending on the number of cycles, depth of discharge, and a variety of other characteristics such as charge and discharge rate, and temperature [47, 163]. The most mature technology is the lead-acid battery. While the Li-ion battery is rapidly evolving and maturing, the flow battery is still in the works. So, the table above, has summarized the features, benefits, and drawbacks of several energy storage technologies such as batteries in terms of round-trip electrical efficiency, capacity, energy density, capital expenses, lifetime, and maturity.

Undoubtedly, electrical vehicle (EV) storage gives the most flexible (dis)charging power [17, 185]. Thus, the goal of this study is to show the flexibility of power consumers by employing energy storage systems (ESSs) as EV batteries. Most EVs are parked practically constantly. To cope with the large penetration of inconsistent RESs, the vehicle to grid (V2G) approach may be considered [4]. The concept of an EV aggregator has been employed in a multi-microgrid system to distribute energy in the event of an emergency, with an emphasis on thermal safety and lithium-ion battery deterioration [194]. Another form of uncertainty might develop during EV scheduling. To decrease the impact on earnings, the energy management of EV parking areas use day-ahead planning, which incorporates a cancelling fee for customers when users modify their original arrival or departure times [87].

Li et al. [96] claims that storage deterioration and battery inefficiencies are vulnerable to battery operating limitations and energy trading demands. To maximize battery life, keep the battery's operating temperature within acceptable limits [168]. The battery's useable capacity and future power costs are affected by the grid's condition and execution time [205]. The anticipated Newton technique discovers optimum (dis)charging operations [214]. The general battery model by Hao et al. [67] also shows the scalability of building energy demand and storage capacity. An internal short circuit diagnosis approach with high resilience to measurement perturbations and capacity fading was also provided in [75].

**Energy density versus power density** It is critical to recognize that power and energy are both essential aspects of storage. This section shows the energy density against power density for several storage devices. High power density but low energy content are common characteristics of capacitors and supercapacitors. These storage units are ideal for reasonably quick power-based services such as transient voltage stability [142, 211].

Batteries and flywheels have adequate power and energy densities. Tesla automobiles, for example, have an energy capacity of  $85 \text{ kWh}$  to  $100 \text{ kWh}$ , which is pretty significant, and the power is also not awful, at approximately  $50 \text{ kW}$  [64]. The power is determined by how the batteries are connected. These battery cells may be linked in parallel or series. If the cells are connected in parallel, one gets greater power since one can draw a larger current. When connected them in series, one gets a high voltage but a low power. A mix of batteries and capacitors would be ideal; this combination of diverse storage technologies is referred to as hybrid energy storage [216].

Because of the usage of liquid fuels, fuel cells have a poor power density with high energy content. Because of the restricted power density, it cannot be given if a significant quantity of power is required. Another essential feature of storage systems is the discharge time, defined as the time necessary to transition from wholly charged to fully discharged. Supercapacitors and superconducting magnetic energy storage typically have a short discharge time of around seconds [215].

The discharge period of a flywheel and most battery technologies (excluding sodium-sulfur and flow batteries) ranges from one minute to tens of minutes. The discharge period of sodium-sulfur and flow batteries, ideal for stationary applications, can be many hours. However, the optimal size of each storage technology will be determined by the individual needs of microgrids. Therefore, it is necessary to know how many microgrid storage technologies are charged or discharged to determine the appropriate size. The Figure 2.4 compares several energy storage methods based on power and energy densities [47].

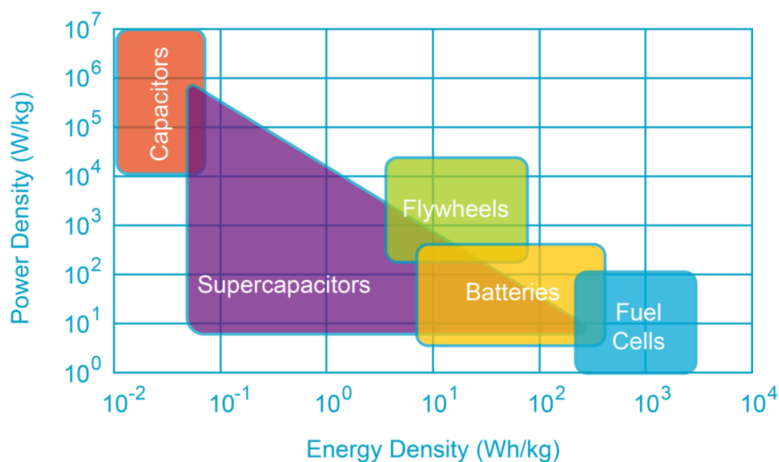


**Figure 2.4:** Comparison of energy storage technologies based on power and energy densities [47].

### 2.2.3 Types of Microgrids

A unified power network incorporates various intelligent energy devices including energy supply entities and as well as energy storage devices [115, 116]. A point of common connection (PCC) connects the microgrid to the upstream network. Therefore, the choice of microgrid design is crucial and must be done carefully to ensure the project's economic feasibility. Among other things, the type of power demands, current and proposed distributed generators, storage devices capacity, difficulties installing additional electrical lines, and existing communication technologies must be considered. In addition, it is vital to comprehend the advantages and disadvantages of various microgrid topologies, layouts, and architectures. An alternative current (AC) microgrid is usually the best solution for existing facilities with AC loads since it requires minor adjustments to the current systems. However, a higher-performing direct current (DC) microgrid might be considered for new installations. Various electrical components link the microgrid to the upstream network. The most common element is an AC or DC circuit breaker. A general illustration of a microgrid layout is shown in Figure 2.5.

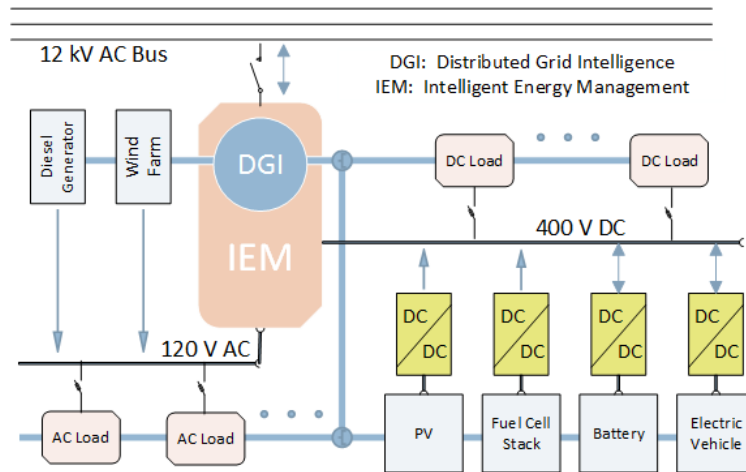


**Figure 2.5:** Microgrid layout.

### AC microgrid

The typical grid operating configuration is grid-connected AC configuration [123]. AC configuration is widely adoptable because of the nature of installed conventional power generating units and the users' load demands. AC microgrids consist of a transformer, a static switch, and several converters for loads, generation, and storage. In a grid-connected AC microgrid, electricity comes straight from the grid, eliminating the need for a series-connected converter. Load demands, power generators, and energy storage devices must all be grid supported [152]. More microgrids feeders may be linked simultaneously while power quality management for voltage and frequency is simple. Static compensators using capacitors and inverters are used to maintain the power quality. The fundamental downside of this arrangement is that it necessitates a high number of sophisticated power converters, which results in more significant power losses and decreased dependability. Nevertheless, the AC microgrid is exceptionally well-suited for integrating the microgrid idea into existing facilities. However, islanded DC distribution systems are becoming popular with the introduction of next-generation efficient renewable energy producers and DC power load components.

### DC microgrid

The utility grid is connected to the Direct current (DC) microgrid through an AC/DC converter. It is hoped that the microgrid will be able to export extra electricity generated by its bidirectional converters. DC microgrids have a relatively higher efficiency if the AC or DC conversion steps can be skipped.

DC microgrid is increasingly gaining more attention due to its many distinct advantages. First, renewable energy sources can be operated on a direct current from the component level's point of view. On top of this, new emerging technologies like electric vehicles are also DC. DC electrical networks may assist in integrating components like renewable energy sources and storage more efficiently. The DC technology is used in various electrical loads such as LED lights, laptops, and inverters for AC motor drives. A microgrid might be a very low-power microgrid, or even a nanogrid if we use our prior definition of microgrids. Apple and Google, among others, agreed that the USB Type-C connection with 100 W is sufficient to

power all DC equipment. Soon, 100 W DC USB type-C outputs will be available for these DC loads [47].

Most distributed generators require an AC/DC electromechanical interface to connect to the DC microgrid bus. To change the bus voltage for the AC loads, a DC/AC converter is required. DC loads can be directly connected or require a DC/DC converter depending on the bus voltage [151]. Without making any electrical contact, capacitors can be added to the bus. The central AC/DC converter controls the voltage on the DC bus. If the distribution grid fails, the microgrid must manage the DC bus voltage without the primary AC/DC converter. DC microgrids have various benefits over AC microgrids, including the use of fewer converters, the ability to adapt DC link voltage to grid demands, and good quality DC link voltage which permits direct connection of some DC loads. In contrast, the series-connected reversible AC/DC inverter regulates the whole flow of power to and from the distribution system, lowering dependability.

The DC connection voltage is independent of battery charge, and no circulating currents are formed, making this DC microgrid easily scalable. The DC/DC converters between the battery and the DC bus may also manage the power flow and hence the system is much controlled. However, despite the apparent benefits, such a system is less stable and more susceptible to DC connection problems. Aside from that, DC/DC converters between the battery and DC connection include power losses, making the system less efficient than a directly linked system.

Multiple AC/DC conversion stages are necessary between the intrinsically DC components and the AC connection. But in an all-DC home, these AC/DC conversion stages may be removed, resulting in the following benefits: First, eliminating AC/DC conversions minimizes the number of power converters required, possibly lowering investment costs. Second, avoiding power losses related with AC/DC conversions increases electrical efficiency. A DC home is more reliable due to the reduced number of power converters that can cause failure in network. Finally, a DC home is easier to govern.

### **Hybrid AC/DC microgrid**

Because it is difficult and costly to convert the whole power supply from AC to DC and operate in islanded mode. In [158, 208] recently have proposed a hybrid AC/DC nanogrid topology that combines the benefits of both AC and DC topologies. This architecture minimizes power conversion steps and integrates dispersed energy resources (DERs) efficiently [111]. Nevertheless, this current scheme has significant hurdles regarding reliability and control. Because the control entity is in charge of achieving dispatched grid power flow and balancing the AC and DC subgrids simultaneously. By intelligently controlling the interlink converter (IC), a smooth transition between AC and DC subgrids may be achieved. Furthermore, the IC must provide grid power flow management and grid-forming performance capabilities. An appropriate control approach is required to coordinate the functioning of the microgrid and maximize the flow of power throughout the AC and DC subgrids.

An asynchronous AC/DC converter connects an AC microgrid to a DC sub-grid in an AC-DC hybrid microgrid. The distributed generators may provide either AC or DC electricity. The AC feeder links the alternating current loads. In contrast, the DC feeder connects the direct current loads with a power converter to modify the voltage level. Depending on the power balance of the DC feeder, the DC sub-

grid may connect or disconnect the AC microgrid. This approach combines AC and DC microgrids to balance its feeders. Existing households mostly using AC supply but the future smart devices can be linked using more straightforward converters through DC feeder. Therefore, it is critical to establish an infrastructure where a direct current load may be connected directly to the DC feeder [151]. This microgrid design is ideal for installations with critical (DC feeder) and resilient loads (at the AC feeder). Solid-state transformers (SSTs) might be employed in a hybrid microgrid instead of conventional ones. Because it can through both AC and DC energy. Multiple AC/DC conversion stages are eliminated with the Solid State Transformer. On the other hand, the SSTs is serially coupled via DC/DC and AC/DC converters, reducing dependability.

Some standard voltage ratings of different typologies of the microgrid are described here. 12 V and 24 V are considered for lights. 48 V is used in telecommunications, rural PV installations, and vehicles. Power over Ethernet uses 50 V. DC voltages exceeding 100 V have a wide variety of uses. Extra low voltage is defined as less than 120 V. 230 V is used for pure resistive and thermal loads. The modulation voltage for a rectifier's DC input is 325 V [47]. 380 V is recommended for DC data centers. And electric cars need 400 V DC. 565 V is believed to directly connect to the three-phase AC grid at low voltage. Trams use 750 V power systems. High DC voltage is desirable for high-power DC applications to decrease power losses. At the same time, in some instances, it is prohibited for safety reasons. However, the maximum low voltage DC is 1500 V, which is used for big solar PV farms and traction systems.

### 2.2.4 Microgrid Configurations

A microgrid combines renewable energy sources and regulated loads as a small-scale power network. Electric vehicles and batteries are essential components of these networks to stabilize the power flow. The commonly known configurations are based on the size and the power capacity of the network and are described as;

#### **Picogrid**

Picogrids are often called “low-power microgrids.” A house, for example, shown in Figure 2.6 is a picogrid. A picogrid typically consists of a few residential appliances, tiny uninterruptible power sources, and photovoltaic (PV) devices. Picogrids may be used to build nanogrids. Their output power varies from hundreds to kilowatts.

#### **Nanogrid**

A nanogrid is a self-contained network of dwellings, photovoltaics, and micro-energy storage devices. Sometimes it consists of several neighboring picogrids as shown in Figure 2.7. Its power output varies from tens to hundreds of kilowatts. Although pico and nanogrids are commonly used interchangeably, it is often essential to describe them individually to illustrate their differences.

#### **Microgrid**

In many cases, the term microgrid also encompasses the concepts of picogrids and nanogrids. However, sometimes it is helpful to classify them this way to accentuate

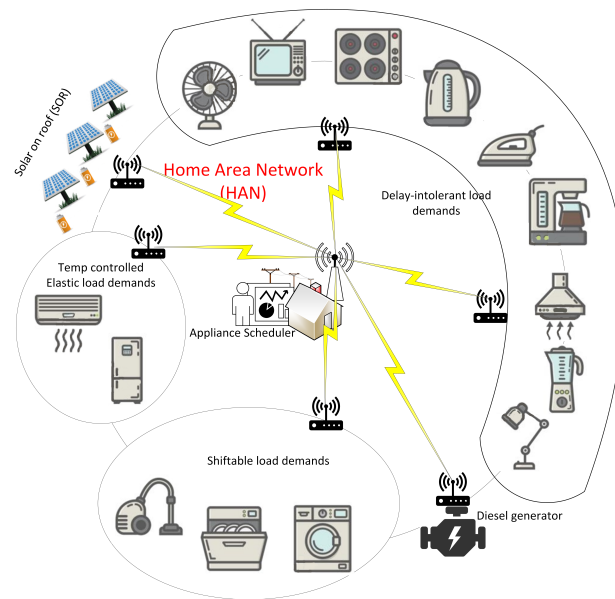


**Figure 2.6:** Picogrid layout.

their differences. A microgrid comprises many nanogrids with medium-scale components such as tiny wind turbines, industrial loads, combined heat and power units, and diesel engines. The size in this scenario ranges from a few hundred  $kW$  to a few  $MW$ . Figure 2.8 describes a detailed layout of a microgrid.

## 2.3 Microgrid Control Architecture

This work is motivated by the notion of a smart home, integrating customer flexibility and clean energy sources. Power related entities play an essential part in a smart home's power network. It is also known as home area power network (HAPN) and is concerned with intelligent energy generation and utilization within the home. This smart home concept has already been described in [8, 76, 85, 147, 153, 159, 161, 170]. Self-sufficiency of the HAPN, integration of new appliances, and communication among various energy agencies are critical components [160]. HAPN also has scheduling or managing policies for energy generators, and load needs citing [173]. Control is vital in microgrids because it keeps the system steady. Control optimizes electricity output and consumption while taking market pricing into account.

The control architecture used in conventional power systems to govern the active power output of generators is also known as Automatic Generation Control. In electrical power systems, the instantaneous active balance of power between the generator and the electric demand must be continually maintained [175]. This requirement must be met during either regular or emergency operations. Power variations arise in normal operation due to either intermittent renewable electricity generation or continuous load fluctuations. These aberrations occur during an emergency owing to abrupt failures of generating units, transmission links, or loads. When there is an imbalance, the system frequency deviates from its nominal value. Primary control is engaged automatically and locally to maintain the system's power balance. This

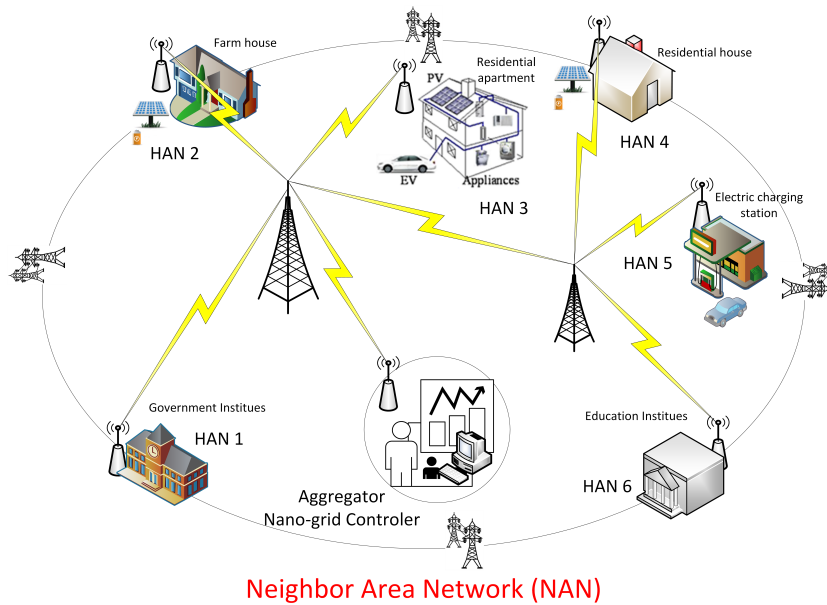


**Figure 2.7:** Nanogrid layout.

balance is done immediately following a contingency event, and it is accomplished decentralized. Following a contingency occurrence, secondary control is in charge of returning the frequency to its nominal value. Load frequency control is another name for secondary control. After that, tertiary control is engaged for times ranging from minutes to hours to replenish the secondary control reserves [68].

Likewise, a hierarchical control shown in Figure 2.9 can also be implemented in microgrids, with some differences. A microgrid is controlled in several ways; grid forming and grid feeding strategies are of primary concern. Grid formation methods are classified as communication-based or non-communication-based. Generally speaking, the structure of a microgrid is made up of four different layers; at the lowest level, this layer has physical infrastructure and local sources, then comes communication layer; above this, there is control and protection layer, and finally on top, the layer on business models and regulatory framework as shown in Figure 2.9.

Whereas, a microgrid's control layer is focused on the lowest layer of microgrid control. Moreover, a microgrid's control architecture may be separated into three layers: microgrid upstream network control, internal microgrid control, and local control, as shown in Figure 2.10.

### 2.3.1 Microgrid Local Control

At the lowest level, where physical components of the power network are present, Local control is responsible for the inner and outer loops, as well as droop control, where dispersed generation, storage, and loads exist. This control is used in power converters that connect various components to the distribution grid. The microgrid local control layer controls a single unit, such as a distributed generator, a storage unit, or a controlled load. Some of the actions performed by this controller are, protection, primary frequency control, primary voltage control, primary active and reactive power control and storage management [44].

Local control is implemented decentralized controlling distributed actuators at

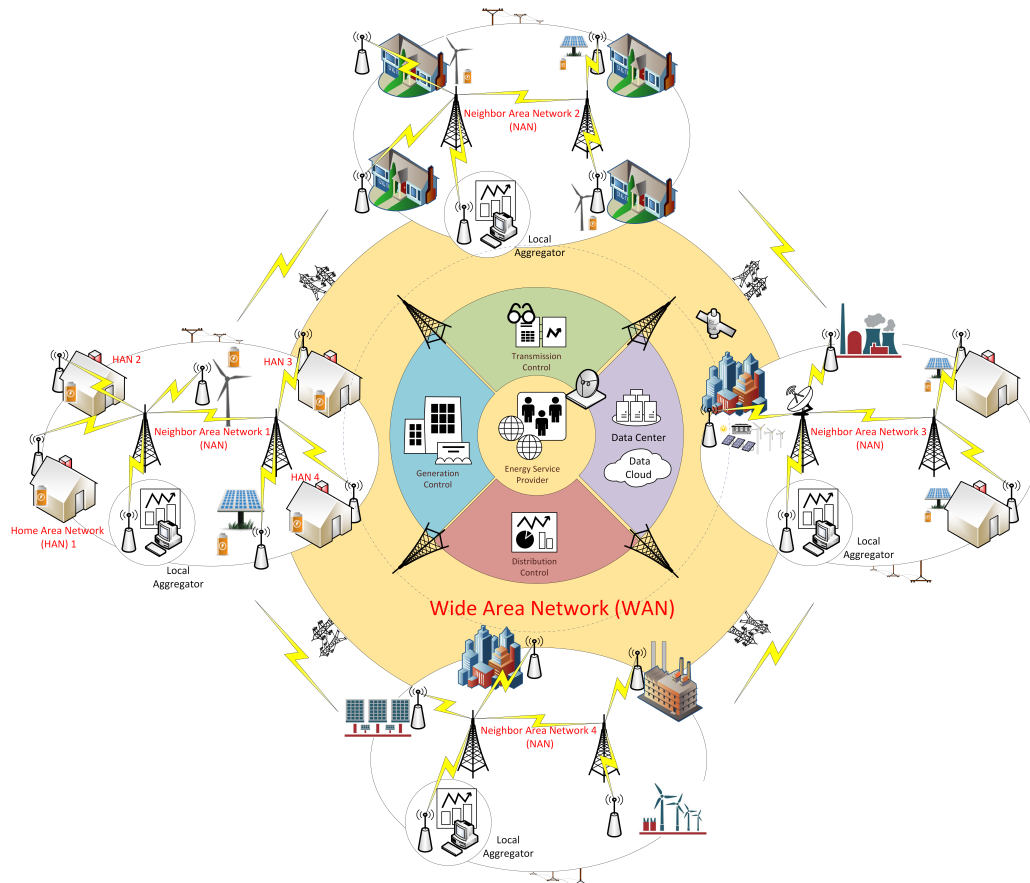


**Figure 2.8:** Microgrid layout.

the lowest level. In microgrids, active and reactive power is controlled locally. The controller receives three-phase current and voltage values from the grid. A distributed generating unit may also help the microgrid provide ancillary services, including inertia simulation, power oscillation damping, islanding assistance, and power quality concerns. Hence, primary local control restores a power system's active power balance. Where control inputs to generators, loads, or batteries are controlled locally. A voltage or current as a control input governs the DC and AC power converters.

### Decentralized architecture of local control in microgrid

In a decentralized control strategy, each controllable unit in the microgrid controls itself. Negotiation among the many actors may occur, particularly if they all have distinct aims. However, it is still possible to centralize standard computations like load forecasting. Four factors determine the performance of control algorithms. First is the energy node count, e.g., the number of dispersed generators and adjustable loads affects complexity and computational time. The second is the message exchange rate. Microgrids frequently include dispersed generators and loads and low-voltage communication networks with limited bandwidth. In some cases, the number of messages required to execute a task is crucial. Third, decentralized control decreases the number of communications, and only a tiny portion of the information is sent up the control hierarchy. Fourth, solution precision and optimality. Finally, the results' convergence and correctness depend on the input data and



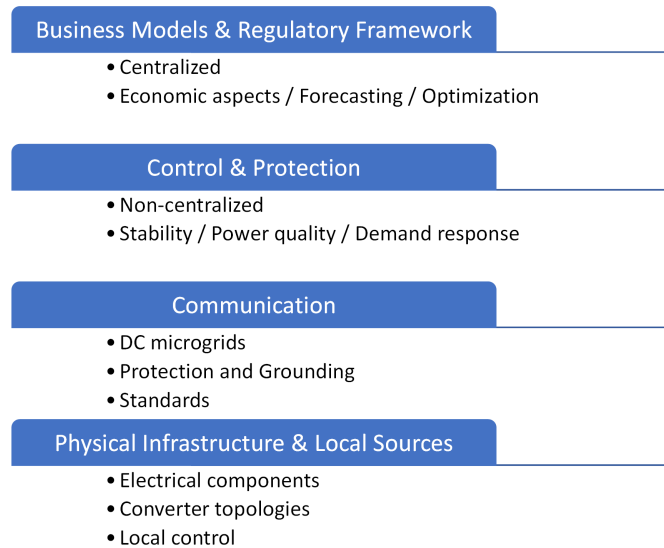


**Figure 2.9:** Microgrid layers [47].

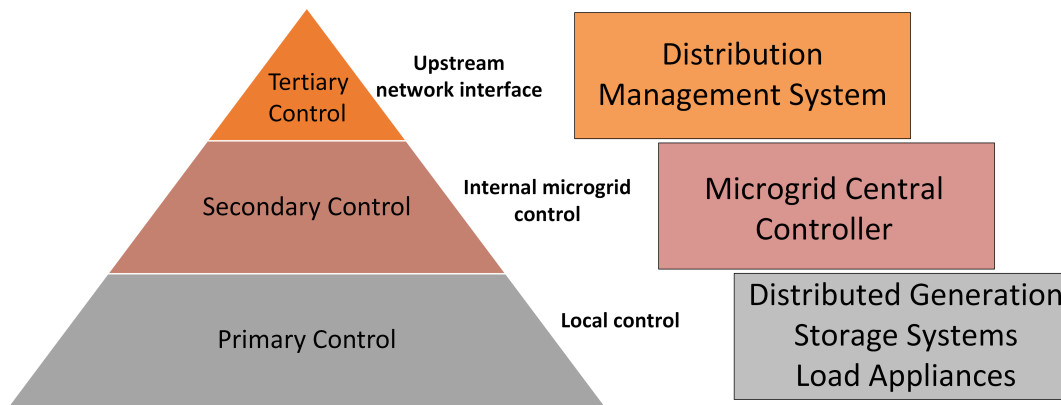


**Figure 2.10:** Microgrid control architecture.

methods.

Thus, decentralized control has several benefits as they are plug-and-play and suited for rapidly changing infrastructures. They are also quite reliable. At the same time, the fundamental drawback of decentralized control is the complexity of multi-ownership and rivalry among the numerous players or agents. It is because each RES's owner strives to maximize its own earnings.

### 2.3.2 Microgrid Internal Control

The internal micro-grid layer executes microgrid activities that need the participation of more than two players. Load and renewable energy source forecasting, load shedding and management, unit commitment economic dispatch, secondary voltage and frequency control, secondary active and reactive power control, security monitoring, black start, and restoration control are some functions [108]. The microgrid central controller has control over the internal control at this level. The primary purpose is to change distributed generator reference points in a microgrid. The internal control maintains synchronization when the microgrid is linked to the external grid. In addition, internal microgrid control modifies the active and reactive

power setpoints. This precise control detects and counteracts grid instabilities.

### **Centralized architecture of internal control in microgrid**

Depending on the control levels' obligations, a microgrid may be run centrally or decentralized. The central controller connects to the microgrid's feeds. This includes power market pricing, grid security, and local production capacities. In a centralized control system, the microgrid central controller is responsible for maximizing value and optimizing operation. The microgrid's central controller decides how much electricity to import from the upstream distribution system, maximizing local output and minimizing consumption. The distribution system operates based on market rates for energy, grid security concerns, and ancillary service requirements. The distribution management system monitors and controls the whole distribution network at the upstream network control layer. It can access real-time data and organize the information. It supplies the energy unit with active and reactive power setpoints based on signals from the transmission system operator or distributors. Control ensures proper power flow in the microgrid. For example, it may be determined if selling electricity to the grid is cheaper than storing it.

When internal microgrid control is centralized, a single unit is in charge of making decisions. This design works well when all microgrid actors have the same aims. For example, transmission system operators (TSOs) usually conduct centralized control in traditional power networks. Similarly, a single entity handles a microgrid's economic dispatch and unit commitment calculations using centralized control. The distribution system operator or a microgrid central controller provides the setpoints while calculating the aggregated load demands, distributed generation, and storage systems. Hence, centralized control gives excellent operational knowledge with well-defined and accomplished targets. So they can deliver the best solutions worldwide for online operation and easily synchronize with the primary grid. But, centralized control systems are computationally costly and time intensive. The central controller must optimize many dispersed generating, load, and storage units. This central controller also has significant communication needs, which increases the grid maintenance expenses.

#### **2.3.3 Microgrid Upstream Control**

On the upstream side is top control level also known as tertiary control. The distribution management system, which manages power transfer in between microgrid and the external power network while taking into account market and regulatory signals, is in charge of this control [57]. Based on market and pricing signals received directly from the distribution system operator or transmission system operator, the upstream control feeds the unit active and reactive power setpoints. Control is in charge of ensuring that electricity flows across power lines at this level. For instance, it is possible to decide which option is most cost-effective; storing the electricity or selling it to the main grid.

The upstream network control layer executes decisions for islanded and interconnected modes of operation, enables market participation, and carries out upstream coordination. It provides an interface for multiple microgrids at medium and low voltage levels. It also enables the provision of ancillary services and carries out

upstream coordination. The upstream network control layer's distribution management system is responsible for monitoring and controlling the entire distribution network. It can access real-time data and gather all the information in a centralized manner.

### 2.3.4 Master Slave Control

The master-slave control approach is an established method of microgrid control for running several distributed generators in parallel. A grid-forming type represents the master unit, which regulates the voltage and frequency of a microgrid. Slave grid feeding units follow the voltage and frequency imposed by the master unit while attempting to maintain their active and reactive power setpoints. Furthermore, grid-supporting equipment may be quickly connected to such a microgrid. In any scenario, supervisory control is required to distribute power correctly across all units. The key advantages of the master-slave control approach are its simplicity, ease of implementation, and resilience. However, the system cannot be readily extended, and supervisory management is required to ensure power is constantly shared appropriately. In addition, this control technique is based on power electronics technologies, which provide reduced dependability owing to unreliable communication channels. Therefore, a multi-master control method is frequently advocated for addressing these issues.

### 2.3.5 Centralized Control

In a centralized system, the primary control is local, but the secondary control is centralized. The microgrid central controller collects data from dispersed generating units, such as active and reactive power. The microgrid then provides updated active and reactive power set-points to all local controllers over the communication channel, such as distributed generators and energy storage units. The internal microgrid control decides how to operate the distributed generators. In addition, the microgrid controller has optimization and scheduling methods. The goal is to optimize the functioning of distributed generating units to meet the microgrid's needs while maximizing revenues. The microgrid central controller notifies users about external market pricing like day-ahead, real-time, or auxiliary service rates. The upstream network interface sends the pricing signals to the central controller. Users may submit their preferred bids to the controller every hour using those price signals. So the microgrid central controller optimizes and distributes the modified set-points to the distributed generators, storage units, and loads. Microgrids may submit hourly supply and demand bids in the centralized control architecture. The market operator aggregates all bids and develops a supply-demand curve depending on demand and supply power. The intersection of the aggregate demand and supply curves determines the unified marginal price.

Also, since low voltage microgrids are linked to the upstream medium voltage network through a transformer, this interconnection must not be overloaded, as this might trigger the transformer's over-current relay. In conclusion, the microgrid should exhibit a smooth transition between linked and isolated modes. Microgrids can be connected to the grid, operate in an isolated manner, or be shut down. The intentional or unintentional disconnection from the main grid of a microgrid connected to the grid may occur. The deliberate disconnection usually occurs dur-

ing maintenance of the primary network, where the switch from grid-connected to isolated mode is deliberately managed.

## 2.4 Microgrid Communication Network

The microgrid communication infrastructure must be highly reliable, with a bidirectional and extensible connection between microgrid resources. The communication network of a microgrid may be thought of as a link between its physical infrastructure and its control and protection operations. This may be compared to the conventional power grid topology, designed to work as a centralized unidirectional system and hence lacks the interconnectedness described above.

A smart residential nanogrid comprises of intelligent energy devices (IEDs) based home area power network (HAPN) [189]. Most IEDs can be operated and monitored remotely (e.g., internet of things devices). For HAPN to work efficiently, controllers and IEDs must communicate data in real time. This information sharing approach is best implemented by wireless sensor and actuator networks [213]. The communication layer is responsible for alerting the control and protection layers about the condition of the physical layer. This phenomenon enables the intelligence layer, the control and protection layer, to function correctly. For example, the size of an electrical grid determines the optimal communication network [21]. Finally, the foregoing techniques need data sharing between energy entities such as irradiation sensors, residential appliances, and grid energy management systems. Given the wide range of devices in HAPN, a standardized communication system network strategy is critical for success [185].

Energy and data transmission bandwidth restrictions frequently limit distributed power systems [92]. It is also advantageous to utilize communication networks efficiently. A resilient distributed control method based on communication was developed to restore voltage and frequency under fixed time delay communication [155]. In [103], a discrete-time distributed communication strategy governs power flow and voltage/frequency restoration during plug-and-play device operations. Continuous information sharing across dispersed DERs is inefficient and might cause congestion [102]. The data exchange between controllers and IEDs causes frequent packet losses and increasing delays [91].

Time-triggered and event-triggered communication techniques may minimize communication traffic. In addition, because event-triggered controls need minor control updating, they demand less data transfer and computation power [92]. It also supports additional configurations without requiring a new system architecture [90]. For example, main local voltage control [199], frequency control [36, 100, 106], and optimal power flow control [54] are all event-based control methods. However, controlling additional DERs increases latency and jitter [188]. Problems emerge while servicing many control loops. Lowering one control loop's latency might influence another's control signal quality. The time-variant controller can rectify jitter. However, it complicates the method and incorporates system functions like as time stamps [98].

Time-triggered approaches, on the other hand, enhance predictability and performance [187]. These have higher latency than event-triggered designs but no jitter if all contributing nodes are aligned to a global time [213]. During periodic services, the time-triggered transmission is controlled by predetermined time frames using

time division multiple access. A control network's offline job scheduling may use time-triggered communication. In this work a time-triggered simplex communication is used to convey decision signals from the scheduler to the device-level robust controller.

Thus, it is essential, practical, and more realistic to investigate the distributed secondary control issue for autonomous microgrids while considering both noise and constrained bandwidth [61]. However, due to the limited capacity of actual network transmission, communication delays are unavoidable, resulting in time-synchronization-loss of energy factors, which affects dynamic response or even causes the microgrid management system to become unstable [202]. Regretfully, limited progress has been made for distributed energy sharing control for enormous distributed generators (e.g., PVs and ESSs) in a microgrid while concurrently addressing communication time delays and constrained bandwidth [54, 169].

Real-time and accurate information exchange among various components of the smart grid is needed for efficient grid operations. The best candidate to implement such an information sharing mechanism would be the wireless sensor and actuator networks (WSANs) [14]. These networks incorporate a large number of low-power, low-cost rapidly deployable sensing and actuating nodes. These networks join several low-power, easily deployable sensing, and actuating hubs. The IEDs (i.e., actuators, sensors ) usually communicating with the controlling hub through relays and switches. The task of sensors is to monitor and collect nodes' data in the form of power frequency, voltages, currents, etc,. Whereas, the actuators perform power controlling tasks at power lines by switching the loads on/off [10].

### 2.4.1 Microgrid Communication Layers and Technologies

A further insight to the applicable communication networks in the power system network is discussed as: The wide area network (WAN) is used for large electrical grids and long-distance data transmission [176, 179]. In addition, this high-bandwidth network supports bidirectional connection for monitoring and automation. The field area network (FAN) links the client and the secondary power substation The near-me area network (NAN) is a collection of smaller power networks that assist the home energy management systems [34]. Furthermore, these power networks comprise multiple home area power networks (HAPN) from various dwellings or flats. It maintains communication inside each building, gathers renewable energy source generation data within a building, collects data on each apartment's usage, and controls intelligent equipment within each apartment [31]. This is frequently accomplished through home energy management systems (HEMS). HEMS include graphical user interfaces for tracking usage and SCADA systems for data storage. Similarly, industrial area networks (IAN) create a communication link between industrial equipment utilized for automation. The lowest stages of the communication architecture are the IAN, and HAPN. Wi-Fi, HomePlug, DSL, ZigBee, ZigBee Smart Energy, and other protocols are commonly utilized in these systems [16]. The ZigBee is based on the IEEE 802.15.4 standard. However, to accommodate the most widely used protocol, TCP/IP, the IP protocol is included in their network layer. A NAN might be used for communications inside a microgrid at a higher level. A FAN may be located at the distribution level, in charge of communications between the substations and the microgrid. These sectors are home to substation and automation standards like IEC 61850. Before each Nanogrid's consumption and production data is transferred

to the distribution system operator, each microgrid has a NAN with a central data hub in charge of collecting and storing data packets [26].

Energy management systems aim to optimize energy use by gathering power consumption and power generation data from various microgrids. The consumption data of houses and industries in each microgrid is shared through intelligent meters to the WAN [123]. A central controller will be present at the WAN, which might be the distribution system operator or any other operator transmitting parameters to the microgrid operator. Current communication drivers in these networks include 3G and 4G LTE, cellular communications, WiMAX or optical fiber, and satellite [47]. For various reasons, several standards are available and applicable to microgrids operations. IEEE 1547 specifies the criteria and standards for connecting dispersed energy resources [174]. Figure 2.11 gives a glimpse over multiple techniques being used as communication standards in microgrid.

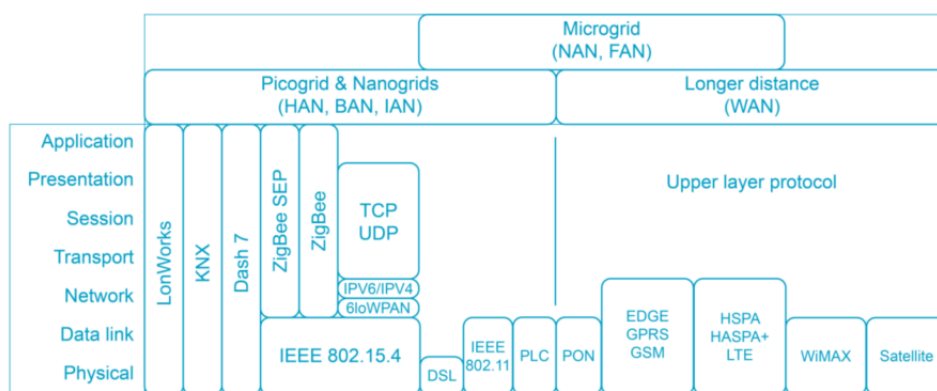


**Figure 2.11:** Microgrid communication Standards and Technologies [47].

## 2.5 Optimal Design and Operations Strategies for Microgrids

This section introduces microgrid forecasting methods and optimization strategies for centralized control [123]. Load consumption curves change based on the day, workday, weekend, or holiday. They may also change by season. Similarly, the generation curves of renewable energy sources, which are highly dependent on meteorological conditions, show much higher daily variations [128]. Therefore, microgrids need accurate forecasting of electricity usage and generation. Proper forecasting improves the performance of a microgrid. However, uncertainty in demand and supply causes forecasting mistakes. The power reserve from the generators often compensates for this [126].

### 2.5.1 Importance of Forecasting in Microgrids

Forecasting approaches are characterized as quantitative or qualitative. When historical data for the units is available, quantitative approaches are used. For example, a numerical time series can be created from data. The process's future behavior is comparable to how it was observed in the past in quantitative methodologies. This

assumption, however, does not hold when significant changes occur in affecting variables such as climate, customer behavior, and electrical market structures. Qualitative approaches are applied when there is little or no quantitative data available. These strategies rely heavily on professional knowledge.

In [12], the management system of the suggested model uses hidden Markov modeling to determine occupant energy use using aggregated power load data and pre-built models. It captures the differences in energy consumption behaviors as part of everyday life. After training the data, the model identified the best fit model and approximated the occupant's current condition. Similarly, [201] introduces an optimum control-based EMS for various storage capacity. It has reduced compensation costs for intra-switching storage and transmission losses. Meanwhile, it kept an eye on each storage component's charge level to maintain supply-demand balance.

### 2.5.2 Stochastic Optimization Strategies

The proposed energy management system attempted to lower energy expenditures by intelligently coordinating household devices and boosting the usage of alternative energy sources [95]. Most energy optimization problems aim to reduce costs, as addressed in [8, 76, 85, 86]. While most research looked at the connection between power rates and customer dissatisfaction [86, 149, 159], others investigated the link between lowering costs and peak-to-average (PAR) power consumption ratio [85]. Getting peaks at off-peak periods is a major drawback when using day-ahead determined dynamic pricing signals [79].

To avoid a large portion of customer load requests favoring the lowest energy price slots, greater extra costs are imposed when the load needs of the user surpass the proposed power limit [79]. Because it may result in a loss of power network diversity and system failure. To avoid fresh power peaks, day-ahead dynamic pricing with additive peak power limiting limits are established. A bi-level model of an energy management system is investigated in [212] to re-examine the PV utilization strategy and ESD capacity estimate to regulate peak power in a smart home.

In microgrids, several optimization strategies may be used. Some of these approaches, such as linear and nonlinear programming, mixed integer programming, stochastic programming, and dynamic programming, have been applied in microgrids to solve multi-objective functions that balance low operating costs and good energy services. The primary goal function of such multi-objective optimization problems is based on a mix of environmental costs such as carbon emissions, capital and operating expenses, power storage expenses such as battery and hydrogen fuel storage, and other costs. Energy or load management is a term used to describe the use of demand-side strategies to electrical loads [205]. Several energy management designs have been presented. One of them is the home energy management system (HEMS) [86, 212]. HEMS incorporates smart energy supply entities (ESEs), such as diesel generator, photovoltaic, etc., and several types of smart load devices (SLDs), such as power flexible and time flexible controlled loads, as well as external grid energy [210]. The ultimate benefit of HEMS is lower power costs for customers. This is only achievable by maximizing the use of inexpensive energy sources, using ESDs, activating low-cost electrical equipment, and limiting network power losses.

To reduce user discomfort when applying DSM techniques is a key job [76, 85, 101, 205]. Ran et al. [160] introduces mathematical models for RES, ESDs, and SLDs, and schedules these entities depending on user happiness. Liu et al. [101]

develops various goals to create a cost-effective residential operation schedule for a smart house while considering inhabitants' desired comfort alternatives. Furthermore, consumers want greater comfort and pleasure by adding a response fatigue index [170], particularly for heat discomfort [198].

The HAPN uses complex optimization methods to operate efficiently. Diverse optimization methods have distinct computational complexity. Among the most often used techniques is MILP, which combines linear models and constraints with a linear objective function [8, 20, 42, 74, 81, 101, 140, 147, 153, 208]. Others focused on heuristic algorithms [76, 85], such as population-based particle swarm optimization (PSO) [79, 160, 161] and genetic algorithms (GA) [86, 95, 212]. Aside from that, some researchers employed stochastic programming [12, 170], while others focused on decision tree algorithms [24, 109]. In [107], a stochastic network calculus theory is used to answer long-term supply and demand uncertainties while meeting energy balancing requirements. Real-time binary backtracking search algorithm (BBSA) is used to optimize home device scheduling to minimize energy consumption without compromising comfort [11]. Xie et al. [198] and Yang et al. [203] discussed model predictive control to deal with unpredictable generation and demand. Moreover, if the constraints or the objective function are nonlinear equations, a nonlinear method, MINLP, may be used [133]. Another real-time SLD operation option ignores uncertainty and uses the Lyapunov optimization method [46, 96, 205].

High load demands, particularly during peak hours, raise power bills. Low generation for plentiful Photovoltaic (PV) electricity results in expensive energy operations [109]. The well-known demand-side management (DSM) or demand response (DR) techniques may be used to solve these issues. DSM can maximize energy output and consumption, lowering power costs and  $CO_2$  emissions [20]. Efficient DR scheduling algorithms are required to enable users to shift loads intelligently during low-cost operating times of the day source [170].

There are also countless alternative solutions to the difficulties listed above. Among them include electric grid, PV, diesel engine generator (DE), and energy storage devices (ESDs) [109, 208]. PV is the cheapest method of power generation, however, it is unreliable [153]. Javaid et al. and Yang et al. [79, 203] says that it is dependent on the sun's irradiation, which is only accessible during the day. Variable PV energy may be compensated in several ways. For example, the PV output could be smoothed using ESDs [95, 107], or the grid energy could be used, or the DE power might be used [24, 81]. If PV power is plentiful, it may be restricted to maintain power flow balance and voltage levels [185]. However, thermal generators and pumped hydro stations may be used extensively to address power generation uncertainties [8, 74]. However, there is a cost trade-off owing to thermal generator starting and shutdown activities [208].

The third approach is to utilize controlled flexible smart load devices (SLDs), which may be operated based on energy availability [46]. There are two kinds of SLDs: power flexible and time flexible (time shiftable and delay-tolerant devices [79, 101, 133]). Some studies exclusively consider HVAC loads as flexible loads [46, 198]. Unlikely, [147] defined electric cars as a new sort of household electricity load. The aggregated power load is a flexible, controllable load, and most researchers distinguish between time shiftable and non-shiftable power loads [20, 76, 85, 160, 205].

Load management may also help shift load, reducing the EV fleet's impact on



the grid [141]. General demand-side management (DSM) or demand response (DR) strategies might be utilized to address smart grid features. As a result, DSM may reduce electricity costs, and CO<sub>2</sub> emissions [20]. Other research has built probabilistic models that may better capture the charging load profile than deterministic charging patterns [166]. Due to minimal energy price slots, Javaid et al. [79] imposed higher extra costs when customer load needs exceeding the proposed power limit. To regulate the peak power in an intelligent home, Zhou et al. [212].

The best flexible load is electric vehicle storage (EVS), which offers a wide range of dynamic charging power [185]. Ahmadi et al. and Dong et al. [8, 42] examine the long-term consequences of varied short-term operations and battery storage component life. Aggregated battery storage systems that operate as energy suppliers or dissipaters reduce ramping while balancing demand with low-cost energy supply. Moreover, [109, 153, 170] offers a pseudo cost function for battery storage degradation, whereas [24, 208] examines storage loss cost.

Battery operating restrictions and energy trading needs also apply to storage degradation and battery inefficiency during operation [96]. To prolong the battery's life, maintain the operating cycle in its safe zone. Because energy prices and user load needs change, the system's worth capacity and future power costs are dependent on the system's condition and operating period [205]. The optimal (dis)charging actions are detected by the predicted Newton approach [214]. Moreover, [67] presents a generalized battery model to depict the flexibility of building energy demand and storage capacity.

In following chapters this book will describe various model predictive iEMS approaches for optimizing energy flow inside HAPN. These concepts of power flow from grid to a vehicle (G2V), PV to a vehicle (PV2V), and vehicle to home (V2H) are believed to be a modernistic alternative to traditional static battery system [17, 97]. As a result, storing energy decreases total power costs, flattens the load curve, and minimizes CO<sub>2</sub> emissions. The moving sliding-window strategy is used to schedule the energy supply entities (ESEs) regularly based on real-time information. Scheduling optimization considers EV (dis)charging phenomena to improve overall operational benefits. The acquired scheduling signals are also supplied to the device level local control for further operations.

A predictive control-based algorithm illustrated in [38] that deals with the forecasting errors of load demands. The provision of real-time ancillary services to the utility grid was demonstrated by integrating vehicle-to-grid technology in [27]. While [83] proposed an energy management technique that designed the sub-problem formulation to introduce different time-slots for appliance scheduling and reduced the load fluctuations to guarantee stability. Moreover, [206] proposed a local control for a house that iteratively interacted with the central control unit and received the information of the planned outage, solving a social warfare optimization problem.

Wang et al. and Minhas et al. [116, 190] created a two-layered power management system, where the top layer depicts the stochastic nature of charging places and time utilizing traffic survey data. The second layer examines the impact of EV penetration on the distribution system's dependability using Monte Carlo simulation [30]. Some research, citing [145, 207], employ time series to assess the effect of EVs in deterministic or stochastic settings, modeling multiple charging scenarios that include start time, residual SOC, and final SOC. These programs were used to regulate the charging and discharging power of the storage batteries [172]. Minhas

et al. [114] uses a multi-objective approach to reduce the cost of EV charging and discharging while also addressing the user's preferences. To improve the flexibility of scheduling algorithms, Abdalla et al. and Trinh et al. used RESs-integrated iEMS [4, 182] adopting the concept of moving sliding window receding horizon. A innovative machine learning-based energy management strategy for a hybrid electric bus is also introduced by Wu et al. [195].

To best of our knowledge, there are just a few HAPN-based studies, and many of the significant research concerns at the microgrid level are identified previously. These studies also did not address optimum cost reduction and energy sharing problems together in both AC and DC sub-grids. Furthermore intensive component based modelling is missing in the previous literature which has a huge impact in decision making for optimal energy solutions. However, it is a great challenge integrating bottom up approach in designing a microgrid with various energy components. Most publications treated grid power as a single entity. However, this study provides a distributed concept of two-staged scheduling and control phenomenon that reduces energy cost and power losses during power distribution in AC/DC home area power network. This thesis carefully investigated the aforementioned constraints in the literature review in order to establish improved operation and design approaches for grid-connected microgrids while taking battery longevity and the grid outage challenge into account.

## 2.6 Conclusion

This chapter provides a detailed overview of the components of the power grid. It describes the evolution process of the intelligent power networks in the context of smart grids. It gives an overview on the history of the power networks revealing how grids are evolving from traditional systems to intelligent smart grids. It also provides information on various grid topologies and setups. This chapter also illustrates a brief literature survey about control and optimization strategies integrating microgrid's primary components and control structures, and discusses a communication network essential for making the microgrid smarter. Finally, several design and operational methodologies are explored in the current academic studies.

## 3 Components Based System Modeling

This chapter presents the mathematical modeling of several innovative home components. Among the components are the energy supply entities (ESEs) such as; photovoltaic (PV) arrays, diesel generators, microgrid structures, and energy storage systems (ESSs). It also includes home energy appliances such as; traditional base load demands and smart load demands (SLDs). Furthermore, energy components, operational costs, and an energy management system are also a part of next-generation perfect power systems. In this chapter, the suggested mathematical modeling of each component provides a complete analysis of the systems' characteristics, performance, and dynamic behavior. It illustrates a predictive model of PV generation, a universal linear diesel generator model, a dynamical working and cost model for the storage batteries, and an approach that accounts for the stochastic characteristics of the individual power appliances' start times and working cycles. Besides, it shows a glimpse of an optimization model that could offer insight into the decision makers' energy policy challenges.

### 3.1 Modelling Energy Supply Entities (ESEs)

#### 3.1.1 Solar Energy

The sun is the primary energy source, and the World has enormous potential for harnessing its energy through solar radiation. The availability of desirable solar radiations on the surface is determined by various climatic factors such as sky clearness index, sky brightness pattern, and reflected and diffuse radiations. These are used to create solar generation models for predicting system capacity, planning operations, and reliably dispatching solar energy. However, these parameters exhibit highly nonlinear features because of the varying atmospheric conditions. These can lead to variations in utility grid power, voltage instability, and frequency deviation at the point of common connection, which is a significant issue with power quality [58]. In order to operate a standalone microgrid, PV generation must be projected. The size, location, and installation angle of PV plants are essential. As a result, its power generation significantly depends on atmospheric conditions, especially solar radiation.

The sun's position and the local meteorological conditions determine the amount and quality of solar energy received at a location. The sun's location is expressed in solar height and azimuth, which may be calculated using solar geometry, as shown in Figure 3.1. Although climatic conditions are challenging to forecast, they may be classified into several sky types. An example of a sky condition is shown in Figure 3.2, where daily sunshine is influenced by the factor of sunny, partly cloudy and cloudy for the whole year. It shows the summer season is less cloudy and more sunny as compared to the winters.

This book emphasizes factors characterizing both the radiation and daylight climate, which are presented in instances with their definition using measured data acquired and is illustrated in Figure 3.3. Data were collected from records of frequent

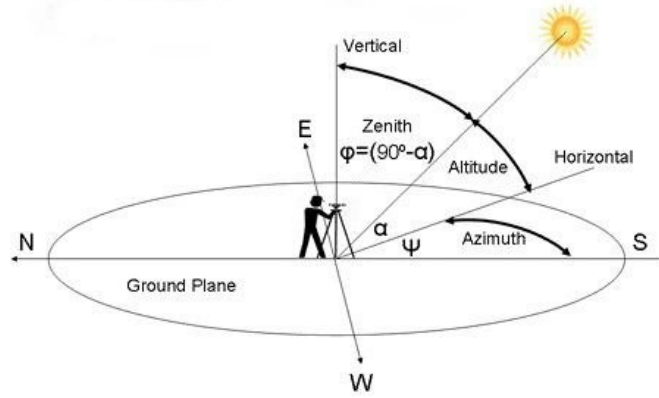


**Figure 3.1:** The solar height and azimuth [25].

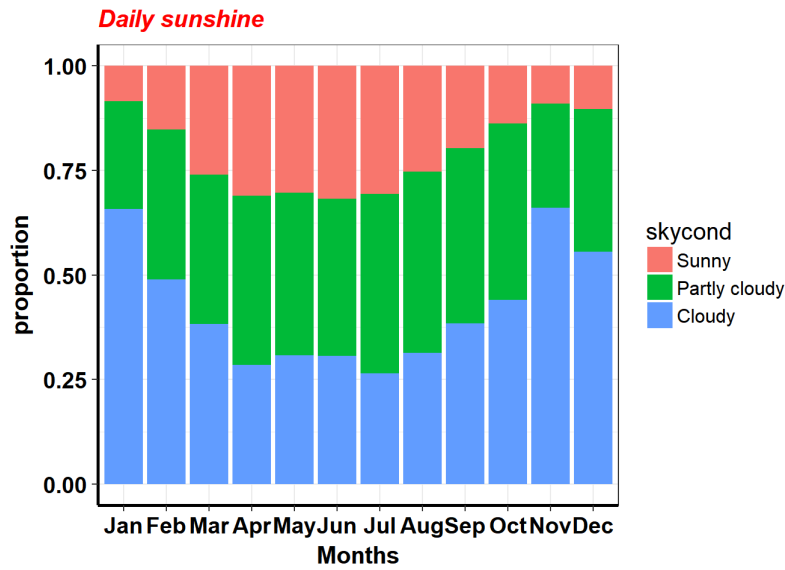


**Figure 3.2:** Sky conditions.

long-term measurements of the most significant parameters taken at 5-min intervals by the Metronome software station in Saarbrücken, Germany ( $49.217^\circ N$  and  $7.117^\circ E$ ). Ground-level solar irradiation is closely related to PV power generation. Consequently, predicting solar irradiance serves as the fundamental principle for forecasting solar energy generation. Predicting global horizontal irradiance (GHI), the total sum of irradiance descending on an area parallel to the Earth's surface, is an important stage in most solar power prediction systems. Cumulative solar irradiance  $G_T$  described in Equation 3.1 is defined as the sum of diffused  $G_D(t, \beta)$ , reflected  $G_R(t, \beta)$ , and direct beam  $G_B(t, \beta)$  solar irradiance reaching the solar cells, and is illustrated in Figure 3.4.

$$G_T(t) = G_B(t, \beta) + G_D(t, \beta) + G_R(t, \beta), \quad (3.1)$$

where  $\beta$  is the pitching angle of the solar panel. The orientation of a photovoltaic (PV) module at an angled slope is intended to increase its overall yearly energy output. As discussed in this book, the isotropic model is employed to assess the amount of solar radiation received by a PV module that is positioned at an inclination [19]. Beam irradiance is the direct irradiance coming from Sun without dispersing, ab-

Location information ×

**General information**

Name: Saarbruecken

Type: Weather station

Coordinates: 49.217 °N Lat, 7.117 °E Lon, WGS84


WMO Number: 107080

Altitude: 325 m a.s.l.

Timezone: 1 UTC

Time reference: -30 min

Situation: Open situation



**Parameters measured at location**

|                           |                            |
|---------------------------|----------------------------|
| Measurements first period | Measurements second period |
| Radiation: 1981-1990      | Radiation: 1996-2015       |
| Temperature: 1973-1992    | Temperature: 2000-2009     |
| Ta Gh FF Td               | Ta Gh FF Td                |
| RR Rd Sd DD               | RR                         |

Source for radiation data: Synop

**Figure 3.3:** Weather measuring location [1] .

sorbing, or scattering. It is possible to compute this irradiance using observed solar irradiation on a horizontal surface by  $G_B(t, \beta) = R_B \overline{G}_B(t)$ . Where  $\overline{G}_B(t)$  is the beam irradiance determined at ground level on a horizontal surface, and  $R_B$  is the ratio of beam irradiance occurring on a heliostat to that received on a horizontal surface. The importance of beam irradiances is shown in Figure 3.5a in the form of a correlation graph between PV production and the  $G_B$ . Further, the distribution of  $G_B$  is shown in Figure 3.5b, showing that it is right skewed and the mean of the distribution is around 130.

Similarly, diffuse solar irradiance does not directly reach a Solar panel but is diffused due to clouds or dust in the air on its way from the sun to the Solar panel. On a slanted surface, diffuse irradiance may be represented as  $G_D(t, \beta) = R_D \overline{D}_D(t)$ . Where  $R_D$  is the ratio of diffuse irradiance occurring on a heliostat to that reaching

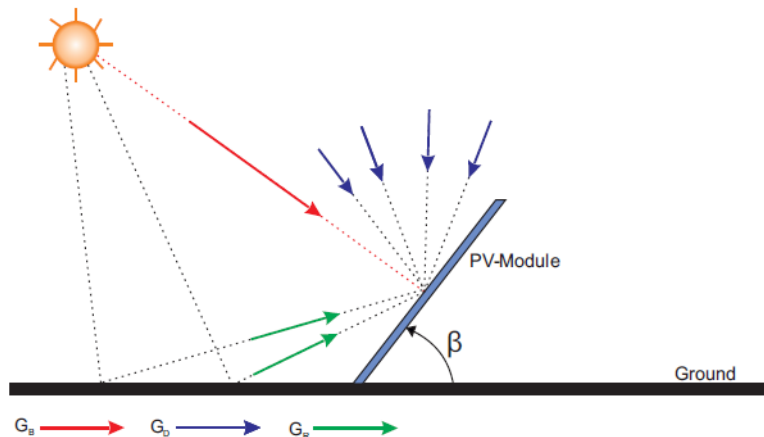


**Figure 3.4:** Solar radiation components falling on a slanted PV-module [19].

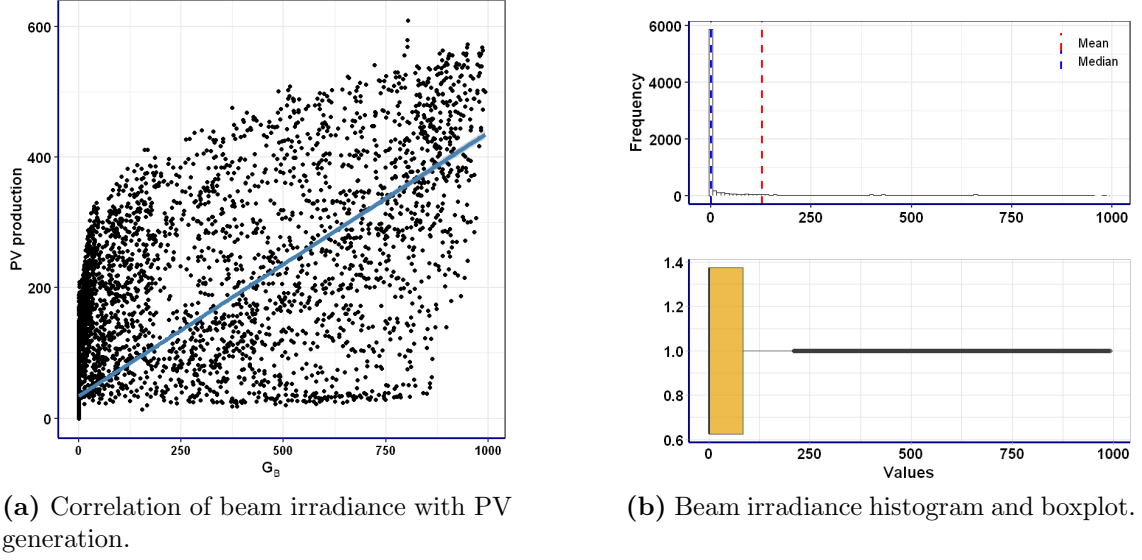


**Figure 3.5:** Correlations and histograms of solar beam irradiation patterns.

on a horizontal plane, and  $\overline{G_D}(t)$  is the diffuse irradiance measured at ground level on a horizontal surface. The significance of diffuse irradiance is shown in Figure 3.6a in the form of a correlation graph between PV production and the  $G_D$ . Further, the distribution of  $G_D$  is shown in Figure 3.6b, showing that it is right skewed and the mean of the distribution is around 130.

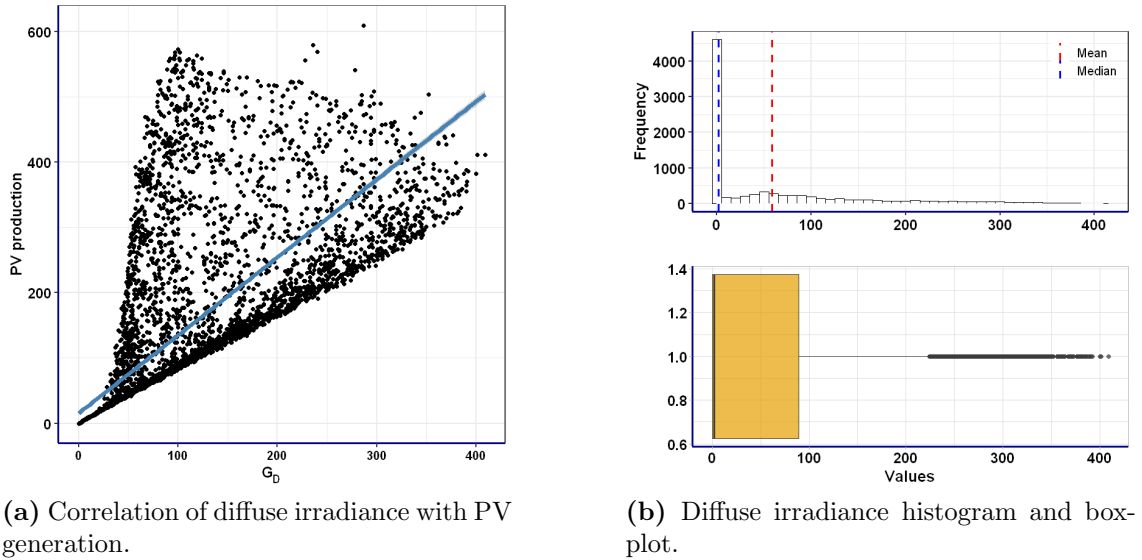
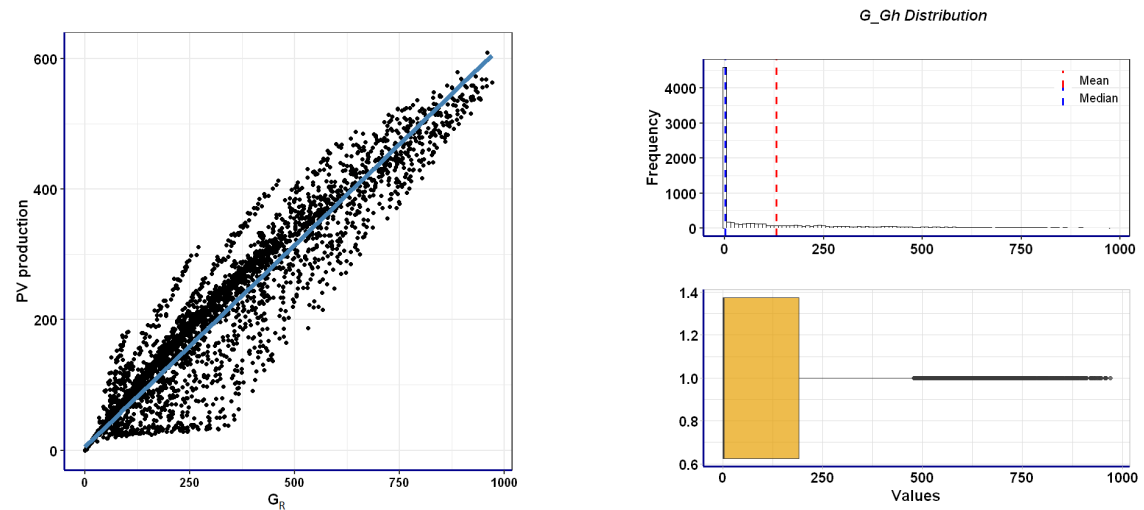


**Figure 3.6:** Correlations and histograms of solar diffuse irradiation patterns.

In addition, reflected irradiance is mirrored by the earth and projected back to the Solar panel, which may be calculated as  $G_R(t, \beta) = \overline{G}(t)\rho\frac{1-\cos\beta}{2}$ . The value of  $\rho$  represents the fraction of diffusely reflected light from the ground, and  $\overline{G_R}(t)$  represents the measured global sun irradiance on a horizontal plane at the ground level. The significance of diffuse irradiance is shown in Figure 3.7a in the form of a correlation graph between PV production and the  $G_R$ . Further, the distribution

of  $G_R$  is shown in Figure 3.7b, showing that it is right skewed and the mean of the distribution is around 130.



(a) Correlation of reflected irradiance with PV generation.

(b) Reflected irradiance histogram and boxplot.

**Figure 3.7:** Correlations and histograms of solar reflected irradiance patterns.

To achieve the performance, the solar cell must be exposed to light. Various weather agencies provide global radiation statistics. These data must be used to compute the incidence of radiation on the slanted solar module surface. The incidence angle may be calculated using the Sun’s location, engine tilt, and orientation. The Sun’s position is determined by the current date, time, and geographical location of the PV system.

### 3.1.2 PV Panel Analytical Model

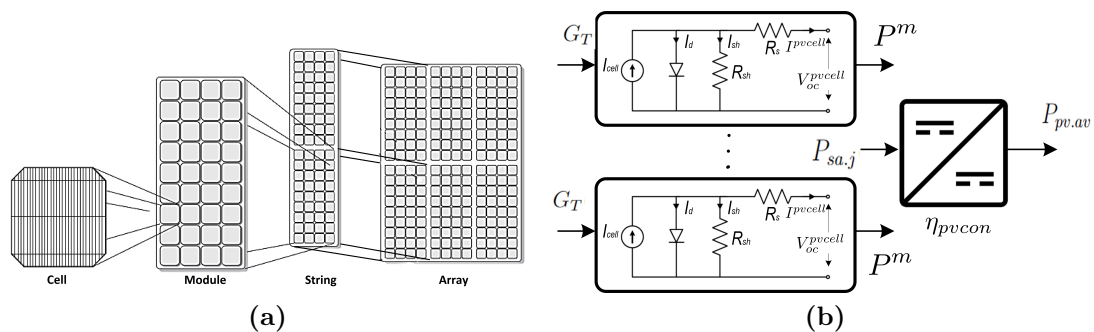


**Figure 3.8:** (a) PV array structure. (b) PV schematic model.

In the proposed HAPN model, a photovoltaic array, as seen in Figure 3.8a, is built on the rooftop, serving as a low-cost and environmentally friendly source of electricity. The available output power of a photovoltaic array ( $P_{pv.av}(t)$ ) is the total power generated by all photovoltaic subarrays  $j \in [1, 2, \dots, J]$  mounted on the roof and the distribution of the obtained PV power on daily, hourly and monthly basis is illustrated in Figure 3.9[66];

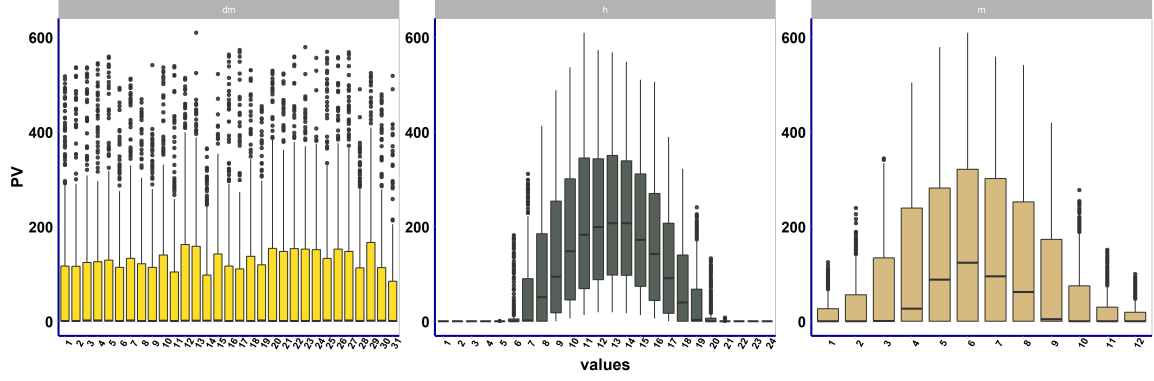


**Figure 3.9:** PV distribution on daily, weekly, and monthly basis.

$$P_{pv.av}(t) = \eta_{pv.con} \sum_{j=1}^J P_{sa.j}(t), \quad \forall t \quad (3.2)$$

where  $\eta_{pv.con}$  denotes the efficiency of a DC-DC maximum power point tracking (MPPT) converter that is connected to the photovoltaic array. The power output of each subarray ( $P_{sa.j}(t)$ ) is computed using the power provided by each PV module ( $P_m(t)$ ), the number of modules ( $N_m$ ) installed in the subarray, and the electrical loss factor ( $F_{sa.j}$ ) associated with it [156].

$$P_{sa.j}(t) = (P_m(t)N_m)F_{sa.j}. \quad \forall t, j \quad (3.3)$$

While,  $F_{sa.j}$  is established on the loss percentage of arrays mismatch loss ( $L_{m.j}$ ) and dc wire loss ( $L_{dc.j}$ ).

$$F_{sa.j} = \left(1 - \frac{L_{m.j}}{100}\right) \left(1 - \frac{L_{dc.j}}{100}\right). \quad \forall j \quad (3.4)$$

Assume that each photovoltaic module produces the power  $P_m(t)$  at its maximum output ( $\bar{P}_m$ ), taking into account predicted solar irradiance ( $G_T(t)$ ) and ambient temperature ( $T_C(t)$ ).

$$P_m(t) = \bar{P}_m \frac{G_T(t)}{G_{STC}} (1 + \alpha (T_C(t) - 25^\circ C)). \quad \forall t \quad (3.5)$$

Where  $G_{STC}$  stands for standard solar irradiance factor and  $\alpha$  for temperature coefficient. Additionally,  $\bar{P}_m$  is reliant on a parameter called the fill factor ( $FF$ ), which is used to determine the maximum power output of a photovoltaic cell, as seen in Figure 3.8b.

$$\bar{P}_m = FF(t) \times V_{oc}^{pvcell} I_{sc}^{pvcell}. \quad (3.6)$$

The short-circuit current ( $I_{sc}^{pvcell}$ ) and open-circuit voltage ( $V_{oc}^{pvcell}$ ) of a photovoltaic cell are the maximum current and voltage, respectively and can be calculates as;

$$V_{oc}^{pvcell} = V_{oc,sc} + K_v (T_C(t) - 25^\circ C). \quad (3.7)$$

$$I_{sc}^{pvcell} = (I_{sc,sc} + K_i (T_C(t) - 25^\circ C)) \frac{G_T(t)}{G_{STC}}. \quad (3.8)$$



The thermal factors of the short circuit current and open circuit voltage of a photovoltaic (PV) module are represented by  $K_i$  and  $K_v$ , respectively. Additionally, the Fill Factor is a parameter that characterizes the relationship between the voltage and current at the highest power point and the open circuit voltage and current in a short circuit. The Fill Factor in Equation 3.9 represents the ratio of the maximum output power of a PV-cell to the product of the PV-open-circuit cell's voltage and short-circuit current. The fill factor is calculated as;

$$FF(t) = FF_0(t)(1 - r_s(t)). \quad (3.9)$$

where  $FF_0(t)$  is the standard nominal PV-cell fill factor, and it is provided by

$$FF_0(t) = \frac{v_{oc.stc}(t) - \ln(v_{oc}(t) + 0.72)}{v_{oc}(t) + 1}. \quad (3.10)$$

Additionally, the normalized series resistance,  $r_s(t)$ , and open-circuit voltage,  $v_{oc}(t)$ , of the PV cell are calculated as follows;

$$r_s(t) = R_s \frac{I_{sc}^{pvcell}(t)}{V_{oc}^{pvcell}(t)} \quad (3.11)$$

$$v_{oc}(t) = \frac{V_{oc}^{pvcell}(t)}{V_t(t)} \quad (3.12)$$

$$V_t(t) = \frac{n_d k_B T_{a.k}(t)}{e} \quad (3.13)$$

The magnitude of the photovoltaic cell's series resistance,  $R_s$ , is influenced by the material of the photovoltaic cell and can be altered by its operating conditions. Nevertheless, these effects might be insignificant or trivial. To calculate the value of  $R_s$ , the relevant information in the photovoltaic module's datasheet can be utilized. The fill factor indicates how closely the actual operating circumstances match the potential power of  $I_{sc}^{pvcell} V_{oc}^{pvcell}$ . However, a fill factor of one is not achievable.

In this study, a prediction model was employed to estimate the photovoltaic (PV) production on both daily and monthly scales. This was accomplished by utilizing standard PV panel parameters and utilizing historical solar irradiance data at the microgrid's location. The model employed linear models that consider various atmospheric and irradiance parameters to make its predictions. To fit the model, historical irradiance data is a requirement. Thus, this approach is particularly well-suited for remote microgrids that lack access to communication infrastructure or real-time weather data.

Various prediction algorithms have been analyzed, and eventually, the ensemble decision tree algorithm was considered best for the PV values. A comparison of daily measured and predicted PV power for any random day is shown in Figure 3.10a, and the error in the values can be assumed in Figure 3.10c, showing high errors during daytime when the irradiation is high. Similarly, the monthly comparison of PV values is shown in Figure 3.10b, and the error rates distribution is illustrated in Figure 3.10d.

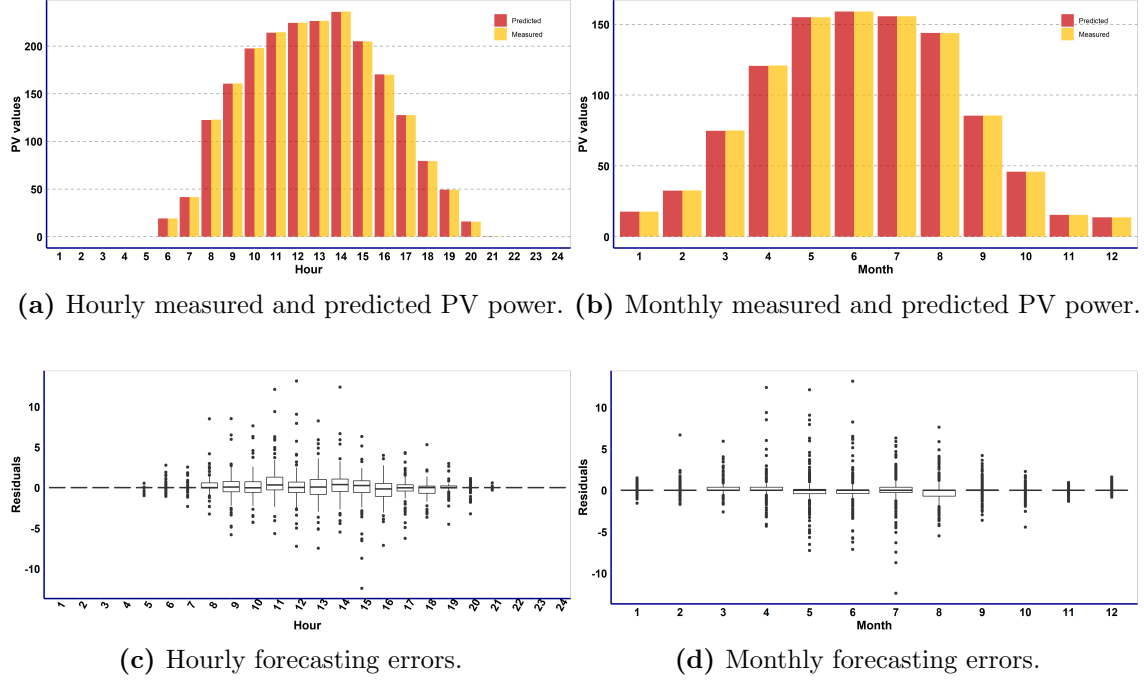


**Figure 3.10:** PV predicted values and forecasting error rates.

### 3.1.3 Grid Tie-line Model

In the context of microgrids, it is possible for them to function both in a grid-connected mode and an off-grid mode. When operating in an off-grid mode, the microgrid is more vulnerable to variations in energy generation and consumption demand. To maintain grid stability in this scenario, grid-forming components such as diesel generators and energy storage systems are necessary. On the other hand, when operating in a grid-connected mode, the microgrid can rely on the assistance of the primary grid, which acts as a grid-forming component, for frequency stability.

The microgrid's stability is not assured despite its link to the primary grid. It is due to grid blackouts or the primary grid load shedding schedule throughout the day when the grid does not have enough generation. This issue occurs in many nations because electricity cannot cover all connected loads to the primary grid [71, 115, 138]. The electricity distribution firms sometimes publicize the grid disconnection timing and duration ahead of time. In contrast, other times, it is uninformed and unplanned, posing a significant challenge to the microgrid operating phenomenon.

In this study the grid's available energy ( $P_{av.g}(t)$ ) can be defined as:

$$P_{g.av}(t) \leq x_{g.ac}(t)\bar{P}_{g.ac}, \quad \forall t \quad (3.14)$$

where

$$x_{g.ac}(t) = \begin{cases} 0, & \text{if grid is disconnected} \\ 1, & \text{otherwise} \end{cases}, \quad \forall t \quad (3.15)$$

In this scenario, the variable  $x_{g.ac}(t) \in 0/1$ , which is defined as a binary value, serves as an indicator of the state of the grid-tie power bus. If  $x_{g.ac}(t) = 1$ , it implies that the grid line is available and the flow of power from the grid is active. Conversely, if  $x_{g.ac}(t) = 0$ , the grid line is inaccessible, and the power flow from the grid is inactive.

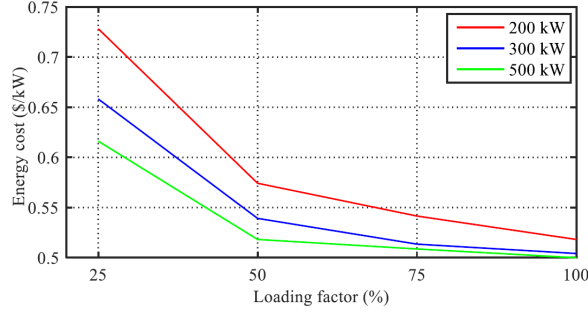


**Figure 3.11:** Diesel generator efficiency characteristics.

It is important to note that while the microgrid is in the grid-connected mode, the dispatched power ( $P_{g,disp}(t)$ ) from the main grid is limited by the capacity of the grid-tie line ( $P_{g,av}(t)$ ).

$$P_{g,disp}(t) \leq P_{g,av}(t), \quad \forall t \quad (3.16)$$

### 3.1.4 Diesel Generator Model

Although the prevalence of renewable energy sources (RES) has increased, the incorporation of traditional diesel generators (DGs) remains necessary in the system. This is due to the substantial uncertainty associated with the generation of RES, which is susceptible to abrupt fluctuations in meteorological conditions. Consequently, the energy yield from RES-based microgrids is limited by their unpredictable nature.

Despite worries that DGs operations are the most expensive and that DGs have significant operating constraints, such as ramp-up/down thresholds for their power production, it is necessary for the microgrid to have secure and reliable options. Consequently, the aggregated power output dispatched from the group of diesel generators ( $P_{de,disp}(t)$ ) with  $m \in \{1, 2, \dots, M\}$  generating units attached to the grid is expressed as;

$$P_{de,disp}(t) = \sum_1^M \eta_{m,dg}(t) P_{m,de,ac}(t), \quad \forall t \quad (3.17)$$

The electrical efficiency of DG ( $\eta_{m,dg}(t)$ ) is determined by the diesel fuel's characteristics and is proportional to the output power of generator [70, 134], and can be seen in figure 3.11.

### DG Operational Cost

The major aspects to consider while looking for the appropriate dispatch method for a microgrid with diesel generators are utilization and fuel economy characteristics. The fuel usage ratios are often indicated on the machine data sheet. The significant running expense of the diesel generator is the engine's fuel utilization for the alternator's active-reactive power production [70]. Furthermore, the startup and shutdown expenses of each DG can also be included in the overall cost formulation associated with the DGs [157]. The cost of power generation ( $C_{m,DE}(t)$ ) for  $m$  diesel generator (DG) units is computed based on the fuel price ( $\sigma^f$ ) which is \$/l, and the

total amount of fuel used ( $F_{m,de.ac}(t)$ ) by  $m$  generators at any time  $t$  and is given as;

$$C_{m,DE}(t) = \sum_1^M (\sigma^f F_{m,de.ac}(t)), \quad \forall t \quad (3.18)$$

where,  $C_{m,DE}(t)$  is the cost of power produced by the  $m$  generator  $P_{m,de.ac}(t)$  at any time  $t$ . Furthermore, the amount of fuel required ( $F_{m,de.ac}(t)$ ) to generate specific amount of power at particular time  $t$  is illustrated as;

$$F_{m,de.ac}(t) = a_{m,de.ac}x_{m,de.ac}(t) + b_{m,de.ac}P_{m,de.ac}(t)x_{m,de.ac}(t) + c_{m,de.ac}P_{m,de.ac}^2(t)x_{m,de.ac}(t). \quad \forall t \quad (3.19)$$

where,  $a_{m,de.ac}$ ,  $b_{m,de.ac}$ , and  $c_{m,de.ac}$  are the price variables of generator unit  $m$  at any time  $t$ .  $x_{m,de.ac}(t)$  is the on/off status of the  $m^{th}$  DG. The fuel cost can be simply linearized by dropping the quadratic term in Equation such that;

$$F_{m,de.ac}(t) = a_{m,de.ac}x_{m,de.ac}(t) + b_{m,de.ac}P_{m,de.ac}(t)x_{m,de.ac}(t). \quad \forall t \quad (3.20)$$

The manufacturer's data sheet may calculate the fuel curve coefficients. Barley et al. [29, 70] offered generic values of  $a_{m,de.ac} = 0.246$  L/kWh and  $b_{m,de.ac} = 0.08415$  L/kWh. Diesel generator manufacturers suggest using generators at or above 30% of their rated capacity. Operating a diesel generator at a reduced output power level can result in decreased efficiency and may increase the frequency of required maintenance due to adverse impacts on the diesel engine [134].

In addition, there are other costs exits which reflects the cold start operational cost  $C_{m,DE}^{su}(t)$  and the shut down operational cost  $C_{m,DE}^{sd}(t)$  of the DG. In this analysis, these costs are modeled in a very simplified way just by using an indicator that when the generator starts or stops and are modelled as [136, 167]; .

$$C_{m,DE}^{su}(t) = \sigma^{su}z_{m,de}(t), \quad \forall m, t \quad (3.21)$$

$$C_{m,DE}^{sd}(t) = \sigma^{sd}v_{m,de}(t), \quad \forall m, t \quad (3.22)$$

while the binary variables  $z_{m,de}(t)$  and  $v_{m,de}(t)$  represent the start-up and shut-down conditions, respectively, of the  $m^{th}$  diesel generator. The start-up indicator is working under the following constraint:

$$x_{m,de.ac}(t) - x_{m,de.ac}(t-1) - z_{m,de}(t) \leq 0, \quad \forall m, t \quad (3.23)$$

whereas the shut-down indicator is activated using following strategy;

$$-x_{m,de.ac}(t) + x_{m,de.ac}(t-1) - v_{m,de}(t) \leq 0, \quad \forall m, t \quad (3.24)$$

### DG Operation Constraints

Lowering the power output of the DG harms the performance of the Diesel engine: poor combustor pressure, cold temperatures, activation problems, poor burns, carbon formation, and cylindrical agglomeration of unburned fuel. As a result, the maximum and lower limitations for gasoline engine power density may be calculated as follows:

$$\underline{P}_{m,de.ac} \leq P_{m,de.ac}(t)x_{m,de.ac}(t) \leq \overline{P}_{m,de.ac}, \quad \forall m, t \quad (3.25)$$

where,  $x_{m,de.ac}(t) = (0/1)$  is the binary on-off status of an individual diesel generator  $m$ .  $\underline{P}_{m,de.ac}$  and  $\overline{P}_{m,de.ac}$  are the minimum and maximum bounds of the power,

respectively. In this work minimum DG power is maintained to 30% of the generator rated output power [136].

Repeated starts and pauses of the DGs wear down the diesel generator. As a result, restricting the generator's minimum up and down duration helps to save maintenance expenses. The following are examples of minimum up and minimum down time constraints:

$$\begin{aligned} z_{m,de}(t) - \sum_{\hat{t}=t}^{t+\pi_{m,de}-1} \left( \frac{x_{m,de,ac}(\hat{t})}{|\hat{t}|} \right) &\leq 0, \quad \text{if } t \leq T - \pi_{m,de} \quad \forall m \\ z_{m,de}(t) - \sum_{\hat{t}=t}^T \left( \frac{x_{m,de,ac}(\hat{t})}{|\hat{t}|} \right) &\leq 0, \quad \text{if } t > T - \pi_{m,de} \quad \forall m \end{aligned} \quad (3.26)$$

Where  $\pi_{m,de}$  represents the minimum time the DG must be operational and  $z_{m,de}(t)$  is a binary status variable indicating the start-up status of generator  $m$  at time  $t$ .

Similarly, the DGs off-time constraint is stated as:

$$\begin{aligned} z_{m,de}(t) + \sum_{\hat{t}=1}^{t-1} \left( \frac{x_{m,de,ac}(\hat{t})}{|\hat{t}|} \right) - 1 &\leq 0, \quad \text{if } t \leq \sigma_{m,de} \quad \forall m \\ z_{m,de}(t) + \sum_{\hat{t}=t-\sigma_{m,de}}^{t-1} \left( \frac{v_{m,de}(\hat{t})}{|\hat{t}|} \right) - 1 &\leq 0, \quad \text{if } t > \sigma_{m,de} \quad \forall m \end{aligned} \quad (3.27)$$

The minimum down time for the diesel generator (DG) is represented by  $\sigma_{m,de}$  while  $v_{m,de}(t) = (0/1)$  denotes the shut-down status of the  $m^{th}$  generator.

Furthermore, the big generating units may also have ramp up and ramp down constraints during variations in load demands and generation requirements. This is due to the limitations in the mechanical operations of the DGs [144]. The ramp up ( $Ru_{m,de}(t)$ ) rate capacity of diesel generator  $m$  is given as:

$$\begin{aligned} P_{m,de,ac}(t) - P_{m,de,ac}(t-1) &\leq \\ Ru_{m,de}(t-1) + \max(\underline{P}_{m,de,ac} - & \\ Ru_{m,de}(t-1), 0)z_{m,de}(t), & \quad \forall m, t \end{aligned} \quad (3.28)$$

Similarly, the ramp down ( $Rd_{m,de}(t)$ ) rate capacity of diesel generator  $m$  is;

$$\begin{aligned} P_{m,de,ac}(t-1) - P_{m,de,ac}(t) &\leq \\ \max(\underline{P}_{m,de,ac}, Rd_{m,de}(t)) - & \\ \max(\underline{P}_{m,de,ac} - Rd_{m,de}(t-1), 0)x_{m,de,ac}(t). & \quad \forall m, t \end{aligned} \quad (3.29)$$

## 3.2 Modelling Energy Storage devices (ESDs)

The fundamental rationale for installing and using ESDs is to ensure that energy must be available at any time of the day. It is critical when renewable energy sources are not providing enough electricity or when the cost of delivering energy from the grid is too high. ESDs can serve as a load-matching solution in small systems along with solar modules. Alternatively, in solar systems with a load that requires a substantial initial current demand (such as an inductive load represented by a

motor), the storage can be employed to supply the initial start-up current. It may also be utilized for peak shifting in grid-connected systems, where the electricity generated by the sun is stored during day during excess energy generation and is used during peak hours at night. In this study, two forms of Energy Storage Devices (ESDs) are considered for utilization in Home Area Power Networks (HAPN). These ESDs are Home Battery Storage (HBS) and Electric Vehicle Storage (EVS) which are chemically similar and hence, have identical operating principles.

The voltage and capacity ratings of the battery are the first critical criteria to consider. Every battery has a specific voltage and capacity rating. The voltage level is formed by cells inside each battery. In this context, the nominal voltage at which the battery is designed to operate is referred to as the battery-rated voltage. The capacity of a battery refers to the quantity of charge it can supply at the rated voltage. The ampere-hour is the unit of measurement for battery capacity (Ah). The battery's energy capacity can also be expressed as a function of its voltage and capacity in amp-hours. The product of these two values results in the total energy capacity of the battery, expressed in watt-hours (Wh). However, the actual energy storage capacities of the battery might differ significantly from the nominal quoted capacity, as the battery capacity is heavily dependent on the battery's age and historical history, charging or discharging regimens, and temperature.

The storage's nominal capacity ( $E_b$ ) is defined as;

$$E_b = I_b \Delta t \times V_b^{oc}, \quad (3.30)$$

which is always limited to its maximum value  $\bar{E}_b$  such that; ( $E_b \leq \bar{E}_b$ ). Where,  $I_b$  and  $V_b^{oc}$  denotes short-circuit current and open-circuit voltage, respectively. However, due to storage internal losses, the available energy capacity ( $E_{av.b}$ ) that can be extracted from storage devices is often less than the  $E_b$ .

$$E_{av.b} \leq E_b. \quad (3.31)$$

The restriction on the maximum permissible discharge of the battery is known as the Depth of Discharge (DoD) and is calculated as follows;  $DoD = 1 - \frac{E_{av.b}}{E_b}$ , which is the counterpart to the state of charge (SoC) of the storage [214].

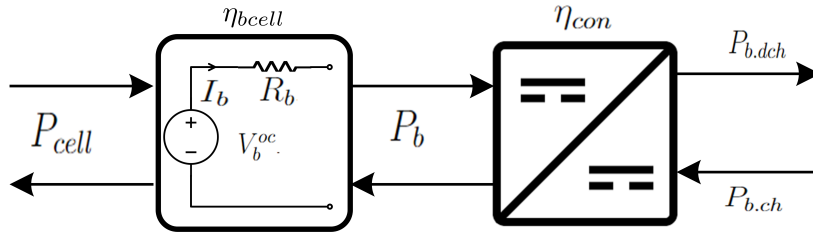


Figure 3.12: ESDs model.

Additionally, storage efficiency is a critical factor affecting battery capacity and is reliant on the internal resistance ( $R_b$ ) and the Battery power ( $P_b$ ) may be defined as follows [56];

$$P_b = V_b^{oc} I_b - R_b I_b^2. \quad (3.32)$$

The efficiency during discharging, when  $I_b \geq 0$  is;

$$\eta_{bcell}^{dch} = \frac{P_b}{P_{cell}} = \frac{V_b^{oc} I_b - R_b I_b^2}{V_b^{oc} I_b} = 1 - \frac{R_b I_b}{V_b^{oc}}, \quad (3.33)$$

where,  $P_{cell}$  represents the power input to the battery circuit.

**Remark 1.**  $\eta_{bcell}^{ch} \approx \eta_{bcell}^{dch} \approx \eta_{bcell} = 1 - \left| \frac{R_b I_b}{V_b^{oc}} \right|$ .

This efficiency is affected by the charging and discharging currents where increasing heat losses may result in reducing overall efficiency. Therefore, in order to determine the economically viable strategy for a storage system, it is imperative to formulate a model that precisely portrays the efficiency of the storage unit by evaluating both the battery and converter losses. Figure 3.12 illustrates a battery storage system's block diagram. It demonstrates two efficiency parameters, one for storage itself ( $\eta_b$ ) and the other one for the converter ( $\eta_{con}$ ) attached next to it.

The charging and discharging rates have an impact on the rated battery capacity. For example, when a battery is depleted rapidly (i.e., the discharge current is strong), the quantity of energy that can be taken from it is reduced, and the battery capacity is lowered. Alternatively, suppose the battery is drained slowly with a low current. In that case, more energy may be taken, and the battery capacity is increased. As a result, the charging/discharging rate should be included when measuring the battery capacity. A popular method of specifying battery capacity is to describe the capacity as a function of the time required to fully drain the battery (note that in practice, the battery often cannot be fully discharged).

The overall power loss associated with the battery and the converter is illustrated as [56];

$$P_{b.loss}(t) = \begin{cases} (\eta_b^{-1} \eta_{con}^{-1} - 1)P_{b.dch} = (\eta_{b.con}^{-1} - 1)P_{b.dch} \\ (\eta_b \eta_{con} - 1)P_{b.ch} = (\eta_{b.con} - 1)P_{b.ch} \\ P_{b.self}(t), \quad \text{if } P_{b.dch}(t) \mid P_{b.ch}(t) = 0. \end{cases} \quad (3.34)$$

where,  $P_{b.dch}$  is established when  $I_b \geq 0$ , and  $P_{b.ch}$  is established when  $I_b < 0$ . Lead acid batteries, on the other hand, often have coulombic efficiencies of 85% and energy efficiencies of 70% [115].

#### 3.2.1 Battery Dynamics

In any PV power generating infrastructure that includes storage devices especially batteries, these are a critical component of the overall installation, influencing the economics, maintenance requirements, reliability, and layout of the solar array significantly. Because of the tremendous effect of batteries in a stand-alone solar module, knowing the properties of batteries is critical in understanding the operation of PV technologies. The battery maintenance needs, battery longevity, available power, and efficiency are all key battery characteristics that determine solar system operation and performance. A perfect battery would be capable of charging and discharging indefinitely despite unpredictable discharging and charging cycles. Furthermore, it is efficient, has a higher power density, has less self-discharge, and is affordable. Such factors are determined not only by the battery's initial choice, yet also by its usage scenarios in the installed power network. For example, what are its charging and discharging rates and what is the operating temperatures.

While in smart power network the switching between intermediate devices is adverse and autonomous and so a storage is critical. It may operate as a buffer, dampening variations caused by fluctuating load demands and the intermittent nature of renewable producers. Additionally, it may be utilized as a backup source

during power outages, periods of low solar energy production or when the grid prices are too high.

The dynamic behavior of an energy storage system can be expressed as the variation in the energy levels, represented by  $E_b(\Delta t)$ , across different time intervals ( $\Delta t = t - (t-1)$ ). This behavior is influenced by various factors, such as the charging and discharging rates of the storage, the (dis)charging efficiency factor ( $\eta_{b.con}$ ), and the self-discharge of the battery ( $P_{b.self}(t)$ ).

$$E_b(\Delta t) = (\eta_{b.con}P_{b.ch}(t) - \eta_{b.con}^{-1}P_{b.dch}(t) - P_{b.self}(t) \times \Delta t). \quad \forall t \in \{2 \dots T\} \quad (3.35)$$

Whereas, the battery *SoC* is limited to its maximum  $\overline{SoC}$  and the minimum  $\underline{SoC}$  threshold:

$$\underline{SoC} \leq SoC(t) \leq \overline{SoC}. \quad \forall t \quad (3.36)$$

Furthermore, the minimum capacity ( $\underline{E}_b$ ) of the storage can be calculated as;

$$\underline{E}_b = (1 - \overline{DoD}_b)\overline{E}_b \quad (3.37)$$

where,  $\overline{E}_b$  and  $\overline{DoD}_b$  represents the maximum capacity and maximum depth of discharge of the storage, respectively. Furthermore,  $P_{b.ch}(t)$  and  $P_{b.dch}(t)$  are also bounded by the maximum and minimum values at any time  $t$ , such as;

$$\underline{P}_{b.ch} \leq P_{b.ch}(t) \leq \overline{P}_{b.ch}, \quad \forall t \quad (3.38)$$

$$\underline{P}_{b.dch} \leq P_{b.dch}(t) \leq \overline{P}_{b.dch}, \quad \forall t \quad (3.39)$$

### 3.2.2 Battery Operation and Degradation Cost Model

The usage of batteries in photovoltaic-based power systems is distinct from other conventional battery uses. The critical technological concerns for photovoltaic systems are the battery's extended endurance at virtually complete depletion circumstances. It is preferable to assess the health state of critical equipment credibly in applications where dependability is vital. The critical example of a RES-based autonomous telecommunications infrastructure is significant because it is employed to achieve equilibrium between the demand and the RES supply. Any deviation from power homeostasis is represented in its SoC, which undergoes repetitive charge/discharge operations of varying intensities.

Ongoing battery deterioration research includes the creation of mathematical aging models. In microgrids, minimizing battery deterioration has been an element of the economic optimization function of the cost minimization issue. To decrease the impact of deterioration, the operation of an energy storage system should be managed in order to maximize its utility at the lowest possible cost. In energy management applications, for example, where the discharged energy dictates the lifespan, the energy storage may be prohibited from discharging over a specific amount of its energy capacity. There are two forms of degradation: a loss in energy delivery capacity and a drop in energy storage capacity. Battery cyclic aging is accelerated by high temperatures, rapid charge and discharge rates, and large Depth of Discharge [43].

The deterioration of battery capacity is most heavily influenced by the interdependence of the following parameters; 1) the storage calendar lifespan, 2) maximum



number of charging/discharging cycles, 3) the battery's charging/discharging regime, 4) the battery's DoD over its life, 5) the average temperature of the battery during its lifespan, 6) the efficiency of the battery, 7) how deep cycling and protracted periods of low charge effect battery capacity and lifetime, 8) the original and continuing battery expenses, 9) and the battery's maintenance needs.

Frequent intense cycling reduces battery capacity by significantly lowering usable energy, as seen in Figure 3.13a. The greater the depth of the discharges, the greater the loss of cumulative capacity. Given the more significant capital outlay and shorter operational lifespan of the battery storage compared to the other energy entities in the power network, the cost associated with ESDs degradation is a crucial function value. As shown in Equation 3.40, the loss penalty ( $C_b$ ) per kWh of ESDs (dis)charge is determine by state of discharge ( $DoD_b$ ), storage investment cost ( $IC_b$ ), number of charging/discharging cycles  $N_{cycle.b}$  [208]. Figure 3.13b shows the degradation cost induced as a function of DoD. Whereas  $N_b$  is showing an exponential functions depends on  $DOD$ .

$$C_b = \frac{IC_b}{N_{cycle.b}(1 - DoD_b)\bar{E}_b} \quad (3.40)$$

$$N_{cycle.b} = \alpha \exp^{-\beta(DoD)} + \gamma \quad (3.41)$$

where  $C_b$  is the cost associated to the capacity loss and is a function of DoD, while  $N_{cycle.b}$  is the total number of cycles required to bring a battery to its total capacity loss when it is periodically discharged at a particular DoD.

The graphs shown in Figure 3.13a depicts a development of battery function as a function of cycle number and depth of discharge for a shallow-cycled lead acid battery. Even with DoD more than 50%, a deep-cycle lead acid battery should be able to retain a cycle life of more than 1,000 cycles. Furthermore, in Figure 3.13b the expected battery operating and maintaining cost is shown as a function of DoD. It shows the cost of storage increases with frequently deep discharges.

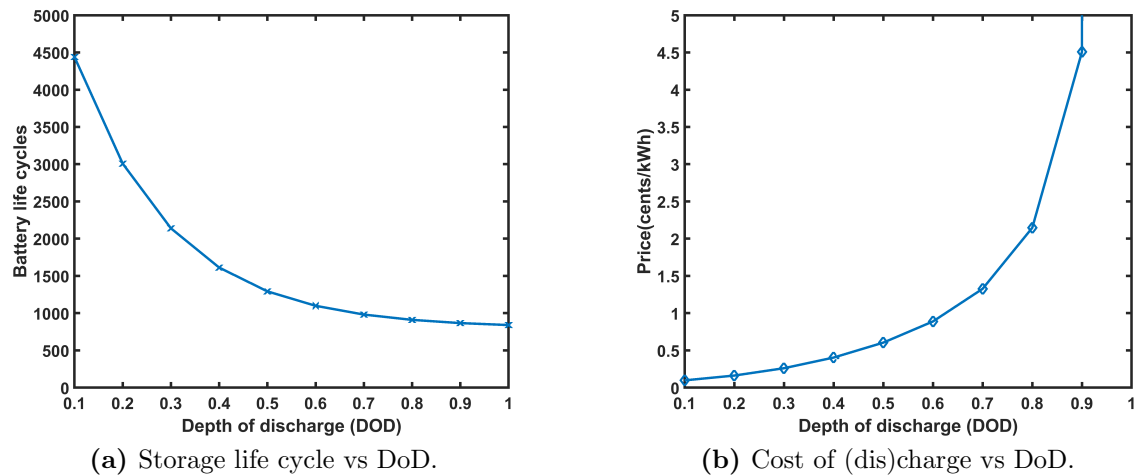


**Figure 3.13:** Storage life cycle degradation and the induced cost with the increasing DoD.

### 3.3 Modelling Home Energy Appliances

One of the work's primary accomplishments is the introduction of the autonomous functioning of smart home appliances. For this purpose, the notion of smart home appliances (a new generation of power appliances that are self-intelligent and energy efficient) has been introduced. An energy management system (EMS) for microgrids can integrate flexible and delay-tolerant smart appliances to operate the grid cost-effectively. Appliances can be classified into two broad groups in the examined innovative home model depending on their technologies. There are two types of appliances; traditional appliances (TA) and smart appliances (SA) [20, 133].

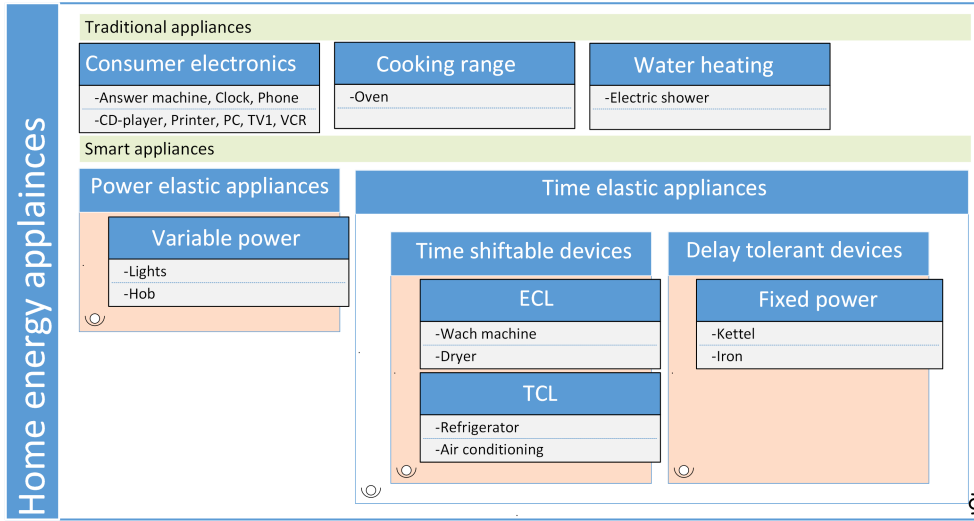


Figure 3.14: Home electrical appliances classification.

#### 3.3.1 Traditional Appliances

This kind of device is sometimes referred to as a critical load. Because these are manually controlled devices with little or limited intelligence, they should be served quickly. These loads are often referred to as a home's base load. These include consumer electronics (CE), cooking range (CR), and instantaneous water heater (WH). As these loads are uncontrolled, this study does not attempt to model these in detail.

**Remark 2.**  $A_{TA} = \{CE \cup CR \cup WH\}$ .

This work considers these loads as deterministic loads that can be anticipated a day in advance. The total energy needed for these loads is modeled as  $E^{TA}$ :

$$E^{TA} = \sum_{t=1}^T \sum_{f=1}^F P_f^{TA-}(t), \quad (3.42)$$

where,  $f \in [1, 2, \dots, F]$  is the index of the appliance and  $P_f^{TA-}(t)$  is the power consumed by a device 'f' at any instant of time  $t$ .

### 3.3.2 Smart Appliances

Typically, this category of the appliance is comprised of energy-efficient and self-aware appliances. These are capable of adjusting their energy consumption and work routines. For example, the scheduling unit may determine how these loads use energy. These devices are assumed to be linked to the central control unit through personal area wireless communication technology (i.e., Zig-bee or WiFi). Additionally, these appliances are categorized into two groups. For example, 1) power elastic appliances (PE) and b) time elastic appliances (TE).

**Remark 3.**  $A_{SA} = \{PE \cup TE\}$ .

#### Power Elastic Appliances

This category of appliances comprises devices with variable power outputs that may change their output magnitudes. Additionally, the power used by these devices can be subject to the consumers' comfort. These appliances might be lights or fans, for example.

**Remark 4.**  $A_{PE} = \{lights \cup fans\}$

The energy demand  $E_a^{PE}$  for a single PE load 'a' is shown as follows:

$$E_a^{PE} = \sum_{t=1}^T P_a^{PE^-}(t), \quad \forall a \in A_{PE} \quad (3.43)$$

where  $P_a^{PE^-}(t)$  denotes the amount of energy consumed by the device  $a$  at any time  $t$ . In this study, these loads may be considered as predictable loads.

#### Time Elastic Appliances

Time elastic (TE) appliances are classified into two types; 1) time shiftable (TS) devices, and 2) delay tolerant (DT) devices. According to optimal choices, TS loads may be planned anywhere on the time scale  $t$ . However, DT loads can only experience delays. TS loads are regarded as dynamic and non-deterministic in this context. The users entrust the home energy management system (HEMS) with the time preference for activating these loads. DT loads, however, are static, predictable, and known in advance. Further, TS loads are classified into electrically controlled loads (ECL) and thermal controllable loads (TCL).

**Remark 5.**  $A_{TS} = \{ECL \cup TCL\}$ .

**ECL** These are fixed energy loads, and the magnitudes of their power can only be adjusted during a single-phase period. The working schedule of these devices may include the alteration in device working phases  $d \in [1, 2, \dots, D]$ . Devices can also postpone activation within a user-defined time preference interval ( $TP_{b,d}^{ECL}(t)$ ). These appliances cannot be turned off once turned on. However, their various operational stages can be delayed based on current power prices and customer satisfaction preferences. This includes, but is not limited to, washing machines (WM), clothes dryers (CD), and water pumps (WP).

**Remark 6.**  $A_{ECL} \in \{WM \cup CD \cup WP\}$ .

The total energy requirement  $E_{b,d}^{ECL}$  of different phases  $d$  of device  $b$  is illustrated as:

$$E_{b,d}^{ECL} = \sum_{t=1}^T P_{b,d}^{ECL^-}(t), \quad \forall d, b \in A_{ECL} \quad (3.44)$$

where,  $P_{b,d}^{ECL^-}(t)$  denotes the power used by a specific phase  $d$  of device  $b$  at any time  $t$ .

**TCL** The Thermal Controllable Loads (TCL), which usually comprise heating and cooling devices, are greatly influenced by fluctuations in ambient temperature [196]. It is, therefore, crucial to accurately model the heat transfer process of these loads. An equivalent Thermal Parameters (ETP) model has been introduced in order to model the electricity consumption of refrigerators and freezers, which is depicted in Figure 3.15. Where,  $C_a$  represents air heat capacity ( $J/^\circ C$ );  $C_m$  depicts

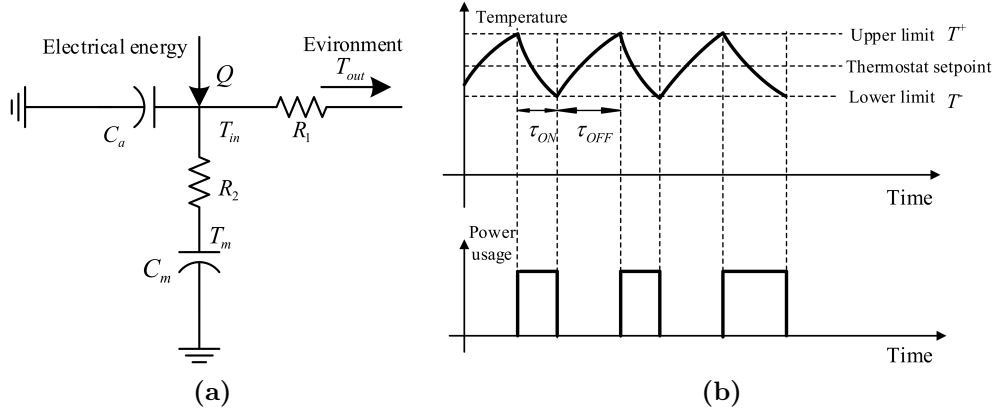


**Figure 3.15:** ETP model and thermal behaviour of a TCL device

mass heat capacity ( $J/^\circ C$ );  $Q$  is heat rate for thermal unit ( $W$ );  $UA$  is standby heat loss coefficient ( $W/^\circ C$ );  $R_1$  is  $1/UA$ ;  $R_2$  is  $1/UA_{mass}$ ;  $T_o$  describes ambient environmental temperature ( $^\circ C$ );  $T_{in}$  represents thermal cabin temperature ( $^\circ C$ );  $T_m$  is mass temperature inside thermal cabin ( $^\circ C$ ).

TCL are fixed power appliances [196]. However, the activation of such devices is conditional on the scheduling unit's temperature-dependent optimum decision values. It takes into account the device's thermal restrictions as well as the ambient environmental temperatures. These energy loads may include but are not limited to air conditioners (AC), water coolers (WC), and refrigerators (RF).

**Remark 7.**  $A_{TCL} \in \{AC \cup WC \cup RF\}$

The energy needed for a particular TCL load  $E_c^{TCL}$  is shown as follows:

$$E_c^{TCL} = \sum_{t=1}^T P_c^{TCL^-}(t), \quad \forall c \in A_{TCL} \quad (3.45)$$

where,  $P_c^{TCL^-}(t)$  is the power required by the particular device  $c$  at any time  $t$ .

**DT loads** These constant power demands cannot be reduced or stopped throughout their operating cycles. Additionally, they cannot be modified in time prior to their activation period. These, on the other hand, maybe postponed from the moment they are initiated until their activation time reaches a specified device starting threshold. Therefore, a notion of a loading queue is developed to regulate their time delays. These queues are formed over time to account for the electricity required to delay and service the loads. With this queue terminology, one may determine the size of the queue and the length of time a given device has been waiting in it. Load delay times can be managed by imposing a limit on queue size and can impose a delay fee on these growing queues. These power load types may include but are not limited to a kettle and an iron.

**Remark 8.**  $A_{DT} \in \{kettle \cup iron\}$

The total energy requirement  $E^{DT}$  for these loads is expressed as:

$$E^{DT} = \sum_{t=1}^T \sum_{e=1}^E P_e^{DT-}(t), \quad (3.46)$$

where  $e \in [1, 2, \dots, E]$  denotes the power load index and  $P_e^{DT-}(t)$  is the power utilized by a specific device  $e$  at any moment  $t$ .

Thus, given a single residence, it may have some random inhabitants  $U$ , who occupy the home randomly during the day as  $U \in \{1, 2, \dots, n^u\}$ . Let  $P_{ac.load}(t)$  be the established total demand for HAPN at any time  $t$ , which is expressed as:

$$\begin{aligned} P_{ac.load}(t) = & \sum_{f \in A_{TA}} P_f^{TA-}(t) + \sum_{a \in A_{PE}} P_a^{PE-}(t) + \sum_{b \in A_{ECL}} \sum_{d=1}^D P_{b,d}^{ECL-}(t) \\ & + \sum_{c \in A_{TCL}} P_c^{TCL-}(t) + \sum_{e \in A_{DT}} P_e^{DT-}(t), \quad \forall t \end{aligned} \quad (3.47)$$

### 3.3.3 Case Study Example

It is critical to obtain device power consumption statistics and a home's load profile information in order to execute load management and schedule loads appropriately. Because physical modeling of individual appliances is outside the scope of this study, the author has designed the loads for our energy demand model using a data-driven method. This research uses a model from [165] to analyze the daily energy consumption profile of a single medium-size residence.

The load profiles of practically all common household appliances are derived at one-second intervals. The Center for Renewable Energy System Technology created this model (CREST). It records the number of inhabitants, their actions, and the activation of desired equipment in the past. Because the energy pattern generated by an individual local home is highly dependent on the residents' activities and their use of electrical appliances. The methodology described below uses historical data from the "UK time use survey" to generate time for residential consumers using statistical models, giving information on occupants' activities and their length. Additionally, it depicts how an actual appliance operates for a certain activity performed by an inhabitant in a house. The occupancy model is developed using a transition

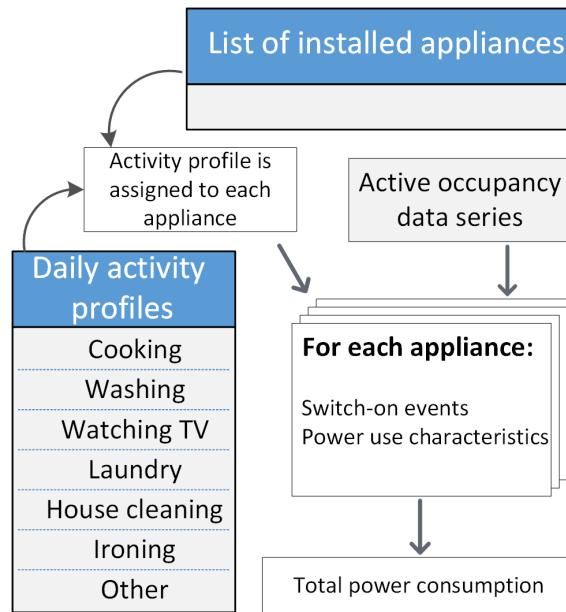


**Figure 3.16:** Electricity demand model architecture [165].

probability matrix for occupants, which yields the precise number of occupants [165].

The activities of each person and the corresponding appliance are determined using historical data. After identifying the appliance, a typical day profile for the appliance is established, and by aggregating the profiles of all the appliances, a load profile for the house is derived. The data obtained includes the average power consumption of each device as well as the operating modes or cycles of each appliance. The model encompasses almost every kind of electrical gadget seen in a domestic environment. It makes use of these gadgets as the fundamental building blocks, with each item representing a particular home power demand, such as a television, clothes dryer, or vacuum cleaner. As a result, it is also referred to as a bottom-up model [12].

As seen in Figure 3.16, the demand model architecture consists of active occupancy, a daily activity profile, and installed devices. The active occupancy approach utilizes randomly allocated inhabitants (one to five). Whereas the time of power usage is predicted based on the individual inhabitants' activity. The resulting activity profiles accurately represent the tenants' actual activities at a given moment. For instance, the most typical activity at dinner is cooking. Similarly, the activity of viewing television is often decided in the evening. Similarly, each occupant's behavior has a daily profile.

Additionally, these activity profiles are associated with a certain appliance. Kitchen, for example, requires the use of an oven, microwave, or other tiny cooking equipment. While viewing the television requires the television to be seen. Thus, rather than calculating specific appliance use data, an activity profile model is utilised to ensure that the appliance is active throughout the intended period of usage [165]. This activity profiling is critical for demand side management because it creates a connection between energy use and occupant activity. This implies that in order to meet variable needs, a user's activity profile must likewise be adaptive. The suggested model of SLDs follows the same technique.

**Table 3.1:** Home appliances activities and classification.

| Activity             | Appliance type       | Mean cycle power (W) | Appliance class |
|----------------------|----------------------|----------------------|-----------------|
| Cooling              | Fridge freezer       | 190                  | TE (TCL)        |
|                      | Refrigertaor         | 110                  | TE (TCL)        |
| Consumer electronics | Answer machine       | 0                    | TA              |
|                      | Cassette / CD-player | 15                   | TA              |
|                      | Clock                | 0                    | TA              |
|                      | Telephone            | 0                    | TA              |
|                      | Hi-Fi                | 100                  | TA              |
|                      | Iron                 | 1000                 | TE (DT)         |
|                      | Personal computer    | 141                  | TA              |
|                      | Printer              | 335                  | TA              |
|                      | TV 1                 | 124                  | TA              |
|                      | TV 2                 | 124                  | TA              |
|                      | VCR / DVD            | 34                   | TA              |
| TV receiver box      | 27                   | TA                   |                 |
| Cooking              | Oven                 | 2125                 | TA              |
|                      | Microwave            | 1250                 | TA              |
|                      | Kettel               | 2000                 | TE (DT)         |
|                      | Small cooking        | 1000                 | TA              |
| Wet                  | Dish wascher         | 1131                 | TE (ECL)        |
|                      | Washing machine      | 406                  | TE (ECL)        |
| Water heating        | Electric shower      | 9000                 | TA              |
| Lighting             | Bulbs                | 190                  | PE              |

The author has identified six distinct activities for the case study example using an existing energy demand model for a house with five residents. Table 3.1 details 22 appliances, including their average power usage and appliance class. The author has categorized these appliances into five distinct types, which were previously explored in Section 3.3.

The often utilized parameter for assessment or control purposes in the aforementioned paradigm is the power value of any device. However, in certain circumstances, more than one parameter may be required to operate the device. For example, as shown in Table 3.2 & Table 3.2, ECL devices (i.e., washing machine and dishwasher) have a distinct number of operating cycles, and each cycle has its own energy consumption and time length constraints [177]. The author re-models these devices' load profiles by including power and time limitations discussed in Section 6.2.2. A similar situation exists with TCL devices (i.e., refrigerator and freezer). In Wu et al. [196], an equivalent thermal parameter (ETP) model is proposed that incorporates both interior and outdoor temperatures as well as the thermal flow mechanism of TCL devices.

**Table 3.2:** Dish washer parameters.

| Energy phase | Energy | Min power | Max power | Op.time |
|--------------|--------|-----------|-----------|---------|
| Wash         | 838 Wh | 1000 W    | 1500 W    | 45 min  |
| Drain & dry  | 261 Wh | 1000 W    | 2500 W    | 15 min  |

**Table 3.3:** Washing machine parameters.

| Energy phase | Energy | Min power | Max power | Op.time |
|--------------|--------|-----------|-----------|---------|
| Movement     | 9.7 Wh | 16 W      | 42 W      | 15 min  |
| Heating      | 720 Wh | 32 W      | 3084 W    | 15 min  |
| Wash         | 77 Wh  | 5 W       | 100 W     | 60 min  |
| Rinse        | 70 Wh  | 17 W      | 170 W     | 30 min  |
| Drain & dry  | 66 Wh  | 203 W     | 1500 W    | 15 min  |

## 3.4 Modelling ESEs Energy Pricing Scheme

To achieve the best results, the cost of various ESEs is assessed throughout the scheduling phase. Fixed operating and maintenance costs are associated with PV operations and EV storage use. While grid prices are changeable, they are determined by open market energy pricing.

### 3.4.1 Utility Grid Energy Price

The demand side management technique (DSM) in scheduling user's load demands may employ standard energy pricing regimes such as; time-of-use pricing (TOU), critical peak pricing (CPP), and real-time pricing (RTP) to minimize peak load and save money. According to recent research, RTP schemes are more adaptable than CPP and TOU price regimes in DSM programs when it comes to expressing dynamic supply-demand connections and influencing consumers' power consumption behavior [181]. However, the provided analysis concentrates on the economic impact of the RTP on the energy consumer or power supplier while ignoring the total power peak to average ratio (PAR) [22], which may result in a situation in which the energy consumer or provider may profit from the pricing model while the power PAR remains unchanged.

In some tasks mentioned in this book use real-time pricing (RTP) data to describe the efficacy of flexible grid pricing strategies for demand side management strategies in the HAPN, which are obtained from Neon et al. [139]. Furthermore, the findings in [84] demonstrated that the RTP could be effectively influenced by the inclining block rate (IBR) method. As a result, in compliance with [22], this work develops a microgrid integrated real-time pricing system that incorporates power resources mismatch and IBR to achieve cost reductions and power demand pattern management.

A hybrid pricing model is devised to coordinate microgrid activities in order to create a cost-effective supply-demand balance. It proposes an inclination block rate-based real-time pricing (IBR-RTP) scheme by merging previously established common tariffs such as real-time pricing (RTP), critical peak pricing (CPP), and time-of-use pricing (TOU) [203][105]. Whereas the RTP price  $\rho(t)$  define for the net



load ( $L(t)$ ) is;

$$\rho(t) = a(t)L(t)^2 + b(t)L(t) + c(t) \quad (3.48)$$

$$L(t) = P_{Load.ac}(t) + P_{dc.b}(t) - P_{b.dc}(t), \forall t \quad (3.49)$$

where  $L(t)$  denotes the net load at any point in time  $t$ ;  $a(t)$ ,  $b(t)$ , and  $c(t)$  denote the coefficients, which may be varied according to the real load requirement at different time increments. The IBR pricing at any instantaneous time  $t$  could be calculated using the system's net load  $L(t)$  and expressed as.

$$IBR(t) = \begin{cases} \sigma^1(t), & 0 < L(t) < \delta^1, \\ \sigma^2(t), & \delta^1 < L(t) < \delta^2, \\ \sigma^3(t), & L(t) > \delta^2. \end{cases} \quad (3.50)$$

Coupling the previously specified common RTP with the IBR pricing technique, the new pricing scheme  $\rho(L(t))$  can be formulated as;

$$\rho(L(t)) = \begin{cases} \rho(t) \times \sigma^1(t), & 0 < L(t) < \delta^1, \\ \rho(t) \times \sigma^2(t), & \delta^1 < L(t) < \delta^2, \\ \rho(t) \times \sigma^3(t), & L(t) > \delta^2, \end{cases} \quad (3.51)$$

where  $\delta^1$  and  $\delta^2$  are the defined net load thresholds for load demand  $L(t)$  at time step  $t$ ;  $\sigma^1(t)$ ,  $\sigma^2(t)$  and  $\sigma^3(t)$  are three IBR price values combined with RTP ( $\rho(t)$ ) to produce the real price  $\rho(L(t))$  of energy providing loads at any time  $t$ . As seen in Figure 3.17, the price varies according on the net load at various time steps.

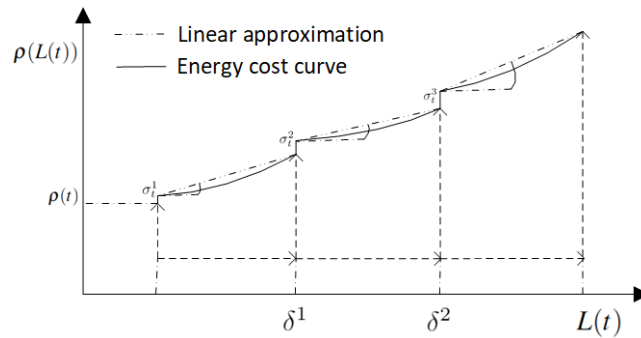


**Figure 3.17:** Energy pricing scheme model.

### 3.4.2 Inverter's Distributed Energy Cost

Inverter power is the power from the battery, PV, and some induced losses due to the DC/AC power conversion inside the inverter. The losses are normally compensated by the power obtained from the source. Hence, in this case the inverter power cost ( $C_{inv.ac}(t)$ ) would be the operating cost of the battery ( $\varphi$ ) and PV ( $\phi$ ) and is illustrated in equation below. The cost per watt for PV and battery operations is obtained from [41]. This operating cost per watt is a function of aggregated investment cost to the working cycle of the component. These operational costs depend on the installation, operation, and management (*O&M*) costs. These expense categories include inverter replacement, operations administration, module replacement,

component replacement, system inspection and monitoring, module cleaning, land lease, property tax, and insurance, as well as asset management and security.

$$C_{inv.ac}(t) = \varphi P_{b.dc}(t) + \phi P_{pv.dc}(t) \quad (3.52)$$

### 3.5 Modelling Optimization Problem

PV storage systems are a popular research topic and are classified as; a) stand-alone systems, b) grid-connected systems. Stand-alone systems off-grid power networks comprises of energy storage systems (ESS) and PV modules which are the mandatory components. At the same time, diesel gensets are commonly used in these systems to meet energy needs when it is impossible to rely on PV and ESS [88]. Whereas, grid-connected PV systems consists at least of a PV systems and an inverter, which enables the connection of the PV modules to the grid [171]. Load and PV generation forecasting are critical inputs for any predictive control approach. While PV prediction is doable given a credible weather forecast, predicting the desired load is a complex problem. Despite technological advancement, vast amounts of electrical energy may not be saved in electrical form. As a result, an optimization method is applied to make the best use of that energy. The consumer-oriented aims are to maximize self-sufficiency and system profitability, and minimize operating expenses, whereas the utility aims to reduce grid congestion and  $CO_2$  emissions. These goals are frequently at odds with one another. As a result, if the control system has to consider more than one target, it is critical to determine the appropriate weighting factors for each objective. A summary of the aims is provided below.

1. Self sufficiency / RE utilization factor indicator: It is defined as the ratio of non-grid-supplied household load to total domestic load. This is accomplished by integrating the battery into the system, allowing surplus PV energy to be used.
2. Components efficiency / Power loss indicator: It illustrates the power losses during energy conversion within the system and calculates the cost of energy wastage due to components' inefficiency rank.
3. Energy storage SoC / Storage device indicator: It demonstrates whether energy storage is cost-efficient at any particular time  $t$ . Alternatively, it costs more by operating unnecessarily, which involves storage degradation costs.
4. Load curtailment / User comfort indicator / Flexible load control indicator: It indicates the priority of user comfort against power load shedding. Flexible loads, however, improve the energy consumers' experiences by adjusting and tolerating themselves according to the situation, which is preferable while handling power cuts and minimizing the energy cost for the consumer.
5. System Return on Investment: It is defined as the ratio of money saved with an investment to the cost of installing and purchasing PV modules and batteries. This aim should be considered at the system design stage by decreasing the system size while achieving system objectives.

6. Operation costs: It relates to reducing the running costs of a certain system with defined capacities. For example, using PV battery systems, one can reduce the power expenses for energy obtained from grid and limits the battery aging phenomenon.
7. Grid congestion: Increasing solar installations' integration into electrical grids causes peak power feed-in congestion. To overcome this issue, peak-shaving algorithms that smoothed out the feed-in power or prohibit feed-in power during peak periods might be introduced to the goal functions.
8.  $CO_2$  emissions: This goal is discussed in systems with a diesel generator and may be reached by reducing the fuel contribution to power generation. Reducing  $CO_2$  emissions is analogous to self-sufficiency in other systems.

#### 3.5.1 Model Predictive Control

Model predictive control (MPC) is a time-ahead optimization approach having many parameters as inputs, outputs, and system limitations. It comprises of two working time horizons, one is known as control and and the other is prediction horizon, and are depicted in Figure 3.18. The prediction horizon is for non-deterministic polynomial (NP) problem, whereas the control horizon is “Nick’s Class” (NC). First, the system model calculates a set of NP expected outputs. Then, the MPC performs the optimization process and calculates a set of NC control values based on this sequence and current system data. The significant benefit of MPC is that it optimizes for the current time slot while considering future time slots within a restricted time horizon. However, the value obtained by optimization is merely implemented for the time being. The exact process should be performed for the next time slot (anticipating future values and the optimization). MPC optimization strategy differs based on the target function and restrictions. The approaches often utilized in MPC-based energy management systems are outlined below.

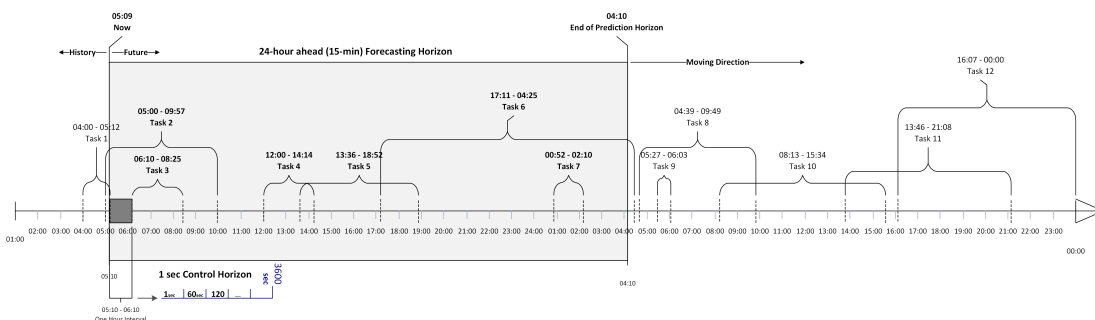


**Figure 3.18:** Predictive control strategy.

#### 3.5.2 Microgrid optimal operation

Many technological and economic issues must be managed during the microgrid (MG) operation to produce steady, dependable, and inexpensive electricity. To meet these needs, the MG control system uses a multi-level and multi-layer architecture to govern the power flow in microgrid, as illustrated in Figure 3.19 [116], with operational (Real-time control), supervisory (scheduling), and planning (scheduling

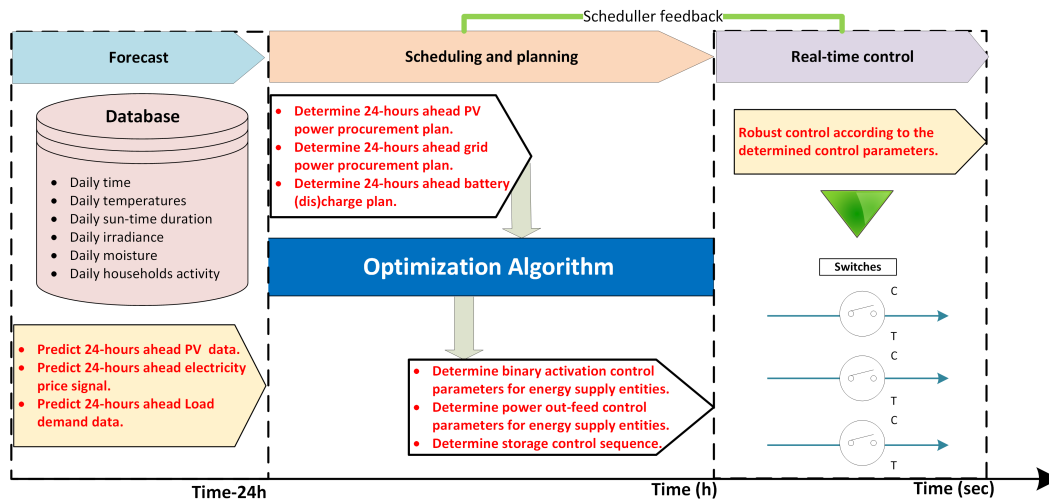


**Figure 3.19:** Illustration of a hierarchical multi-layer structure for MGs control system.

and forecasting) levels. From right to left, each level is distinguished by its control parameters and execution speed resolution. Real-time controllers attached to the significant elements of the microgrid at the functional level are responsible for observing and controlling the voltage and frequency within milliseconds. The supervisory layer comes next, with a time window ranging from seconds to minutes. The scheduler at this layer assures steady functioning of the MG components based on the set points provided by the management layer. The planning layer is at the topmost level, in which the controller operates in increments of few minutes to many hours while keeping costs to a minimum given their technological and operational limits. It is responsible for predicting load needs dependably and cost-effectively.

### 3.5.3 Optimization Algorithms

The MATLAB Optimization Toolbox is utilized to find the optimal solution to most of the problems discussed in this publication. This toolbox comprises functions that facilitate the identification of parameters that minimize or maximize objectives while satisfying constraints imposed by the system. The optimization problem can be defined with functions and matrices, resulting in faster and more accurate solutions, and automatic differentiation of objective and constraint functions can be leveraged. The toolbox's solvers can be utilized to determine optimal solutions to both continuous and discrete problems, evaluate trade-offs, and incorporate optimization techniques into algorithms and applications. Furthermore, the toolbox can be employed to carry out design optimization tasks such as parameter estimation, component selection, and parameter adjustment [113].

Because of complex mathematical models and to reduce the time of getting results from optimization algorithms, the objective functions and the system constraints are designed as linear equations. Hence a linear programming strategy is implemented to deal with these linear equations. Mixed-integer linear programming (MILP) optimizes linear objective functions for a given set of linear equations and inequalities. Unlike linear programming, the variables in integer optimization can only take integer values rather than arbitrary fundamental values. Despite its abil-

ity to handle problems with many variables and constraints, adding integers to the issue raises the processing cost compared to only linear programming. The following mathematical illustrations show the function implemented as MILP syntax:

$$\min_x f(x_1, x_2, \dots, x_n) = \sum_{t=0}^T c_t x_t, \quad (3.53)$$

subject to the linear conditions as follows:

$$\begin{aligned} x(\text{intcon}) \text{ are integers} \\ A_{eq}x = b_{eq} \\ Ax \leq b \\ lb \leq x \leq ub \end{aligned} \quad (3.54)$$

In general,  $f(x)$  is a scalar function  
 whereas  $c_t$  is constant parameter,  
 $x_t$  are the set of control variables,  
 $A$  and  $A_{eq}$  are system input matrices,  
 $b$ ,  $b_{eq}$ ,  $lb$ , and  $ub$  are constraint vectors, and

The parameter “intcon” is a vector of positive integers containing the integer-valued controlled components. Optimization approaches are used to identify a combination of design variables,  $(x = x_1, x_2, \dots, x_n)$ , that may be described as optimal in some sense. In the most basic scenario, this process may be the minimization or maximizing of some system feature that is dependent on  $x$ . In a more sophisticated formulation, the objective function  $f(x)$  to be reduced or maximized may be constrained in one or more of the following ways; a) constraints on equality, b) inequality constraints, and c) parameter’s lower and upper bounds [2].

A problem-based rational functions technique is employed for creating an optimization strategy that employs optimization variables to describe goals and constraints. Variables and expressions in the problem reflect an operating system model. The procedures outlined below are suggested for implementing an optimization expression.

1. Get a broader overview of the issue.
2. Determine the goal (maximizing or minimizing).
3. Determine the variables names.
4. Determine the constraints and limitations.
5. Identify the control variables.
6. Use mathematical terminology to specify all quantities.
7. Examine the model for reliability and consistency.
8. For each problem variable, construct an optimization variable.
9. Make a container for optimization problems. Include the problem’s objective function.

10. Create and incorporate linear constraints such as; linear equalities/inequalities and boundary conditions.
11. After finishing the problem formulation, use an optimization solver (in this thesis, “linprob” with the “dual-simplex” or “interior-point” method is used) to solve the problem.

Solvers, in general, return a local minimum (or optimum). The outcome may be a global minimum (or optimal), but this is not guaranteed. A local minimum of a function is a position where the function value is less than that of adjacent points but may be larger than that of a distant point.

## 3.6 Conclusion

This chapter delves into the examination of several grid component models and presents novel analytical approaches to system modeling. Among the components are the energy supply entities (ESEs) such as; photovoltaic (PV) arrays, diesel generators, and energy storage devices (ESDs). Because in further chapters, the concept of demand-side management is also introduced. So the modeling of home energy appliances (i.e., traditional base load demands and smart load demands (SLDs)) is also critical to be described here. The recommended mathematical modeling of each component in this chapter comprehensively examines the system’s attributes, performance, and dynamic behavior. In addition, various components of cost models are also explained, with the help of which an optimization model could offer insight into the decision makers’ energy policy challenges.

## 4 Home Area Power Network Design Framework and Power Scheduling Algorithms

As the world endeavors to produce cost-effective and environmentally friendly electricity, the use of photovoltaic (PV) and electric vehicle (EV) systems has gained substantial attention. However, the fluctuating nature of PV power generation, the variability of energy consumers' load demands, and the restrictions of EV storage capacity can result in instability in the power grid. To examine these challenges, a behavior of a small scale home area power network (HAPN) is studied by incorporating an intelligent energy management system (iEMS). This chapter focuses on the grid connected HAPN framework integrating photovoltaic modules, electric vehicle storage, residential households, and the power scheduling algorithms. Two different techniques have been investigated for energy management. The first technique is fixed horizon based day-ahead rule-based energy management system, whereas the second one is rolling horizon based optimal energy management system.

The methodology put forth in this study employs a real-life case study of yearly datasets relating to household energy demands, electric vehicle driving patterns, and battery charging and discharging patterns. The purpose of this demonstration is to showcase the actual capabilities of energy management. The simulation results present a comparative analysis of various energy sources in terms of their monthly and yearly evaluation indices, such as penetration levels and utilization factors. A battery storage capacity loss percentage is determined on daily, monthly and yearly basis by integrating a battery life-cycle degradation model in the system. Additionally, consumers' comfort and low energy costs are ensured by balancing their power needs with the least expensive energy supply sources.

### 4.1 Critical Analysis of Optimization Strategies

The main problem of the modern power network is that the RESs are exceptionally intermittent. Intermittence is induced by varying wind speeds and time-limited sun irradiation [117]. Incorporating RESs into the traditional grid is also challenging due to the inherent unpredictability of RESs. The inadequacy of measuring technology to monitor grid status adequately cites [114]. Due to the low system inertia, a grid with significant RESs uptake may experience frequency and voltage instability. The intermittent nature of dispersed energy supplies further complicates system stability [166].

To solve this issue, Li et al. [96] proposes a distributed grid design. It connects RESs to regular power grids by storing and controlling energy. Decentralized generation re-imagines the existing electrical network. Using energy storage systems (ESSs) like batteries is a simple solution to the issue cited by [123]. This work uses the ESSs to optimize PV and EV serving capacity in grid-connected nanogrids (NGs). It helps managing nanogrid energy by storing energy to EV battery, when RESs production exceeds load needs (i.e., PV to vehicle (PV2V)) and returning energy to the home (i.e., vehicle to home (V2H)) when energy demands are high.

**Table 4.1:** Objectives, limitations, and critical analysis of the past literature.

| Ref # | Objectives   | Technique(s)                                | Scheduling entities |    |    | Dynamic EV Charging | Battery degradation | Cost reduction | Energy balancing | Limitation(s)   |
|-------|--|---|---------------------|----|----|---------------------|---------------------|----------------|------------------|---|
|       |  |   | Grid                | PV | EV |                     |                     |                |                  |   |
| [166] | According to this study, using battery storage for PV and EV hosting capacity optimization as well as grid voltage maintenance was critical.   | Model Predictive Control                    | ✓                   | ✓  | ✓  | ✗                   | ✗                   | ✓              | ✗                | The case study is fictitious. It was confirmed that the generation of DG and PVs exceeds the consumption of the load and EV charging and that the ESS maintains all BUS voltages within the permitted limit.  |
| [145] | The purpose of this study is to propose a methodology for simulating plug-in electric vehicle charging in order to quantify the impact of this type of load on power systems.  | Monte Carlo Simulation                      | ✓                   | ✓  | ✓  | ✗                   | ✗                   | ✗              | ✓                | The proposed technique focused on transmission networks and provides a deterministic representation of the EV charge distribution across the network. It made no reference to any real-world data collection. |
| [214] | Dynamic programming is used to govern the charging and discharging of the storage device in order to extend the life of the battery.   | Adaptive Dynamic Programming                | ✓                   | ✓  | ✗  | ✗                   | ✗                   | ✓              | ✗                | The model was confined to battery storage alone and did not include specific information about load needs. Additionally, constraint functions that do not have an exact model of the device were estimated.   |
| [205] | The author discussed the challenge of minimizing the total energy and thermal discomfort costs. The suggested system stabilised developing queues for indoor temperature control, electric car charging, and energy storage.   | Lyapunov Optimization                       | ✓                   | ✓  | ✓  | ✗                   | ✗                   | ✓              | ✓                | The energy demand model was limited in scope since it examines only thermal loads. Additionally, the algorithm was incapable of addressing the issue of peak forms.   |
| [133] | Maximizing the utility sums of residential customers while keeping energy consumption costs in check is explored in this article. It is decentralized, but it protected the residents' private information at the same time.   | Generalized Benders Decomposition algorithm | ✓                   | ✓  | ✗  | ✗                   | ✗                   | ✓              | ✗                | The technique might not operate successfully if the homes' demand information is inaccurate. It also didn't address the peak-to-average power demand ratio (PAR).   |
| [20]  | A two-stage optimization approach is devised, in which peak reduction signals are discovered and their flexibility provision determined by aggregating individual users' energy use histories.                                 | Mixed Integer Linear Programming            | ✓                   | ✓  | ✗  | ✗                   | ✓                   | ✓              | ✗                | This study made no allowance for incentives for postponing loading or for the penalty cost associated with reducing customer suffering.   |
| [172] | The control method outlined in this work is intended to address power factor concerns associated with EV charging stations while still allowing for full PV generation.  | Optimal Dynamic Programming                 | ✓                   | ✓  | ✓  | ✗                   | ✗                   | ✓              | ✗                | The effort was done to boost the power factor. The battery management system was designed to adjust only the power factor, ignoring the demand-supply balance and ignoring real-world data.                   |
| [35]  | This research provided a model for optimizing the operation of storage batteries and appliance usage for each consumer, as well as the operation of a photovoltaic plant within a community to maximize load factor increases. | Mixed Integer Linear Programming            | ✓                   | ✓  | ✓  | ✗                   | ✗                   | ✓              | ✗                | The battery deterioration model outlined in this study is critical to the model's success. Realistic information about the actions of prosumers was also not included.  |
| [4]   | The suggested technique uses time-of-use pricing, time-varying residential power demand, solar generating profiles, and EV specifications to reduce electricity prices and flatten the load curve.                             | Rule Based Optimization                     | ✓                   | ✓  | ✓  | ✗                   | ✗                   | ✗              | ✓                | The battery degradation model is an important factor in this study's model. But, realistic data sets on prosumer actions were not included in the investigation.  |
| [15]  | The PV produced more energy than needed to meet load demands and charge the batteries. Battery discharge happens when PV panel output falls short of load needs. The controller prevented over(dis)charging.                   | Fuzzy Logic Design                          | ✓                   | ✓  | ✗  | ✗                   | ✗                   | ✗              | ✓                | The focus of this paper was solely on the supply and demand for energy. Cost reduction and customer satisfaction were not adequately addressed.   |

Thus, EVs may act as prosumers for NGs, reducing the need for separate residential batteries [30]. A homeowner, for example, may utilize the EV's storage to power several residences at peak periods and high energy costs while charging it later in the night when energy costs are lower [48]. Also, enabling their EVs to act as dispersed energy supplies may earn them rewards [204].

Moreover, the concept of a regulated home area power network (HAPN) makes it simple to cope with power production and consumption uncertainties [115]. Self-reliability and resilience are essential HAPN traits. Other qualities like self-sufficiency, integrating appliances, and coordination among multiple energy devices are also vital [160]. To optimize the HAPN's cost-effectiveness, an intelligent energy management system (iEMS) using advanced optimization techniques may be used. A nanogrid management system can better regulate the unpredictable and intermittent nature of RESs and load demands.

A critical analysis of prior research on energy sources, EV charging behavior, storage life cycle deterioration, cost reduction, and scheduling strategies is shown in Table 5.1.

In comparison to past studies, this study adds the following noteworthy contributions:

1. This chapter is a response to the special issue of Energies on "Demand Side Management of Distributed and Uncertain Flexibilities". It presents a novel approach to demonstrate the practical capabilities of an energy management system (iEMS) using real-life yearly datasets of household energy demands, electric vehicle (EV) driving patterns, and EV battery charging and discharging patterns. To the author's knowledge, this is the first study that employs such explicit data sets in the development of an iEMS methodology.
2. A detailed converter-based nanogrid model is presented. This model incorporates real-world data sets as well as operational constraints for conventional and renewable energy power sources. The proposed model takes into consideration the gradual decrease in storage capacity over time of the electric vehicle.



The data utilized in MATLAB undergoes pre-processing before being utilized in the analysis.

3. A two-stage co-simulation framework was implemented to construct a multi-time scale Integrated Energy Management System (iEMS) and control approach. A reliable decision-based operating method is proposed to use the least expensive energy supply sources while maximizing consumer satisfaction.
4. To address forecast errors and create cost-effective scheduling decisions for supply sources, we propose a computationally efficient mixed integer rule-based sliding horizon dynamical method. Furthermore, the first step compares daily and seasonal scheduling selections for diverse supply sources.

## 4.2 Home Area Power Network Design and Scheduling Strategies

The dynamical scheme represented in Figure 4.1, includes daily load curves for household appliances, solar power curves from PV systems, grid electricity pricing signals, EV loading, charging, and driving indications. The smart meter includes a home energy management system (HEMS) that allows for cost-effective day-ahead scheduling and real-time power flow control in HAPN gathers the above signals for further processing. The built architecture can accommodate plug-and-play energy sources, such as electric automobiles.

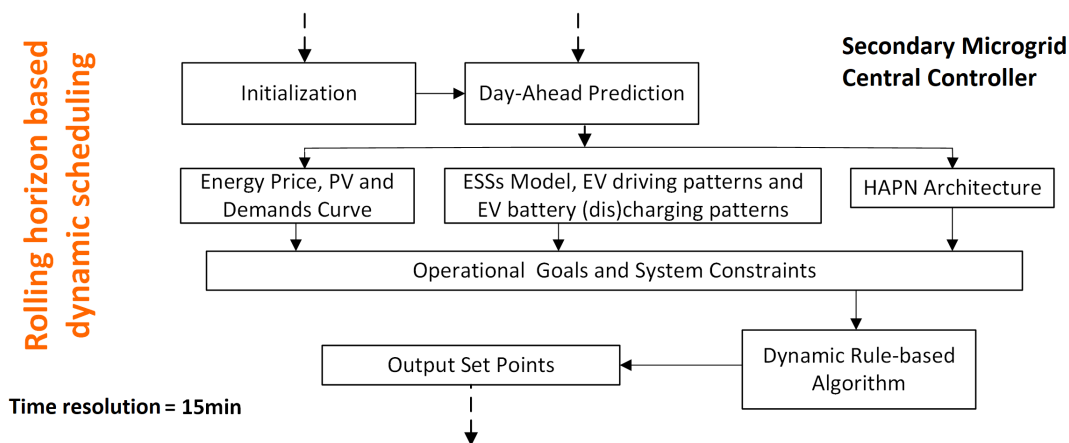


**Figure 4.1:** Proposed dynamic scheduling scheme.

The suggested framework’s energy management tactics are divided into two sub-problems and solved in two ways. A cost-effective approach to acquiring schedule control signals for different energy supply entities (ESEs) is discussed initially. The signals are repeatedly tuned with a year-ahead temporal resolution of 15 minutes. It anticipates solar energy and residential load demand uncertainty. The second component deals with energy balance and user satisfaction, using the first section’s data as reference signals for real-time electrical device performance. Each energy device has a powerful controller that follows the planned signal during its operating time. A device-level robust control mechanism continually monitors the power levels and regulates the device’s activation depending on the received reference signal. The

proposed strategy works for any home with solar panels and an electric car as a storage entity. With increased energy costs and extra solar electricity, it helps the homeowner financially to act optimally and reduce its energy costs.

#### 4.2.1 Home Area Power Network Architecture

Figure 4.2 shows the HAPN architecture in question. The Utility grid (discussed in Section 3.1.3) is attached directly to the home's AC bus. However, the PV array (model stated in Section 3.1.2) and EV storage (as stated in Section 3.2) are linked to the grid AC bus through inverters and converters. The system includes controllable switches for the nanogrid's binary operations.

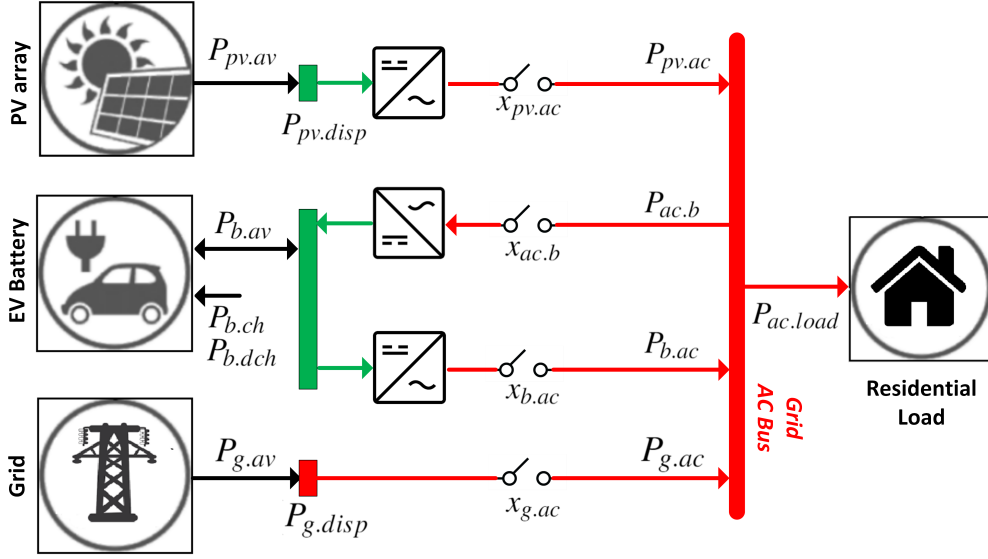


Figure 4.2: HAPN architecture.

As shown in the figure, the grid supply power at the AC bus ( $P_{g.ac}(t)$ ) is;

$$P_{g.ac}(t) \leq \min [x_{g.ac}(t)P_{g.disp}(t), P_{ac.load}(t)], \quad \forall t \quad (4.1)$$

where  $x_{g.ac}(t) \in \{0, 1\}$  represents the grid Boolean operator,  $P_{g.disp}(t)$  represents the controlled dispatchable grid power, and  $P_{ac.load}(t)$  represents the desired load demands. The power provided by solar panels  $P_{pv.ac}(t)$  on the AC bus, on the other hand, is restricted to;

$$P_{pv.ac}(t) \leq \min [P_{pv.disp}(t), P_{ac.load}(t) + P_{ac.b}(t)] x_{pv.ac}(t) \eta_{pv.con}, \quad \forall t \quad (4.2)$$

where,  $P_{pv.disp}(t)$  represents the controlled dispatchable photovoltaic power,  $P_{ac.b}(t)$  represents the power utilized to charge the EV battery, and  $\eta_{pv.con}$  represents the inverter efficiency, and  $x_{pv.ac}(t) \in \{0, 1\}$  represents the PV Boolean operator.

Additionally, the HAPN incorporates a battery in the form of an electric car that acts as a storage entity with instantaneous available power ( $P_{b.av}(t)$ ) that is restricted by the EV battery's maximum capacity ( $\bar{E}_b$ ), such as

$$P_{b.av}(t) \leq (\bar{E}_b / \Delta t). \quad \forall t \quad (4.3)$$

The instantaneous power transfer from attached EV to AC bus ( $P_{b.ac}(t)$ ) during discharging is:

$$P_{b.ac}(t) = \min [\eta_{b.con}P_{b.dch}(t), \eta_{b.con}P_{b.av}(t), P_{ac.load}(t)] x_{b.ac}(t), \quad \forall t \quad (4.4)$$

where,  $x_{b.ac}(t) \in \{0, 1\}$ ,  $P_{b.dch}(t)$  is the battery discharge rate, and  $\eta_{b.con}$  denote the battery converter efficiency. However, the instantaneous power necessary to recharge the EV battery ( $P_{ac.b}(t)$ ) is illustrated in Equation 4.5, coupled with a Boolean operation of  $x_{ac.b}(t) \in \{0, 1\}$ .

$$P_{ac.b}(t) = \min [P_{pv.ac}(t) + P_{g.ac}(t) - P_{ac.load}(t), \eta_{b.con}^{-1} P_{b.ch}(t), \dots, (\bar{E}_b / \Delta t) - (\eta_{b.con}^{-1} P_{b.av}(t)) x_{ac.b}(t), \quad \forall t \quad (4.5)$$

where,  $P_{b.ch}(t)$  denotes the battery's charge rate. Additionally,  $E_b(t)$  represents the capacity of energy in the battery influenced by the capacity degradation  $Q_{AM/SEI}(t)$ , which is restricted by its maximum  $\bar{E}_b$  and the minimum  $\underline{E}_b$  threshold;

$$\underline{E}_b \leq E_b(t) - (Q_{AM}(t) + Q_{SEI}(t)) \leq \bar{E}_b. \quad \forall t \quad (4.6)$$

Further,  $P_{b.ch}(t)$  and  $P_{b.dch}(t)$  are constrained by a maximum ( $\bar{P}_{b.ch} | \bar{P}_{b.dch}$ ) and lowest ( $\underline{P}_{b.ch} | \underline{P}_{b.dch}$ ) value at any point in time, including the following:

$$\underline{P}_{b.ch} \leq P_{b.ch}(t) \leq \bar{P}_{b.ch}, \quad \forall t \quad (4.7)$$

$$\underline{P}_{b.dch} \leq P_{b.dch}(t) \leq \bar{P}_{b.dch}, \quad \forall t \quad (4.8)$$

besides, the AC bus exchanges power transfer as;

$$\begin{aligned} x_{pv.ac}(t)P_{pv.ac}(t) + x_{b.ac}(t)P_{b.ac}(t) + x_{g.ac}(t)P_{g.ac}(t) \dots \\ = x_{ac.b}(t)P_{ac.b}(t) + P_{ac.load}(t). \quad \forall t \end{aligned} \quad (4.9)$$

Additionally, one constraint on battery functioning is that charging and draining cannot occur simultaneously.

$$x_{b.ac}(t) + x_{ac.b}(t) \leq 1. \quad \forall t \quad (4.10)$$

Additionally, the battery's immediate state of energy ( $E_b(t)$ ) may be computed as follows:

$$E_b(t) = E_b(t-1) + \int_{t-1}^t ((\eta_{b.con} P_{ac.b}(t) \times \Delta t) - (\eta_{b.con}^{-1} P_{b.ac}(t) \times \Delta t)) dt. \quad \forall t \quad (4.11)$$

#### 4.2.2 Battery Capacity Loss Model

A typical characteristic of battery ageing or deterioration is noticed during battery operation. There are two distinct forms of deterioration that are often investigated: 1) the diminishment of a battery's ability to provide energy; 2) and the reduction of its capacity for storage. According to [192], the aforesaid degrading event is characterized by high temperatures, high charge and discharge rates, and a substantial depth of discharge (DOD).

Jin et al. [82] developed a reduced-order physical model to anticipate the degraded state of lithium-ion phosphate cathode and graphite anode battery cells. Individual storage cells with a capacity of 2.3 Ah are being investigated, which will be combined in series and parallel to form a battery pack with a given capacity power. At each time step  $t$ , the capacity loss owing to solid electrolyte interface

(SEI) layer development ( $Q_{\text{SEI}}(t)$ ) and active material (AM) loss ( $Q_{\text{AM}}(t)$ ) at any time  $t$  are calculated using Equation 4.12 and 4.13, respectively.

$$Q_{\text{SEI}}(t) = \int_{t-1}^t -\frac{k_{\text{SEI}} \exp\left(-\frac{E_{\text{SEI}}}{RT}\right)}{2(1 + \lambda\theta)\sqrt{t}} dt, \quad (4.12)$$

$$Q_{\text{AM}}(t) = \int_{t-1}^t k_{\text{AM}} \exp\left(\frac{-E_{\text{AM}}}{MN}\right) \cdot \text{SOC}(t) \cdot |I_{b.dch}(t) - I_{b.ch}(t)| dt, \quad (4.13)$$

A detailed description of the model is given in [130].

### 4.2.3 Energy Supply Entities Cost Modeling

For demand side management (DSM) strategies in the HAPN, the usefulness of dynamic grid pricing methods ( $\theta(t)$ ) is highlighted by obtaining real-time pricing (RTP) data from [3, 139]. Whereas the cost per watt for solar photovoltaic ( $\phi$ ) and battery storage ( $\varphi$ ) operations is derived from [41]. These operating expenses are proportional to the costs of installation, operation, and management (*O&M*). Additionally, *O&M* expenditure categories include inverter replacement, operations administration, module replacement, component replacement, system inspection and monitoring, module cleaning, land leasing, property taxes, and insurance, as well as asset management and security [41].

## 4.3 Rule-based Energy Scheduling Scheme

The Home Area Power Network (HAPN) is a single-phase power network that receives energy from the utility grid, solar panels, and electric vehicle batteries, and distributes it to individual residences at a predetermined voltage level. This is a novel solution to the problem of providing energy to residential areas, as it allows for efficient and reliable energy distribution. Additionally, the HAPN provides a cost-effective alternative to traditional power networks, making it an attractive option for many residential areas. The article demonstrates energy allocation from various energy sources via the use of a cost-effective energy management technique. This technique is utilized at the secondary level scheduling stage to generate set points for charging and discharging electric cars, solar power feed-in, and grid power consumption. Additionally, a limit on satisfying users' load requirements is imposed. It ensures that energy supply is always equal to or greater than energy consumption. Additionally, cost reductions are realized by employing readily accessible, inexpensive energy sources at any time  $t$ . The next part discusses the proposed method, which provides a practical strategy for scheduling available power sources.

The operational aim of the energy management phase is to boost customer satisfaction and EV charging while maintaining HAPN's operating expenses as low as possible. This implies that preference should always be given to energy sources that produce relatively inexpensive power and that, if required, a part of the EV charging load may be served as another source of energy to balance the power demands. At each time  $t$ , the EMS collects data on solar energy, the status of electric vehicle storage, and user load needs.

The purpose is to build a scheduling mechanism  $\mathbf{u}(t) \in \{\mathbf{u}_x(t), \mathbf{u}_p(t)\}$ , that balances power from the grid, photovoltaics, and a battery for an electric car. Whereas

$\mathbf{u}_x(t) = [x_{pv.ac}(t), x_{b.ac}(t), x_{g.ac}(t), x_{ac.b}(t)]$  denotes Boolean decision variables. The variables listed in the previous section represent the availability of various energy sources at the start of each iteration of the algorithm, and are denoted as follows:

$$\begin{aligned} x_{g.ac}(t) &= \begin{cases} 1 & \text{if } P_{g.av}(t) > P_{g.disp}(t) \\ 0 & \text{otherwise} \end{cases}, & x_{pv.ac}(t) &= \begin{cases} 1 & \text{if } P_{pv.av}(t) > P_{pv.disp}(t) \\ 0 & \text{otherwise} \end{cases}, \\ x_{b.ac}(t) &= \begin{cases} 1 & \text{if } P_{b.av}(t) > \underline{E}_b(t) \\ 0 & \text{otherwise} \end{cases}, & x_{ac.b}(t) &= \begin{cases} 1 & \text{if } P_{b.av}(t) < \overline{E}_b(t) \\ 0 & \text{otherwise} \end{cases}. \end{aligned} \quad (4.14)$$

Thus, the aforementioned discrete variables contribute to the reduction of computation complexity by allowing for an earlier determination of whether or not to activate a specific energy supply entity. Additionally,  $\mathbf{u}_p(t) = [p_{pv.ac}(t), p_{b.ac}(t), p_{ac.b}(t), p_{g.ac}(t)]$  denotes a vector of continuous power control variables applicable to a variety of energy sources. The aforementioned management approach is designed to establish a load and supply balance while accounting for the cost of operating HAPN. As a result, we identify two unique formulations of the issue.

$$\begin{aligned} \mathbf{P} &= \min_{\mathbf{u}(t)} \sum_{t=1}^T \{ \theta(t) \times x_{g.ac}(t) P_{g.ac}(t) + \phi \times x_{pv.ac}(t) P_{pv.ac}(t) + \varphi \times x_{b.ac}(t) P_{b.ac}(t) \} \quad (4.15) \\ & \quad \text{s.t.} \quad \text{ref, eq. (1-2), (4-14), (16-17)} \end{aligned}$$

The first one is the cost minimization issue shown in Equation 4.15, and the second one is the energy balancing problem depicted in Equation 4.17, in which the house's load needs (as defined in Equation 4.16) must be met with the least amount of electricity possible. This issue can be rectified by enforcing some of the security constraints stated above. On the other hand, the power needs ( $P_{ac.load}(t)$ ) for each time slot  $t$  must be met by a combination of power provided by various sources. As a consequence, the following principles outline the inherent energy balance restriction associated with achieving the aforementioned objective. As a result, the target power that must be attained is as follows:

$$P_{ac.load}(t) = \begin{cases} \max(0, P_{ac.load} + x_{ac.b}(t) P_{ac.b}), & \text{if } x_{pv.ac}(t) | x_{b.ac}(t) | x_{g.ac}(t) = 1 \\ 0, & \text{otherwise} \end{cases} \quad \forall t \quad (4.16)$$

The EMS places a premium on the usage of solar energy, and battery power is used if solar is insufficient to fulfill load requirements. If required, energy may also be drawn from the grid. The net power that will be allocated at every time slot  $t$  will be as follows:

$$P_{pv.ac}(t) + P_{b.ac}(t) + P_{g.ac}(t) \geq P_{ac.load}(t). \quad \forall t \quad (4.17)$$

### 4.3.1 Algorithms and Implementation

We have demonstrated three unique operating techniques for supply-side management that may be compared to achieve the best results. Among them are the following:

1. Scheme 1: Conventional rule-based strategy involves only EV storage and grid energy supply (Conv-EG).

2. Scheme 2: Conventional rule-based strategy involves PV supply along with EV storage and grid energy supply (Conv-PEG).
3. Scheme 3: Proposed model predictive intelligent energy management system (MP-iEMS).

For all three optimization schemes, the system model is identical to that presented in Section 4.2, except that the PV is missing in Scheme 1.

To address the problems expressed in Equation (4.15 & 4.17), we suggest a set of establishing priorities for acquiring power values from the absolute cheapest and most dependable source of energy. This set includes two continuous power indicators and three binary indicators. One of the power indicators cover both the actual load and storage charging requirements ( $P_{ac.load}$ ) and the other is EV consumption when driving ( $P_{drv}(t)$ ). While binary indicators such as drive bool ( $EV_{drv}(t) \in \{0, 1\}$ ), electric vehicle charging Bool ( $EV_{ch}(t) \in \{0, 1\}$ ), and electric vehicle loading Bool ( $EV_{load}(t) \in \{0, 1\}$ ) are also accessible. The feasible solution set is composed of 16 distinct conditions based on these four indicators. Only six of them are plausible, and we used a rule-based expert system to apply them over the operating window. The remaining 10 candidate sets are not feasibly operational and so cannot be adopted. Considering the above binary loading signals the author has developed the control policy  $\mathbf{u}(t)$ .

#### **Scheme 1: Conv-EG**

The scheduling strategy (Conv-EG) is a priority-based decision algorithm as shown in Figure 4.3. We assume that the system model used to apply this algorithm only contains a supply from the grid and EV storage. In this algorithm, the EV storage has priority over the grid to supply power to the load demands. It is due to the assumption that the EV storage might be charged at low peak hours at comparatively lower rates. Hence, at the initial stage, EV storage is analyzed to determine whether it can fulfill the load demands completely by itself or not. If the EV is parked at home and the loading Boolean is enabled, it will automatically discharge. Additionally, if the charging Boolean is active, then it is capable of charging as well. However, if the EV drive Boolean is set to true, the EV will drive on the road and will charge itself via charging stations, while the home loads will be entertained by grid electricity. The detailed workflow of the algorithms is illustrated in Figure 4.3.

#### **Scheme 2: Conv-PEG**

The scheduling method (Conv-PEG) incorporates a rooftop photovoltaic system along with EV storage and grid power adding another low-cost source of power. In the algorithm shown in Figure 4.4, the PV source is considered to be the cheapest source of energy, as it requires only solar energy to generate freely available power. The Conv-PEG is initiated by initializing the decision window's system variables and anticipating new values for PV in-feed and load demands. Additionally, it updates the battery's state of charge (SOC), charging power rate, and battery capacity.

Thus, the first stage of the algorithm assesses if there is enough solar power available to suit the demands of the clients. If the answer is "yes," the PV immediately satisfies all of the load requirements for the time period  $t$ . Then it comes to the

## 4. Home Area Power Network Design Framework and Power Scheduling Algorithms

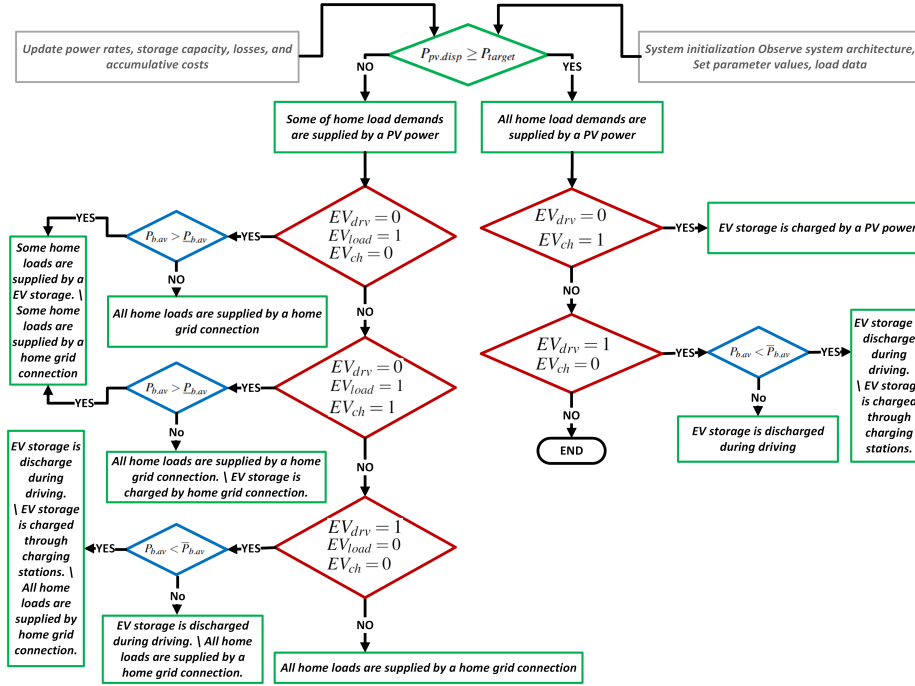


Figure 4.3: Flowchart of the conventional rule-based scheduling scheme (Conv-EG).

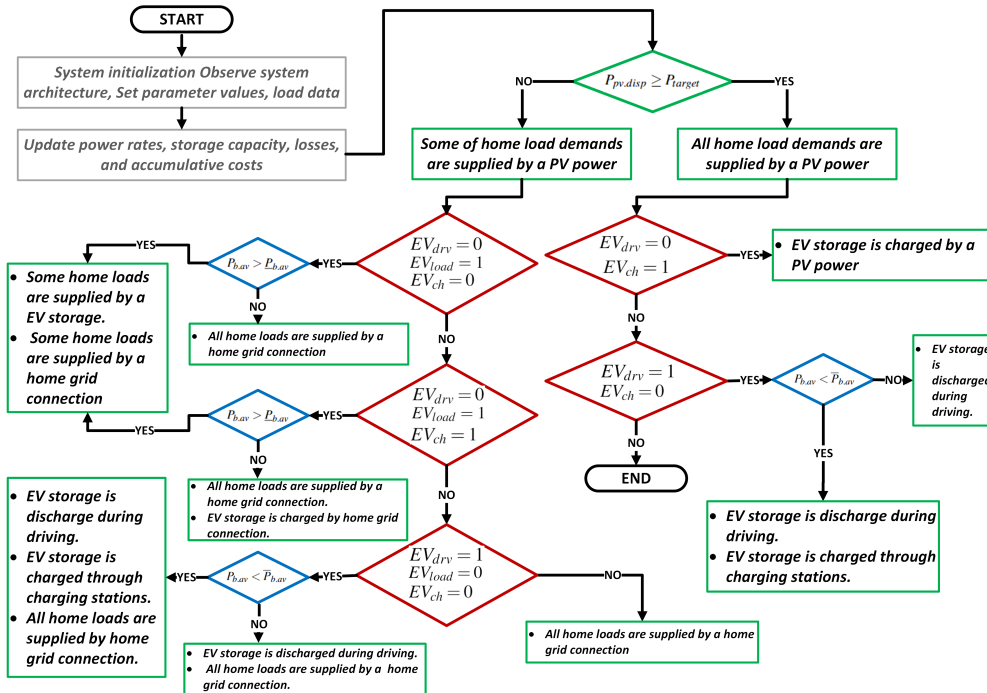


Figure 4.4: Flowchart of the conventional rule-based scheduling scheme (Conv-PEG).

binary indicators, and analyses if the electric cars can be charged at home or on the road. It is essential to note that the grid is disconnected while the battery is being charged with the unused photovoltaic (PV) energy generated at home. The battery would be charged up to its fullest capacity or until it is able to absorb as much energy from the PV as possible. This process of charging the battery with

the unused PV power generated at home provides a viable way of meeting the load needs. However, if the car is on the road, there are two possibilities. It may be able to charge itself while on the road if it comes across a charging station. Otherwise, it will continue until it runs out of charge.

In comparison to the previous choice, if the available PV capacity is less than the load demand, and the needs are partially met by the PV power, using EV storage becomes a secondary consideration if it is available for discharging as shown in Figure 4.4. While, in the worst-case scenario, the remaining unsatisfied loads are fulfilled by the grid. The grid will deliver power on a demand basis and charges according to the market price of energy. Similarly, while the EV is at home and linked to the HAPN, the EV acts as temporary storage. The home will benefit from this EV storage by balancing and providing low-cost electricity during periods of poor solar production and high grid costs. Additionally, during periods of high solar energy output, this EV may charge itself using the HAPN battery charging system.

### Scheme 3: MP-iEMS

Furthermore, the author suggests a model predictive iEMS framework with a hierarchical structure, as seen in Figure 4.1. The first step entails the development of an energy scheduler that will ensure that the net cost of energy produced is maintained as low as possible. It combines a predictive sliding window module with a rule-based decision algorithm that operates at a 15 minute sample rate, i.e.,  $t \in [1, 2, \dots, T]$ . While the sliding window maintains a 24-hour temporal resolution, i.e.,  $T \triangleq (t+24)$ . The proposed MP-iEMS is shown schematically in Figure 4.5, which illustrates the rolling horizon rule-based decision technique.

Observing the system architecture in Figure 4.5, the system parameters are set, the input data is loaded, and rolling horizon control variables are defined. The rolling horizon's current time  $t$  is then determined, and the sliding window's parameters are established. The MP-iEMS algorithm begins at each instantaneous time step by initializing the decision window's system variables and expecting fresh values for solar in-feed and load needs. Additionally, it keeps track of the battery's state of charge SOC, charging power, and capacity. The operational window is implemented using a receding horizon approach, with the next step  $t$  sliding over every 15 minutes. By using this method, it is possible to obtain the decision values for the control variables for the next whole year.

The rolling window technique has the benefit of accounting for uncertainty in PV production, EV charging connections, and changing load requirements every 15 minutes. Furthermore, the HAPN operations are optimized using the time-varying day-ahead grid power pricing. At each time step, the MP-iEMS technique resolves the scheduling issue for the whole operating window and stores the results in the database. It does, however, communicate only real-time data to the device's primary controller, which operates the device at the designated power set point. For example, in the case of a real-time disconnect between the secondary level scheduling stage and the main level device controller, the saved 24-hour window choice values may be utilized to assure HAPN functionality by using previously recorded set points in the database.

To solve the problem described in Equation 4.15, the priority criteria for getting power values from the least expensive and most dependable energy source choice is



#### 4. Home Area Power Network Design Framework and Power Scheduling Algorithms

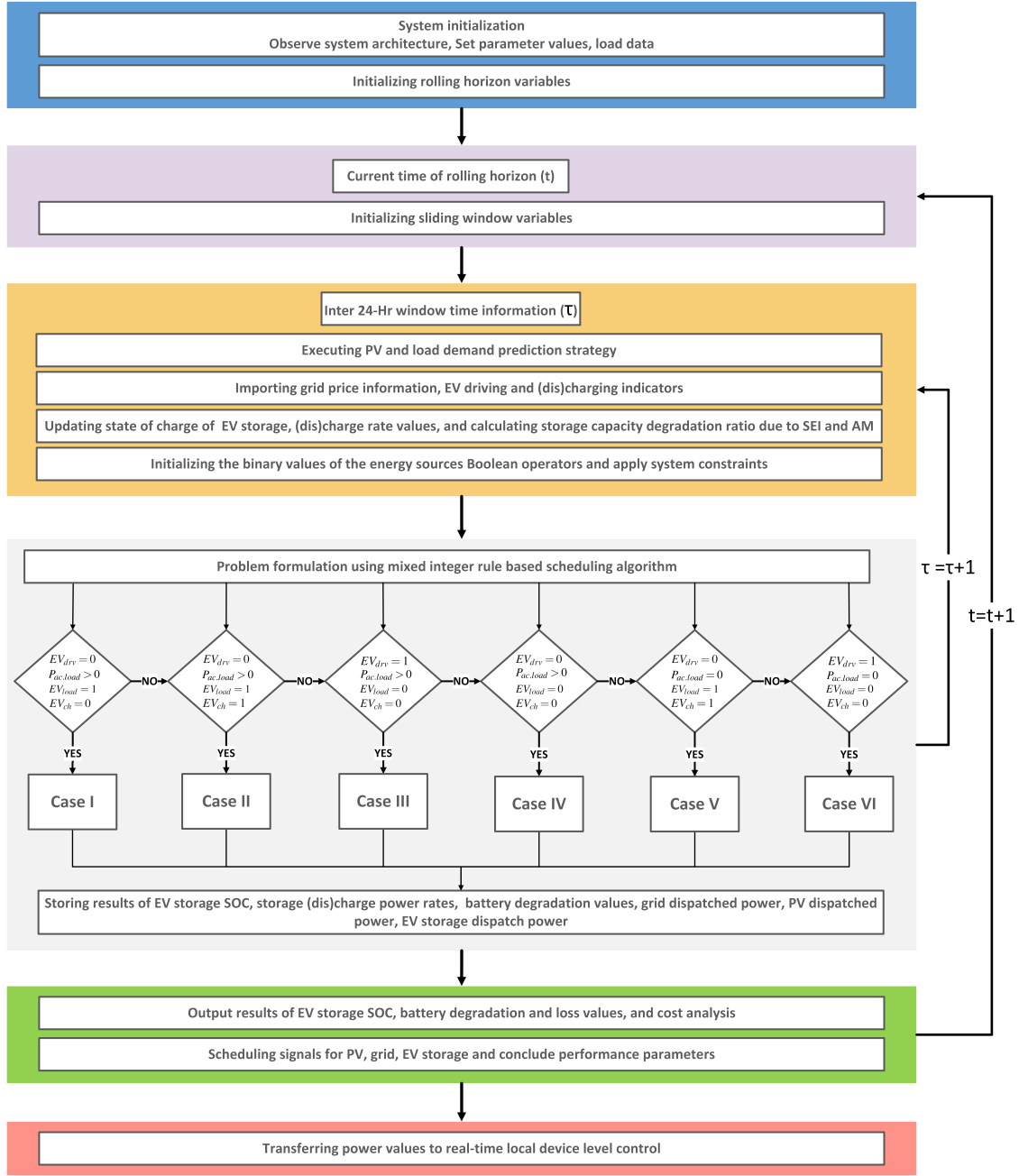


**Figure 4.5:** Flowchart of the mixed integer rule-based scheduling scheme.

introduced. The algorithm suggests alternative cases that are defined in accordance with the scenarios produced using the data set's system input parameters.

1. Case 1:  $EV_{drv}(t) = 0 \& P_{ac.load}(t) > 0 \& EV_{load}(t) = 1 \& EV_{ch}(t) = 0$ :
2. Case 2:  $EV_{drv}(t) = 0 \& P_{ac.load}(t) > 0 \& EV_{load}(t) = 1 \& EV_{ch}(t) = 1$ :
3. Case 3:  $EV_{drv}(t) = 1 \& P_{ac.load}(t) > 0 \& EV_{load}(t) = 0 \& EV_{ch}(t) = 0$ :
4. Case 4:  $EV_{drv}(t) = 0 \& P_{ac.load}(t) > 0 \& EV_{load}(t) = 0 \& EV_{ch}(t) = 0$ :
5. Case 5:  $EV_{drv}(t) = 0 \& P_{ac.load}(t) = 0 \& EV_{load}(t) = 1 \& EV_{ch}(t) = 1$ :
6. Case 6:  $EV_{drv}(t) = 1 \& P_{ac.load}(t) = 0 \& EV_{load}(t) = 0 \& EV_{ch}(t) = 0$ :

## Case I

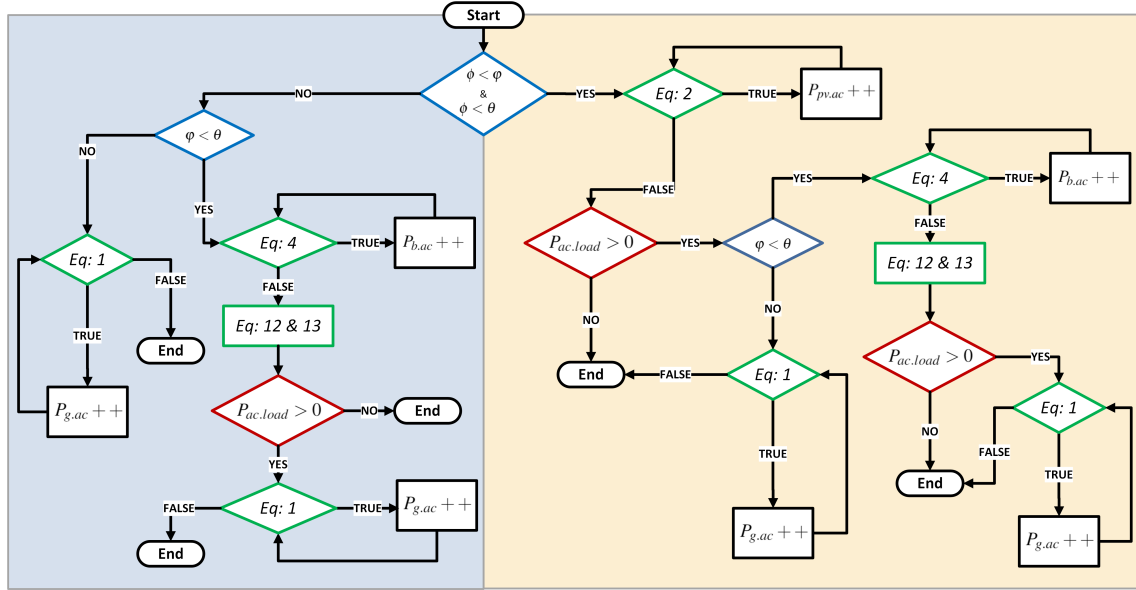


Figure 4.6: Case I flow chart.

This scenario is shown in Figure 4.6, which demonstrates that the EV is parked at home and is connected to HAPN to power the household appliances. Nonetheless, the charging function of the EV is disabled and it cannot be charged in any way; however, it may be discharged to meet load needs. Additionally, PV and grid electricity may be used to meet load needs. To determine the lowest source of energy to provide, per unit energy costs are first compared between photovoltaic (PV), electric vehicle (EV) battery, and grid power sources (i.e., guaranteeing Equation 4.15). If the cost of PV energy is the lowest, electricity is pulled from the PV source until demand is fulfilled or there is no more PV energy available. If demand continues to be high, the next power source is chosen based on its low unit cost. If the power from the battery is inexpensive and the battery's state of charge is more than the threshold, the power is received from the battery. Otherwise, in the worst-case situation, the loads are matched by grid electricity. It's important mentioning here that grid pricing are dynamic, and the cost per unit of energy might be cheaper in certain situations than the cost of PV or battery energy.

## Case II

The flow chart for the case II approach shown in Figure 4.7 illustrates that the case II strategy operates in a manner remarkably similar to case I when it comes to meeting load needs. The only difference is that the EV battery gets charged at the HAPN. As a result, the battery may be charged using photovoltaic or grid electricity. According to the flow chart, if the user's load demand is totally met by the PV power, the leftover PV power may be utilized to charge the EV until the battery is fully charged or until the PV production capacity is reached. However, if the PV power generated does not meet the battery charging needs, the grid steps in and charges the battery until it reaches its maximum capacity.

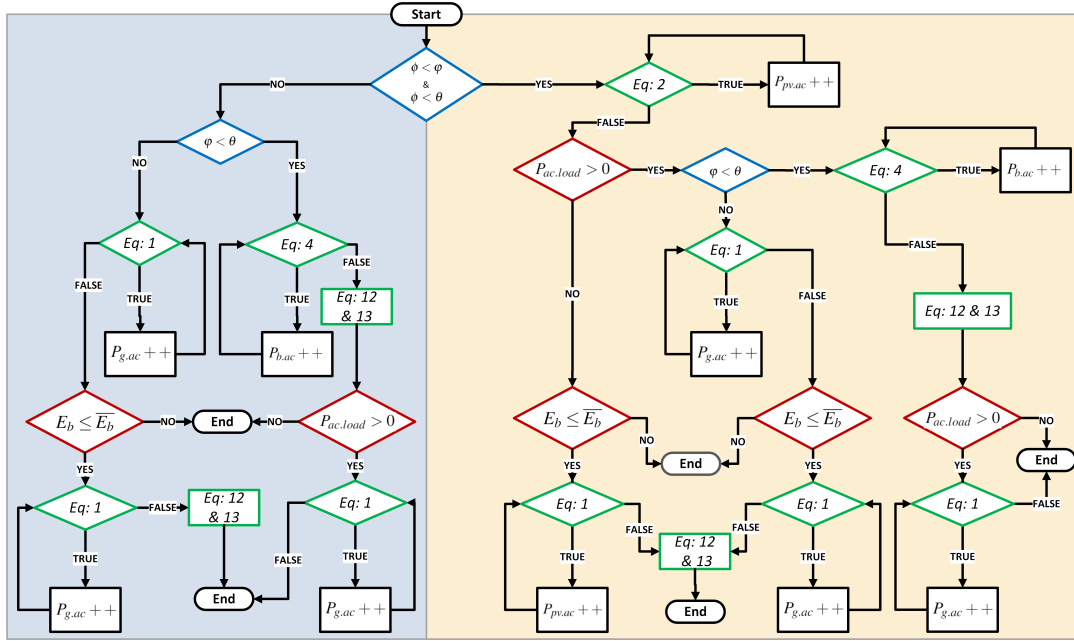


Figure 4.7: Case II flow chart.

### Case III

It illustrates the EV's drive Boolean here. This signifies that the car may drive away from the residence. As a result, it is also obvious that the EV storage would be utilized only for driving reasons. However, HAPN must first meet the household's load requirements. Thus, the choices for meeting demand include the use of photovoltaic (PV) and grid electricity. Again, depending on the cost comparison, a scheduling choice is made on whether PV or grid electricity should be used (i.e., guaranteeing Equation 4.15). Because the EV is not connected to the HAPN, there is no possibility of charging or discharging the EV storage in this circumstance. Case III's flow chart is shown in Figure 4.8.

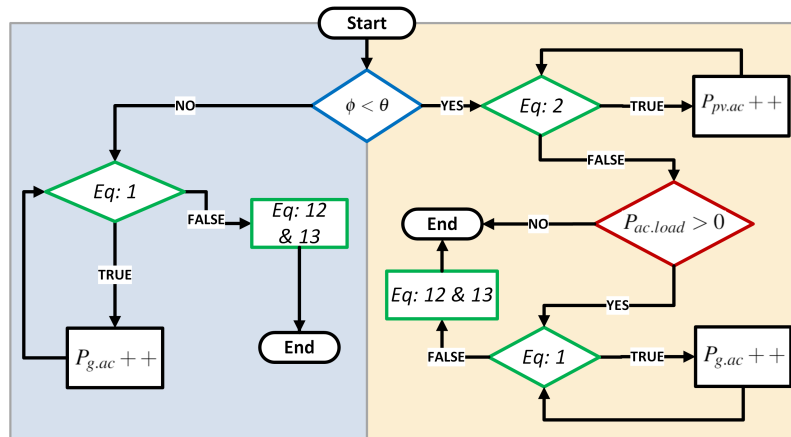


Figure 4.8: Case III flow chart.

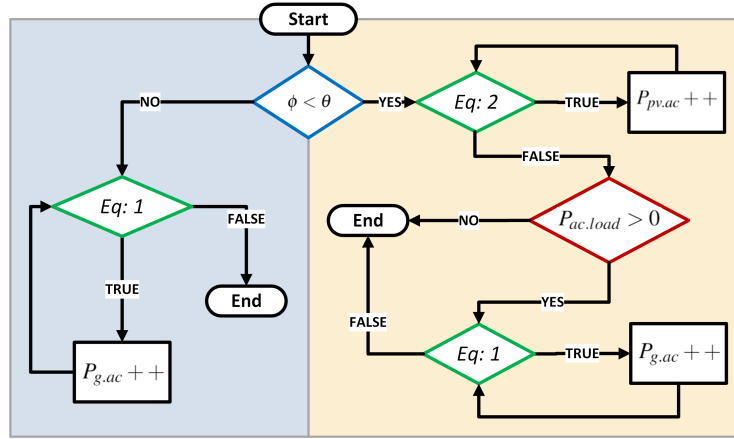


Figure 4.9: Case IV flow chart.

#### Case IV

As seen in Figure 4.9, the car is parked at home but not participating in the demand response program. This implies that the EV storage will neither charge or discharge in order to meet the HAPN's load demand needs. Thus, the EV user foregoes the option of accessing EV storage in order to meet the extra limits, i.e., to save battery life. In this situation, the user's energy demand is met by PV and grid electricity, using the least expensive scenario feasible (i.e., guaranteeing Equation 4.15).

#### Case V

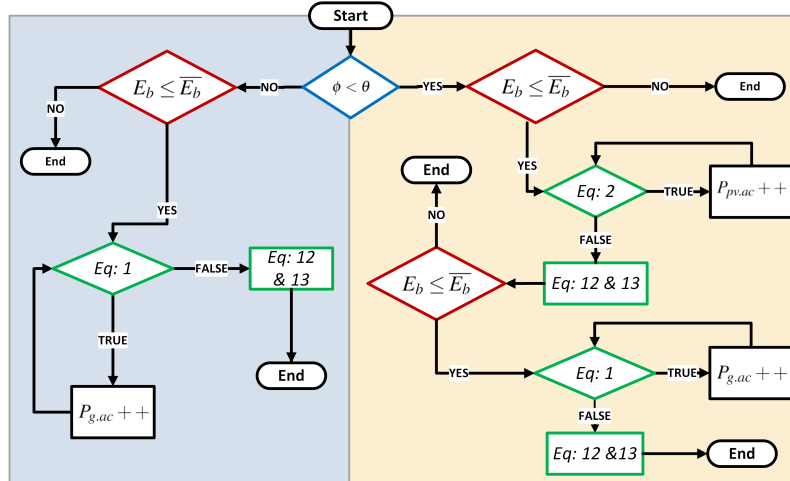


Figure 4.10: Case V flow chart.

The electric car parked at the residence is connected to the home power grid and participates in a demand response program for a HAPN in this scenario. However, as seen in Figure 4.10, there are now no user power demands to be met. However, the EV has the option of capitalizing on the scenario and charging through a low-cost power source (i.e., assuring Equation 4.15). Thus, if the cost of electricity sent from PV is cheaper and the storage is self-charging, the EV battery will be charged by the PV source until it reaches 100% capacity or the PV source is exhausted. In

the worst-case scenario, the battery may be charged completely with grid electricity at any cost.

### Case VI

Case VI in Figure 4.11 demonstrates that the EV is on the road and is solely reliant on its storage for driving. Additionally, there are no power requirements at home. As a result, if any PV power is available, it is curtailed and no grid power is required at this time.

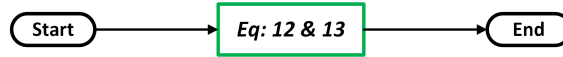


**Figure 4.11:** Case VI flow chart.

During the scheduling process, the internal nanogrid control assumes the responsibility of adjusting the active power set-points for various energy supply components. This information is passed on to the local controller of the device through a communication channel. Subsequently, the specified set-point signal is utilized as a reference signal for the device's real-time controller. The device level controller applies a robust control mechanism to continually monitor the reference signal and, based on the monitored power levels, controls the activation of the device.

### 4.3.2 Evaluation Indices

The following critical performance criteria are created to assess the system's performance and to identify the optimal mix of different energy resources:

**PV utilization factor ( $K_{PV.UF}$ )** It is the ratio of the total PV power used to meet load needs to the total PV power available. The preceding section established that the real PV power usage is always less than the available power, which is caused by converter losses. It may be expressed as follows:

$$K_{PV.UF} = \frac{\sum P_{pv.ac}(t)}{\sum P_{pv.av}(t)}. \quad (4.18)$$

**PV penetration level ( $K_{PV.PL}$ )** It is the ratio of total photovoltaic electricity utilized to meet the percentage of load demands that comprise a home's total power requirement. This may be expanded as follows:

$$K_{PV.PL} = \frac{\sum P_{pv.ac}(t)}{\sum (P_{ac.load}(t) + P_{ac.b}(t))}. \quad (4.19)$$

**Grid utilization factor ( $K_{G.UF}$ )** It is the ratio of the total grid power used to meet load demands to the total grid power available. The preceding section revealed that real grid power use may be less than what is available, owing to HAPN's request. It may be expressed as follows:

$$K_{G.UF} = \frac{\sum P_{g.ac}(t)}{\sum P_{g.av}(t)}. \quad (4.20)$$

**Grid penetration level ( $K_{G.PL}$ )** It is the ratio of total grid power utilized to meet the fraction of load needs that are smaller than the total power demands of a residence due to the usage of solar and electric vehicle batteries. This is stated as follows:

$$K_{G.PL} = \frac{\sum P_{g.ac}(t)}{\sum (P_{ac.load}(t) + P_{ac.b}(t))}. \quad (4.21)$$

**EV storage utilization factor ( $K_{EV.UF}$ )** The ratio of the total energy discharged from an electric vehicle's storage system to satisfy household energy needs in relation to the entire storage capacity and the power charged in the battery is quantified. The preceding section established that the actual storage power use in HAPN is always smaller than the available storage power. This is because of the losses incurred as a result of conversion losses. Additionally, the majority of energy is used for driving purposes. It may be expressed as follows:

$$K_{EV.UF} = \frac{\sum \eta_{b.con}^{-1} P_{b.ac}(t)}{\sum (P_{b.av}(t) + \eta_{b.con} P_{ac.b}(t))}. \quad (4.22)$$

**EV storage penetration level ( $K_{EV.PL}$ )** It is the ratio of the total discharge power from the EV storage to the fraction of load demands met by the EV storage. This may be expanded as follows:

$$K_{EV.PL} = \frac{\sum \eta_{b.con}^{-1} P_{b.ac}(t)}{\sum P_{ac.load}(t)}. \quad (4.23)$$

**Degree of self-sufficiency ( $K_{SS}$ )** The percentage of total energy demand met by PV and EV storage is described as the degree of self-sufficiency and is expressed as;

$$K_{SS} = \frac{\sum (P_{load}(t) - P_{g.ac}(t))}{\sum P_{ac.load}(t)}. \quad (4.24)$$

## 4.4 A Case Study

A simple HAPN is utilized to show the true potential of the suggested MP-iEMS approach. According to [164], the algorithm is given input data from a real-world yearly data set of (dis)charging of EV storage, solar power, and grid energy pricing. It then calculates the actual output power of each energy source entity. Additionally, scheduling decisions are determined by the use of a mixed-integer rule-based decision-making technique. The following Table 4.2 highlights the parametric values associated with the different power entities in our system model.

**Table 4.2:** System parameters.

| Parameters        | Value   | Parameters      | Value      | Parameters        | Value        |
|-------------------|---------|-----------------|------------|-------------------|--------------|
| $P_{g.disp}$      | 20 kW   | $\eta_{b.con}$  | 0.98       | $\Delta t$        | 15 min       |
| $E_{b,0}$         | 110 kWh | $\eta_{pv.con}$ | 0.98       | $\Delta k$        | 1 s          |
| $\bar{E}_b$       | 120 kWh | $\phi$          | 130 \$/MWh | $\bar{P}_{b.ch}$  | Dynamic [72] |
| $\underline{E}_b$ | 1 kWh   | $\varphi$       | 201 \$/MWh | $\bar{P}_{b.dch}$ | Dynamic [72] |

While scheduling, the cost of different ESEs is taken into account for the best output. The cost parameter that is most essential is the dynamical grid energy cost, which fluctuates with time  $t$ . Additionally, the characteristic parameters affecting the deterioration of the EV battery bank as modelled in Section 4.2.2 are listed in Table 4.3.

**Table 4.3:** The simplified reduced-order battery model’s coefficients.

| Parameters | Value    | Unit                 | Parameters  | Value                | Unit  |
|------------|----------|----------------------|-------------|----------------------|-------|
| $k_{SEI}$  | 6684.8   | $\sqrt{\frac{1}{s}}$ | $E_{SEI}$   | 39,146               | J/mol |
| $k_{AM}$   | 1.368    | 1/Ah                 | $E_{AM}$    | 39,500               | J/mol |
| $R$        | 8.314    | J/K·mol              | $\lambda$   | $5.5 \times 10^{-5}$ | -     |
| $F$        | 96,485.3 | C/mol                | $U_s^{OCP}$ | 0.4                  | -     |

The proposed MP-iEMS is meant to illustrate the scheduling framework’s reaction across a time horizon of 15min for 24 hours. The algorithm that optimizes for cost also optimizes for self-consumption and self-sufficiency of a HAPN. PV and user load demand forecasting are critical components of the overall process. Additionally, minimum and maximum energy restrictions are defined to create a realistic operating range for energy supply and demand entities.

#### 4.4.1 Data Preparation

Rheinberger et al. [164] has provided the whole dataset for one year utilized in the simulations. It is subdivided into the following subsets:

- Day-ahead energy market prices for the bidding zone Germany-Austria-Luxembourg [49]
- Photovoltaic production in a localized place in Germany [139]
- Photovoltaic production prediction [52]
- Electric vehicle usage from UK [45]
- Household demand from Ireland [40]

#### 4.4.2 Comparative Analysis of Power Scheduling Scenarios

The author has investigated the performance of the suggested scheduling method over a variety of time domains. It examines daily, monthly, and year scenarios, noting how scheduling choices are made and their effect on aggregated cost projection.

The system model is similar to that provided in Section 4.2, except that the PV is connected with HAPN, which operates as a very inexpensive source of energy and is therefore prioritized for energy distribution. However, in rare circumstances when the cost of electricity from the grid is less than the cost of operating the photovoltaic system, the photovoltaic system will be unplugged. Similarly, while the EV is at home and linked to the HAPN, it acts as a temporary store for the HAPN. This EV storage will aid HAPN in balancing and delivering inexpensive power during times of low solar production and high grid prices. If there is surplus power generated

after the solar array has met the demand, it will be utilized to charge the battery bank.

### Daily analysis

Author chooses two random days throughout the year to demonstrate the suggested scheduling strategy in this case. A time step of 15 *min* is chosen, which means that the scheduling analysis is conducted for each 15 *min*. At each time step, a fresh forecasting is made for the next complete day, and the results for the next 24 hours are stored in the database. Unless the algorithm fails or the secondary HEMS is detached from the main device level control, a day-ahead decision values are used in HAPN for different control entities.

Additionally, a predictive energy demand model is integrated that calculates the correct amount of energy necessary for a household's energy use. Figure 4.12 illustrates the total energy consumption with a temporal granularity of 15 *min*. It displays how drastically energy needs shift during the day. It considerably rises just before and throughout the day, as a result of the activation of high-power loads. The energy demand model is based on aggregated data from all loads engaged at any point in time  $t$ , and it scales up to about 1.5 *kW*.

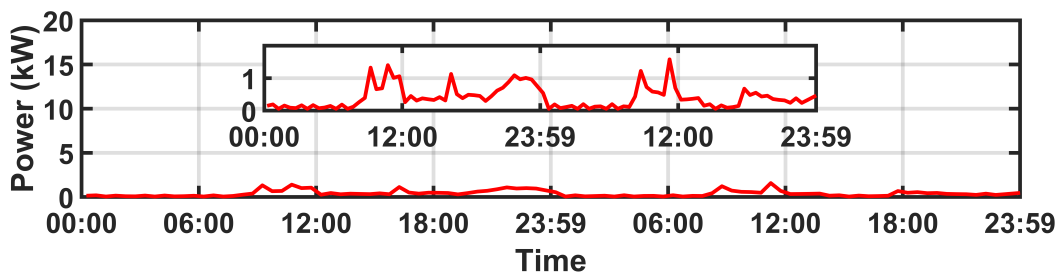


Figure 4.12: Predicted load demands.

Additionally, the availability of photovoltaic energy is represented in Figure 6.9, which shows a daily peak around midday. The greatest photovoltaic power generated is around 0.8 *kW*. Notably, the actual output power of the photovoltaic module may

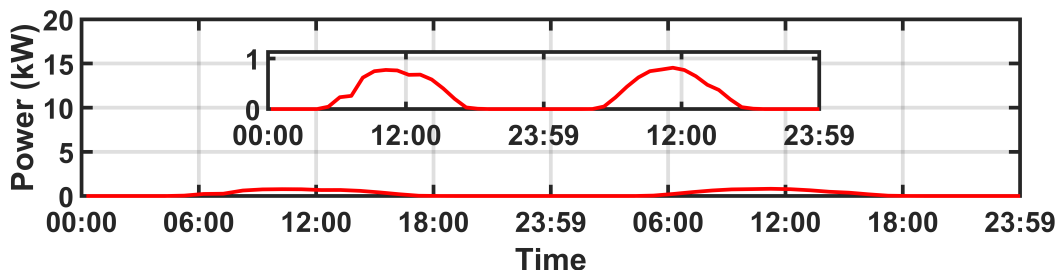


Figure 4.13: Predicted PV power.

be less than the rated power.

Additionally, Figure 4.14 depicts the varying SOC of the EV storage in green during a two-day period. The blue and red lines illustrate the dynamics of storage's charging and discharging power rates. Additionally, discharge may occur as a result of power dissipation during vehicle driving on the road or during the transmission



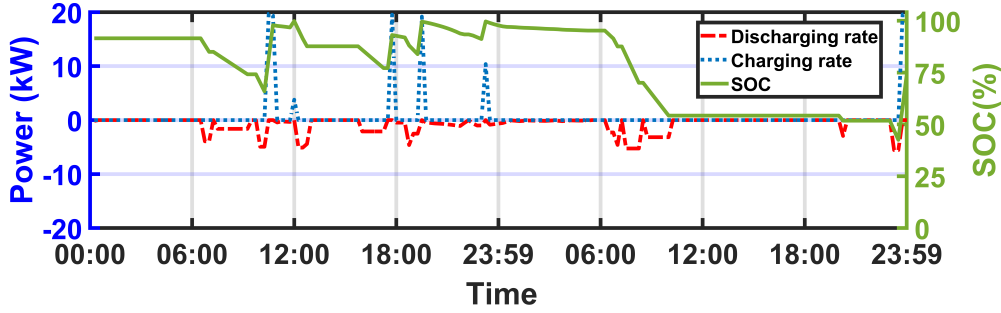


Figure 4.14: EV (dis)charge rates and SOC.

of energy to a dwelling. The initial level of charge indicates that the EV’s storage capacity is roughly 80 %, which begins to deplete after 06:00 due to battery drain. This discharge occurs when the vehicle’s storage is utilized for road travel, as demonstrated in Figure 4.15. The green driving indication on the car comes from the data set [45, 164], which also includes deterministic power levels utilized by the vehicle throughout the voyage. The vehicle usage indication, as seen in the image, is distributed throughout the day and represents the vehicle’s activity from dawn to night, although morning seems to be busier. The EV’s power consumption is determined by the driver’s behavior. The greatest amount of electricity used by the car while draining its battery is around 5 kW, as specified in the suggested dataset [45]. During driving intervals, the vehicle’s indicator often indicates that it is in

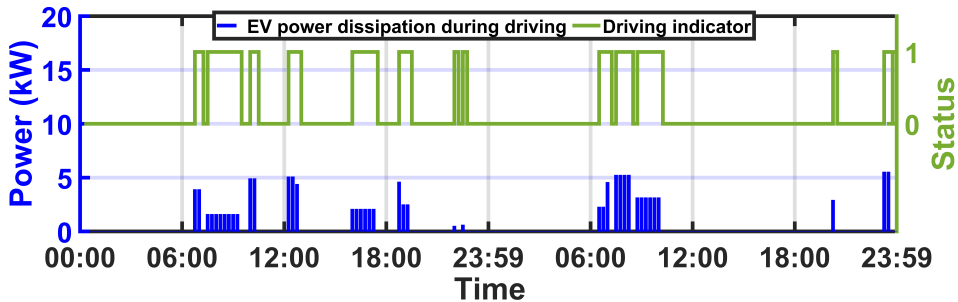


Figure 4.15: Driving indicator and EV power dissipation.

a stationary position. The length of this position fluctuates, suggesting that the car is sometimes parked at home and sometimes outdoors. However, if it is parked at home, there is a greater likelihood that it is connected to the HAPN. Thus, it may charge or discharge itself through the HAPN by employing its access power to meet home load needs or by charging itself during periods of high or low grid energy costs, respectively. Again, the (dis)charging status is determined using the previously gathered information, which includes the time and length of the EV’s connection to the grid. The EV loading indicator in Figure 4.16 reveals if the EV storage is sufficiently charged to meet the household’s needs. Thus, our system determines whether or not to drain the battery depending on certain pre-defined criteria and indicators. According to the data obtained after executing the algorithm, the battery is preferably to drain during sometimes in the day and later at night when grid energy costs are high, as seen in Figure 4.14, and Figure 4.16. However, the next day, there is no discharge for homes since the battery loading status is inactive, indicating that the vehicle has been out of use for the whole day, as verified by the

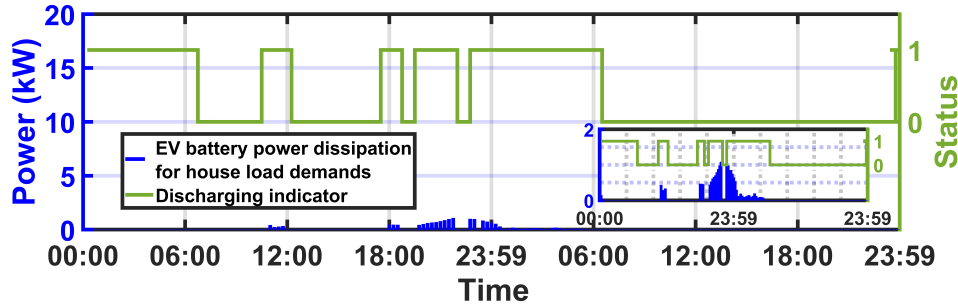


Figure 4.16: Discharging indicator and EV discharge rates.

signs in Figure 4.15. The highest discharge rate required to power the residences shown in the illustration is around  $1kW$ . This indicates that the home load needs are much lower than the vehicle's power consumption when traveling.

Additionally, there is another method of charging the battery while the car is parked at home and the charging state for the EV storage is active. The pace at which the EV storage is charged is shown in Figure 4.17, assuming the car is parked at home and connected to the HAPN. The charging indication provided by [45, 164] is depicted in Figure 4.17, which indicates the time and duration of the EV's self-charging using solar or grid electricity. Due to the restricted capacity of the storage, the charge and discharge rates are relatively limited. Additionally, a pre-condition for utilizing EV storage at home is set at 50 % of SOC. This ensures that there is sufficient storage for the EV to be driven on the road. When connected to the grid,

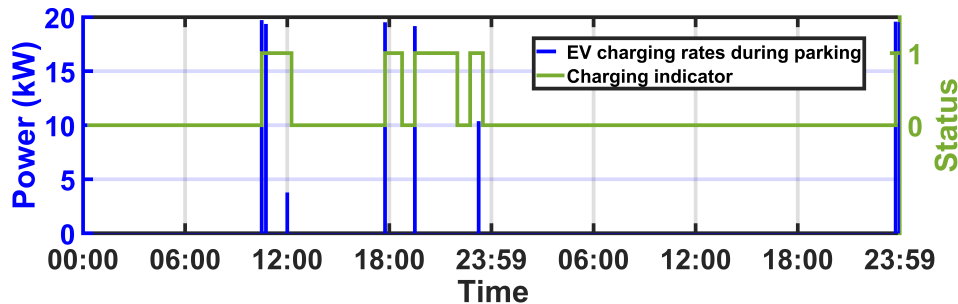


Figure 4.17: Charging indicator and EV charge rates.

the EV storage may charge itself instantly upon receipt of the charging signal. This is due to the low SOC, which occurs around midday and in the evening on the first day, as already seen in Figure 4.14. However, since the car is not at home on the second day, there is no charge sign for that day. The maximum power available to charge the battery is about  $20 kW$ , which is the maximum amount of grid electricity available at any moment  $t$ . Before the next day, when the car is scheduled to travel for the whole day, the battery's state of charge is fully established over 90 %.

Additionally, a conceptual model of battery degradation created in Section 4.2 illustrates the percentage capacity deterioration during time of use and is shown in Figure 4.18. Additionally, Figure 4.19 depicts the two-day power pricing data obtained from [49, 164]. Energy companies often determine these prices for their customers. So that customers may take advantage of the shifting energy prices and buy energy when it is most convenient for them. Additionally, the same picture demonstrates the activation of numerous ESEs. The recommended scheduling

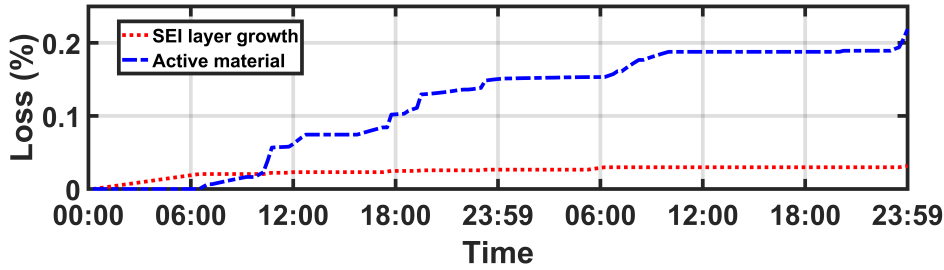


Figure 4.18: EV battery capacity loss.

strategy determines the activation mechanism to use. A decision-based cost minimization problem is devised that takes into account changing energy grid prices and a range of system constraints, including capacity limitations on power sources. Our scheduling algorithm assessed the lowest practical power cost and made the greatest use of available energy resources by using the different planned scenarios. It lets one to use the ideal combination of ESEs at any moment in time  $t$ .

As seen in this illustration, the grid supplies electricity, especially in the afternoon and evening. This is because the PV system is currently unable to satisfy energy needs, and the EV battery is being charged to guarantee that adequate power is available to run the vehicle. When the EV storage is quite fully charged and grid energy prices are fairly high, however, the EV storage is also utilized in combination with the grid (i.e., around 12:00 and between 09:00 and 23:00 on the first day). Furthermore, photovoltaic energy is entirely used throughout the day. The high grid power input is used to charge electric car storage, which costs around 20  $kW$ .

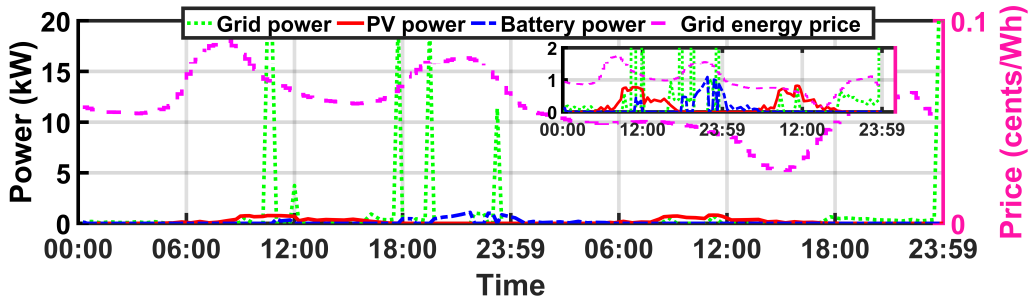


Figure 4.19: a) Electricity prices. b) Power mix by various ESEs.

Similarly, Figure 4.20 depicts the utilization factor (UF), penetration level (PL), and cumulative energy shares of several ESEs integrated into HAPN.

Additionally, as seen in Figure 4.21, the scheduling strategy balanced the required and generated energy in the manner specified in Equation 4.17. All loads are met adequately using an intelligent power mix. The scheduling of different ESEs is performed via the development of a cost-cutting plan. The scheduling system activates energy sources that are economically equal at any point  $t$  in time.

### Monthly analysis

To illustrate the seasonal fluctuations in the given dataset of the load profile, PV-system, and the consequence of our proposed algorithm, one month from each season

| Parameters  | Value  |
|-------------|--------|
| $K_{PV.UF}$ | 0.6990 |
| $K_{G.UF}$  | 0.0300 |
| $K_{EV.UF}$ | 0.0693 |
| $K_{PV.PL}$ | 0.1644 |
| $K_{G.PL}$  | 0.7559 |
| $K_{EV.PL}$ | 0.0801 |
| $K_{SS}$    | 0.2441 |

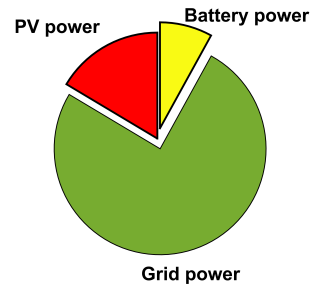


**Figure 4.20:** a) ESEs utilization factor (UF). b) Energy shares.

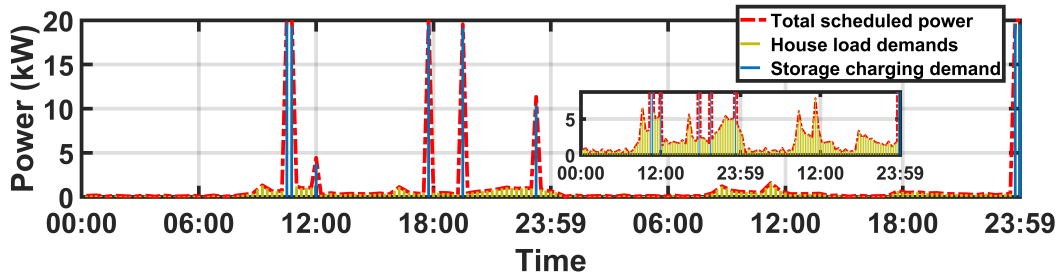


**Figure 4.21:** Total load demands and the scheduling power.

of a year is chosen. In this scenario, the system model stays constant as discussed before in the daily analysis.

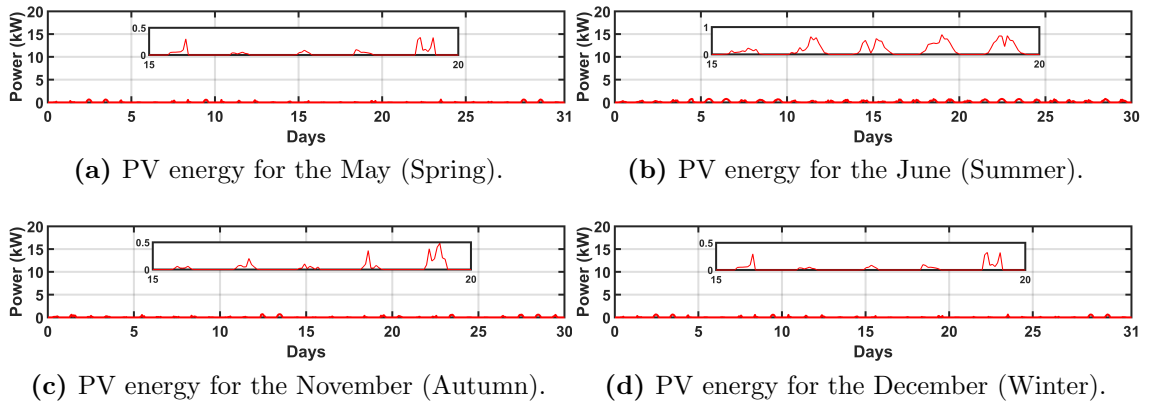


**Figure 4.22:** Seasonal comparison of PV power generation.

The Figure 4.22 compares the monthly PV estimated power output for four distinct seasons. It demonstrates that throughout the summer, solar power peaks at  $1 \text{ kW}$ . Then comes Spring and Autumn. Finally, winter is the poorest season for solar energy production, with the lowest peaks.

The Figure 4.23 depicts an average household's expected seasonal load requirements. In contrast to PV production, load demand is strong in the summer as well as the winter, with peaks above  $8 \text{ kW}$  and significant month-to-month volatility in load. Whereas the first half of Winter has a steady load curve, the second half has greater dynamic loads. Then comes Autumn and Spring, with peaks of up to  $5 \text{ kW}$  and a very steady pattern throughout the month.

#### 4. Home Area Power Network Design Framework and Power Scheduling Algorithms

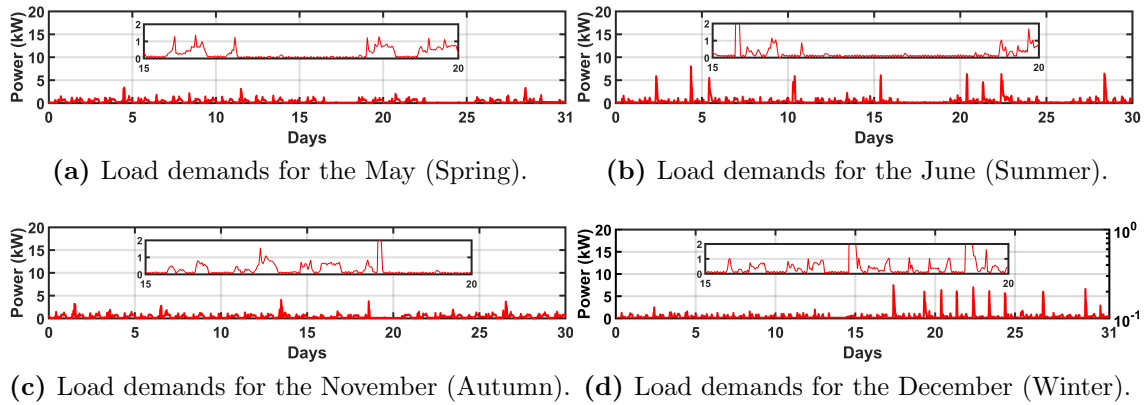


**Figure 4.23:** Seasonal comparison of users' load demands.

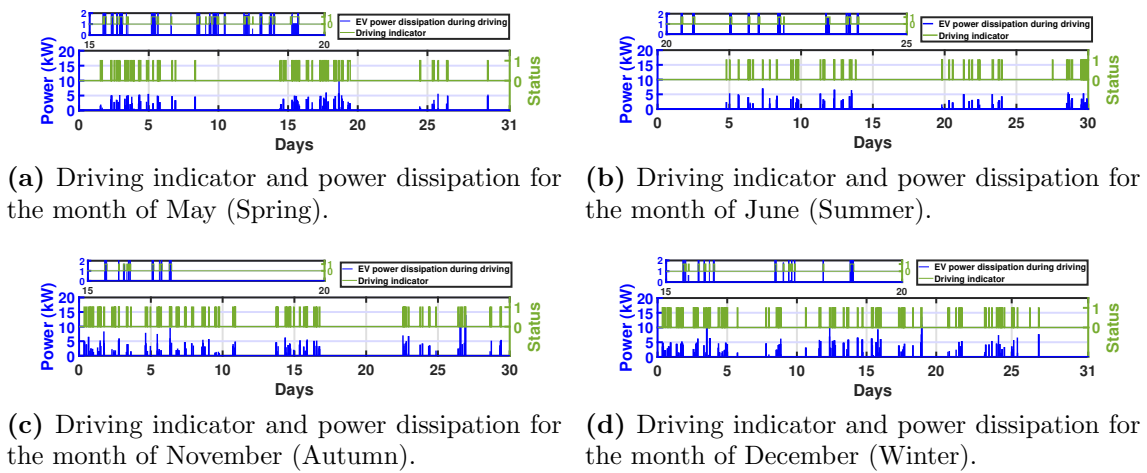


**Figure 4.24:** Seasonal comparison of driving indicator and EV power dissipation.

The Figure 4.24 illustrates the behavior of an EV driver throughout each of the four seasons. Additionally, it specifies the quantity of energy expended throughout each journey. Autumn and Winter seem to have a higher number of driving excursions, with peak dissipated power exceeding  $10\text{ kW}$ . In comparison to Spring and Summer, these seasons provide a greater number of high-peak road excursions. Summer is the least-utilized season for EVs, with the highest power dissipation from the EV battery hardly exceeding  $5\text{ kW}$ . However, in the spring, power dissipation is consistent for virtually all excursions except those above  $10\text{ kW}$ . Thus, as seen in the image, Autumn and Winter are extremely variable seasons for using EVs for road trips, requiring higher EV power for driving.

Additionally, Figure 4.25 illustrates the EV power discharge indicators and the home power rates. Autumn and Winter continue to have a high number of discharging power. This indicates that EV storage has been heavily used during the last months. One cause for this might be the lack of surplus photovoltaic electricity during these seasons, as opposed to the Spring and Summer seasons. However, the power dissipated by EV storage is relatively low in Autumn and Winter, when peak power consumption reaches  $500\text{ W}$  and  $1000\text{ W}$ , respectively. Whereas in the spring and summer, peak power is  $8\text{ kW}$  and  $4\text{ kW}$ , respectively. Thus, it is obvious from the comparison that in Autumn and Winter, the EV store is discharged more often

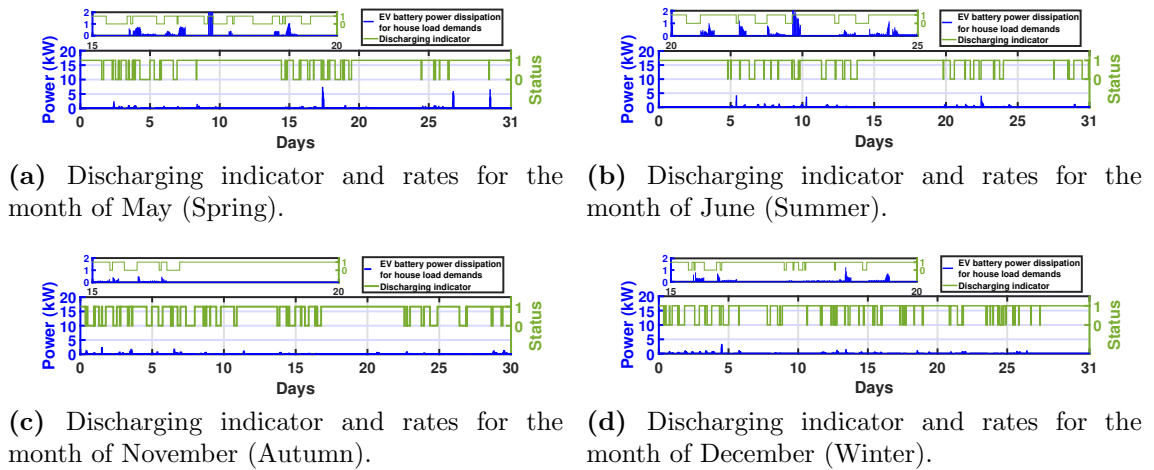


**Figure 4.25:** Seasonal comparison of EV battery discharge indicator and their power rates.

with lower power peaks than in Spring and Summer, when the storage is discharged less frequently but with higher peaks.

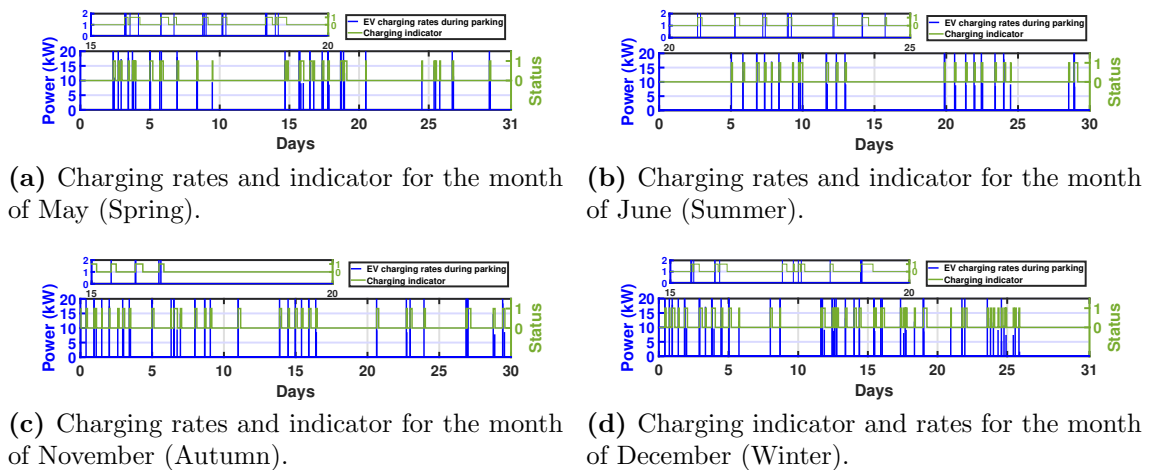


**Figure 4.26:** Seasonal comparison of EV battery charging rates and the indicators.

The Figure 4.26 compares the charging indicators and charging power rates for each of the four seasons. As is the case with discharge signs, charging states are also elevated in Autumn and Winter. Clearly, the number of discharges was large throughout these seasons, and the number of charges should have been as high to compensate. However, in virtually all circumstances, the EV storage must be charged using grid power, and grid in-feed is capped at  $20\text{kW}$  for a home. Thus, the maximum power output is restricted to a maximum of  $20\text{kW}$  for each charge. The Figure 4.27 compares the state of charge (SOC) of an EV battery over all four seasons. Winter and Autumn have more volatile SOC changes owing to the increased frequency of charging and discharging cycles, as seen in previous figures. Generally, the depth of discharge reaches 50 % of the capacity, except in the Autumn, when the battery discharges to its full capacity owing to prolonged high discharge while road driving. Summer's SOC stays at 60 % for an extended period of time because to the absence of charging, discharging, and driving signs during this time period.

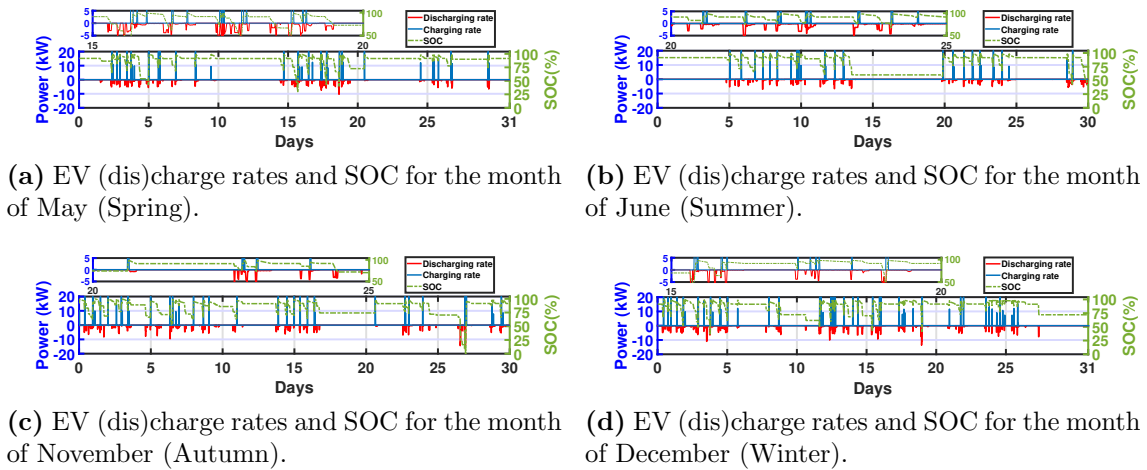


**Figure 4.27:** Seasonal comparison of EV (dis)charge rates and their SOC.

Perhaps it refers to certain holiday seasons. The Figure 4.28 provides a comparison

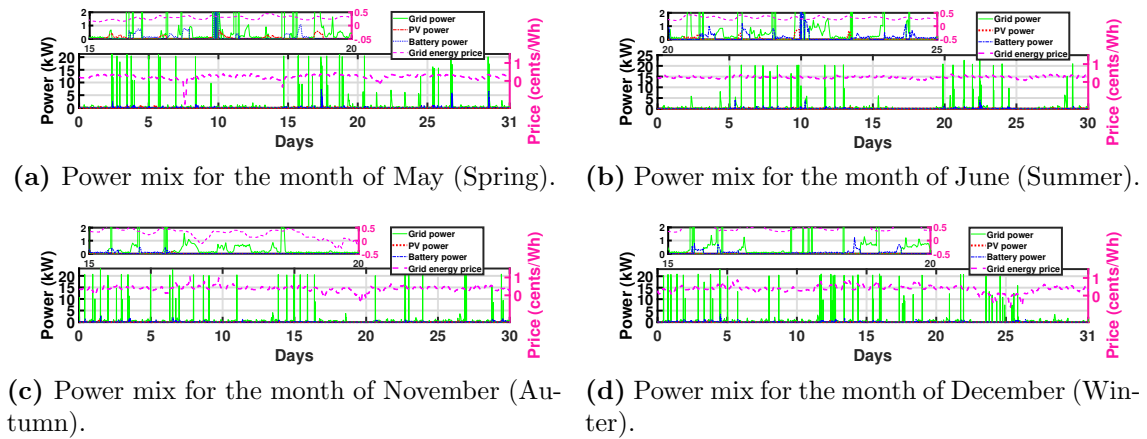


**Figure 4.28:** Seasonal comparison of power mix.

of the various power sources used to meet a household’s load needs. Additionally, grid energy price indications are shown here. Prices fluctuate continually during the season, although the fluctuating behavior is almost consistent throughout all seasons. The average price stays about 0.05 *cents/Wh* throughout the year, with the exception of Spring, which has a negative high. Perhaps this is owing to the high level of renewable energy output at the moment. In Autumn, around the 20<sup>th</sup> day, and in Winter, around the 25<sup>th</sup> day, a somewhat tiny negative surge may also be noted. One may see more grid activity on this day of Winter as a result of low-cost power availability, which is also contingent upon load needs, and as previously said, load demands are quite high in the second half of Winter.

Additionally, by zooming into the figures’ magnified window, one can view the power mix of PV, grid, and EV batteries used to meet the load needs of a dwelling. This combination is derived by the suggested MP-iEMS, which takes into account the cost of various energy sources. This figure makes the most sense when seen in conjunction with Figure 4.29, which depicts the energy shares of different sources for a given season.

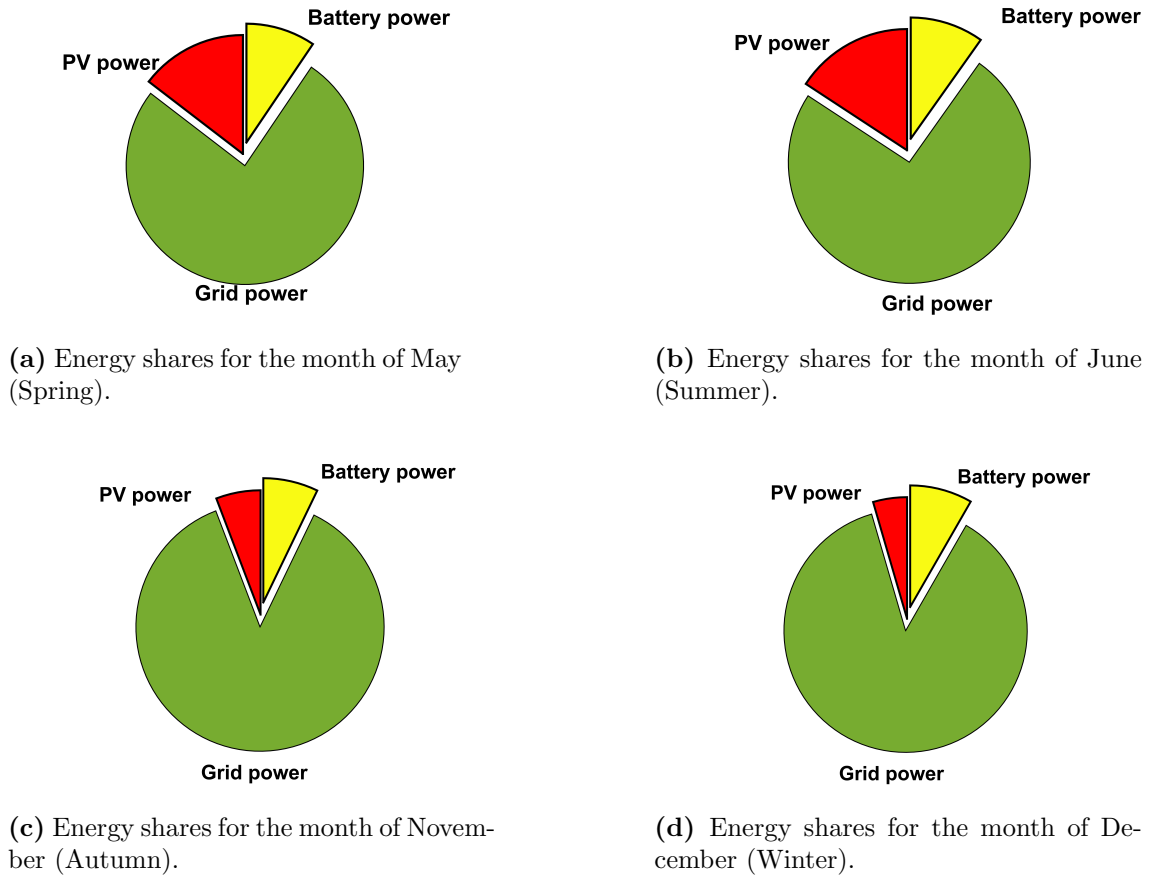


**Figure 4.29:** Seasonal comparison of energy shares.

The Figure 4.30 compares the proportion of battery loss by season. This implies that the EV storage suffers the greatest loss percentage in December, when the battery is most often used for driving the vehicle and hence charged most frequently. As a consequence of the high consumption of battery cycles, the SEI layer grows rapidly in storage, resulting in rapid capacity loss. Then come Spring and Autumn, and finally Summer, when EV storage use is at its lowest. The battery's overall capacity loss is more than 2% during the Winter season, 2% during the Spring and Autumn seasons, and 1.65% during the Summer season.

While looking at Table 4.4, one can notice that Winter has the highest PV usage factor, followed by Autumn, Spring, and Summer. This is because PV power output is lower in the winter and autumn, and the PV system is more heavily used during these seasons. Winter, on the other hand, has the highest grid use, followed by Autumn, Spring, and Summer. Due to the limited amount of solar energy generated, grid electricity is in great demand throughout the winter and autumn. Additionally, Summer has the highest EV use factor, followed by Spring, Winter, and Autumn.

Additionally, PV penetration is highest in the summer and lowest in the winter owing to seasonal fluctuations in PV production. Additionally, the degree of grid penetration is greatest in the winter and lowest in the summer. This is because in the summer, the majority of loads are provided by RESs, whilst in the winter, the reverse is true. Similarly, EV penetration is highest in the summer and lowest in the winter. Additionally, the HAPN is most self-sufficient in the Summer, followed



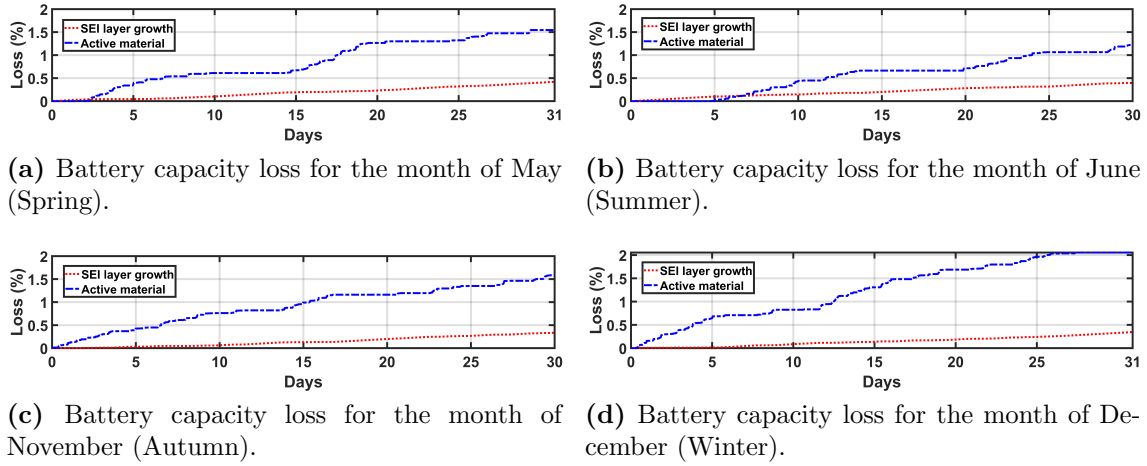


**Figure 4.30:** Seasonal comparison of battery capacity loss.

**Table 4.4:** Seasonal comparison of ESEs utilization factor (UF) and penetration level (PL).

| Parameters  | Spring Values | Summer Values | Autumn Values | Winter Values |
|-------------|---------------|---------------|---------------|---------------|
| $K_{PV,UF}$ | 0.6017        | 0.6619        | 0.7919        | 0.7942        |
| $K_{G,UF}$  | 0.8622        | 0.7527        | 0.9928        | 1.0578        |
| $K_{EV,UF}$ | 0.1969        | 0.2337        | 0.1383        | 0.1422        |
| $K_{PV,PL}$ | 0.1460        | 0.1579        | 0.0580        | 0.0451        |
| $K_{G,PL}$  | 0.7600        | 0.7445        | 0.8710        | 0.8726        |
| $K_{EV,PL}$ | 0.0947        | 0.0983        | 0.0716        | 0.0830        |
| $K_{SS}$    | 0.2400        | 0.2555        | 0.1290        | 0.1274        |

by the Spring. While Winter is the coldest season, Autumn is the warmest. This is because RESs are used at a higher rate during the summer and at a lower rate during the winter.

### Yearly analysis

A annual study is performed to determine the total power mix from all power sources and the algorithm’s ability to handle massive amounts of data. The utilization and penetration levels of the various energy sources, as well as their respective energy shares, are shown in Figure 4.31 for the whole year. Similarly, an investigation of EV storage capacity loss reveals a total loss of capacity of 14 % over a one-year period, as seen in Figure 4.32. This loss study is performed physically using the battery model data provided from [82].

Within the scope of supply side management, we have examined and compared the operating expenses of various energy supply entities. We chose three distinct operating strategies to compare for the best outcomes. Among these are: (1) Scheme 1: Conv-EG, (2) Scheme 2: Conv-PEG, and (3) Scheme 3: MP-iEMS.

Schemes 1 and 2 represent greedy priority-based algorithms. In which attention is given to a low-cost energy source such as PV and EV storage. Scheme 3, on the other hand, makes use of intelligence by anticipating future changing grid energy

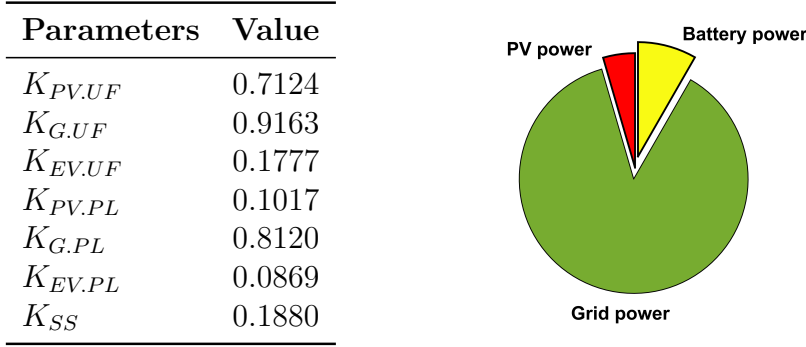


**Figure 4.31:** a) ESEs utilization factor (UF) and penetration level. b) Energy shares for whole year.

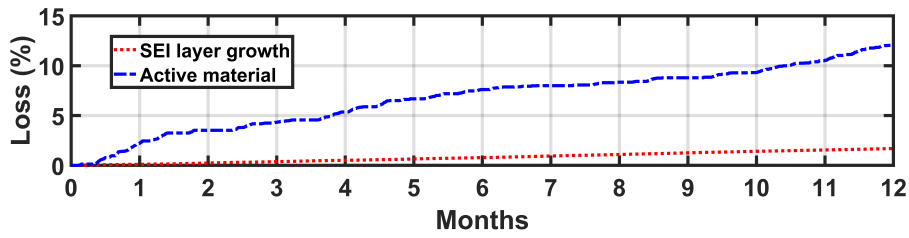


**Figure 4.32:** Yearly battery capacity loss.

costs and optimizing the capacity usage of EV storage and the PV source. All of these techniques provide for the required power to be accessible from any supply entity at the lowest feasible cost, while also ensuring maximum comfort for energy users by meeting their demands with their immediate energy requests, as indicated in Equation 4.17.

Initially, an examination of several performance measures is presented that are previously mentioned in Section 4.3.2. Table 4.5 compares the indices for various ESEs among various optimum schemes.

**Table 4.5:** Comparison of ESEs utilization factor (UF) and penetration level (PL) for various schemes.

| Scheme / Parameters  | $K_{PV,UF}$ | $K_{G,UF}$ | $K_{EV,UF}$ | $K_{PV,PL}$ | $K_{G,PL}$ | $K_{EV,PL}$ | $K_{SS}$ |
|----------------------|-------------|------------|-------------|-------------|------------|-------------|----------|
| Scheme 1: (Conv-EG)  | 0           | 0.0307     | 0.9597      | 0           | 0.8598     | 0.4198      | 0.1402   |
| Scheme 2: (Conv-PEG) | 0.6634      | 0.0268     | 0.9598      | 0.1129      | 0.7639     | 0.4098      | 0.2361   |
| Scheme 3: (MP-iEMS)  | 0.6272      | 0.0269     | 0.9579      | 0.1175      | 0.8447     | 0.3533      | 0.1553   |

It shows that the typical optimum scheme that does not incorporate PV has a high grid utilization factor ( $K_{G,UF}$ ) and penetration level ( $K_{G,PL}$ ) when compared to other schemes, which is understandable. Nevertheless, the grid usage factor for Schemes 2 and 3 is nearly the same. However, the grid penetration level in Scheme 2 is high, indicating that Scheme 3 uses grid electricity a slightly less than Scheme 2. Furthermore, the PV usage factor ( $K_{PV,UF}$ ) in Scheme 2 is high, even though the penetration level ( $K_{PV,PL}$ ) in both schemes is very similar. It demonstrates that in Scheme 3, when grid prices are negative, as shown in Figure 4.28a, the MP-iEMS algorithm disconnects the PV and instead obtains energy from the grid. This would

also reduce energy conversion losses from DC to AC, thereby increasing the shelf life of PV modules. Furthermore, the EV usage factor ( $K_{EV,UF}$ ) is about identical for Schemes 1 and 2, while it is somewhat lower in Scheme 3. Similarly, the penetration level of the EV storage ( $K_{EV,PL}$ ) is also lower in Scheme 3, which indicates that the MP-iEMS algorithm engages the EV operations sporadically in comparison to Scheme 2. In this way, the storage has been utilized more efficiently. In comparison, the self-sufficiency indicator ( $K_{SS}$ ) is high in Scheme 2, where the operations of PV and EV storage are involved more often. However, due to the optimal and efficient utilization of PV and EV storage, this factor is less in Scheme 3 while it is at its lowest in Scheme 1 due to the absence of the PV energy source.

In addition, Figure 4.33 depicts the comparative contribution of various ESEs in various energy optimal schemes. Where Scheme 3 uses less energy overall due to lower energy losses incurred during battery and PV operations.

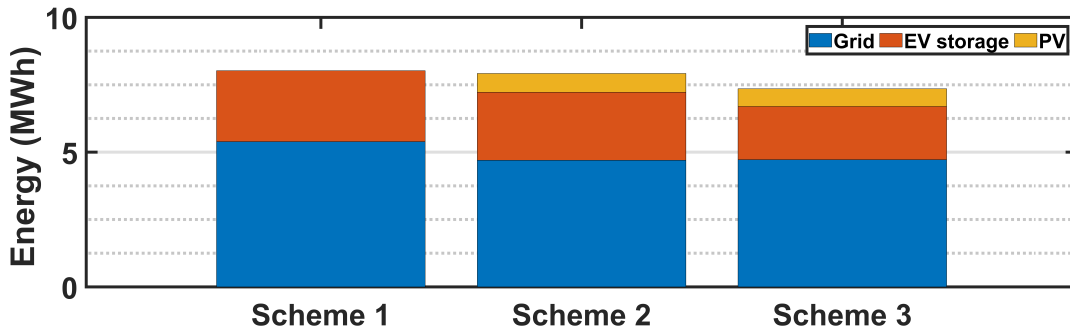


Figure 4.33: Comparative power utilization.

We also investigate the yearly accumulative price of the energy associated with grid power utilization, PV usage, and EV storage utilization as shown in following figures. Figure 4.34 demonstrates that Scheme 3 has overall exhibited a lower energy cost, followed by Schemes 1 and 2, respectively. Scheme 1 exhibits high costs due to the absence of a cheap energy source, i.e., PV, as shown in Figure 4.33. The load demands are satisfied exclusively by grid power, where the grid power is also used for charging the EV storage when needed.

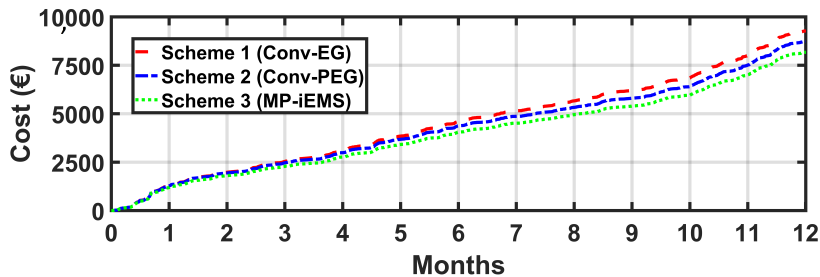


Figure 4.34: Total energy cost.

Figure 4.35 and 4.36 refer to the high grid cost and storage operating cost for Scheme 1, respectively. It may be due to the high charge and discharge rates associated with high grid energy prices.

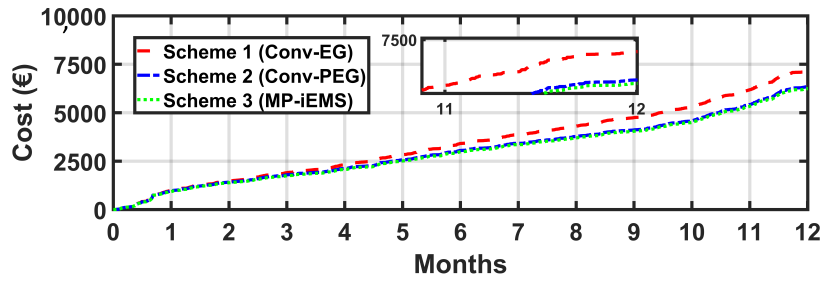


Figure 4.35: Total grid energy cost.

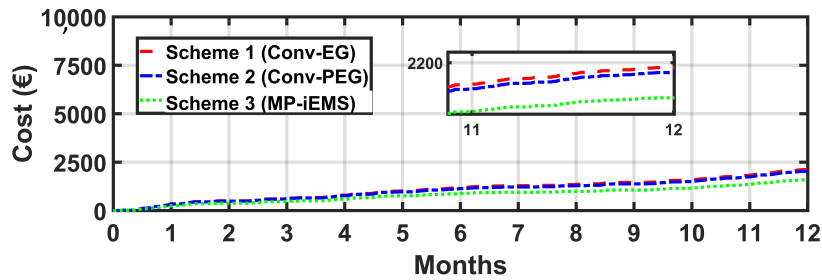


Figure 4.36: Total EV storage utilization cost.

On the other hand, in Scheme 2, the PV source is added. It is then utilized to satisfy the loads along with charging the EV storage when the grid energy prices are high and extra power is available from the PV source. However, both of these schemes opt for the same price for the EV operational costs, and so the storage utilization is almost the same.

Furthermore, in Scheme 3 the system model is similar to that of Scheme 2 where the cheap PV source is included, however in this scheme, an extra intelligence is placed to look into the cheapest option of energy available at any instance of time. As seen in Figure 4.19, sometimes the grid energy prices become negative or gaining energy from the grid is sometimes cheaper as compared to the energy obtained from the PV (i.e., due to operational and maintenance costs). Hence, our proposed MP-iEMS algorithm used in scheme 3 can have this intelligence about when to use PV or when it is cheap to utilize grid power both for satisfying user load demands and charging the EV. One can see in Figure 4.33 that the PV utilization is lower in Scheme 3 in comparison to Scheme 2. It takes more energy from the grid at the lowest possible price and still exhibits a quite lower grid energy price when looking into the zoom window of Figure 4.35. However, on the other hand, this scheme also utilizes EV storage quite efficiently and achieves the lowest battery operational costs as compared to other schemes as shown in Figure 4.36.

Moreover, if we want to know the difference in the behavior of utilizing EV storage especially for Scheme 2 and Scheme 3, a histogram of state of charge (SOC) in Figure 4.37 shows that Scheme 2 maintains a quit low range of SOC in between 25% to 75%. While Scheme 3 maintains this SOC approximately in between 55% to 75%. It indicates that Scheme 2 experiences deep discharges and high battery utilization as compared to Scheme 3.

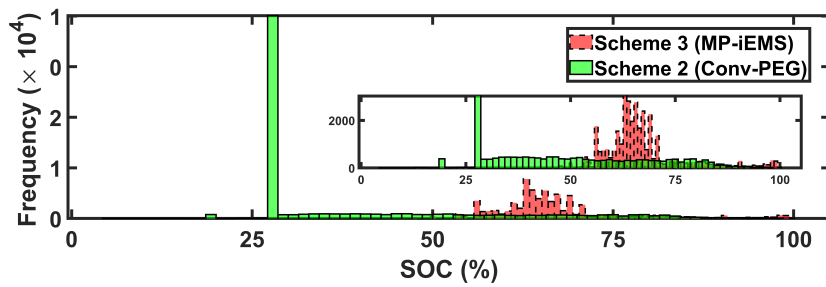


Figure 4.37: Histogram of EV storage SOC.

Similarly, if we look into Figure 4.38, Schemes 1 and 2 opt for normally high charge rates around 23 kW, while Scheme 3 experiences low charge rates in comparison to other schemes around 12 kW.

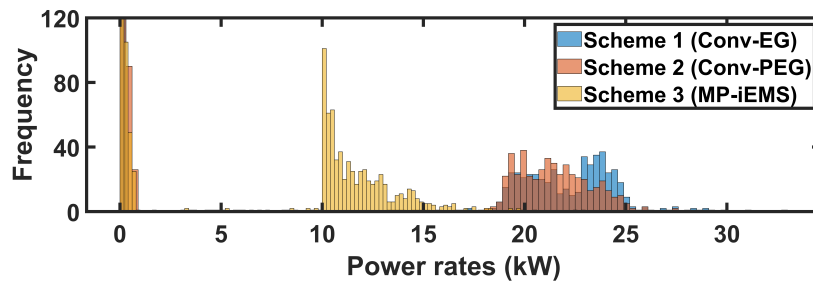


Figure 4.38: Histogram of EV storage charge rates.

Another comparison in terms of yearly accumulative charge and discharge energy for various schemes is shown in Figure 4.39. It demonstrates that Scheme 1 encounters a significant amount of energy exchange throughout the battery's charge and discharge cycles. It is due to the absence of a third source of energy when compared to Scheme 2, where these values are comparatively low around 2.6 MWh, and it is due to the induction of the PV source. Which takes over some of the supply from EV storage. However, Scheme 3 experiences the lowest charge and discharge energy exchange of around 2 MWh, and it is due to the intelligence of utilizing the optimum share of energy from each source at a very optimal price.

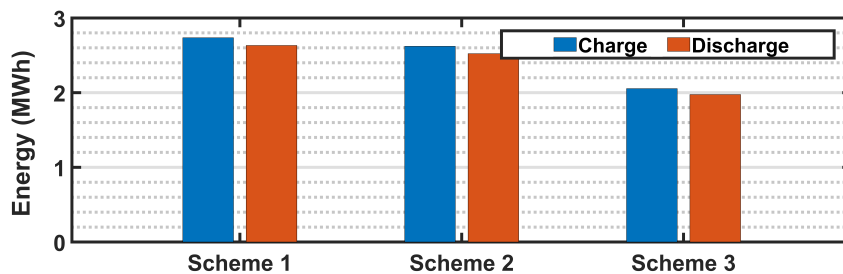


Figure 4.39: Annual accumulative charge and discharge energy for EV storage.

Moreover, Figure 4.40 demonstrates the accumulative EV storage losses. These losses are evident during the charge and discharge of EV storage and are due to the inefficiency of the conversion (i.e., AC-DC or DC-AC). As illustrated above, Scheme 3 experiences less EV storage utilization, so it also exhibits less storage loss as compared to Scheme 2 and 3. It is worth mentioning that the driving behavior and

EV consumption on the road are the same for all the study schemes. However, there are differences in the number of times the EV battery is charged and discharged

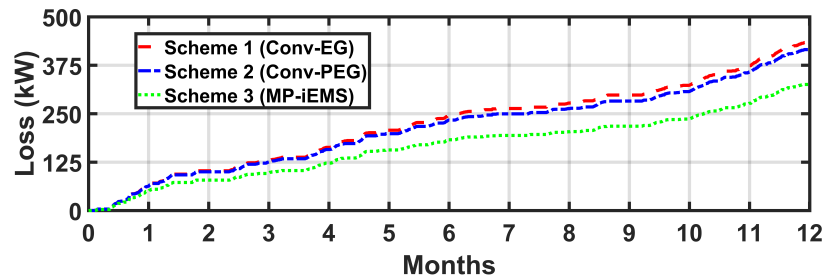


Figure 4.40: Total EV storage loss.

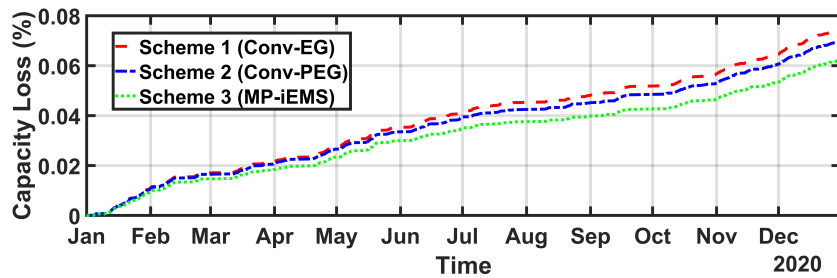


Figure 4.41: Comparison of total capacity loss.

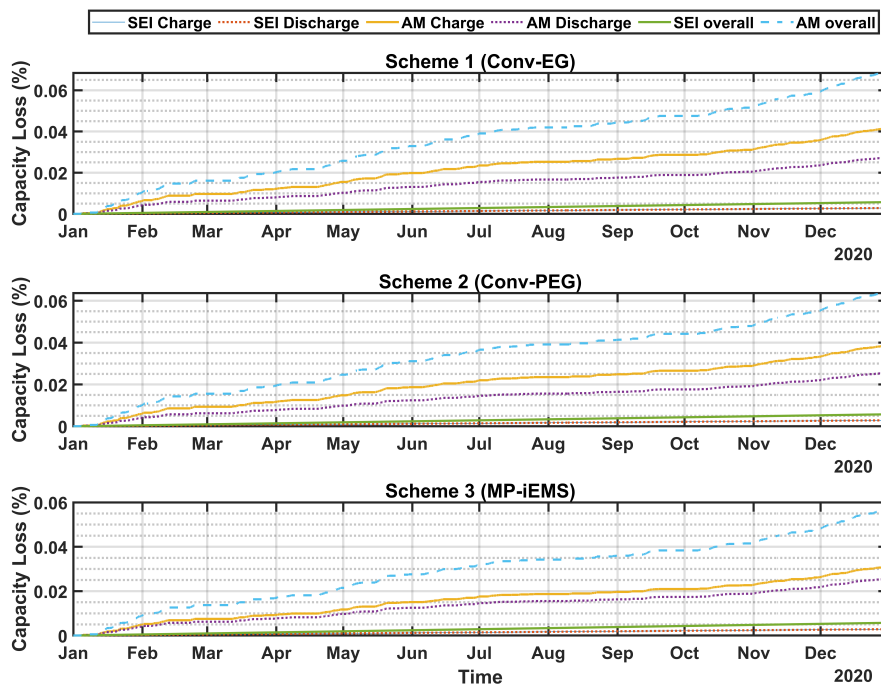


Figure 4.42: Comparison of various capacity losses among different schemes.

Furthermore, EV storage capacity loss analysis is carried out to demonstrate the effects of dynamic storage SOC and (dis)charge rates. This loss analysis is done using the battery model data available from [82]. The battery SOC, charge/discharge

power, and the elapsed lifespan are all inputs into the storage degradation model, which then determines the percentage capacity loss. Degradation models are usually complex and non-linear.

Figure 4.41 shows the variations in the accumulative capacity loss of the storage for the whole year. While Figure 4.42 illustrates individual scheme-based capacity losses induced due to charge, discharge, and the SOC of the storage. Moreover, two types of losses (e.g., SEI and AM capacity loss) are shown individually for every scheme.

All three systems have active material (AM) losses greater than solid electrolyte interface (SEI) losses, as seen in the figure. The charging and discharging rates affect the AM losses, hence higher rates result in higher losses. With increasing SOC, such as Scheme, the AM capacity loss grows in a monotone pattern. The AM variation pattern is time-invariant since it is unaffected by the amount of time the battery has been in use. Due to high charge rates, AM charge losses are larger than AM discharge losses, especially when the car charges itself using the charging station’s high charge power option. SEI losses are reliant on the storage’s SOC, whereas SOC losses are independent. With increasing net discharge power, the SEI capacity loss reduces in a linear fashion. The battery run duration has an adverse effect on the SEI capacity decrease rate.

Compared to the other three schemes, the overall AM losses in Scheme 3 are lower. Scheme 2 and 3 have very little difference, on the other hand. However, there is not a significant difference in overall SEI losses between these schemes. This may be because there are not as many changes in SOC between them, and that the battery runs for a long time i.e., the whole year. In addition, a heat map can provide another perspective to analyze the losses during the hour of the day and the month of the year. Figure 4.43–4.45 show the heat maps for Schemes 1–3, respectively. In all these schemes it is evident that the storage capacity losses are high in winter, especially during 3:00 p.m. to 8:00 p.m. It is due to higher driving utilization of battery during the winter season.

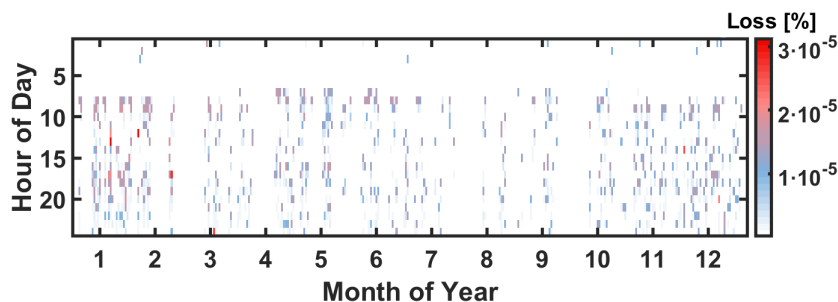


**Figure 4.43:** Hourly mean total loss increment for Scheme 1 (Conv-EG).

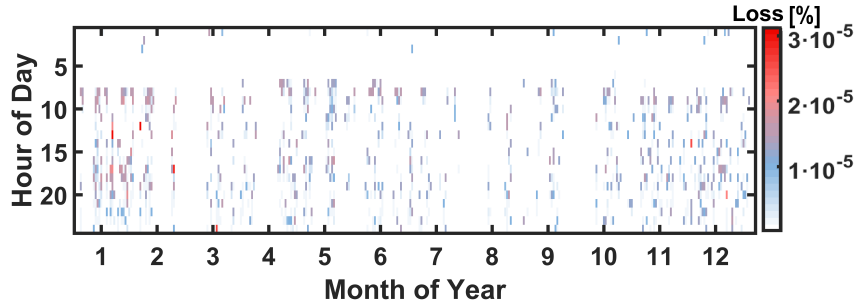


Figure 4.44: Hourly mean total loss increment for Scheme 2 (Conv-PEG).

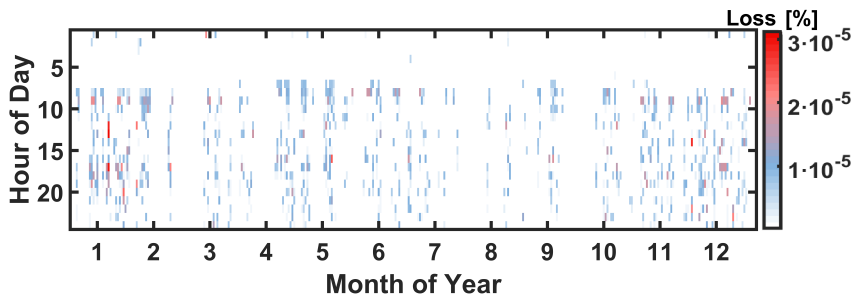


Figure 4.45: Hourly mean total loss increment for Scheme 3 (MP-iEMS).

## 4.5 Conclusion

This chapter presents an overview of the basic principles of a small-scale home area power network (HAPN). It includes an empirical battery degradation model in the analysis of the behavior of storage devices in power networks. The aim is to develop a cost-effective energy management system by incorporating optimization techniques. The proposed energy management system uses a mixed integer dynamic algorithm based on a receding horizon rule to make time-ahead scheduling decisions. The objective is to enhance the self-sufficiency of the HAPN and reduce the energy costs for consumers by utilizing the most cost-efficient energy source available at any given time. A case study is conducted using real-life yearly data sets of household energy demands, EV driving patterns, and EV battery charging/discharging patterns to demonstrate the capability of the proposed model for precise energy management and to illustrate the scheduling algorithms in action. The simulation results analyze the impact of energy suppliers' penetration levels and utilization variables on a daily, monthly, and annual basis.



## 5 Time-Triggered Model Predictive Optimal Distributed Control for AC/DC HAPN

This chapter is an extension to the previous one integrating mixed integer linear programming (MILP) based optimization strategy for further analysis of energy cost minimization and power balancing in a HAPN. Furthermore a reactive power control is rolled out in addition to previously established active power control for the energy supply entities. Moreover, this chapter presents a co-simulated intelligent home energy management system (CO-iHEMS) that integrates the robust rolling horizon-based predictive scheduling framework with the real-time power electronics-based control mechanism. A time-ahead scheduler incorporating an ideal method for predicting cost-optimal decision signals for various Energy Supply Entities (ESEs) can be utilized to optimize load following. This approach is beneficial in ensuring that optimal decisions are taken with respect to the cost associated with running different ESEs. Also, a real-time distributed robust control technique involving an auxiliary power source is devised. The central scheduler sends time-triggered low-jitter wireless signals to the distributed device level local controller to execute the control law. The development of a real-time distributed robust control strategy is achieved by implementing a coordinated energy sharing mechanism that incorporates an auxiliary power source. The proposed model is assessed by comparing several AC/DC microgrid models for home area power network (HAPN).

### 5.1 Communication Based Scheduling Policy for HAPN

For an intelligent grid, smart nanogrid (NG) is a crucial component. A unified power network includes energy supply entities, energy storage devices, and intelligent energy devices [115, 116]. Qiu et al. and Zhao et al. [158, 208] have recently proposed a hybrid AC/DC nanogrid topology that combines the benefits of both AC and DC topologies. Since the standard grid topology is a grid-connected AC configuration. The AC configuration is widely adaptable because of installed AC conventional power generating units and the users' load demands. However, the islanded DC distribution system is emerging with the advent of next-generation efficient renewable energy generators and DC power load components. Therefore, it is difficult and cost-inefficient to migrate the whole power system from AC to DC and operate in islanded mode.

The hybrid AC/DC nanogrid architecture minimizes power conversion steps and integrates dispersed energy resources (DERs) efficiently [111]. However, this new system has enormous challenges regarding stability and control, since the control entity is responsible for achieving a dispatched grid power flow and balances both AC and DC subgrids simultaneously. A smart residential NG is an intelligent energy

devices (IEDs) based home area power network (HAPN). Most IEDs can be operated and monitored remotely (e.g., internet of things devices). However, for HAPN to work efficiently, controllers and IEDs must communicate data in real-time. The wireless sensor and actuator networks best implement this information-sharing approach [213].

However, in wireless architecture, data transmission bandwidth restrictions frequently limits the working of power systems [92]. Therefore, it is also advantageous to utilize communication networks efficiently. A resilient distributed control method based on communication was developed to restore voltage and frequency under the condition of fixed time delay communication [155]. In [103], a discrete-time distributed communication strategy governs power flow and voltage/frequency restoration during plug-and-play device operations. Continuous information sharing across dispersed DERs is inefficient and might cause congestion [102]. The data exchange between controllers and IEDs causes frequent packet losses and increasing delays [91].

Event-triggered communication techniques may minimize communication traffic. In addition, because event-triggered controls need minor control updating, they demand less data transfer and computation power [92]. It also supports additional configurations without requiring a new system architecture [90]. Time-triggered approaches, on the other hand, enhance predictability and performance [187]. These have higher latency than event-triggered designs but no jitter if all contributing nodes are aligned to a global time [213]. The time-triggered transmission is controlled by predetermined time frames using time division multiple access during periodic services. A control network's offline job scheduling may use time-triggered communication. In this chapter, the time-triggered simplex communication approach is employed to transmit decision signals from the scheduler to the robust controller at the device level.

This work's primary goal is to show cost-optimal power-sharing phenomena. This chapter presents a new approach to optimizing power flow in a Home Area Power Network (HAPN) with a hierarchical control architecture, as illustrated in Figure 5.1. This control hierarchy comprises two main control frameworks: Stage 1: Secondary control rolling horizon-based scheduler; Stage 2: Primary distributed real-time controller. Moreover, a wireless communication infrastructure connects both of these two stages.

The first stage discusses the optimization challenge of obtaining cost-effective scheduling signals for various ESEs. Initially, the parameters connected with the optimization algorithm are featured, which then executes a forecasting algorithm to estimate future load needs and electricity pricing information, [129]. This chapter presents analytical models for the solar power generation, storage, and HAPN architecture. These models specify the operating rules and system restrictions in more detail, thus increasing the complexity of the investigated power system. Additionally, it identifies the convergence difficulties associated with the suggested optimum method. Scheduling choices are optimized repeatedly for a 24-hour receding horizon. The scheduler's optimal signals are then wirelessly delivered to numerous IEDs located around the residence. The model includes a packet-based transmitter and receiver to exhibit genuine communication phenomena. A multi-path fading channel is introduced, coupled with additive white Gaussian noise (AWGN) to improve the practicality of the model.

In the second step, a robust control approach is used to trace down the signals received at the targeted IED. It guarantees that the device operates according to the scheduler’s optimum decision values. As a result, it always maintains the previously acquired values until the controller receives a new signal. Additionally, a distributed power-sharing phenomenon can be observed at this stage by implementing a proportional energy sharing strategy. It includes energy reserves (e.g., fuel cells, capacitors, or battery storage) for auxiliary operations during grid failure, demand uncertainty, and scheduler signal loss.

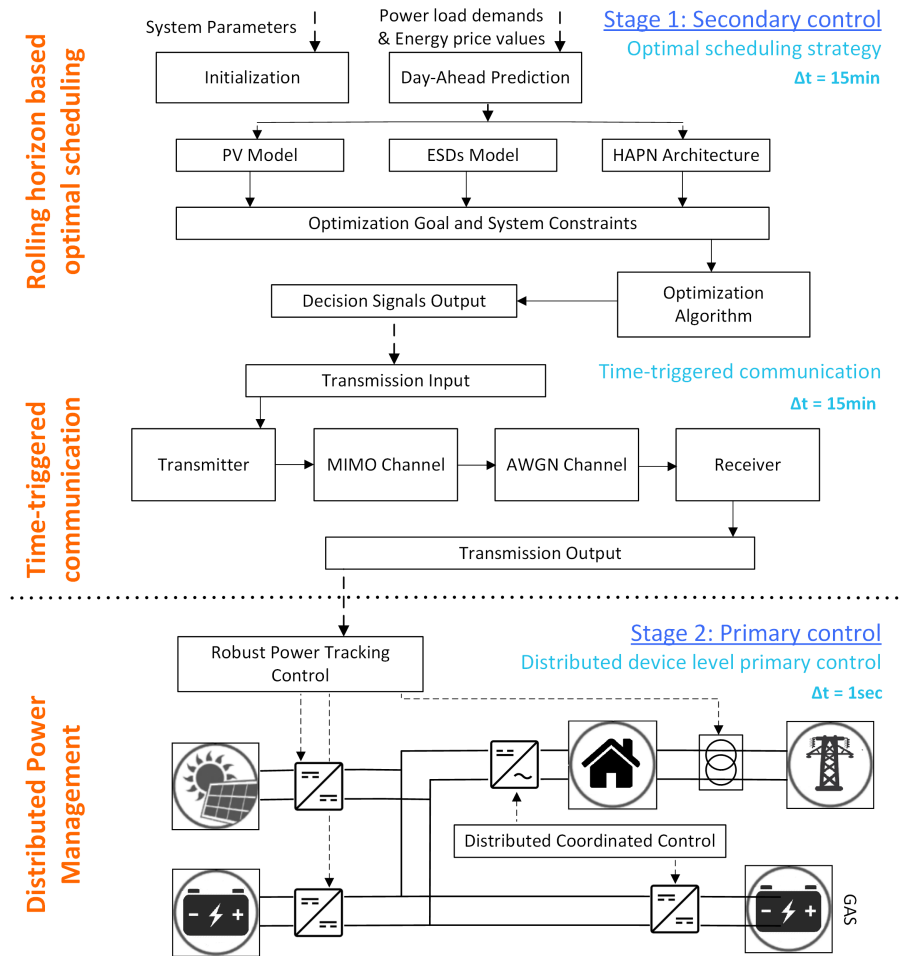


Figure 5.1: Proposed control strategy and system model.

Furthermore, the literature mentioned in Table 5.1 shows that most critical research concerns at the microgrid level, and there are just a few HAPN-based studies to our knowledge. Furthermore, the previous research did not address solution techniques for hybrid AC/DC systems in HAPN that incorporate system losses. As a result, they did not accomplish optimal cost reduction in AC and DC subgrids while sharing comparable energy. Furthermore, to simplify the complexity of the energy flow, the energy scheduling across interconnected microgrids was accomplished using a DC or AC network. Most papers treated grid power flow as if it were a single entity with a single controller. This chapter provides a two-staged scheduling and control framework as a distributive optimization technique for reducing power losses during power distribution.

This chapter optimizes the total cost of energy and more effectively distributes

**Table 5.1:** Critical analysis of past work. (Con, converter; P, active power; Q, reactive power; RT, real-time; DA, day-ahead.)

| Ref #. | Domain    | Topology | Technique(s)   | Energy supply entities |    |     | Entity losses |    |     | Power supply |   | Battery deg-model | Communication topology | Time horizon | cost reduction | Energy balancing |
|--------|-----------|----------|----------------|------------------------|----|-----|---------------|----|-----|--------------|---|-------------------|------------------------|--------------|----------------|------------------|
|        |           |          |                | Grid                   | PV | HBS | Con           | PV | HBS | P            | Q |                   |                        |              |                |                  |
| [83]   | Microgrid | AC       | Heuristic algo | ✓                      | ✓  | ✓   | ✗             | ✗  | ✗   | ✓            | ✗ | ✗                 | ✗                      | RT           | ✗              | ✓                |
| [73]   | Microgrid | AC       | MILP\fuzzy     | ✓                      | ✓  | ✓   | ✗             | ✗  | ✗   | ✓            | ✗ | ✓                 | ✗                      | DA\RT        | ✓              | ✗                |
| [38]   | Microgrid | AC       | Pareto Optimal | ✓                      | ✓  | ✓   | ✗             | ✗  | ✗   | ✓            | ✗ | ✗                 | ✗                      | DA           | ✓              | ✗                |
| [78]   | Nanogrid  | AC       | fuzzy          | ✓                      | ✓  | ✓   | ✗             | ✗  | ✗   | ✓            | ✗ | ✗                 | ✗                      | RT           | ✗              | ✓                |
| [69]   | Microgrid | AC\DC    | Droop control  | ✓                      | ✓  | ✓   | ✗             | ✗  | ✗   | ✓            | ✗ | ✗                 | ✗                      | RT           | ✗              | ✓                |
| [187]  | Nanogrid  | AC\DC    | Droop control  | ✓                      | ✓  | ✓   | ✗             | ✗  | ✗   | ✓            | ✓ | ✗                 | ✗                      | RT           | ✗              | ✓                |
| [206]  | Microgrid | AC       | Heuristic algo | ✓                      | ✓  | ✓   | ✗             | ✗  | ✗   | ✓            | ✗ | ✗                 | ✗                      | DA           | ✓              | ✓                |
| [154]  | Nanogrid  | AC       | Lyapunov-opt   | ✓                      | ✓  | ✓   | ✗             | ✗  | ✗   | ✓            | ✗ | ✗                 | ✗                      | RT           | ✓              | ✗                |
| [37]   | Microgrid | AC\DC    | PSO\GA         | ✓                      | ✓  | ✓   | ✗             | ✗  | ✗   | ✓            | ✗ | ✗                 | ✗                      | DA           | ✓              | ✗                |
| [27]   | Microgrid | AC\DC    | Droop          | ✓                      | ✓  | ✓   | ✗             | ✗  | ✗   | ✓            | ✓ | ✗                 | ✗                      | RT           | ✗              | ✓                |

it across numerous IEDs by considering an efficient low-latency communication connection and system inefficiency. When compared to prior efforts, this study makes the following significant contributions:

1. A complex hybrid AC/DC nano-grid model for a HAPN is presented. This model incorporates real-world operational constraints for conventional and renewable energy sources. It also accounts the cost for battery life loss and component-based power losses during DC/AC sub-grid energy exchange. Previously, as cited in [69, 89, 200], AC/DC power models for higher-level distributed microgrids were constructed neglecting significant component power losses.
2. This work introduces a two-stage co-simulation framework to construct a multi-time scale energy management and control solution, which differs from the Specifically Proportional Power-Sharing (SPPS) approach presented in [32, 69, 94]. Moreover, the AC/DC hybrid nanogrid’s dispatch can be optimized offline to reduce total energy costs. Furthermore, a real-time coordinated power sharing scheme is utilized to balance the power network.
3. The previously proposed distributed event-triggering communication in [36, 89, 90] is entirely dependent on local control data and settings. While in this work, a robust local controller utilizes time-triggered communication to monitor the ideal data acquired from the scheduler. Nevertheless, a lossless connection between device-level control and actuators is envisioned. Furthermore, this work dramatically minimizes the transmission latency, jitter, and computation power associated with the communication between the offline scheduler and the local controller using the time stamp feature.
4. Unlike the typical hierarchical control structure of microgrids [32, 69, 89, 200], the suggested design includes secondary predictive control and main distributed robust control layers. It increases system predictability, redundancy and facilitates HAPN plug-and-play. The secondary control layer implements the HAPN analytical model, whereas the main control layer implements the HAPN physical model.
5. A performance comparison is made with some previous works (i.e., [158, 200, 208]) based on the inclusion of various types of losses and system topologies. Moreover, the impact of the hierarchical control framework on the stability and economic operation of the AC/DC hybrid HAPN is thoroughly analyzed.

## 5.2 Hybrid AC/DC Home Area Power Network

The present study proposes a three-layer system design for hybrid AC/DC HAPN, as illustrated in Figure 5.1. This system comprises of an optimized scheduling layer, a cyber communication layer, and an electrical physical layer. The physical layer consists of necessary power electronics and the robust coordinated device level controllers. A physical device is linked to the scheduler through a cyber network, from where it receives a reference power signal for the actuators. The cyber layer enables the scheduler's data to be exchanged with various power electronics converters. Additionally, a local energy sharing controller coordinates the functioning of an additional energy reserve device (for emergency operations). This coordinated control is connected to the physical network through sensors and actuators.

### 5.2.1 HAPN Architecture

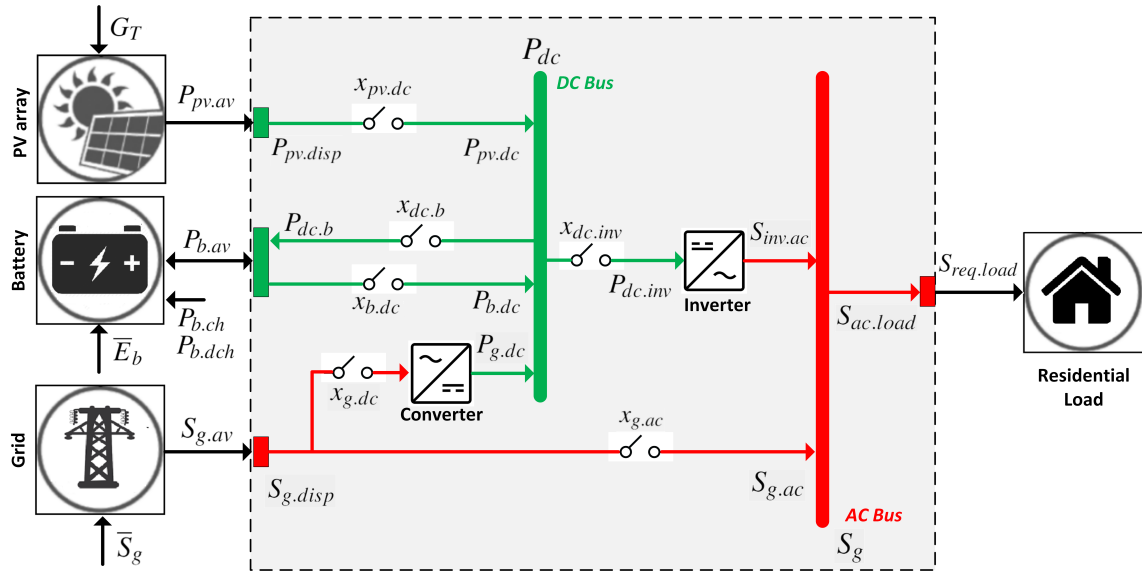


**Figure 5.2:** HAPN architecture (Scheduler perspective).

Figure 5.2 illustrates the HAPN architecture under discussion. The service grid line is directly linked to the HAPN's AC sub-grid and to the DC sub-grid through an AC/DC converter. The photovoltaic array and Home Battery Storage (HBS) are coupled together through the incorporation of DC/DC converters, thus allowing for direct connection to the DC line. To further facilitate the connection between the DC sub-grid and the primary grid, a DC/AC converter is employed. Controllable switches are included in the system to implement the nanogrid's binary operating restrictions.

#### Grid-tie line

Grid connection model is taken from Section 3.1.3, transforming the exact model using apparent energy transmitted from the utility grid ( $S_{g,disp}(t)$ ) is always less than the power available ( $S_{g,av}(t)$ ). Whereas the electrical grid is restricted to its top limit by its maximum threshold  $\bar{S}_g$ .

$$S_{g,disp}(t) \leq S_{g,av}(t) \leq \bar{S}_g \quad \forall t \quad (5.1)$$

The electricity supplied by the utility company to the AC sub-grid ( $S_{g.ac}(t)$ ) is;

$$S_{g.ac}(t) = S_{g.disp}(t) - x_{g.dc}(t) (\eta_{con}^{-1} P_{g.dc}(t)), \quad \forall t \quad (5.2)$$

where,  $x_{g.dc}(t) \in \{0, 1\}$  and  $\eta_{con}$  denote the efficiency of the converter. The available power from the utility grid at the DC sub-grid ( $P_{g.dc}(t)$ ) is shown in Equation 5.3; given that,  $x_{g.ac}(t) \in \{0, 1\}$ .

$$P_{g.dc}(t) = \eta_{con} (S_{g.disp}(t) - x_{g.ac}(t) S_{g.ac}(t)). \quad \forall t \quad (5.3)$$

### PV-array Connection

The dispatched power ( $P_{pv.disp}(t)$ ) from the photovoltaic array is constrained by the availability power ( $P_{pv.av}(t)$ ), and it is always less than that of the maximum power produced by the photovoltaic array ( $\bar{P}_{pv}(t)$ ), since some of it is lost during the maximum power point tracking (MPPT) algorithm processing.

$$P_{pv.disp}(t) \leq P_{pv.av}(t) \leq \bar{P}_{pv}(t), \quad \forall t \quad (5.4)$$

given  $x_{pv.dc}(t) \in \{0, 1\}$ . The power available from PV at DC sub-grid is;

$$P_{pv.dc}(t) = x_{pv.dc}(t) P_{pv.disp}(t), \quad \forall t \quad (5.5)$$

### Battery Storage Connection

The nanogrid incorporates a battery that serves as both a storage and a buffer, with available power ( $P_{b.av}(t)$ ) restricted by the battery's capacity ( $\bar{E}_b$ ) such as;

$$P_{b.av}(t) \leq (\bar{E}_b / \Delta t). \quad \forall t \quad (5.6)$$

During discharging, the battery's available power at DC sub-grid ( $P_{b.dc}(t)$ ) during discharging is;

$$P_{b.dc}(t) = \min [P_{b.dch}(t), P_{b.av}(t)] x_{b.dc}(t), \quad \forall t \quad (5.7)$$

where,  $x_{b.dc}(t) \in \{0, 1\}$ . The power available from DC line to battery ( $P_{dc.b}(t)$ ) is shown in Equation 5.8, given that  $x_{dc.b}(t) \in \{0, 1\}$ .

$$P_{dc.b}(t) = \min [P_{dc}(t), P_{b.ch}(t), (\bar{E}_b / \Delta t) - P_{b.av}(t)], \quad \forall t \quad (5.8)$$

where ( $P_{dc}(t)$ ) is the power available at DC sub-grid.

**Remark 9.** *In order to prevent battery overheating, the maximum (dis)charging current should be restricted as;  $\bar{P}_{b.ch}(t) \approx \bar{P}_{b.dch}(t) \leq \gamma V_b(t) I_b(t)$ . Where  $\gamma$  serves as a limit on the current charging rate.*

### DC Sub-grid Connection

The power exchanged at DC bus is

$$\begin{aligned} & x_{g.dc}(t) P_{g.dc}(t) + x_{b.dc}(t) P_{b.dc}(t) + \dots \\ & x_{pv.dc}(t) P_{pv.dc}(t) = x_{dc.b}(t) P_{dc.b}(t) \dots \\ & \quad + x_{dc.inv}(t) P_{dc.inv}(t), \quad \forall t \end{aligned} \quad (5.9)$$

where,  $x_{dc.inv}(t) \in \{0, 1\}$ . Whereas, additional limits are enforced at the DC sub-grid level, including the following: The charging and discharging of a battery cannot occur concurrently:

$$x_{b.dc}(t) + x_{dc.b}(t) \leq 1, \quad \forall t \quad (5.10)$$

DC sub-grids cannot draw electricity from the grid while transferring power to the AC sub-grid through the inverter:

$$x_{g.dc}(t) + x_{dc.inv}(t) \leq 1, \quad \forall t \quad (5.11)$$

The battery discharge and the utility grid electricity cannot be enabled concurrently:

$$x_{b.dc}(t) + x_{g.dc}(t) \leq 1, \quad \forall t \quad (5.12)$$

### AC Sub-grid Connection

The power exchanges at AC sub-grid is;

$$x_{g.ac}(t)S_{g.ac}(t) + x_{dc.inv}(t)S_{inv.ac}(t) = S_{ac.load}(t), \quad \forall t \quad (5.13)$$

where,

$$S_{inv.ac}(t) = P_{dc.inv}(t) - P_{inv.loss} \quad (5.14)$$

**Remark 10.** *Additionally, the passengers' comfort is ensured by ensuring that the supply power is always higher than the load needs i.e.,  $S_{req.load}(t) \leq S_{ac.load}(t)$ .*

## 5.2.2 Model Dynamics for Energy Entities

### PV Array Dynamics

To illustrate a PV array power output to be used for a standalone home grid, a model obtained from Section 3.1.2 is used showing available power  $P_{pv.av}(t)$ .

### Battery Storage Dynamics

To show a storage system's cost-optimal solution, a model obtained from Section 3.2 describing the real power losses ( $P_{b.loss}(t)$ ) connected with the storage system is used [115].

### Inverter Efficiency Model

The inverter acts as a conduit, facilitating the transformation of electrical energy from the DC to AC sub-system. This transformation process is not without a certain degree of energy loss, which is manifested as heat. Furthermore, the inverter is responsible for establishing the phase angle of the current that is injected into the AC line. Moreover, the AC sub-grid is subjected to both active and reactive power due to the reactive load demands. The current transmitted to the AC line is restricted to the inverter's maximum apparent power handling capacity ( $\bar{S}_{inv.ac}$ ).

The phenomenon of self-consumption is augmented due to the reactive power flow originating from the inverter. It is considered to be the additional losses having an additional impact on the operational costs. As a result, it is demonstrated that an inverter may suffer power loss due to power flow. However, the losses induced

by the reactive power supply can be compensated with the help of an additional active power supply. This energy might come from solar panels or a battery. If this is not practicable, electricity may be obtained from the primary grid. The inverter's consumption is derived by the efficiency figures supplied in the datasheets or by  $\eta_{inv} = P_{inv.ac}/P_{dc.inv}$ , where  $P_{dc.inv}(t) = P_{inv.ac}(t) + P_{inv.loss}(t)$ .

### Energy Demands Model

This chapter utilizes a daily energy demand profile for a single residence that was previously established in [115]. This model is being developed by the center for renewable energy system technologies (CREST). This model collects data on the amount of energy used by a certain number of inhabitants. In addition, it contains their daily activities at home and the likelihood of activating a particular device weekly for the whole year [65]. Hence, it is assumed that a single home may have maximum occupants  $u \in [1, 2, \dots, U]$  utilizing various AC load devices. These devices are activated randomly throughout the day. The device randomness is incorporated using the load prediction strategy. The user energy demands ( $S_{req.load}(t)$ ) may further categorize as active ( $P_{req.load}$ ) and reactive power ( $Q_{req.load}$ ) demands depending on the house power factor as:

$$S_{req.load}(t) = \sqrt{P_{req.load}^2(t) + Q_{req.load}^2(t)} \quad (5.15)$$

### 5.2.3 Entities Operating Cost Model

#### Battery Lifetime Loss Cost

Battery life is often represented in terms of the manufacturer-specified number of storage life cycles. A generalized ampere-hour (Ah) life-cycle storage model is utilized to assess the storage life loss. At each step, the loss in storage life ( $L_f(t)$ ) is the ratio of effective consumed power ( $A_c = SOC(t) \times A'_c(t)$ ) to the total effective capacity ( $A_{total} = \eta_{b.con} \times \bar{E}_b$ ) [209] and is shown as;

$$L_f(t) = A_c/A_{total}. \quad \forall t \quad (5.16)$$

The battery bank's effective used power is dependent on both the actual consumed power ( $A'_c(t)$ ) and the storage's operational state of charge ( $SOC(t)$ ) as seen in [209]. Whereas the average productive capacity of a lead-acid battery is derived using data from the producer of deep-cycle lead-acid batteries [80]. Moreover, discharging the battery at a high state of charge increases its lifespan. The calculated value of  $L_f(t)$  in Equation 5.16 can be utilized to determine the cost associated with the reduction in battery life, which is represented as;

$$C_{b.l}(t) = L_f(t)C_{b,inv}, \quad \forall t \quad (5.17)$$

where  $C_{b,inv}$  is the investment cost of the battery bank.

### Grid Energy Pricing

This chapter employs a unique hybrid pricing approach for utility grid active and reactive electricity. This scheme will help reduce grid power input and encourage



RES use of RESs. A real-time pricing (RTP) scheme based on inclined blocked rate (IBR) is developed, taking into account RTP ( $\theta(t)$ ) for active power utilization [203] and IBR ( $\vartheta(t)$ ) for reactive power usage [105]. The dynamic grid pricing scheme  $C_g(t)$ , previously discussed in Section 3.4.1, is a preliminary step for this chapter's energy cost optimization problem.

### Inverter Power Cost

As discussed in Section 3.4.2, inverter power combines a battery power, photovoltaic power, and inverter-induced power losses. Thus, the inverter power cost ( $C_{inv.ac}(t)$ ) is equal to the operating costs of the battery ( $\phi$ ) and the photovoltaic system ( $\varphi$ ), as demonstrated in Equation 5.18. This operational cost per watt is a function of the component's total investment cost throughout its useful life.

$$C_{inv.ac}(t) = \varphi P_{pv.dc}(t) + \phi P_{b.dc}(t). \quad \forall t \quad (5.18)$$

## 5.3 Multi-Stage Power Scheduling and Energy Sharing Control

The HAPN is a single energy network that integrates grid-connected power, solar arrays, and household energy storage. Additionally, it supplies electricity to household appliances at a set voltage standard [13]. The energy allocation tactics and robust real-time power sharing mechanism described in this article are shown via the implementation of a home energy management system (HEMS) that incorporates power scheduling and control algorithms. Where a main control unit decodes the scheduler's reference signals and activates the devices appropriately. Additionally, it adjusts for voltage fluctuations that occur as a result of load uncertainty or grid disconnection. It initiates distributed coordinated control for the energy balancing mechanism, which in this instance is the grid auxiliary storage (GAS). GAS with an energy status of ( $E_{gas}(k)$ ), is responsible for providing ancillary services to HAPN (i.e., support with island operation and power quality issues) citing [143]. GAS power management monitors the disparity in the power network through its dispersed organized control unit, which consists of a proportional and integral control system. It utilizes the network's excess capacity and supplies electricity during blackouts.

In Figure 5.3, a two-staged model predictive control (MPC) scheduler and control infrastructure are provided. The first stage is to establish an energy scheduler at the secondary control level, which minimizes the net cost of produced energy. It includes a prediction module and an optimization algorithm to forecast the production of time-ahead photovoltaic energy and the customer's load needs. Alternatively, an ideal algorithm optimizes ESE scheduling and produces optimal decision signals in the form of device power set-points. These set-points are sent to the system's principal controller through a communication channel.

Furthermore, a forecasting and scheduling strategy that uses rolling time horizons is presented to reduce forecasting errors. This strategy operates at a minute-level time scale, i.e.  $t \in [1, 2, \dots, T]$ . Meanwhile, the second level implements a robust control approach for power allocation that operates at a second-level time scale, i.e.  $k \in [1, 2, \dots, k]$ , and is based on a coordinated energy sharing strategy. The robust

control mechanism of the system controller continuously evaluates the received reference signal and adjusts the device activation and power levels accordingly [95, 116].

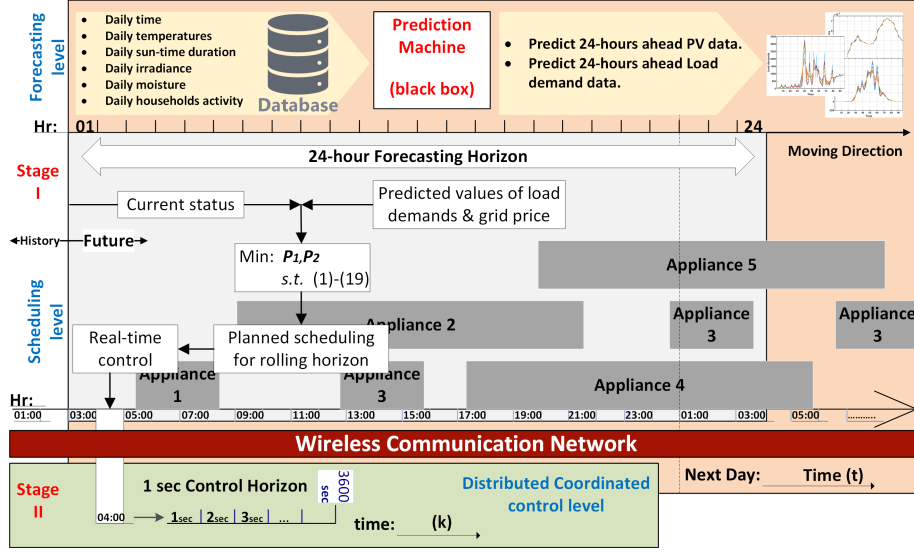


Figure 5.3: Energy management system Architecture.

The following algorithm demonstrates an energy management method that is based on a two-stage scheduling and regulating mechanism. The scheduling strategy is operated using a linear programming method that considers the length of the whole day and analyzes future knowledge of the resources and load needs. The best control variable values are determined using mixed integer linear programming (MILP), which minimizes the objective function shown in Equation 5.19. As a result, the statistical horizon is shifted to the subsequent time period, and the procedure is repeated. The sample period is set to  $t = 15 \text{ minutes}$ , and the prediction horizon is set to  $T = 24 \text{ hours}$ .

### 5.3.1 Rolling-Horizon Based Optimal Power Scheduling

The goal is to reduce the overall cost of energy provided by ESEs as much as feasible. This conundrum is regarded as a problem of energy scheduling on a time-dependent basis, such as:

$$\mathcal{P}_1 = \min_{\mathbf{u}_P^G(t), \mathbf{u}_x^G(t)} \sum_{t=1}^T \{C_g(t)(S_{g.ac}(t) + P_{g.dc}(t)) + C_{b,l}(t) + C_{inv.ac}(t)\}. \quad (5.19)$$

$s.t. \quad (5.1) - (5.14).$

Our management technique places a premium on the usage of photovoltaic energy. As a result, if the load conditions are not met, battery power is used. If necessary, power can be taken from the grid. For every time period  $t$ , the energy requirements ( $S_{req.load}(t)$ ) must be met by any type of the ESEs.

Considering a HAPN, which necessitates the association of a collection of energy dispatchable entities  $\mathcal{G} = \{1, 2, \dots, n^G\}$  with a single operational domain (Home). Let  $u_P^G \in \mathbb{R}_+$  denote the power shared throughout the time-slot  $t \in \mathcal{T} = \{\tau, \dots, \tau + T - 1\}$  represents the individual energy entity, and  $u_x^G \in \mathbb{R}_+$  represents the entity's binary activation set. A subset of entities (i.e., grid power, load needs) is connected

---

**Algorithm 1** Algorithm for Power Cost/Balance Reciprocity

---

```

procedure DYNAMIC SCHEDULING & CONTROL ALGORITHM
  System Initialization
  Set parameter values
  Set system bounds
  Determine control variables initial values
  for ( $t \leq T - 1$ ) do
    Executing PV and load demand prediction strategy
    Initialize system constraints
    Initialize components constraints
    while  $\mathcal{P}_1 \neq \min(\text{Cost})$  do
      Executing optimal scheduling algorithm
    Store scheduling variables set ( $\mathbf{u}_x^{\mathcal{D}}(1)$  &  $\mathbf{u}_P^{\mathcal{D}}(1)$ )
    Transmit decision signal to the device level controller through WLAN.
    Initializing distributed robust control
    for ( $k \leq K - 1$ ) do
      Executing robust control scheme on received signals
      Tracking and applying signals decisions set ( $\mathbf{u}_x^{\mathcal{D}}(k)$  &  $\mathbf{u}_P^{\mathcal{D}}(k)$ )
      while  $\mathcal{P}_2 \neq \max(\text{Balance})$  do
        Executing coordinated control strategy for auxiliary power sharing
        Integrate real-time control variable set ( $\mathbf{u}_{ch}(k)$  &  $\mathbf{u}_{dch}(k)$ )
       $k \leftarrow k + 1$ 
     $t \leftarrow t + 1$ 
  Conclude total energy utilization cost
  Conclude real-time balancing phenomenon
  Conclude ESEs utilization factor and penetration level
  Conclude EEs loss factor and loss cost

```

---

to the HAPN AC line through  $\mathcal{G}_{AC}$ , while a tuple of generators (i.e., PV, HBS) is connected to the DC line via  $\mathcal{G}_{DC}$ . HEMS evaluates the objective functions set  $\mathcal{P}t : \mathbb{R}^+ \mapsto \mathbb{R}^+$ , determines the cost of electricity supply for households at time-slot  $t$ , and balances the power network at time-slot  $k$ .

### Time-Triggered Communication Strategy

A model of HAPN is constructed in this chapter by combining a time-triggered WLAN 802.11ac high-throughput communication connection [14]. Additionally, it incorporates an AWGN fading channel [10] to highlight the noise disturbances that occur in the channel during transmission. Because the scheduler and the IEDs are located close together inside a home, there should be less noise and ambiguity in the communication channel. Author assumes that the IEDs are immobile and that communication between the HEMS and the IEDs takes place in a low-bandwidth simplex mode. This is a straightforward unidirectional time-triggered communication approach that dramatically eliminates needless transmissions and bandwidth usage while optimizing communication connection use. Author establishes that signals transfer frequently at equidistant sampling instants. Because the off-line scheduling pre-defines the time slots for all activities, the result is a time system with constant latencies and no jittering. Because the delays are consistent, global synchronization is achieved with no jitter. Whatever the number of IEDs running, each one has its own allocated time slot for communication with the scheduler, and time invariant techniques are employed. For data transfer, the MATLAB communication toolbox is used to perform TCP/IP-specific identification, retransmission, as well as management of the router's queue length using the random early detection method and congestion avoidance. The communication model has three main parts components:

**Transmitter** It consists of two primary levels of communication networks: the data connection layer and the physical layer. The data connection layer creates signals carrying data and control information. It facilitates the communication of protocol and service information between the peer levels of communicating IEDs. A transmitter generates a physical layer convergence method service data unit and compresses the bits into a single packet waveform. Additionally, data is sent using a quadrature amplitude modulation (QAM) technology.

**Channel** The suggested WLAN model works on the unlicensed  $2.4GHz$  radio frequency band, with a bandwidth of  $20MHz$  and a maximum throughput of  $800Mbps$ . The bandwidth of a WLAN channel is specified as  $5MHz$ .

**Receiver** A receiver's basic operation is to retrieve a message from a sent packet. There are two components to the receiver: packet detection and packet recovery. The receiver must perform a variety of tasks, including packet identification, time and frequency synchronization, carrier frequency offset correction, MIMO channel estimation, received packet demodulation, and data decoding.

### 5.3.2 Distributed Coordinated Control for Energy Balancing

Due to pre-planned or unanticipated disturbances, the nanogrid may operate in an off-grid mode. As a result, backup energy sources must be employed in voltage/current-controlled inverter (VSI) mode in order to offer rapid voltage/frequency support. By compensating for a part of the power needed for voltage and frequency reconstruction, VSI may offer active and reactive power assistance for HAPN. The goal here is to create a balance of supply and demand inside the HAPN. The problem is then rewritten as a real-time energy balancing problem, as seen below:

$$\begin{aligned}
 \mathcal{P}_2 = \min_{\mathbf{u}_{gas}(k)} \{ & S_{g.ac}(k) + P_{g.dc}(k) + P_{pv.dc}(k) + P_{b.dc}(k) \\
 & + \mathbf{u}_{gas}(k) - S_{ac.load}(k) - P_{dc.b}(k) \}, \forall k \\
 s.t. & \\
 \underline{E}_{gas} \leq E_{gas}(k) \leq \bar{E}_{gas}, & \quad \forall k \\
 \bar{P}_{gas.ch} \leq \mathbf{u}_{gas}(k) \leq \bar{P}_{gas.dch}, & \quad \forall k
 \end{aligned} \tag{5.20}$$

where,  $\mathbf{u}_{gas}(k) = [x_{gas}(k)P_{gas}(k)]$  is the control signal used to activate the auxiliary storage power ( $P_{gas}(k)$ ) with  $x_{gas}(k)$  as a binary activation variable. The available energy in grid auxiliary storage (GAS) is constrained by higher ( $\bar{E}_{gas}$ ) and lower energy thresholds ( $\underline{E}_{gas}$ ). Although the charging and discharging rates of the storage are regulated by the maximum  $\bar{P}_{gas.dch}$  and lowest values  $\bar{P}_{gas.ch}$  specified in Equation 5.20.

### 5.3.3 Robust Power Tracking Control

#### ESDs converter control

Typically, the DC buck/boost converter connected to the ESDs supports voltage levels on both the storage and DC sub-grid sides. Figure 5.4a illustrates the schematic of a converter and the related control framework. The converter's essential control

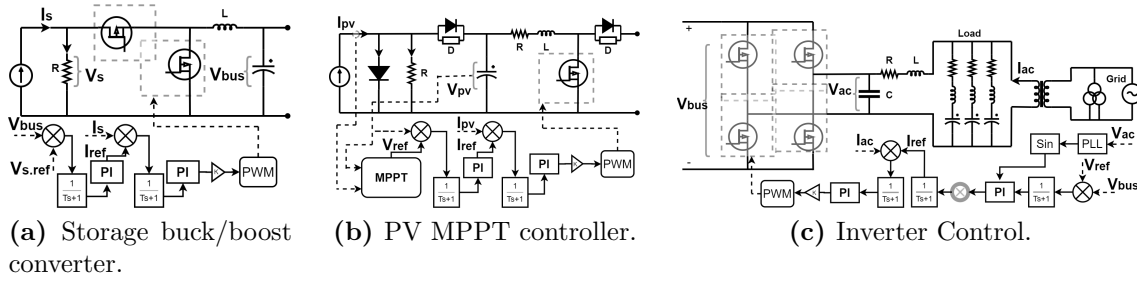


**Figure 5.4:** HAPN components architecture (Primary robust control perspective).

parameters are the output voltage on the DC sub-grid side ( $V_{bus}$ ), the output voltage on the storage side ( $V_s$ ), and the current flowing through the converter ( $I_s$ ). Furthermore, the control strategy for the energy storage system is based on a conventional robust control method that encompasses an external voltage control loop and an internal current control loop. Both loops employ Proportional and Integral (PI) controllers to regulate the reference voltage and current values, respectively [197]. The reference input voltage ( $V_{s.ref}$ ) is the voltage at which the DC sub-grid operates.

### PV power support control

Figure 5.4b illustrates the structure of the photovoltaic power converter and the control method used to facilitate the flow of energy from the photovoltaic generator. Through the use of an MPPT converter, the solar panels are connected to the DC sub-grid. The voltage between the terminals of the photovoltaic panel is denoted by the symbol  $V_{pv}$ . Where  $V_{bus}$  is the output voltage and  $I_{pv}$  is the solar panel's output current.

In practice, the PV panel's voltage and current data are sent into the MPPT controller, which outputs the reference voltage value for control by the main controller coupled to the converter. The MPPT controller employs the perturbation and observation approach described in [197]. While the basic control method utilizes a PI controller in conjunction with two-staged control loops, such as the outer voltage loop and the inner current loop. The PV voltage ( $V_{pv}$ ) is pushed to follow the reference voltage value ( $V_{ref}$ ) acquired via MPPT through a PI-based voltage controller.

### Voltage source inverter control

This section illustrates the inverter's structure and control schematic. The power load is connected to the AC sub-grid in this chapter, and the DC supply is prioritized above the AC grid supply to meet load needs. To enable optimal power transmission from the DC sub-grid to the AC sub-grid, the DC sub-voltages grid's must be constant. As a result, the inverter is constantly stressed. A voltage-controlled VSI is used to regulate the unexpected behavior of renewable energy sources. Figure 5.4c illustrates the grid-connected VSI and its control framework schematically. The outside voltage control loop, as depicted, determines the DC sub-grid voltages applied to the inverter input. The voltage regulator is basically responsible for determining the quantity of current injected into the AC bus. While maintaining a steady DC

bus voltage. In general, proportional and integral (PI) controllers are utilized to update the voltage regulator. [186].

The power shared by the GAS through VSI can be described as [89];

$$P_{gas} = v^{gd}i^{gd} + v^{gq}i^{gq}, \quad Q_{gas} = v^{gq}i^{gd} - v^{gd}i^{gq}, \quad (5.21)$$

where  $i^{gd}$  and  $i^{gq}$  represent the direct and quadrature components of the AC bus current ( $I_{ac}$ ), respectively, and  $v^{gd}$  and  $v^{gq}$  represent the direct and quadrature components of the AC bus voltage ( $V_{ac}$ ), respectively. VSI control is used to implement a direct and quadrature (d-q) reference frame transition that rotates with the common reference frequency ( $\omega$ ). The objective is to replicate the operation of synchronous generators by modulating the input power as a function of power, frequency, and voltage. The phase-locked loop (PLL) is used to synchronize the phase angle of the system. Additionally,  $L$  and  $R$  indicate the inductance and resistance between the VSI and the feeder bus, which together create an output filter. The fact that the local power control is always compatible with the bus voltage (i.e.  $v^{gd} = V_{ac}$  and  $v^{gq} = 0$ ).

## 5.4 A Case Study Based Performance Validation

To test the scheduling algorithm's and real-time control strategy's performance, an AC/DC HAPN architecture similar to that depicted in Figure 5.2 is employed, along with suggested energy allocation scenarios. A modified case study from [115] is used to include electricity pricing data, load profiles, and solar radiation profiles. Table 5.2 illustrates the parametric values for the different power entities employed.

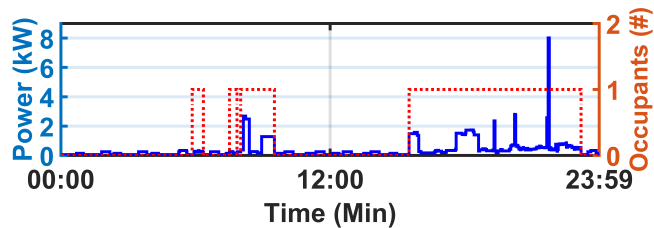
**Table 5.2:** System parameters

| Par:              | Value   | Par:                      | Value   | Par:              | Value  |
|-------------------|---------|---------------------------|---------|-------------------|--------|
| $S_{g.av}$        | 5 kVA   | $\bar{P}_{pv.ac}$         | 1.05 kW | $\bar{E}_{b/gas}$ | 5 kWh  |
| $\bar{P}_{b.dch}$ | 1.28 kW | $\bar{P}_{b.ch}$          | 0.8 kW  | $P_{b.self}$      | 2 KW   |
| $SoE_{initial}$   | 2 kWh   | $\eta_{b.con}$            | 0.95    | $\delta$          | 0.8    |
| $\bar{E}_{b/gas}$ | 2 kWh   | $\eta_{inv}/\eta_{dc/ac}$ | 0.95    | $\eta_{ac/dc}$    | 0.95   |
| $C_{b.iwt}$       | 2000    | $\phi$                    | 0.001   | $\varphi$         | 0.0012 |
| $t$               | 15 min  | $k$                       | 1 sec   |                   |        |

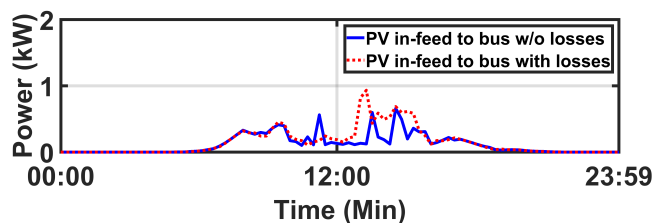
Additionally, a quantitative energy demand model is created that accurately estimates the amount of energy required for a particular household's energy use. The estimated number of active residents in a home and their associated energy consumption are shown in Figure 5.5a with a temporal resolution of 1min. Whereas, Table 5.3 contains a list of frequently used power devices.

### 5.4.1 Comparison Study for Power Scheduling Scenarios

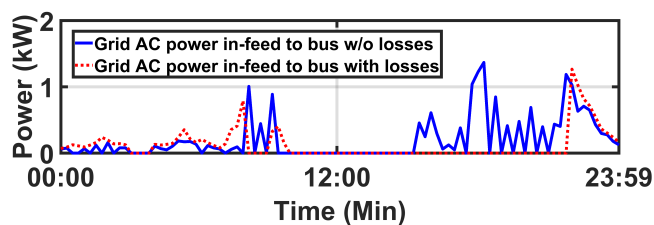
Utilizing the ‘‘MATLAB’’ optimization toolbox, the mixed-integer linear programming (MILP) optimization approach is employed to find the best solution. The MILP solver ‘‘intlinprog’’ is used to find a plausible solution (the minimal need for convergence guarantee). The proposed problem is bit computationally expensive implying;



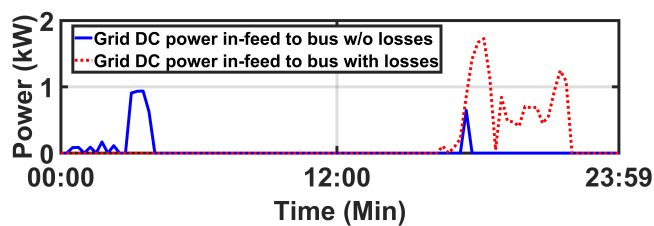
(a) House occupants and their energy demands.



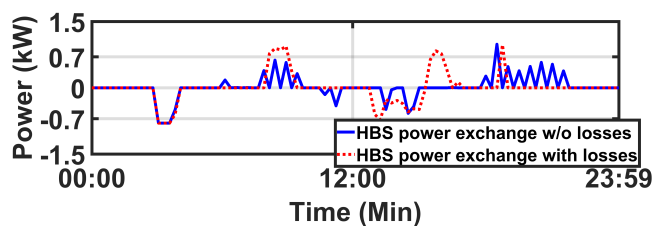
(b) PV power in-feed.



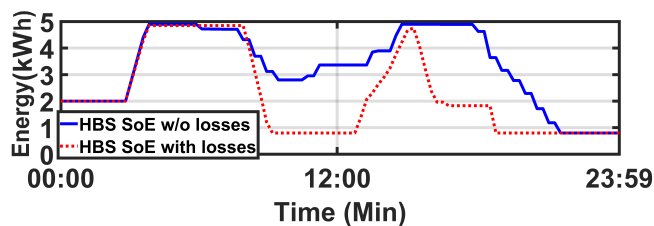
(c) Grid AC power in-feed.



(d) Grid DC power in-feed.

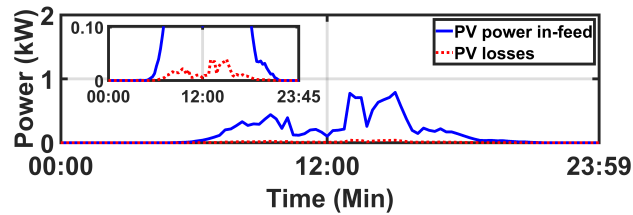


(e) HBS power exchange.

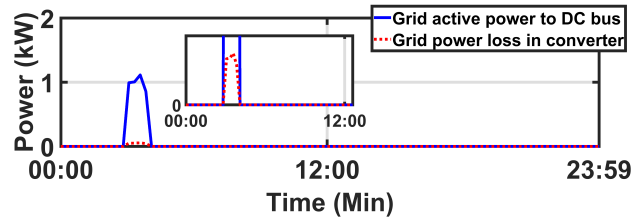


(f) HBS state of energy.

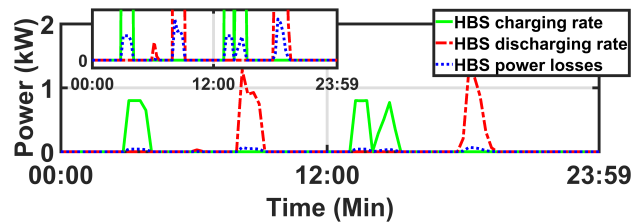
**Figure 5.5:** AC/DC bus (w/o losses) Vs AC/DC bus (with losses).



(a) PV power and losses.



(b) Grid DC power and losses.



(c) HBS power exchange and losses.

**Figure 5.6:** Hybrid AC/DC bus with losses.

- It has total of 12 binary and continuous optimization variables.
- It has 3 linear equality constraints.
- It uses 3 linear inequality constraints.
- It uses 12 bounding condition constraints.

Each iteration takes 3 seconds to get an integer solution to the required optimality level. The required degree of optimality in this issue is a “integer viable solution” and a relative gap of 0. The preceding analysis demonstrates that implementing the recommended approach is feasible in the offline scheduling of home appliances.

In the first section of discussing findings, the author has generated four distinct HAPN architecture scenarios to compare the scheduler’s output. These situations are as follows:

- **A:** AC bus without losses [116].
- **B:** Hybrid AC/DC bus with PV losses [158].
- **C:** Hybrid AC/DC bus with PV and HBS losses [115].
- **D:** All in *Scenario C* with additional converter losses.

On the basis of cost estimation for consuming energy from different ESEs, a link is established. Additionally, author has monitored the utilization factors and penetration levels of different power sources inside a HAPN. Table 5.4 and Table 5.5



**Table 5.3:** Home appliances activities and classification.

| Activity             | Appliance type       | Mean cycle power (W) |
|----------------------|----------------------|----------------------|
| Cooling              | Refrigertaor         | 110                  |
|                      | Cassette / CD-player | 15                   |
| Consumer electronics | Hi-Fi                | 100                  |
|                      | Iron                 | 1000                 |
|                      | Personal computer    | 141                  |
|                      | Printer              | 335                  |
|                      | TV                   | 124                  |
|                      | VCR / DVD            | 34                   |
|                      | TV receiver box      | 27                   |
| Cooking              | Oven                 | 2125                 |
|                      | Microwave            | 1250                 |
|                      | Kettel               | 2000                 |
|                      | Small cooking        | 1000                 |
| Wet                  | Dish wascher         | 1131                 |
|                      | Washing machine      | 406                  |
| Lighting             | Bulbs                | 190                  |

**Table 5.4:** ESEs utilization factor and penetration level.

| Parameters              |              | Scenario A | Scenario B | Scenario C | Scenario D |
|-------------------------|--------------|------------|------------|------------|------------|
| PV ulitization factor   | $(PV_{uf})$  | 0.80       | 0.74       | 0.60       | 0.80       |
| PV loss factor          | $(PV_{lf})$  | –          | 0.05       | 0.05       | 0.05       |
| PV penetration level    | $(PV_{pl})$  | 0.46       | 0.43       | 0.35       | 0.46       |
| HBS ulitization factor  | $(HBS_{uf})$ | 0.80       | 0.82       | 0.63       | 0.73       |
| HBS loss factor         | $(HBS_{lf})$ | –          | –          | 1.5        | 2.5        |
| HBS penetration level   | $(HBS_{pl})$ | 0.17       | 0.20       | 0.09       | 0.16       |
| Grid ulitization factor | $(G_{uf})$   | 0.04       | 0.04       | 0.045      | 0.04       |
| Grid loss factor        | $(G_{lf})$   | –          | –          | –          | 0.005      |
| Grid penetration level  | $(G_{pl})$   | 0.52       | 0.55       | 0.64       | 0.6        |
| Inverter loss factor    | $(I_{lf})$   | –          | –          | –          | 0.00018    |

compare the previously indicated scenarios A, B, C, and D using performance indexes.

Specifically, while examining Table 5.4, the maximum PV usage factor is found in *scenario D*. This is because, in comparison to other circumstances, surplus energy is used to compensate for converter losses. The DC sub-grid compensates for the majority of the system’s power losses. In comparison to energy acquired from the AC sub-grid, it is less expensive to deliver electricity using photovoltaic and battery technology. While the cost is quite high owing to utility grid interconnection, particularly for power loss compensation. However, it is the cheapest in *scenario C* since there is no converter loss and getting power from the DC bus is not cheap. Additionally, it utilizes an alternating current bus when utility grid energy rates are quite cheap. Additionally, the PV loss factor is almost same in all circumstances since the efficiency factor is constant for every given power amount. Whereas the PV penetration level is maximum in *scenarios A* and *scenario D*, it is lowest in

**Table 5.5:** Estimated aggregated energy cost for one day.

| Parameters (“cents”)    |               | Scenario A | Scenario B | Scenario C | Scenario D |
|-------------------------|---------------|------------|------------|------------|------------|
| PV energy cost          | $(C_{pv})$    | 31         | 29         | 24         | 31         |
| HBS energy cost         | $(C_B)$       | 14         | 16         | 7          | 13         |
| HBS lifecycle loss cost | $(C_{b,l})$   | 2.7        | 2.8        | 2.7        | 2.5        |
| Grid energy cost        | $(C_G)$       | 202        | 204        | 240        | 221        |
| Total energy cost       | $(C_{total})$ | 250        | 252        | 274        | 268        |

*scenario C.*

Additionally, as indicated in Table 5.4, the HBS utilization factor is highest in *scenario B*, followed by *scenario A*. One explanation is that these scenarios did not account for battery losses, making it more effective to utilize the full amount of battery to power the loads in these situations. In comparison, it is the smallest in *scenario C* because to the battery losses. Additionally, in *scenario D*, battery losses increase again due to the low cost of using the battery to compensate for converter losses. Thus, if the usage factor for HBS grows, the loss factor increases proportionately. Whereas the amount of HBS penetration is greatest in *scenario B* and is least in *scenario C*. This might be the case with the usage aspect as well.

Additionally, the grid usage factor is high in *scenario C* since utility electricity is inexpensive to utilize and also serves to charge the battery linked to the DC bus. A portion of which is utilized to compensate for the losses of the AC-DC converter. It is, however, smaller in other circumstances since the HBS and converter losses are ignored. As seen in *scenario D*, the grid loss factor is raised by adding converter losses. The usage factor also increases the penetration level.

The cost analysis of ESEs is mostly determined by the usage factor. As a result, if one examine Table 5.5, it can be observed that the operating cost of a photovoltaic source is highest in *scenario D* and *scenario A* and lowest in *scenario C*. Similarly, the operating cost of the HBS is higher in *scenario B* than in *scenario C*. Additionally, the cost of battery life-cycle loss is greatest in *scenario B* since the battery is fully charged, and according to Equation 5.14 battery deterioration plays a significant role in this scenario. While it is the lowest in *scenario D*, which involves less alterations in the battery’s level of energy, it is the highest in *scenario E*. Power from the grid is more expensive in *scenatio C*, where grid penetration is somewhat greater than in the other situations. Finally, after examining the HAPN’s total operating expenses and component loss factors, author proposes that the optimal architectural scenario to operate with is *scenario D*.

Additionally, Figure 5.5 illustrates the graphical comparison of two extreme circumstances. It compares two AC/DC topologies for a HAPN in terms of lossless and lossy power networks. *Scenario A* has no losses, but *scenario D* contains all losses. As seen in Figure 5.5b, the PV in-feed in both cases follows a similar pattern throughout the day with little fluctuations. However, in *scenario A*, the PV in-feed is more volatile than in *scenario D*. This is because more power is necessary to compensate for losses. Additionally, the grid’s AC in-feed is much greater throughout the network without incurring losses, as seen in Figure 5.5c. Due to the fact that the combined in-feed from batteries and PV is less expensive than the network with losses. However, as seen in Figure 5.5d, the grid DC in-feed is in the other direction. This is due to the DC bus compensating for power loss. As a result,

there is always the option of charging the battery using an AC-DC converter. The battery power exchange rates shown in Figure 5.5e are relatively comparable and follow the same trend. However, electricity rates are more volatile in *scenario A*. Additionally, when losses are included, the state of energy (SoE) of the battery is often lower, suggesting high use for power loss compensations.

The further analysis for *scenario D* is presented in Figure 5.6, which shows the power consumption and converter losses. This scenario is more realistic and practical in nature since it illustrates the actual system losses caused by the power flowing via multiple converters. In illustration, as depicted in Figure 5.6a, the power actually delivered by the photovoltaic module is consistently lower than the power obtained from the photovoltaic array. This is a result of the losses brought about by the DC/DC converter that is linked to the photovoltaic array for maximum power point tracking operations. The efficiency of the converter has been estimated to be around 95 percent, as reported in [115]. The zoomed-in graphic clearly illustrates the losses associated with the actual power generated by the photovoltaic module.

Furthermore, Figure 5.6b demonstrates the utility grid’s contribution to the DC bus voltage. As demonstrated in Figure 5.2, the AC source is connected to the DC bus through an AC/DC converter that exhibits inefficiencies. As a result, these power losses are visible during power transmission. This power transfer is often initiated when the utility grid’s energy price is relatively low and the batteries are charged during off-peak hours.

Furthermore, as shown in Figure 5.6c, the simulation of power transfer via the battery is depicted. The battery’s charging and discharging cycles are cyclically activated according to Equations 5.7 and 5.8, which take into consideration the combined losses from both the battery and the converter. Both charging and draining processes might result in battery capacity losses. These losses are seen more clearly in the figure’s magnified pane. Additionally, an inverter is installed between the DC and AC buses to connect the DC energy sources (i.e., battery and photovoltaic array) to the AC loads. This inverter has the ability to provide electricity to the load side. As mentioned in Section 5.2.2, the inverter incurs considerable power losses during power transmission, which may be dissipated as heat.

#### 5.4.2 Communication Link Performance Parameters and Experimental Setup

The parameters of the communication system under investigation are given in Table 5.6. Additionally, the signal-to-noise ratio is used to determine the signal in-

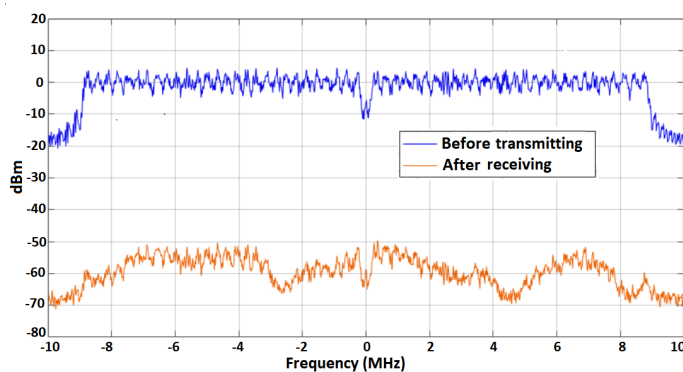
**Table 5.6:** Communication system parameters

| Model Parameters        |           | Channel Parameters  |        |
|-------------------------|-----------|---------------------|--------|
| Distance within Tx & Rx | 3 m       | Breakpoint distance | 10 m   |
| Carrier frequency       | 5.25e9 Hz | RMS delay spread    | 50 ns  |
| Channel bandwidth       | 20 MHz    | Maximum delay       | 390 ns |
| Modulation              | 16-QAM    | Rician K-factor     | 3 dB   |
| Noise model             | AWGN      | Number of clusters  | 3      |
| SNR                     | 28 dB     | Number of taps      | 18     |

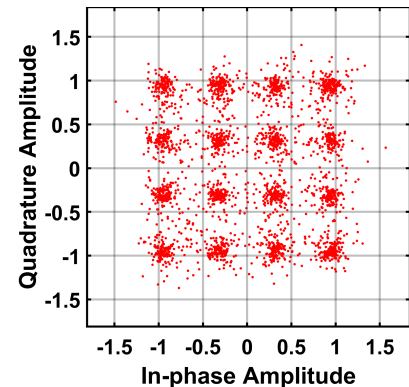
tensity (SNR). It has an effect on the output of the system (e.g., signal intensity

decreases as SNR decreases with rising bit error rate (BER)) and decreases sensitivity. Figure 5.7a displays the difference in signal strength between the broadcast and received signals, or may be interpreted as a route loss that accounts for about 50 to 60 dB of segregation between the waveforms before and after they transit through the communication channel. This route loss is caused by the 3 meter distance between the transmitter and receiver, which includes shadowing effects and AWGN noise. The variances in the received signal level represent the channel delay profile's frequency selectivity over the frequency spectrum. The author computes the SNR ratio required for effective communication to be 28 dB. The likelihood of inaccuracy increases as the SNR value decreases.

Additionally, Figure 5.7b displays the equalized data symbols for each packet analyzed. The picture depicts the output constellation of equalized symbols. It demonstrates that the middle of each quadrature amplitude modulation (QAM) constellation is almost perfect, but the red dots around the midway represent the analytical location of each data point with noise. The fact that these data points are less spaced out (have a smaller range of constellation spread) implies that they have low bit error rates. By increasing the channel noise, the different constellation points may spread, leading in an increase in error rates. A total of  $1.416 \times 10^{09}$  packets are created and transferred in this job throughout a 24-hour period. In



(a) 20 MHz waveform before transmitting and after receiving through AWGN channel.



(b) Frequency spectrum and data symbols output.

**Figure 5.7:** Frequency spectrum and data symbols output

the present architecture, author has employed one of the raspberry pi as master (secondary controller) and one as slave (primary controller) nodes, with a communication link between them as shown in Figure 5.8. The raspberry pi which serves as a slave, gathering data from devices/sensors (i.e., internet of things) and acting as a main controller for those devices. The other one is a scheduler that generates optimum control signals. For connectivity, Linux operating system of the raspberry pi built-in network stack is utilized. In this scenario, TCP is utilized as the network layer, with IP as the underlying protocol. The choice is taken on the basis of data integrity taking precedence above speed. Additionally, author wants to use current internet infrastructure. TCP/IP is utilized to communicate between the master and slave nodes for these reasons. Additionally, Figure 5.9 illustrates the master-slave communication between these two nodes. TCP/IP is also justified in this case since no packet is lost and all packets that are dropped are retransmitted. The data

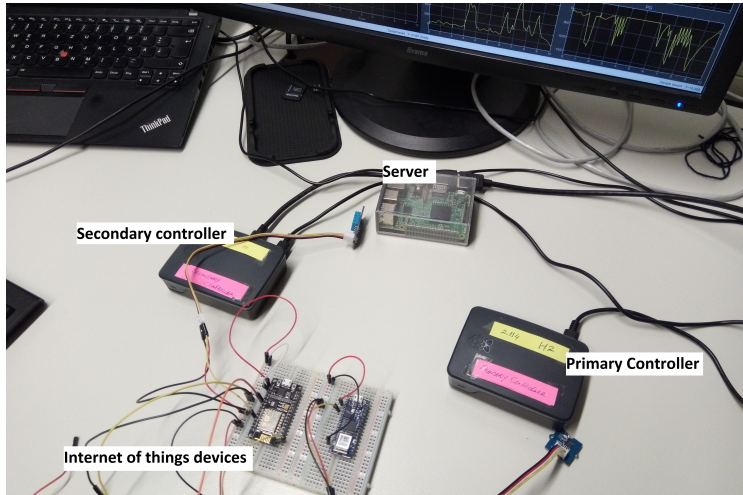


Figure 5.8: Master slave communication experimental setup.

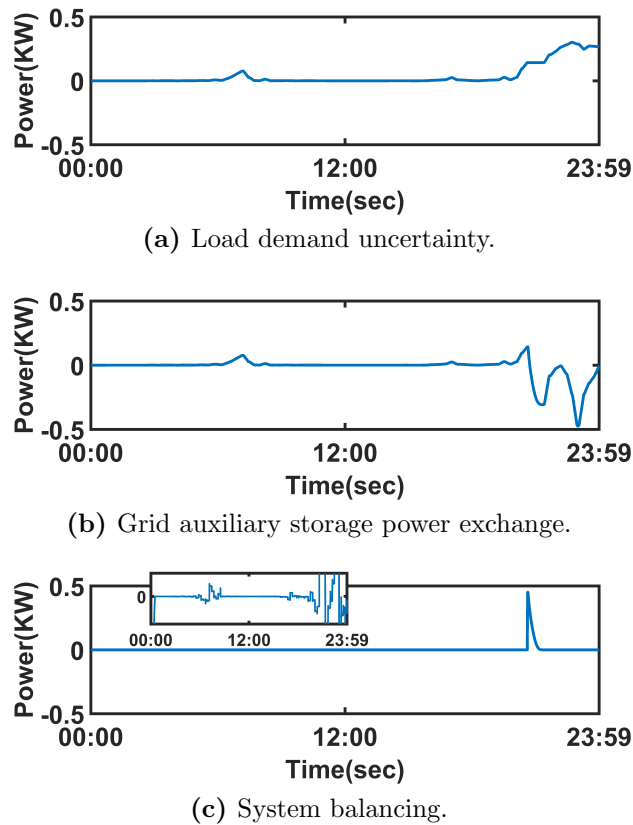
| Time      | 192.168.1.249 | 192.168.1.14                             | Comment  |
|-----------|---------------|--|--|
| 19.353206 | 61508         | 61508 → 12000 [SYN] Seq=0 Win=64240      | TCP: 61508 → 12000 [SYN] Seq=0 Win=64240 Le...   |
| 19.353211 | 61508         | [TCP Out-Of-Order] 61508 → 12000 [SYN]   | TCP: [TCP Out-Of-Order] 61508 → 12000 [SYN] ...  |
| 20.364187 | 61508         | [TCP Retransmission] 61508 → 12000 [SYN] | TCP: [TCP Retransmission] 61508 → 12000 [SYN]... |
| 20.364208 | 61508         | [TCP Retransmission] 61508 → 12000 [SYN] | TCP: [TCP Retransmission] 61508 → 12000 [SYN]... |
| 21.305064 | 61508         | 12000 → 61508 [SYN, ACK] Seq=0 Ack=...   | TCP: 12000 → 61508 [SYN, ACK] Seq=0 Ack=1 ...    |
| 21.305064 | 61508         | [TCP Out-Of-Order] 12000 → 61508 [SYN]   | TCP: [TCP Out-Of-Order] 12000 → 61508 [SYN, ...  |
| 21.305292 | 61508         | 61508 → 12000 [ACK] Seq=1 Ack=1 Win=...  | TCP: 61508 → 12000 [ACK] Seq=1 Ack=1 Win=1...    |
| 21.305301 | 61508         | [TCP Dup ACK 933#1] 61508 → 12000        | TCP: [TCP Dup ACK 933#1] 61508 → 12000 [AC...    |
| 21.344529 | 61508         | 61508 → 12000 [PSH, ACK] Seq=1 Ack=...   | TCP: 61508 → 12000 [PSH, ACK] Seq=1 Ack=1 ...    |
| 21.344533 | 61508         | [TCP Retransmission] 61508 → 12000 [PSH] | TCP: [TCP Retransmission] 61508 → 12000 [PSH,... |
| 21.345115 | 61508         | 61508 → 12000 [FIN, PSH, ACK] Seq=7      | TCP: 61508 → 12000 [FIN, PSH, ACK] Seq=7 Ac...   |
| 21.345118 | 61508         | [TCP Out-Of-Order] 61508 → 12000 [FIN]   | TCP: [TCP Out-Of-Order] 61508 → 12000 [FIN, ...  |
| 21.353497 | 61508         | 12000 → 61508 [ACK] Seq=1 Ack=7 Win=...  | TCP: 12000 → 61508 [ACK] Seq=1 Ack=7 Win=6...    |
| 21.407205 | 61508         | 12000 → 61508 [ACK] Seq=1 Ack=211        | TCP: 12000 → 61508 [ACK] Seq=1 Ack=211 Win...    |
| 23.058033 | 61508         | 12000 → 61508 [FIN, ACK] Seq=1 Ack=...   | TCP: 12000 → 61508 [FIN, ACK] Seq=1 Ack=21...    |
| 23.058145 | 61508         | 61508 → 12000 [ACK] Seq=211 Ack=2        | TCP: 61508 → 12000 [ACK] Seq=211 Ack=2 Win...    |
| 23.058151 | 61508         | [TCP Dup ACK 1002#1] 61508 → 12000       | TCP: [TCP Dup ACK 1002#1] 61508 → 12000 [A...    |

Figure 5.9: Time-triggered communication setup between nodes.

transferred from the secondary controller and received at the main controller are accurately analyzed.

### 5.4.3 Power Sharing During Communication Failure and Load Uncertainties

The Simulink model of a nanogrid shown in Figure 5.1 is used to evaluate the real-time control strategy for *scenario D*. To handle the dynamic nature of load demand, an unforeseen volatile load demand model composition is assimilated into the real-time power system, as shown in Figure 5.10a. To maintain the energy network's power balance, auxiliary storage is connected, which compensates for any system imbalance caused by unplanned changes in solar power production, load demands, or scheduling signal loss. Finally, a load interruption model is merged into the previously anticipated load demand model. For example, the predicted power load is disengaged for 3600 *seconds* at 20*h* of the day, presumably as a result of the communication breakdown. This phenomena simulates an uncertain circumstance



**Figure 5.10:** Real-time HAPN operation.

that a main controller must respond to immediately. The grid auxiliary storage (GAS) is capable of handling both load increase and load discontinuities. As seen in Figure 5.10b, it functions as a buffer, absorbing excess energy in the system and adding energy when the system is at a low energy level.

Figure 5.10c illustrates the onset of power network imbalance. The auxiliary storage system corrects the irregularity quickly by providing more power throughout the night when the load is disconnected. Even in the event of a load interruption or ambiguity, the ESEs are designed to deliver energy in accordance with the scheduling management decision. As a result, the GAS compensates for the projected imbalance energy. It is worth noting here that the grid might directly balance the HAPN. However, large on-demand energy costs may result in a rise in the customer's cost. The insignificant variations in the magnified pane of Figure 5.10c demonstrate the chattering effect caused by the controller's activity.

## 5.5 Conclusion

This chapter elaborates on an AC/DC hybrid home area power network with rolling horizon-based time-triggered scheduling and distributed coordinated control. The chapter introduces the innovative multi-time scale co-simulated intelligent home energy management system where the energy entities are scheduled and controlled on two separate time resolutions. The recommended secondary control scheduler delivers the optimised cost scheduling decision vector for various dispatchable energy supply entities. It is transferred wirelessly to the primary local control, where the

reference signals are tracked systematically. The effects of amplification of additive noise and bandwidth constraints on decision vectors during wireless communication are analysed. The robust control method at the local control uses proportional and integral control that ensures the reference signal tracking. Moreover, when a signal is lost or a power imbalance occurs, a distributed coordinated control balances that intermittency using auxiliary grid power served by local storage. The influence of energy losses due to the components' inefficiencies on the total energy costs is illustrated in several HAPN architectural scenarios incorporating active and reactive powers of various energy entities. The suggested control strategy's output is also verified using the MATLAB/SimPowerSystems toolbox.

---

## 6 Co-scheduling of Energy Supply Entities with Flexible Smart Load Demands: A Case Study of Demand Side Management

One significant critical characteristic of the current power system paradigm is the capacity to regulate load demand rather than just expanding generation to meet ever-rising consumption. Demand-side management may be described simply as any measures that impact the energy consumer's consumption efficiency. This only sometimes implies that consumption should be decreased but somewhat optimized. This study presents a framework for the component-based modeling of various Energy Supply Entities (ESEs) and Smart Load Demands (SLDs). It implements a co-scheduling strategy between ESEs and SLDs within the small-scale energy nano grid referred to as the Home Area Power Network (HAPN). The HAPN integrates roof-top Photovoltaic (PV) panels, backup Diesel Engine (DE) generators, Energy Storage Devices (ESDs), and smart load demands with grid electricity. The scheduling model utilizes a mixed-integer linear programming (MILP) based min-max optimization technique to minimize daily energy expenses, ensure high consumer comfort, and advance home energy self-sufficiency. Incorporating various energy entities (EEs) in an established optimization framework may help make day-ahead cost-optimal scheduling choices using dynamic energy price signals and SLDs of different kinds. This chapter proposes a linearized component-based model that incorporates energy inefficiencies, power phase modes of smart demands, and the deterioration phenomenon of Energy Storage Devices (ESDs). The validity of the proposed Home Area Power Network (HAPN) model is verified through a numerical case study. The implemented technique optimizes the cost-effective balance of various energy entities in the HAPN, demonstrating practical potential in real-world applications.

### 6.1 Critical Analysis of Demand Side Management Techniques

Confronting the problem of uncertainty in energy demands and PV generation, a decentralized smart grid, also known as distributed grids (DGs), is designed. With energy storage and control techniques, it better integrates RESs with the traditional electricity network [96]. Intelligent, self-contained and robust, the smart grid reinvents the classical electricity network. It also promotes the internet of energy idea. [185]. It encourages customer energy savings and trading via demand-side management (DSM) and demand response (DR) techniques. DR or DSM programs may help minimize RESs intermittency by assuming the load demands flexible [12].

The smart grid's DSM and DR features encourage energy customers to utilize energy effectively and cheaply. It helps design strategies for flexible energy entity (EE) operations that maintain the electricity grid stable [20]. It also incorporates



## 6. Co-scheduling of Energy Supply Entities with Flexible Smart Load Demands: A Case Study of Demand Side Management

**Table 6.1:** Objectives and limitations in state of the art work.

| Techniques  | Domain   | Objectives   | Limitations  |
|---|--|--|--|
| Adaptive dynamic programming [214]                | Adaptive dynamic programming for multi-battery energy storage systems                          | Due to the efficient control capabilities of dynamic programming, it is used to optimally control the charging and discharging of the storage device and make its life prolonged.  | The model is limited to only battery storage and the detailed information about load demands is missing. Moreover, the constraint functions are approximated which lack the accurate model of the device.  |
| Lyapunov optimization [205]                       | Energy management for a sustainable smart home with an HVAC Load and Random Occupancy          | The study examines the reduction of the combined cost of energy and thermal discomfort and proposes stabilizing queue development for indoor temperature, electric vehicle charging, and energy storage to minimize the cost and improve efficiency and comfort.                                     | The energy demand model is narrow as it only considers thermal loads. Moreover, the algorithm is unable to address the problem of peak formations.   |
| Mixed integer linear programming [210]            | Optimal Demand Side Response in Hybrid AC/DC Systems   | This study presents a simplified mathematical representation of a hybrid AC/DC energy system to reduce variables and constraints, improve efficiency and modeling accuracy, and increase search effectiveness. The simplified model can improve understanding and performance of the energy systems. | Piecewise linear function is computationally expensive and is not suitable if the number of decision variables increases.  |
| Dynamic optimization [203]                        | Demand Side Management for a Microgrid Considering Uncertainties                               | A two-stage optimization method using model predictive control with dual-time scale is introduced to balance supply and demand, reduce operational costs, and manage uncertainty. The method considers both short- and long-term objectives for an efficient solution.                               | Aggregated load demand is utilized and it does not show the insight of component level based device behaviour which is crucial for device level energy management system.  |
| Stochastic programming [149]                      | Demand Response Technique for Peak Load Reduction  | A heuristic approach optimizes household appliance scheduling to reduce power consumption's PAR and maintains consumer appliance information confidentiality.  | A probabilistic model for supply and demand is presented which is prone to forecasting errors. Moreover the model complexity is not discussed in detail.   |
| Generalized Benders Decomposition algorithm [133] | Multi-Residential Demand Response Scheduling with Multi-Class Appliances                       | The optimization problem balances energy consumption cost and residential customer utility while being executed in a secure, distributed manner.   | The strategy may not work well if there is an error in the demand information provided by the residences. Moreover, it does not address the problem of a peak to average ratio (PAR) of the power demand.  |
| Metaheuristic algorithm [104]                     | Home Energy Management System with Demand Charge Tariff and Appliance Operational Dependencies | A demand charge pricing scheme is instituted with the objective of minimizing the community's daily electricity cost while considering the monthly peak power consumption penalty.   | The concept of demand charge tariff is usually proposed for a community or large-scaled industrial loads. However, a single residential unit's power capacity would be too small to implement the proposed strategy.   |
| Lyapunov optimization [96]                        | Residential Energy Storage Management with Bidirectional Energy Control                        | A real-time bidirectional energy control algorithm is proposed to minimize the net energy cost. It also includes battery deterioration and storage inefficiency in its system model.   | The constraint of electric line power flow has not been adequately addressed in the current discourse. Furthermore, there is a lack of information provided regarding the setting of selling and purchasing prices, as well as the impact of battery inefficiency on storage behavior. |
| Coordination algorithm [67]                       | Optimal Coordination of Building Loads and Energy Storage                                      | An optimized coordination algorithm has been implemented to deliver power grid and end-user services, including energy arbitrage, frequency regulation, spinning reserve, cost reduction, and demand charge reduction.   | Need to investigate further about scalable and distributed coordination strategies for building loads and energy storage systems to provide services to the grid and end-users.  |
| Mixed integer linear programming [20]             | Flexibility of Residential Loads for Demand Response Provisions                                | A two-stage optimization framework is developed, where the peak reduction signals are identified by aggregating individual users energy consumption patterns, and determines their flexibility provision.  | This work does not consider the incentives that may be provided for delaying the loads and the penalty cost for lowering the discomfort of the consumers.  |

financial incentives like variable energy pricing and low energy use prizes. This is realized by postponing, transferring, or limiting non-priority load needs [79]. These tactics include peak clipping, valley filling, and critical load management. In order to aid in demand response programs, a variety of energy pricing schemes have been devised, including time-of-use pricing (ToU), day-ahead pricing (DAP), real-time pricing (RTP), critical-peak pricing (CCP), and inclined-block rate pricing (IBR). These tariffs aim to incentivize customers to shift their energy usage to off-peak periods, thereby reducing overall demand on the energy grid and improving its reliability [86]. Table 6.1 and Table 6.2 demonstrates the limitation of previous work in the context of above mentioned next generation power system.

The cost-effective functioning of various energy entities (EEs) in a home is the focus of this Chapter. EEs consist of both energy generators and electrical appliances. So far, most pieces of literature have only studied the energy generating side for cost-optimal operations (i.e., scheduling of energy supply entities (ESEs)) [121]. But in this work, the DSM techniques are also explored along with supply-side management. Thus the author recreates the cost reduction and customer satisfaction problem using the concept of the internet of energy (IoE), where every energy entity is carefully regulated using an intelligent energy management system (iEMS). The ultimate goal is to combine supply and demand management of cheap, clean, and uncertain EEs. The benefit of adding energy storage devices (ESDs) and diesel engines (DEs) in reducing power costs throughout the day is also studied, considering grid outages and thermal device temperature requirements. The optimization problem formulated in this Chapter is challenging because of the large number of EEs and their temporal coupling limitations.

This proposed work's notable features include:

1. Analyze detailed PV and ESDs models to identify component inefficiencies

**Table 6.2:** Critical analysis of past work. (PE, power elastic loads; ECL, electric controllable loads; TCL, thermal controllable loads; DT, delay tolerant load demands; Occ, occupancy behaviour; Ss, Self-sufficiency; Ps, pricing scheme; Cr, cost reduction; DA, day-ahead; Roll, rolling time horizon.)

| Ref.  | Domain     | Technique(s)   | Scheduling ESEs |    |    |      | Scheduling SLDs |     |     |    | Occ | Ss | Ps | Cr | Time horizon |   |         |   |          |
|-------|------------|----------------|-----------------|----|----|------|-----------------|-----|-----|----|-----|----|----|----|--------------|---|---------|---|----------|
|       |            |                | Grid            | PV | DE | ESDs | PE              | ECL | TCL | DT |     |    |    |    |              |   |         |   |          |
| [8]   | Micro-grid | MILP           | ✗               | ✗  | ✓  | ✓    | ✗               | ✗   | ✗   | ✗  | ✗   | ✗  | ✗  | ✗  | ✗            | ✗ | Fixed   | ✓ | 24h-DA   |
| [208] | Micro-grid | MILP           | ✗               | ✓  | ✓  | ✓    | ✗               | ✗   | ✗   | ✗  | ✗   | ✗  | ✗  | ✗  | ✗            | ✗ | Fixed   | ✓ | 24h-DA   |
| [46]  | Micro-grid | Lyapunov-opt   | ✗               | ✓  | ✗  | ✗    | ✗               | ✗   | ✓   | ✗  | ✗   | ✗  | ✗  | ✗  | ✗            | ✗ | RTP     | ✓ | 24h-Roll |
| [95]  | Nano-grid  | GA             | ✓               | ✓  | ✗  | ✓    | ✗               | ✗   | ✗   | ✓  | ✗   | ✗  | ✗  | ✗  | ✗            | ✗ | RTP     | ✓ | 24h-Roll |
| [147] | Nano-grid  | MILP           | ✓               | ✗  | ✗  | ✓    | ✗               | ✗   | ✗   | ✓  | ✗   | ✗  | ✗  | ✗  | ✗            | ✗ | Dynamic | ✓ | 24h-DA   |
| [153] | Nano-grid  | MILP           | ✓               | ✓  | ✗  | ✓    | ✓               | ✗   | ✓   | ✓  | ✗   | ✗  | ✗  | ✗  | ✗            | ✗ | Fixed   | ✓ | 24h-DA   |
| [170] | Nano-grid  | Stochastic     | ✓               | ✓  | ✗  | ✓    | ✗               | ✓   | ✗   | ✓  | ✓   | ✓  | ✓  | ✓  | ✓            | ✓ | F/D     | ✓ | 24h-DA   |
| [161] | Nano-grid  | PSO            | ✓               | ✓  | ✓  | ✓    | ✗               | ✓   | ✓   | ✗  | ✓   | ✓  | ✓  | ✓  | ✓            | ✓ | TOU     | ✓ | 24h      |
| [85]  | Nano-grid  | Heuristic      | ✓               | ✓  | ✗  | ✗    | ✗               | ✓   | ✓   | ✓  | ✗   | ✗  | ✗  | ✗  | ✗            | ✗ | TOU     | ✓ | 24h-DA   |
| [101] | Nano-grid  | MILP           | ✓               | ✓  | ✗  | ✓    | ✓               | ✗   | ✓   | ✓  | ✗   | ✗  | ✗  | ✗  | ✗            | ✗ | RTP     | ✓ | 24h-DA   |
| [107] | Nano-grid  | MILP           | ✓               | ✓  | ✗  | ✓    | ✗               | ✗   | ✗   | ✗  | ✗   | ✗  | ✗  | ✗  | ✗            | ✗ | Fixed   | ✓ | 24h-DA   |
| [160] | Nano-grid  | Stochastic     | ✓               | ✓  | ✓  | ✓    | ✗               | ✓   | ✓   | ✗  | ✗   | ✗  | ✗  | ✗  | ✗            | ✗ | Fixed   | ✓ | 24h-DA   |
| [79]  | Micro-grid | Meta-Heuristic | ✓               | ✓  | ✗  | ✓    | ✗               | ✓   | ✓   | ✗  | ✗   | ✗  | ✗  | ✗  | ✗            | ✗ | Dynamic | ✓ | 24h-DA   |
| [86]  | Nano-grid  | Heuristic      | ✓               | ✗  | ✗  | ✗    | ✓               | ✓   | ✗   | ✗  | ✗   | ✗  | ✗  | ✗  | ✗            | ✗ | F/D     | ✓ | 24h-D/R  |
| [212] | Nano-grid  | GA             | ✓               | ✓  | ✗  | ✓    | ✗               | ✗   | ✗   | ✗  | ✗   | ✗  | ✗  | ✗  | ✗            | ✗ | F/D     | ✓ | 24h-DA   |
| [201] | Micro-grid | Opt-Algo       | ✓               | ✗  | ✗  | ✓    | ✗               | ✗   | ✗   | ✗  | ✗   | ✗  | ✗  | ✗  | ✗            | ✗ | TOU     | ✓ | 24h      |

and energy losses. ESDs model also gives the outlook of the storage device life cycle.

2. Incorporate a constraint-based mathematical model for different flexible smart load demands (SLDs) attributing the DSM strategies.
3. Add a reward and penalty component allows cheap activation of power elastic and delay-tolerant loads while considering user comfort.
4. A novel “min-max co-scheduling (MMCS)” optimization technique is proposed. It successfully handles the cost reduction and customer satisfaction optimization problems inside a single optimization framework. The resolution of the model is achieved through the application of a branch and bound approach based on mixed-integer linear programming (MILP).
5. Validate the optimum scheduling issue using a signal house simulation, and use auctioned electricity price information [3] for realistic numerical analysis.

## 6.2 Analytical Modeling of Home Area Power Network and the Attached Power Devices

The suggested operational nanogrid model for scheduling EEs optimally is a small-scaled HAPN. The HAPN operates autonomously as a nanogrid, balancing supply and demand while maximizing energy efficiency. It functions as a low voltage distribution nanogrid, enabling ESDs, integrating energy from RESs, and delivering energy to (in)flexible household smart appliances. A smart meter that links a residence to the external grid serves as the doorway to this HAPN.

The suggested structure of a nanogrid is shown in Figure 6.1. Where, power loads ( $P_{ac.load}(t)$ ), diesel power generator ( $P_{de.ac}(t)$ ) and grid power ( $P_{g.ac}(t)$ ) share alternative current (AC) line. While, direct current (DC) line is shared by the power

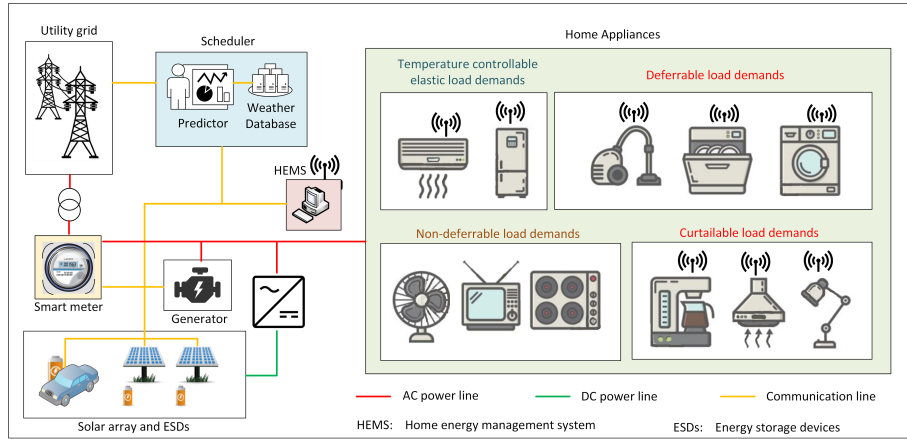


**Figure 6.1:** Home area power network system model

obtained from PV ( $P_{pv.dc}(t)$ ) and the ESDs ( $P_{b.dc}(t)$ ). To create a plausible scenario for off-grid operation, a nanogrid is assumed to be situated in a rural region where grid power is more often disconnected. As a result, a backup diesel generator is included to assure an uninterrupted power supply for the whole day. The hybrid AC/DC grid exchanges power using a bidirectional converter that supplies power to both the DC and AC lines [210]. Normally, it is assumed that the nanogrid distributes electricity over DC lines to avoid line losses. However, most electrical appliances run on AC power and, thus, transforming electricity from DC to AC at the appliance level is not a cost-effective option. In comparison, a one-time DC to AC conversion is less expensive and results in fewer conversion losses.

Furthermore, a PV power model assumed in Section 3.1.2 is introduced in this chapter to reflect the inherit problem of inflexibilities in PV generation. The day-ahead solar irradiances are calculated and the PV power is forecasted using a prediction algorithm incorporating solar irradiance model. In addition, a battery as an energy storage device (ESD) already described in Section 3.2 is introduced in this work. ESDs can act as an energy buffer and storage device in a smart power networks.

### 6.2.1 Energy Usage Cost Formulations

Establishing an ideal and efficient system is crucial in minimizing the daily electricity costs within an intelligent home area power network (HAPN). This strategy may integrate a variety of EEs (i.e., energy sources and electrical appliances) in a cost-efficient way so that only sufficient energy is drawn for the appliance from the cheapest energy source at any instantaneous time  $t$ . While scheduling various EEs it is necessary to guarantee that energy supply and demand are balanced and that customer satisfaction is met.

Additionally, to execute such a scheduling model, a problem formulation is standardized to a specified cost function. For example, both the quantity of energy used and the degree of customer satisfaction are expressed as cost parameters. The cost formulation of various EEs is illustrated as follows:

1. **Grid energy delivery cost:** The cost per unit of energy obtained from the

grid ( $\rho(t)$ ) at any time  $t$  is derived from [3] and is illustrated as:

$$C_g(t) = (P_{g.ac}(t)x_{g.ac}(t))\rho(t), \quad \forall t \quad (6.1)$$

where  $P_{g.ac}(t)$  represents the grid's power input to the AC line of the home, and  $x_{g.ac}(t) \in [0/1]$  indicates the grid's on/off state.

2. **PV operating cost:** Theoretically, PV has no operating costs since it generates power using plentiful, free solar energy. It does, however, incur certain fixed operating and maintenance expenses  $\varphi$ . This covers the cost of the photovoltaic equipment's replacement as described in [41]. The per unit energy cost insured by the PV is calculated as;

$$C_{PV}(t) = (P_{pv.dc}(t)x_{pv.dc}(t))\varphi, \quad \forall t \quad (6.2)$$

where  $\varphi$  is the fixed cost derived from disaggregating the installation and maintenance cost over the period of some years. Whereas,  $x_{pv.dc}(t) \in [0/1]$  denotes the on/off status of the PV array.

3. **Diesel engine operating cost:** The time intensive operating and running cost of a diesel engine (DE) unit is dependent on the quantity of fuel used to produce the desired amount of electricity at any given time  $t$  of the day. However, the fuel consumption model for a diesel engine is often represented by a quadratic function as described in Section 3.1.4 [29, 74]. Hence, the power cost is established as;

$$C_{DE}(t) = (a_{de}x_{de.ac}(t) + b_{de}P_{de.ac}(t)x_{de.ac}(t)), \quad \forall t \quad (6.3)$$

Additionally, each time the generator starts or stops, it incurs charges, which are denoted by start-up ( $\sigma^{su}$ ) and shutdown costs ( $\sigma^{sd}$ ), respectively. These expenditures are incurred as a result of staff costs, pre-heating, and idle circumstances of the generator and is discussed in Section 3.1.4, [208]. In the case of steam power plants, this cost is often exponential, however in our instance, the cost is constant due to the presence of a tiny diesel unit. These expenses are shown as follows:

$$C_{DE}^{su}(t) = z_{de}(t)\sigma^{su}, \quad \forall t \quad (6.4)$$

$$C_{DE}^{sd}(t) = v_{de}(t)\sigma^{sd}, \quad \forall t \quad (6.5)$$

where  $z_{de}(t) \in [0/1]$  and  $v_{de}(t) \in [0/1]$  denote the start-up and shutdown state of diesel engine, respectively.

Furthermore, there are certain operating and maintenance expenditures  $\sigma^{om}$  associated with filter or oil changes, as well as the replacement of some components of the DE unit. These expenses are depicted for any time  $t$  as follows:

$$C_{DE}^{om}(t) = x_{de.ac}(t)\sigma^{om}. \quad \forall t \quad (6.6)$$

Besides, DE causes harmful  $CO_2$  emissions. As a result, there is a penalty cost of  $\xi$  associated with the production of a mass of carbon element. This amount of carbon grows as the generator's output increases [148]. The total cost of emitting  $CO_2$  at any point in time  $t$  is defined as

$$C_{DE}^{co2}(t) = (CO_2 \times P_{de.ac}(t)x_{de.ac}(t))\xi, \quad \forall t \quad (6.7)$$

4. **Energy storage devices operating cost:** The running cost of a storage component is the most critical metric in an energy management system and is indirectly refers to the maintenance cost of the storage. The expense of storage deterioration is not insignificant. There are two methods for extending the life of a storage battery. One approach is to restrict the depth of discharge (DoD) of storage to a specific value at which the battery performs optimally well while disregarding the number of cycles  $N_{cycle.b}(t)$  in a day. The cost of the battery is fixed in this case, reflecting the cost of replacing the battery after a certain length. The second is to define a cost function that estimates the deterioration of storage capacity in terms of cycles and DoD which is already discussed in Section 3.2.2. In this chapter the later approach is used to calculate a variable cost operator  $C_b(t)$ , which is the ratio of the battery's total investment cost ( $IC_b$ ) to its total energy throughput [8].

$$C_b(t) = \frac{IC_b}{N_{cycle.b}(t)(1 - DoD(t))\bar{E}_b}, \quad \forall t. \quad (6.8)$$

This implies that if the battery is cycled at a high DoD for an extended period of time, a relatively large cost is imposed. Hence the cost of power obtained from the storage is dependent on the battery deterioration and replacement cost and is determined as;

$$C_{b.deg}(t) = (P_{b.dc}(t)x_{b.dc}(t) + P_{dc.b}(t)x_{dc.b}(t))C_b(t), \quad \forall t \quad (6.9)$$

where,  $P_{dc.b}(t)$  and  $P_{b.dc}(t)$  shows the battery's charging and discharging power rates along with charging and discharging status  $x_{ac.b}(t) \in [0/1]$  and  $x_{b.dc}(t) \in [0/1]$ , respectively.

5. **User discomfort penalty for power elastic (PE) load demands:** PE loads discussed in Section 3.3 may be interrupted and their power can be reduced to save energy consumption. However, this occurrence will exacerbate the consumers' discomfort. As a result, a discomfort penalty is introduced that an optimization strategy takes into account while constructing different scheduling schemes. The penalty rate  $\zeta$  is proportional to the amount of the curtailed power, and the total penalty cost at any time  $t$  is as follows:

$$C_{PE}^{pen}(t) = \sum_{a \in A_{PE}} (L_a^{PE}(t) - P_a^{PE^-}(t)x_a^{PE}(t))\zeta, \quad \forall t \quad (6.10)$$

where,  $L_a^{PE}(t)$  is the required energy for PE load and  $(L_a^{PE}(t) - P_a^{PE^-}(t))$  reflects the quantity of curtailed demand given  $x_a^{PE}(t) \in [0/1]$  on/off status of the appliance.

6. **Delay tolerant (DT) demands Queue costs:** DT loads discussed in Section 3.3 may be delayed up to a certain time interval till the grid prices become lower in order to reduce the overall cost of power used by these devices. Integrating DT queues enables the delayed activation of DT loads. However, there is a cost associated with building these queues and maintaining them for an extended period of time. This cost increases with the waiting time

representing the users' growing displeasure [119]. This delay cost is illustrated as;

$$C_{DT}^{del}(t) = \sum_{e \in A_{DT}} Q_e^{DT}(t)\delta, \quad \forall t \quad (6.11)$$

where,  $\delta$  is the fixed delay penalty rate for putting the loads in the queue and  $Q_e^{DT}(t)$  represents the queue length.

### 6.2.2 HAPN Component Level Constraints

#### Grid constraints

- Incoming power from the utility grid: It is possible to receive a wide range of electricity from grid at any one moment using the following equation  $t$ .

$$\underline{P}_{g.ac} \leq P_{g.ac}(t)x_{g.ac}(t) \leq \overline{P}_{g.ac}. \quad \forall t \quad (6.12)$$

#### PV array constraints

- Power in-feed from PV panel: The following limitation dictates the maximum amount of PV power that may be derived from the PV array at any given moment  $t$ .

$$P_{pv.dc}(t)x_{pv.dc}(t) \leq \overline{P}_{pv.dc}. \quad \forall t \quad (6.13)$$

#### Diesel engine (DE) constraints

- DE power capacity: In order for a diesel engine generator to provide power in the range of lowest to maximum, this limitation must be met.

$$\underline{P}_{de.ac} \leq P_{de.ac}(t)x_{de.ac}(t) \leq \overline{P}_{de.ac}. \quad \forall t \quad (6.14)$$

- DE start-up indicator: The indication  $z_{de}(t)$  changes to 1 whenever the generator moves from a static to a dynamic mode.

$$-x_{de.ac}(t-1) + x_{de.ac}(t) - z_{de}(t) \leq 0. \quad \forall t \quad (6.15)$$

But we think that shutting off the DE will cost nothing, thus we don't utilize any signal for that.

#### ESDs constraints

- Evolution of ESDs' energy states The difference in energy levels between the ESDs for various time slots ( $\Delta t = t - (t-1)$ ) is shown in the following equation. Charge and discharge rates and efficiency variables cause this disparity in energy levels.

$$\begin{aligned} \eta_{b.con}P_{ac.b}(t) \times \Delta t - \eta_{b.con}^{-1}P_{b.ac}(t) \times \Delta t \\ = E_b(t) - E_b(t-1). \quad \forall t \in [2 \dots T-1] \end{aligned} \quad (6.16)$$

**Remark 11.** *ESDs are expected to have the same initial and final SoC, such that the storage must have the same value of SoC starting the following day;  $E_b(1) \simeq E_b(T) \simeq \varepsilon$ .*

- Actual capacity of the ESDs: The maximum and lowest values of the ESDs limit the available storage capacity.

$$\underline{E}_b \leq E_b \leq \bar{E}_b. \quad \forall t \quad (6.17)$$

- Maximum (dis)charge rates for ESDs: The ESDs' charging and discharging rates are limited by the specified restrictions.

$$\underline{P}_{ac.b} \leq P_{ac.b}(t)x_{ac.b}(t) \leq \bar{P}_{ac.b}, \quad \forall t \quad (6.18)$$

$$\underline{P}_{b.ac} \leq P_{b.ac}(t)x_{b.ac}(t) \leq \bar{P}_{b.ac}. \quad \forall t \quad (6.19)$$

### Power elastic (PE) demands constraints

The greatest amount of energy required to meet these needs is stated as follows:

$$P_a^{PE^-}(t)x_a^{PE}(t) \leq \bar{P}_a^{PE^-}. \quad \forall a, t \quad (6.20)$$

### Time elastic electrical controllable load (ECL) demands constraints

#### Energy constraints

- Appliance phase energy specification: Each device's  $b$  phase  $d$  has a certain amount of energy it needs. Total power for one phase must meet these limits in order to satisfy the stated demand.

$$\sum_{t=1}^T P_{b,d}^{ECL^-}(t) - E_{b,d}^{ECL} \leq 0. \quad \forall b, d \quad (6.21)$$

- Appliance phase power limits: There is a maximum amount of power that can be fed into a device during any phase of operation. In the following constraint, we provide this upper limit as;

$$\underline{P}_{b,d}^{ECL} \leq P_{b,d}^{ECL^-}(t)x_{b,d}^{ECL}(t) \leq \bar{P}_{b,d}^{ECL}. \quad \forall b, d, t \quad (6.22)$$

#### Time constraints

- Appliance phase time bounds: There is a time restriction for each phase of a gadget to be used. This time-bound is shown in the form of;

$$\underline{\tau}_{b,d}^{ECL} \leq \sum_{t=1}^T x_{b,d}^{ECL}(t) \leq \bar{\tau}_{b,d}^{ECL}. \quad \forall b, d \quad (6.23)$$

- Appliance intra-phase operations: Every stage must be completed in its entirety, without interruption. Cycles are completed via an auxiliary variable  $s_{b,d}^{ECL}(t)$  that is set to 1 when a given phase has been completed [177]. Then it must stay constant for the duration of the device's operation.

$$x_{b,d}^{ECL}(t) + s_{b,d}^{ECL}(t) \leq 1, \quad \forall b, d, t \quad (6.24)$$

$$x_{b,d}^{ECL}(t-1) - x_{b,d}^{ECL}(t) - s_{b,d}^{ECL}(t) \leq 0, \quad \forall b, d, \forall t = 2, 3, \dots, T \quad (6.25)$$

$$s_{b,d}^{ECL}(t-1) - s_{b,d}^{ECL}(t) \leq 0. \quad \forall b, d, \forall t = 2, 3, \dots, T \quad (6.26)$$

- Appliance inter-phase operation: To begin the following step, a device must have completed the previous phase first;

$$x_{b,d}^{ECL}(t) - s_{b,(d-1)}^{ECL}(t) \leq 0, \quad \forall b, t, \forall d = 2, 3, \dots, D \quad (6.27)$$

- Appliance inter-phase delay: The following delay limitation guarantees that the start time of the next phase may be flexible.

$$d_{b,d}^{ECL}(t) = s_{b,(d-1)}^{ECL}(t) - (x_{b,d}^{ECL}(t) + s_{b,d}^{ECL}(t)), \quad \forall b, t, \forall d = 2, 3, \dots, D \quad (6.28)$$

As a result of the trade-off between cost and comfort, the delay  $d_{b,d}^{ECL}(t)$  is customizable.

$$\underline{D}_{b,d} \leq \sum_{t=1}^T d_{b,d}(t) \leq \overline{D}_{b,d}, \quad \forall t, b, \forall d = 2, 3, \dots, T \quad (6.29)$$

### Time elastic thermal controllable load (TCL) demands constraints

- Appliance power limits: The operational device's power range is limited to a certain phase;

$$\underline{P}_c^{TCL} \leq P_c^{TCL^-}(t)x_c^{TCL}(t) \leq \overline{P}_c^{TCL}, \quad \forall c, t \quad (6.30)$$

- Appliance temperature limits: The user determines the device's operating temperature range, and the permissible fluctuations are constrained by the following restrictions.

$$\underline{T}_c^{TCL} \leq T_c^{TCL}(t) \leq \overline{T}_c^{TCL}, \quad \forall c, t \quad (6.31)$$

- Temperature variations in thermal devices: The changing temperature situation inside a thermal chamber (i.e., refrigerator, freeze) is shown as [46, 205];

$$\begin{aligned} T_c^{TCL}(t) &= T^{room}(t) - P_c^{TCL^-}(t)R_c^{TCL} \\ &- (T^{room}(t) - P_c^{TCL^-}(t)R_c^{TCL} - T_c^{TCL}(t-1))e^{-\Delta t/R_c^{TCL}C_c^{TCL}}, \end{aligned} \quad (6.32)$$

$$\forall c, \forall t = 2, 3, \dots, T$$

where,  $T_c^{TCL}(t)$  represents inside temperature;  $R_c^{TCL}$  depicts equivalent thermal resistance;  $C_c^{TCL}$  represents equivalent heat rate;  $P_c^{TCL^-}(t)$  is equivalent heat capacity. The model is already explained in Section 3.3.2.

### Time elastic DT demands constraints

- Appliance power limitation: The amount of energy dissipated by these demands is limited by their maximum energy need, which is specified as;

$$\underline{P}_e^{DT} \leq P_e^{DT^-}(t)x_e^{DT}(t) \leq \overline{P}_e^{DT}. \quad \forall e, t \quad (6.33)$$



- Load queue: A demand queue is constructed, which enforces the DT load scheduling architecture [119]. At every point in time  $t$ , the cumulative load demands in a queue are denoted by the symbol  $Q_e^{DT}(t)$  and are summarized as;

$$Q_e^{DT}(t) = \max[Q_e^{DT}(t-1) - P_e^{DT^-}(t)x_e^{DT}(t), 0] + L_e^{DT}(t), \quad \forall e, t \quad (6.34)$$

where, Loads entering the queue are referred to as  $L_e^{DT}(t)$ , while those leaving the queue are referred to as  $P_e^{DT^-}(t)$ . This queue emptying rule must be enforced in order to maintain the above queue steady.

**Remark 12.**  $P_e^{DT^-}(t) \geq L_e^{DT}(t)$ .

### 6.2.3 HAPN System Level Constraints

- Power balancing constraints: The following equation assures supply and demand equilibrium to keep the power network stable and to minimize the power losses.

$$\begin{aligned} P_{g.ac}(t) + P_{pv.ac}(t) + P_{de.ac}(t) + P_{b.ac}(t) \\ = P_{ac.load}(t) + P_{ac.b}(t). \quad \forall t \end{aligned} \quad (6.35)$$

- Operations of ESDs: The following limitations prohibit concurrent charging  $x_{ac.b}(t) \in [0/1]$  and discharging  $x_{b.ac}(t) \in [0/1]$  operations of ESDs at any time  $t$ .

$$x_{ac.b}(t) + x_{b.ac}(t) \leq 1. \quad \forall t \quad (6.36)$$

- Prohibition of charging ESDs from grid power: ESDs cannot be charged from the grid because of the following restrictions;

$$x_{ac.b}(t) + x_{g.ac}(t) \leq 1. \quad \forall t \quad (6.37)$$

- Prohibiting inter-ESDs energy sharing: With the following limitations, one may deny the inefficient charging of ESDs from each other.

$$x_{b.ac}^{HBS}(t) + x_{ac.b}^{EVS}(t) \leq 1, \quad \forall t \quad (6.38)$$

- Prohibiting energy export: The following restrictions specifies the HAPN's no-export guidelines.

$$\begin{aligned} P_{de.ac}(t) + P_{pv.ac}(t) + P_{b.ac}(t) \\ - P_{ac.load}(t) - P_{ac.b}(t) \leq 0. \quad \forall t \end{aligned} \quad (6.39)$$

- Time preferences for (dis)charging of EV storage: The following limitations illustrate the time restrictions requirement for charging and discharging EV batteries.

$$x_{b.ac}^{EVS}(t) - TP_{b.ac}^{EVS}(t) \leq 0, \quad \forall t \quad (6.40)$$

$$x_{ac.b}^{EVS}(t) - TP_{ac.b}^{EVS}(t) \leq 0. \quad \forall t \quad (6.41)$$

The user time preference for discharging and charging of EV storage are expressed in terms of  $TP_{b.ac/ac.b}^{EVS}(t)$ .

- ECL user time preference: The ECL demands requirements are flexible and may be changed at any point in time  $t$ . A user's preferred time zone ( $TP_{b,d}^{ECL}(t)$ ) may be customized for a specific phase of a particular device.

$$x_{b,d}^{ECL}(t) - TP_{b,d}^{ECL}(t) \leq 0. \quad \forall b, d, t \quad (6.42)$$

- Demand response signal: Security constraints on the maximum amount of electricity that may be provided to the whole load of a smart home. As a precaution, the utility is sending out a warning signal to prevent overloading in the power grid.

$$P_{ac.load}(t) - P_{ac.load}^{peak}(t) \leq 0. \quad \forall t \quad (6.43)$$

## 6.3 Demand Side Management Problem Formulation and Optimization Strategy

This section provides a mathematical treatment of the evaluation issue. The objective is to reduce the total cost of electricity, to alleviate inhabitants' discomfort, and to maximize the self-sufficiency of local energy generation.

Consider a HAPN that has a collection of generators  $\mathcal{G} = \{1, 2, \dots, n^G\}$  and a set of demands  $\mathcal{D} = \{1, 2, \dots, n^D\}$ . The model is made up of a collection of energy entities  $A_{EEs} \in [\mathcal{G} \cup \mathcal{D}]$  that are all connected in a single operational domain (Home).

Let  $P_t^{\mathcal{G}} \in \mathbb{R}_+$  be the power given by the individual power source at time-slot  $t \in \mathcal{T} = \{\tau, \dots, \tau + T - 1\}$  and  $x_t^{\mathcal{G}} \in \mathbb{R}_+$  is the sources binary activation set. Similarly,  $P_t^{\mathcal{D}} \in \mathbb{R}_+$  be the power demand of each kind of load connected to the HAPN,  $x_t^{\mathcal{D}} \in \mathbb{R}_+$  is the appliances' on/off set. A subset  $\mathcal{G}_{AC}$  of generators (i.e., Grid, DE) are connected to the HAPN's AC line, while a subset  $\mathcal{G}_{DC}$  of generators (i.e., PV, ESDs) are connected to the DC line. The requests, on the other hand, are presumed to be AC and are connected only to the AC line.

The HEMS performs an evaluation of a collection of cost functions  $\mathcal{C}_t : \mathbb{R}_+ \mapsto \mathbb{R}_+$ , defining the cost of delivering energy to houses, the operation and maintenance of ESEs, and the penalty costs related with user discomfort during time-slot  $t$ .

**Remark 13.** *Given the HAPN's power sources feasible binary schedule sets  $\mathcal{X}^{\mathcal{G}} = [x_t^{\mathcal{G}}, \dots, x_{\tau+T-1}^{\mathcal{G}}]$  and their activation profile will be  $\mathbf{x}^{\mathcal{G}} \in \mathcal{X}^{\mathcal{G}}$ .*

**Remark 14.** *Given the HAPN's generators feasible power schedule sets  $\mathcal{P}^{\mathcal{G}} = [P_t^{\mathcal{G}}, \dots, P_{\tau+T-1}^{\mathcal{G}}]$  and their power supply profile will be  $\mathbf{P}^{\mathcal{G}} \in \mathcal{P}^{\mathcal{G}}$ .*

**Remark 15.** *Given the HAPN's load demands feasible binary schedule sets  $\mathcal{X}^{\mathcal{D}} = [x_t^{\mathcal{D}}, \dots, x_{\tau+T-1}^{\mathcal{D}}]$  and their activation profile will be  $\mathbf{x}^{\mathcal{D}} \in \mathcal{X}^{\mathcal{D}}$ .*

**Remark 16.** *Given the HAPN's load demands feasible power dissipation schedule sets  $\mathcal{P}^{\mathcal{D}} = [P_t^{\mathcal{D}}, \dots, P_{\tau+T-1}^{\mathcal{D}}]$  and their power demand profile will be  $\mathbf{P}^{\mathcal{D}} \in \mathcal{P}^{\mathcal{D}}$ .*

By adopting the general issue formulation as follows, the HEMS may minimize

the overall cost of power required per scheduling horizon  $T$ .

$$\begin{aligned}
 \min_{\mathbf{u}(t)} \quad & \sum_{t=0}^T \mathbf{C}(t)(\mathbf{u}(t)), \\
 \text{s.t.} \quad & A_{eq}\mathbf{u} = b_{eq} \\
 & A\mathbf{u} \leq b \\
 & lb \leq \mathbf{u} \leq ub
 \end{aligned} \tag{6.44}$$

where,  $\mathbf{u}_t \in [(\mathbf{x}^G \in \mathcal{X}^G) \cup (\mathbf{P}^G \in \mathcal{P}^G) \cup (\mathbf{x}^D \in \mathcal{X}^D) \cup (\mathbf{P}^D \in \mathcal{P}^D)]$ ,  $A_{eq}$  &  $A$  are coupling constraint matrix, and  $lb$  &  $ub$  represents lower and upper bound, respectively.

Additionally, a modeling system is implemented to maximize the variability in the operating expenses of HAPN's numerous components (e.g., variable prices of grid energy, fuel and maintenance costs of DE, operational costs of DE, PV, and ESDs). The suggested supply and demand “min-max” co-scheduling system (MMCS) integrates the scheduling mechanisms of energy supply sources and energy-consuming devices. It optimizes the supply and load profiles of a HAPN by combining source-controlled loads (i.e., SLDs, ESDs) and load-driven energy sources (i.e., grid, DE, ESDs), despite the fact that the PV source is often uncontrolled. As a result, the issue is a MILP problem, which falls into the group of NP-hard problems, which are notorious for becoming unmanageable as they grow in size. The accumulative cost reduction issue for the day ahead is mathematically stated as follows:

$$\begin{aligned}
 \mathcal{C}_1 = \min_{\mathbf{u}(t)} \quad & \sum_{t=0}^T \{C_g(t) + C_{pv}(t) + C_{DE}(t) + C_{DE}^{su}(t) + C_{DE}^{sd}(t) \\
 & + C_{DE}^{om}(t) + C_{DE}^{co2}(t) + C_{b.deg}(t) + C_{PE}^{pen}(t) + C_{DT}^{del}(t)\}, \\
 \text{s.t.} \quad & (1), (13 - 54)
 \end{aligned} \tag{6.45}$$

The objective of increasing customer satisfaction is expressed indirectly by lowering the penalty cost associated with reduced load requests and the queue evolution cost associated with delayed load demands. Additionally, the author stresses the self-sufficiency of the HAPN in this article by optimizing the self-generation ratio (SGR). This ratio typically refers to the maximal usage of the photovoltaic source, and the ESDs linked to the HAPN and is calculated as follows:

$$\begin{aligned}
 \mathcal{C}_2 = \max_{\mathbf{u}(t)} \quad & \sum_{t=0}^T \{-P_{ac.load}(t) + P_{b.ac}(t)x_{b.ac}(t) + P_{pv.ac}(t)x_{pv.ac}(t)\}, \\
 \text{s.t.} \quad & (1), (13 - 54)
 \end{aligned} \tag{6.46}$$

The suggested HEMS is shown in Figure 6.2. Solar irradiance, price signals, and power use are determined using historical and climatic data. The issue is defined in conjunction with the time horizon  $t$ .

### 6.3.1 Co-scheduling Optimization Algorithm

The objective is to develop a scheduling strategy for  $\mathbf{u}(t)$  that regulates the in-feed from the grid, PV, and DE, as well as the out-feed to the smart load devices (SLDs). The policy is based on the following criteria:

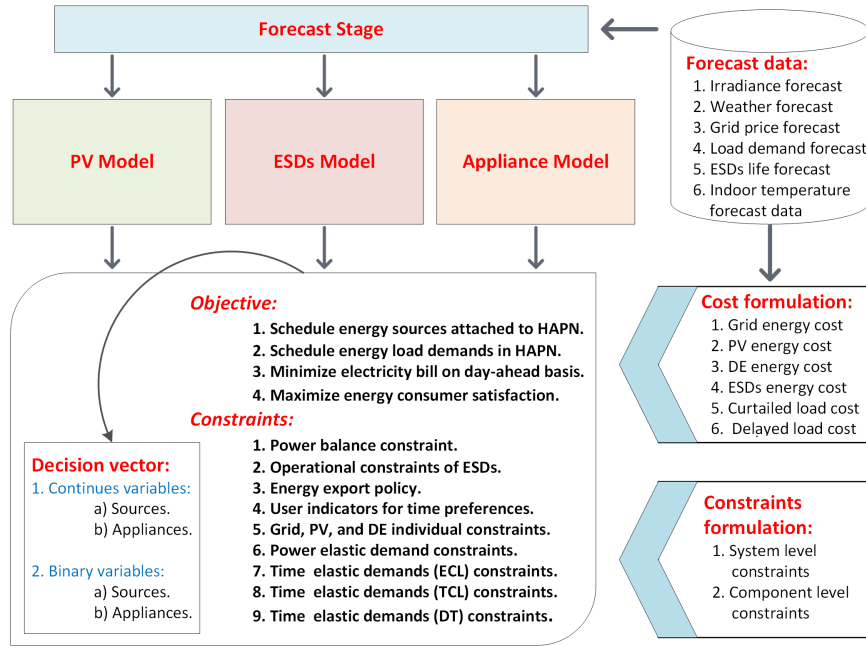


**Figure 6.2:** The multi-objective optimization problem for HEMS.

1. Minimize the overall cost of energy used.
2. Maximize customer satisfaction.
3. Maximizing the consumption of photovoltaic energy.
4. Optimum operating of ESDs.

Similarly, it is implemented within the limits imposed by different system and component-level constraints. These restrictions contribute to system stability by imposing lower and upper boundaries on supply and demand, hence imposing physical restraints on the nanogrid's important energy entities.

When the HEMS is activated, it takes into account the prices associated with various energy sources (including forecasted grid price signals, degradation costs of the storage devices, and DE operating costs). Additionally, it included information on proposed penalty or award values for SLDs (curtailed and delayed loads). Additionally, HEMS incorporates pre-configured information about appliance operation circumstances, including consumer settings, time preferences for activation loads, device type of usage, load power profile, achieving precise energy requirements, and optimum cooling temperature for TCLs. While it also incorporates anticipated inside temperature data over the following 24 hours in order to generate a TCL activation profile. The optimal scheduling sequence for both ESEs and SLDs is determined using an optimization technique. These scheduling sequences ensure that a residential user pays the least amount of power possible while maintaining a high degree of satisfaction across the time horizon  $T$ . It consists of the following workload model:

- The optimal time slots and cost for grid energy use.
- The ideal charging and discharging arrangement of ESDs to maximize energy savings.

- The diesel engine’s shut-down time.
- The power that is restricted for power elastic loads.
- The maximum delay time that should be used for queuing loads.
- The time at which time elastic ECL loads begin to act.
- The trade-off between temperature and load activation for TCL devices.

The optimization algorithm mentioned below encompasses the optimization formulation’s iterative process.

---

**Algorithm 2** Algorithm for Cost-Comfort Reciprocity

---

```

1: procedure MILP(System & cost parameters)
2:   System Initialization
3:   Set parameter values
4:   Set consumer preferences
5:   Set system bounds
6:   while  $\mathcal{C}_1 \neq \min(\text{Cost})$  &  $\mathcal{C}_1 \neq \max(\text{SGR})$  do
7:     for ( $t \leq T - 1$ ) do
8:       Initialize system constraints
9:       Initialize components constraints
10:      Implementing Branch & Bound algorithm
11:      Store scheduling variables set ( $\mathbf{u}_t$ )
12:       $t \leftarrow t + 1$ 
13:      Execute problem set:  $\mathcal{C}_1$  &  $\mathcal{C}_2$ 
14:       $\mathbf{u}_t \rightarrow [\mathbf{x}^G, \mathbf{P}^G, \mathbf{x}^D, \mathbf{P}^D]$  ▷  $\mathbf{u}_t \in [\mathbf{u}_1, \mathbf{u}_2, \dots, \mathbf{u}_{T-1}]$ 
15: Conclude day-ahead total electricity cost
16: Conclude day-ahead self-sufficiency
17: Conclude SLDs satisfaction level (SL)
18: Conclude ESEs utilization factor (UF)

```

---

Laptop with Intel Core i7 CPU and 20GB of RAM is used for the simulation of the suggested optimization model. “MATLAB” toolkit for optimization is used to calculate the results. A linear objective function is given that can solve the linear programming problem using the intlinprog solver. Nonetheless, “primal-simplex” is a linear programming algorithm used to solve this problem, and the search strategy is “Branch and bound” to find the best answer. Energy supply entities (ESEs) costs and the 24-hour day-ahead power profile of several SLDs were calculated using a time slot resolution ( $\Delta t$ ) of 15 minutes.

Thus, our scheduling problem is a mixed-integer linear problem that traces previously predicted values of day-ahead photovoltaic supply and user load demand and generates a cost-optimal decision vector for obtaining energy from multiple supply sources and intelligently activating various types of user load demand. To demonstrate how to construct the appliance scheduler framework, the next part presents a case study using several kinds of household appliances with variable energy usage patterns.

## 6.4 Numerical Analysis of DSM Technique

The study illustrates power allocation techniques via the use of an optimum scheduling algorithm. The scheduling choices are made using a MILP-based optimization approach. Consider a smart house that operates autonomously as a nano-grid. To demonstrate the energy network model for a single house with a variable number of occupants. The author has coined the acronym home area power network (HAPN). Table 6.3 summarizes the parametric values for the different power entities included in the system model:

**Table 6.3:** System parameters. (pred, predicted)

| Parameters   | Value (Watts)   | Parameters                             | Value                             |
|--|-----------------|--|-----------------------------------|
| $\underline{P}^{GR}/\overline{P}^{GR}$             | 1/5000          | $\underline{P}^{DE}/\overline{P}^{DE}$ | 1000/3500                         |
| $\overline{P}^{PV}$                                | $\max[0, pred]$ | $\epsilon$                             | $0.5 \times \overline{E}_k^{bat}$ |
| $C^{HB}$   | 5120 Wh         | $E_{HB}^{bat}$                         | $0.8 \times C^{HB}$               |
| $C^{EV}$   | 22000 Wh        | $E_{EV}^{bat}$                         | $0.7 \times C^{EV}$               |
| $\underline{E}_{HB}^{bat}/\overline{E}_{HB}^{bat}$ | 800/4900        | $\eta_{HB}$                            | 0.96                              |
| $\underline{E}_{EV}^{bat}/\overline{E}_{EV}^{bat}$ | 4400/19800      | $\eta_{EV}$                            | 0.96                              |
| $\overline{P}_{(ch/dch),HB}^B$                     | 800/1280        | $\overline{P}_{(ch/dch),EV}^B$         | 7000/14000                        |
| $TP_t^{EV-}$                                       | 18:00→09:00     | $\Delta t$                             | 15 min                            |

While the cost parameters associated with various EEs are given as:

**Table 6.4:** Cost parameters (cents/Watt). (pred, predicted)

| Parameters     | Value              | Parameters                | Value              |
|----------------|--------------------|---------------------------|--------------------|
| $q_t$          | $\max[0, pred]$    | $\varsigma$               | 0.01               |
| $\beta/\gamma$ | 0/1                | $\xi$                     | 5.45               |
| $\sigma^f$     | 0.3                | $\sigma^{sd}/\sigma^{su}$ | 200                |
| $\sigma^{om}$  | 100                | $\pi_{k,t}$               | 0.5                |
| $\zeta$        | $3 \times 10^{-3}$ | $\delta$                  | $2 \times 10^{-5}$ |

The suggested HEMS is intended to demonstrate the scheduling framework's response to a dynamic goal function. The optimization method that seeks the lowest cost also has the goal of increasing a HAPN's self-sufficiency. The procedure as a whole involves predicting grid energy costs, solar irradiance, and room temperature, as well as addressing the optimization issue. The impact of the price signal being indirectly linked to a peak power indication is also discussed in terms of daily peak demand. Additionally, minimum and maximum energy constraints are established for each energy supply and demand entity to ensure a realistic range of activities. Finally, the proposed home energy management system (HEMS) is evaluated for five distinct ESEs profiles and two different SLDs profiles. From Section 3.3 the realistically generated SLDs profiles are utilized to illustrate the scheduling scheme's success in reducing energy costs and peak load demands.

### 6.4.1 Load Demand Prediction Module

The author has implemented the predicted energy demand model from Section 3.3, determining the precise amount of electricity required by activating actual household appliances [165]. This model incorporates active inhabitants, who have an effect on the energy demand pattern. The maximum number of occupants is assumed to be 5. A probabilistic strategy is used to account for the activation of various appliances in a residence. Table 6.5 illustrates the characteristic values associated with different home appliances.

**Table 6.5:** Energy demands parameters. (pred, predicted)

| Parameters                        | Value                  | Parameters                        | Value                     |
|-----------------------------------|------------------------|-----------------------------------|---------------------------|
| $L_{a,t}^{PE}$                    | $max[0, pred]$         | $L_{e,t}^{DT}$                    | $max[0, pred]$            |
| $\bar{P}_a^{PE}$                  | $max[0, L_{a,t}^{PE}]$ | $\bar{P}_e^{DT}$                  | $max[0, L_{e,t}^{DT}]$    |
| $(\underline{P}/\bar{P})_R^{TCL}$ | 100/105                | $(\underline{T}/\bar{T})_R^{TCL}$ | 0/4                       |
| $(\underline{P}/\bar{P})_F^{TCL}$ | 160/170                | $(\underline{T}/\bar{T})_F^{TCL}$ | -20/ - 16                 |
| $\underline{P}_W^{ECL}$           | [16, 32, 5, 17, 66]    | $\bar{P}_W^{ECL}$                 | [42, 3084, 100, 170, 203] |
| $\underline{P}_D^{ECL}$           | [1500, 1000]           | $\bar{P}_D^{ECL}$                 | [2500, 1000]              |
| $\underline{\tau}_W^{ECL}$        | [15, 15, 60, 30, 15]   | $\bar{\tau}_W^{ECL}$              | [15, 15, 60, 30, 15]      |
| $\underline{\tau}_D^{ECL}$        | [45, 15]               | $\bar{\tau}_D^{ECL}$              | [45, 15]                  |
| $(\underline{D}/\bar{D})_{W,d}$   | [0, 0, 0, 0, 0]        | $(\underline{D}/\bar{D})_{D,d}$   | [0, 0]                    |
| $R_R^{TCL}$                       | 0.408                  | $C_R^{TCL}$                       | 2599                      |
| $R_F^{TCL}$                       | 0.608                  | $C_F^{TCL}$                       | 2599                      |
| $T_t^{room}$                      | $max[0, pred]$         | $\bar{Q}_{e,t}^{DT}$              | 10000                     |
| $TP_{b,d,t}^{ECL}$                | 24 hr                  | $P_t^{L,peak}$                    | 5000                      |

As previously stated, the load demands taken are alternating current (AC) loads. Thus, AC power flow is often described in terms of nonlinear and complicated equations that are incompatible with the suggested scheduling problem describes in [99]. As a result, the equations are approximated as linear real power equations by substituting the power factor nomenclature for the power load needs and neglecting the actual characteristics of the power lines. This approximation has no effect on the investigated scheduling model's solution.

Whereas, in the proposed model, the average number of active inhabitants in a home on any given day of the week and their total energy consumption at any time instant  $t$  are illustrated in Figure 6.3. It demonstrates that the highest number of inhabitants is often activated in the afternoon and evening, at an average number of 3 occupants for the whole day in a dwelling. While energy needs fluctuate significantly during the day. The demand spikes dramatically at night owing to the activation of a large power load, which is most likely the heating load. As seen in the graph below, the average energy consumption forecast is around 1 kWh for each given day.

Similarly, the author has included a predictive PV energy model in [120] that anticipates the precise PV power output based on expected solar irradiance, ambient temperature, and day of the week data. Thus, the entire production of photovoltaic energy may be determined by assessing Section 3.1.1. Solar irradiance data is derived using the "Meteonorm Irradiation Data" program for any given location of the

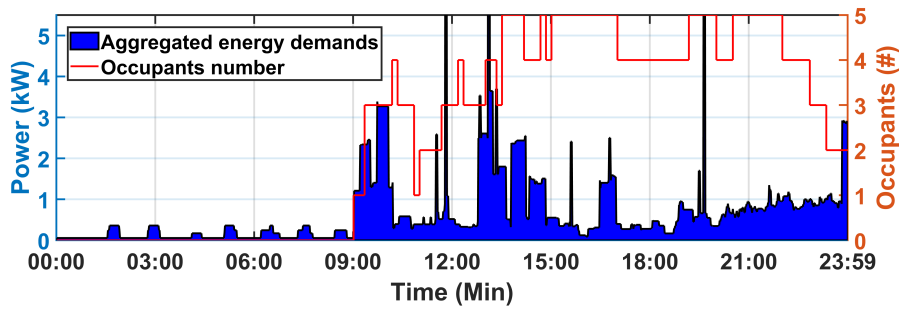


**Figure 6.3:** House occupants and their energy demands.

United Kingdom [1]. This anticipated photovoltaic energy is used to improve the planning of energy storage and load scheduling activities at a specific area.

Additionally, because pricing markets are frequently characterized by non-linearity and inconstancy, price prediction can assist energy producers and purchasers in optimizing their respective scheduling techniques, thereby increasing their profit margins and lowering electricity prices, respectively [118]. This day-ahead energy price may be set by a power company. It may have its own renewable energy sources and may also import electricity from the power grids as needed. The price of electricity varies during the day, based on the state of accessible renewable energy sources and the cost of import from the power grid. The advantage of a utility setting the electricity cost is that it may adjust the cost of power for each energy consumer required to participate in DSM plans. Figure 6.4 displays daily power prices. In this scenario, the author uses a day-ahead price from [3] to analyze the scheduling challenge, ensuring that energy loads are scheduled at low rates.

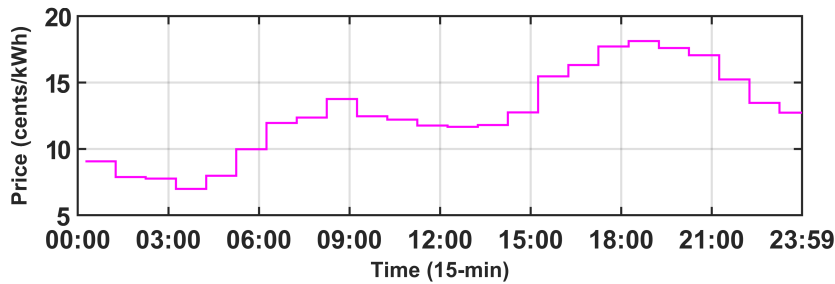


**Figure 6.4:** Day-ahead predicted price.

Additionally, to meet the TCL requirements described in Equation 6.30-6.32, they must work in accordance to the ambient temperature. Thus, for the proposed TCL device, a day-ahead room temperature is anticipated based on previously accessible data, such as the dimensions of the home, the thermal conductivity of the house, the season, the month, the day of the week, and the time of day [146]. The expected indoor temperature for a typical house is shown in Figure 6.5.

#### 6.4.2 Energy Supply Entities Utilization

As described earlier in Section 6.2, the model can run without electricity from the main grid. A grid shutdown signal, as seen in Figure 6.6 is included to demonstrate HAPN's off-grid behavior. The grid's actual power output is shown in Figure 6.7. Here, a high-power load of  $3kW$  is serviced in the early morning about 04:00. At this



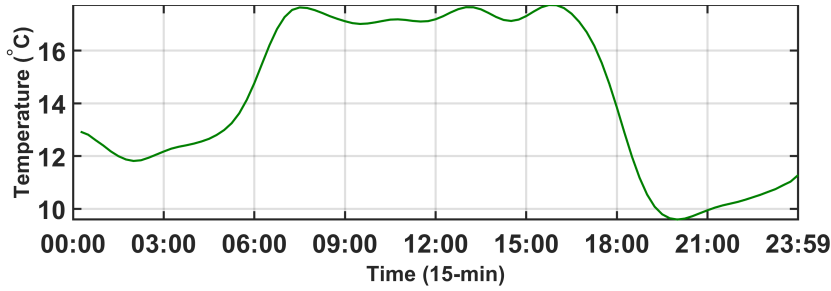


Figure 6.5: Predicted room temperature.

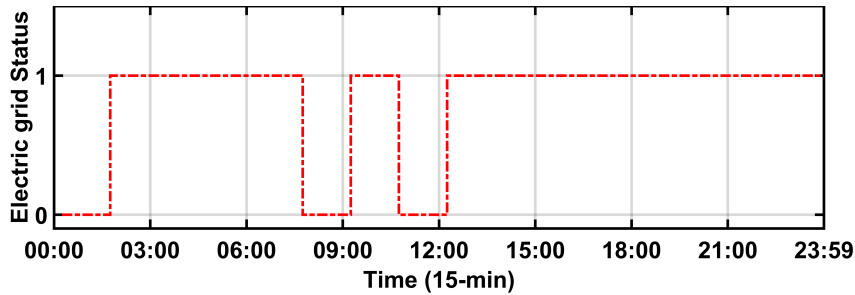


Figure 6.6: Electric grid power outage signal.

time of year, power prices are at their lowest, and when examining the anticipated load needs in Figure 6.3, it is clear that the forecasted loads are little. As a result, it's clear that a shiftable load is being utilized at this moment. Similarly, at the night after 21:00 and before midnight users consume the most energy on average. This is owing to the average low cost of power and the fact that the day is ending. Or, it is the only affordable source of energy available to meet the remaining load needs in any form.

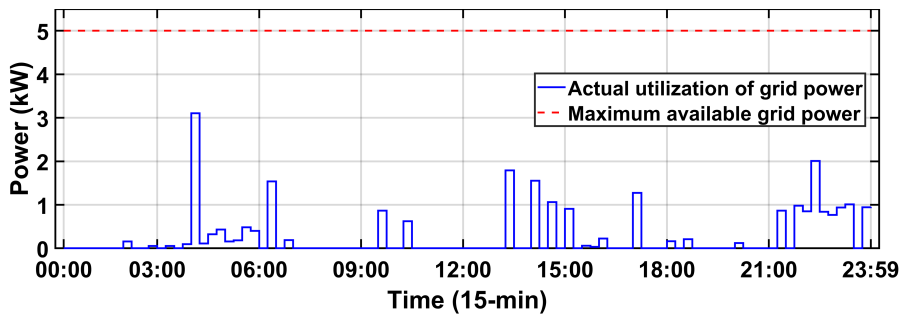


Figure 6.7: Grid power utilization.

Additionally, the power generated by the diesel generator is shown in Figure 6.8. One of the reasons DE power was activated was due to a grid failure. If no other alternative is available during a grid outage, the DE will run. While it can also be run if the cost of producing electricity is quite cheap in comparison to other energy sources.

Similarly, the power generated by the photovoltaic arrays is shown in Figure 6.9. PV energy is intended to power only domestic appliances, and export to the grid is not permitted in this example. In addition, surplus energy may be utilized for recharging energy storage batteries. The only component accessible to store this inexpensive energy is a home battery storage system, which also boosts the HAPN's

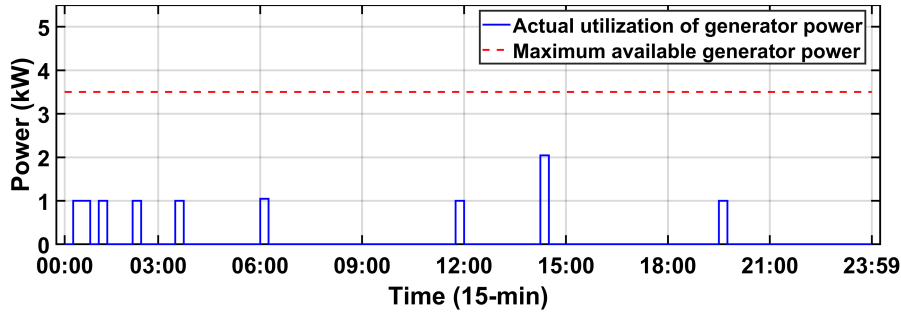


Figure 6.8: Diesel generator power production.

self-sufficiency. When looking to the Figure 6.9, about 08:00, it is clear that the actual use of the photovoltaic source is less than the available. The reason for this is that all loads have been met and charging the home battery storage at this time is not the most cost-effective choice. While the extra PV generation is lost in this situation.

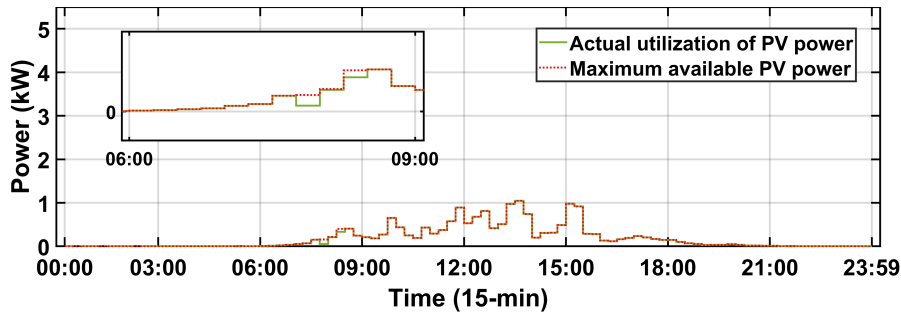


Figure 6.9: Power procured from the PV.

### 6.4.3 Activation of Smart Load Devices

#### Power elastic (PE) demands

Figure 6.10 depicts planned and reduced load requirements. The PE load in this example is mostly comprised of light bulbs that are often triggered at night. As a result, one may see a sizable load being supplied by ESEs throughout the night. Around 14:30, one detects a little load execution, and around 19:45, one witnesses a significant load curtailment. Of course, there is a cost associated with this load reduction step, but it is relatively manageable given our cost function. The greatest load that may be supplied, however, is restricted to Equation 6.43.

#### Electrical controllable load (ECL) demands

Additionally, the estimated number of operational dishwashers and washing machines is described in the load prediction module. These appliances need only to be scheduled once every day and are constrained in two ways (energy and time). A minimum energy level for each operating phase of the device is estimated, as seen in Equation 6.21. While the phase-by-phase power limiter is established in Equation 6.22. Additionally, the phase time constraints are established in accordance with Equation 6.23. As seen in Figure 6.11a, the washing machine is operational

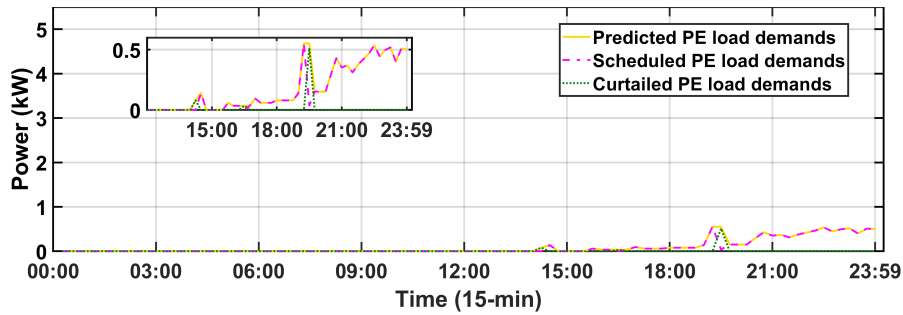


**Figure 6.10:** Power elastic load demands.

from 04:00 to 06:00. The peak power consumption of the washing machine reaches  $3kW$  owing to the heating element that heats the water to the proper temperature prior to cleaning the garments. As mentioned in Table 3.3, there are a total of five stages of WM operations. There is no delay between the device’s various phase actions. While the phase indicator, as illustrated in Figure 6.11b, shows that all of the appliance’s operational stages have been completed successfully.

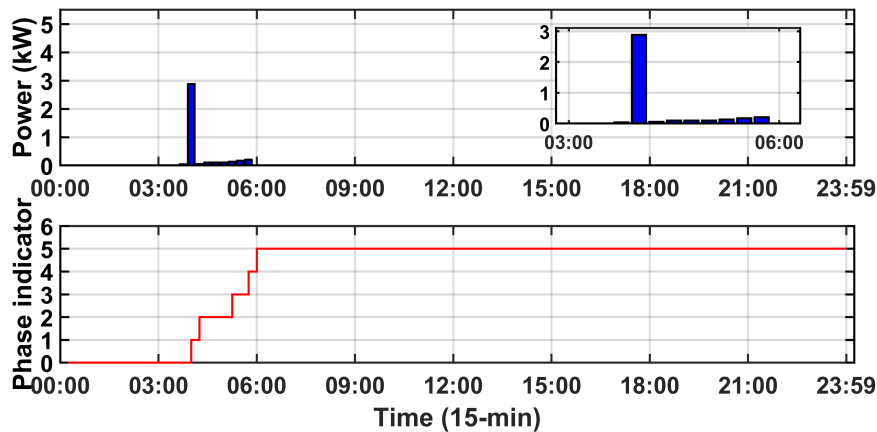


**Figure 6.11:** a) Power profile of WM. b) Phase indicator.

Similarly, the dishwasher begins operation immediately after the washing machine at 06:00, as seen in Figure 6.12a. The rationale for this is because relatively low-cost grid electricity is available at that time. Additionally, the average power is near  $1kW$ , indicating that each of the two phases requires a distinct amount of energy to operate the gadget. Table 3.2 discusses these phases. As with a washing machine, there is no delay between the various phases of the dish washer’s operation. The phase indications, as illustrated in Figure 6.12b, indicate that the appliance has successfully completed all of its operational stages. By concluding, the ECL requests are the only non-deterministic loads that may be completed on demand.

### TCL demands

In this investigation, just one form of TCL load requirement is considered, and that is the cooling load. However, two distinct types of cooling loads are presented for illustration purposes, namely refrigerators and freezers.

Both of these appliances operate in the same manner. The only distinction is that the working temperatures are different. The temperature is set through

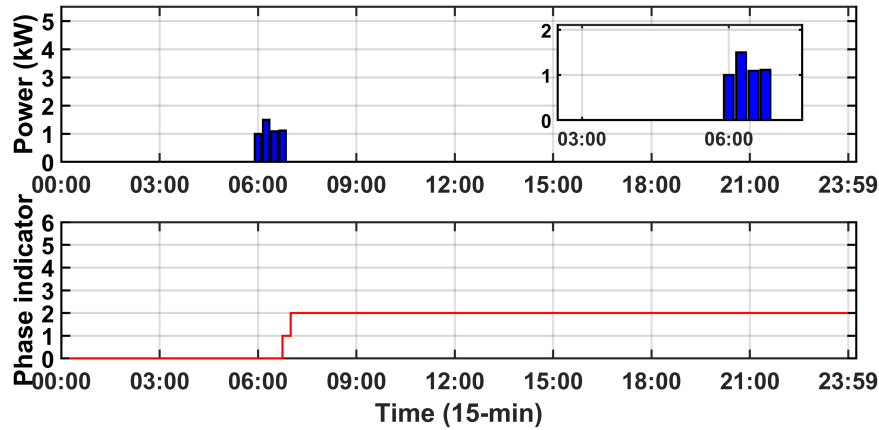


Figure 6.12: a) Power profile of DW. b) Phase indicator.

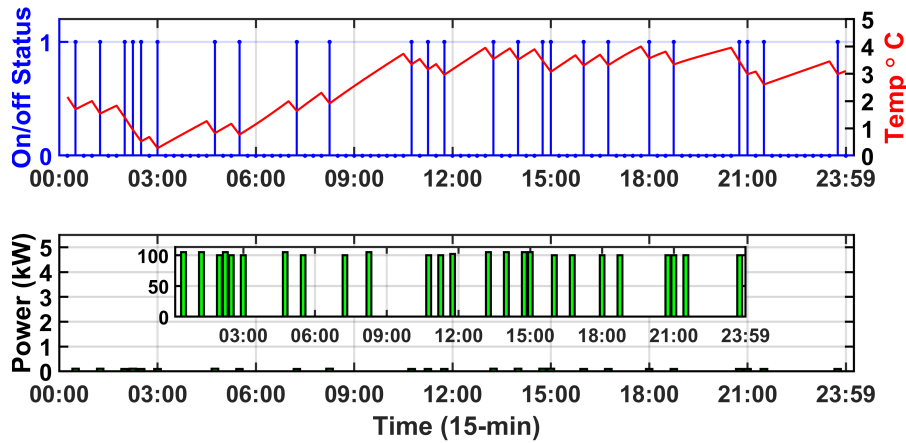


Figure 6.13: a) Temperature profile and on/off status of a refrigerator. b) Power profile of a refrigerator.

Equation 6.31, which is about  $0 \rightarrow 4^{\circ}\text{C}$  for refrigerator and  $-16 \rightarrow -20^{\circ}\text{C}$  for freezer. The refrigerator's activation state is shown in Figure 6.13a, along with its interior temperature profile moving ideally between its lower and higher limits. Additionally, the power profile is presented in Figure 6.13b, which shows almost constant operational power for all of its phases throughout the course of a day.

Similarly, the freezer exhibits the same phenomena as the aforementioned device. The power constraints are represented in Equation 6.30, and the device's temperature changes are regulated through Equation 6.32. Figure 6.14a depicts the freezer's activation and temperature profiles. While Figure 6.14b depicts the daily power profile dispersion.

## DT demands

DT loads are day-ahead deterministic power requirements projected by the prediction module. Equation 6.33 illustrates the power constraints of DT loads, and Equation 6.34 establishes the cumulative load demands. Figure 6.15a depicts the expected rate of real DT demands, while Figure 6.15b depicts the precise quantity of load demands satisfied at any moment  $t$ . Additionally, Figure 6.15c shows the pace at which DT demands enter and exit the load queue. As seen in the image,

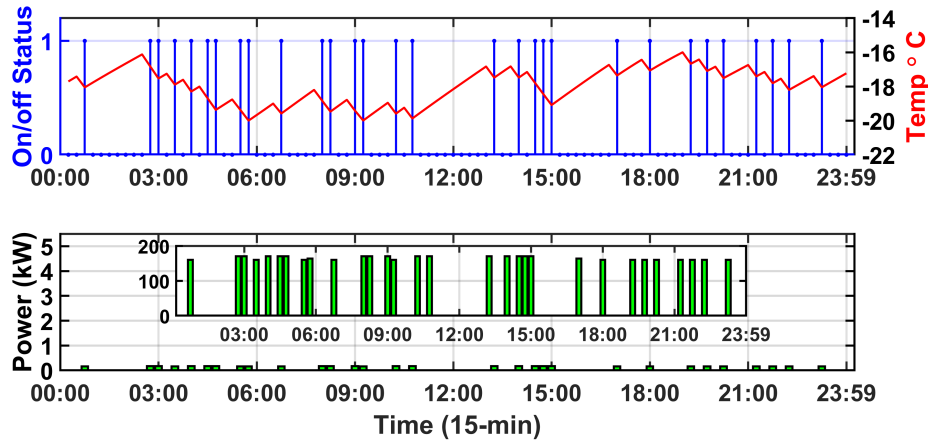


**Figure 6.14:** a) Temperature profile and on/off status of a freezer. b) Power profile of a freezer.

loads are met at the end of the day, but the distinct disparity between projected and planned load needs illustrates the queue's operation.

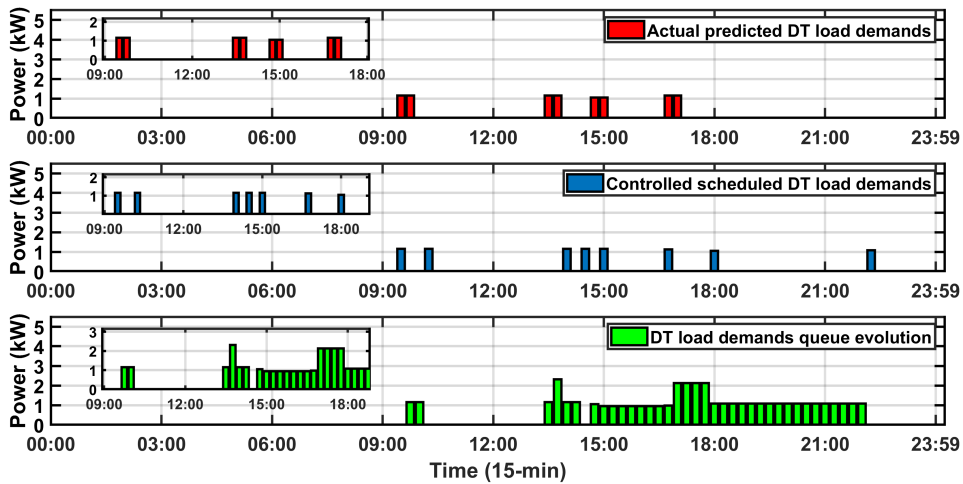


**Figure 6.15:** a) Predicted DT demands. b) Scheduled DT demands. c) DT demands queue backlog.

#### 6.4.4 Incorporation of Energy Storage Devices

The rate at which the ESDs are charged and discharged is shown in Figure 6.16a. Due to the restricted capacity of the storage, the charge and discharge rates are similarly limited, which are determined according to the manufacturer's data. An initial and ultimate SoC( $\epsilon$ ) for ESDs is specified in order to get the necessary quantity of energy in the storage at the end of each day, as seen in Figure 6.16b&c. Setting SoC may also assist in limiting the amount of discharge cycles performed on the storage, which has a significant effect on battery life. When one employ deep cycle discharge (e.g., 80% of DoD), the battery life drops significantly in comparison to 20% DoD. As seen in Figure 6.16b, the house battery is charged throughout the day with extra solar energy. It charges itself in the morning using DE power. Additionally, it is released at a time when energy prices are rising and photovoltaic (PV) power is

diminishing. Similarly, EV storage is charged throughout the day someplace else (often at the office), and a part of it is used at home at times of high grid energy prices, as seen in Figure 6.16c. Due to the capacity restrictions of these ESDs, one can only use them for a short period of time.

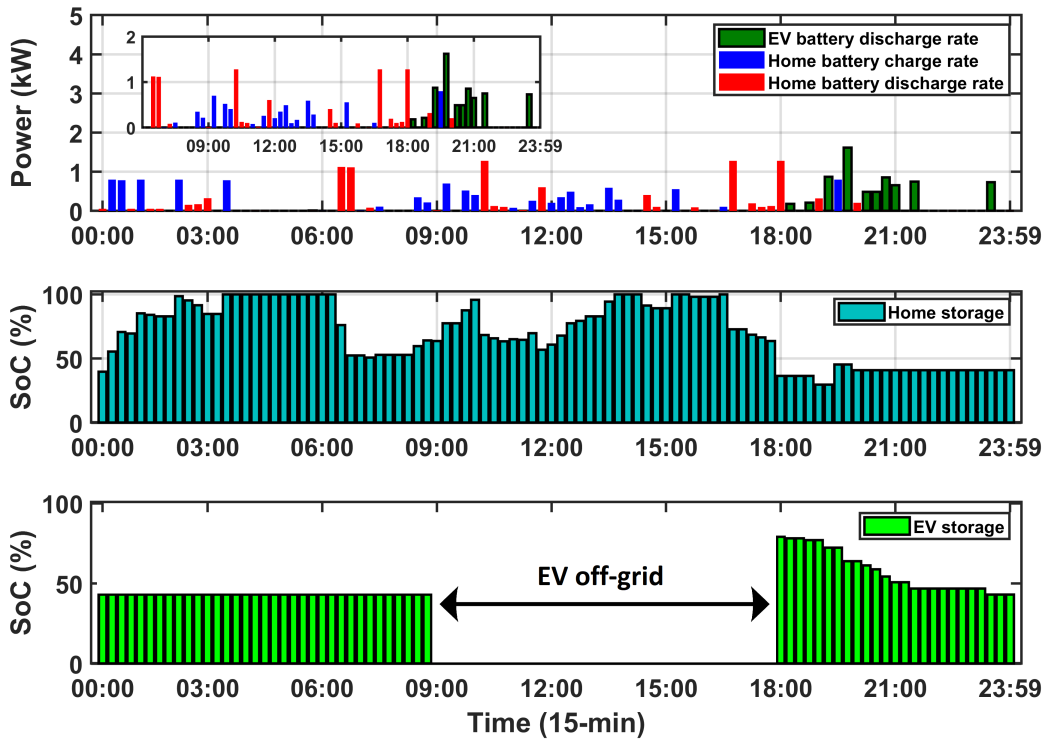


**Figure 6.16:** a) ESDs (dis)charging rates. b) SoCs of HB and EV storages.

#### 6.4.5 Power Mix in a Single HAPN

Figure 6.17 illustrates the day-ahead power auction price. Typically, energy providers set these pricing for their clients. So that clients may take advantage of these fluctuating energy rates and buy energy at their convenience. Additionally, one can notice the activation of other ESEs in the same picture. This activation choice is made by the suggested scheduling mechanism. The cost reduction challenge has been framed in light of the changing energy grid pricing and other system restrictions. The scheduler determines the lowest feasible power cost for employing the optimal mix of accessible ESEs at any given moment,  $t$ . As seen in this picture, power is supplied by the grid throughout the night (21:00 to 24:00) and early morning (04:00 to 06:30), when electricity prices are comparatively cheap. While, about 06:30 a.m., the grid's energy costs are raised and the home battery storage is activated. As soon as the sun rises, energy is obtained from the photovoltaic source. Around midday, energy is redistributed between grid, home battery storage, diesel generator, and photovoltaic sources. However, when the PV power diminishes in the evening, the home battery storage compensates. The storage SoC is still sufficient for discharge. Thus, when PV and diesel generator energy are available, the battery charges itself and discharges itself in the evening when no other source of inexpensive energy is available. Soon after 06:30, the charge in home battery becomes depleted, and another storage electric vehicle becomes accessible. As a result, it is favoured above

all other energy sources until grid electricity prices fall again.

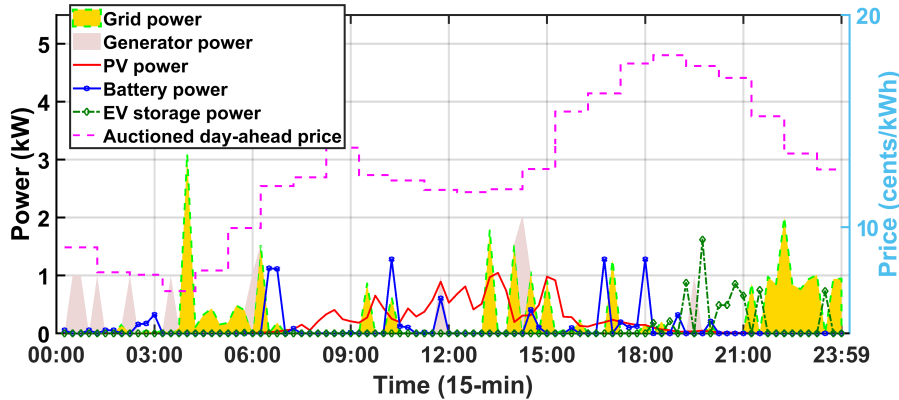


**Figure 6.17:** a) Changing electricity prices. b) Scheduling various ESEs.

Similarly, Figure 6.18 demonstrates the utilization factors and cumulative energy shares of several ESEs incorporated into HAPN. Additionally, it illustrates that the average daily aggregated cost of energy is roughly 310 *cents*. Whereas the total power used by household appliances over the previous 24-hours is around 73 *kW*.

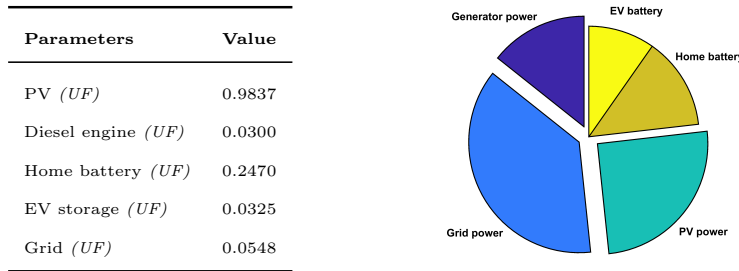


**Figure 6.18:** a) ESEs utilization factor (*UF*). b) Energy shares.

Similarly, Fig. 6.19, illustrates the satisfaction level and the accumulated load demand shares of various SLDs integrated into HAPN.

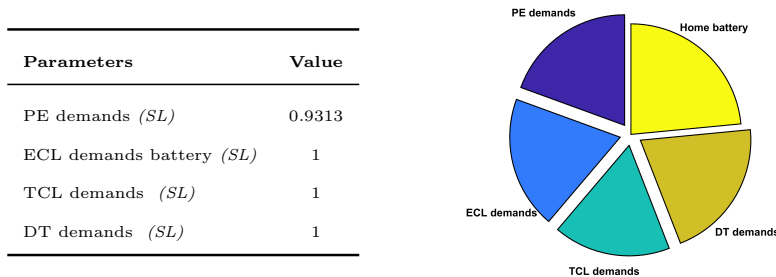


**Figure 6.19:** a) SLDs satisfaction level (*SL*). b) Load shares.

Additionally, as indicated in Figure 6.20, the scheduling approach properly balance the required and generated energy as in Equation 6.35. There is a distinct distinction between typical baseload requirements and SLDs. With an optimal power mix, all loads are fulfilled satisfactorily. Scheduling several ESEs is accomplished by the formulation of a cost minimization and user satisfaction maximization issue.

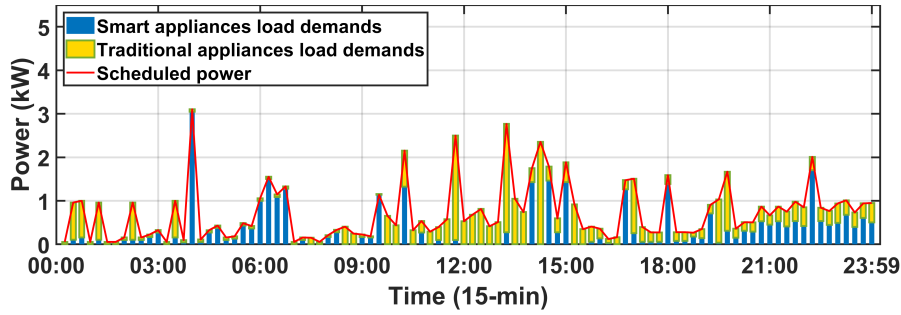


**Figure 6.20:** Total load demands and the scheduling power.

Our scheduling algorithm activates energy sources that are equivalent in price at any given moment  $t$ .

Finally, as seen in Figure 6.21, one can notice a clear difference in load demands before to and after the establishment of a scheduling system. A significant amount of peak load demand is transferred to off-peak times, primarily in the early morning when power prices are lowest. As a result, the peak load is now restricted to  $3kW$ , down from  $3.5kW$  earlier. Similarly, between 00:00 and 09:00 in the morning, the averager anticipated a load demand of less than  $500W$ , which has now increased to approximately  $1kW$ . As a result, one can infer that by implementing the sug-

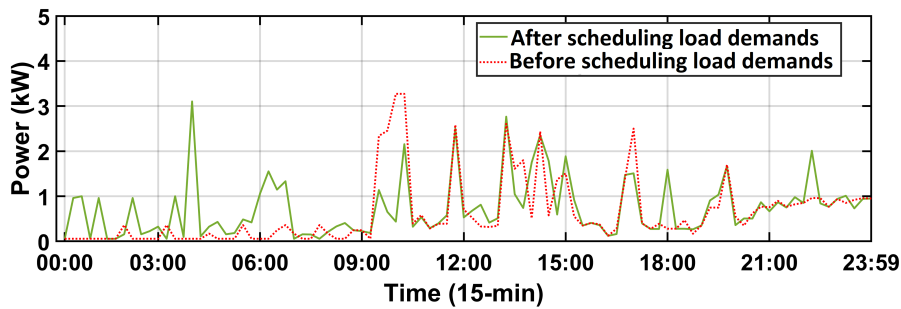


**Figure 6.21:** Pre and post scheduling load demands.

gested HAPN model and optimizing the HEMS, it reduces the cost of power used. Additionally, the peak clipping, valley filling, and load shifting phenomena in the day-ahead EEs scheduling data are also noticed.

#### 6.4.6 Computational Results

The results are generated using the “MATLAB” optimization toolset. The optimization issue is solved using the mixed-integer linear programming (MILP) approach. The MILP solver “intlinprog” is utilized to discover a plausible solution in the preceding analysis (the minimum requirement of supply and demand scheduling problem). This solver is capable of abruptly terminating the practice of looking for an optimum solution. It might be halted if it discovers a realistic solution. Additionally, regardless of whether a viable solution is discovered, the “intlinprog” allows the operator to specify a time limit beyond which the solving must be completed.

The suggested problem resolution is quite huge, means;

- It has 40 optimization variables that take integer values.



- It has 9 linear equality constraints.
- It uses 17 linear inequality constraints.
- It uses 20 bounding condition constraints.

As a result, it is recommended that the sub-optimal energy profiles acquired by the early halted solver are sufficient replacements for the true perfect profiles, which are substantially more time consuming to locate. It takes 21 seconds in this scenario to optimize an integer answer to the desired degree of optimality. The needed degree of optimality in this issue is a “integer viable solution” with a 360 percent relative gap. Thus, it is shown that a fair approximation may be obtained in a reasonable period of calculation time (e.g., around 30 seconds). The preceding analysis demonstrates that it is feasible to implement the suggested framework in the real-time scheduling of home appliances. The amount of time required to make scheduling choices is dependent on the number of decision factors.

## 6.5 Conclusion

A concept of demand side management (DSM) integrated smart home area power network (HAPN) is presented in this chapter. It combines time-varying photovoltaic (PV) energy with two forms of storage (home battery and electric car), and a diesel engine generator (DE) for backup is added. It also includes baseload and smart load devices (SLDs), i.e., power and time elastic appliances. “min-max co-scheduling” home energy management system (HEMS) is introduced, that forces the HAPN’s energy entities (EEs) to coordinate and creates a cost-optimal scheduling framework for powering SLDs. The suggested system also optimizes customer satisfaction factor and  $CO_2$  footprints. The suggested “min-max” multi-objective optimization problem seeks to maximize self-sufficiency and customer satisfaction while reducing cumulative power costs. In addition, a storage degradation model and efficiency metrics of energy storage devices (ESDs) are introduced to calculate storage capacities and prices of the storage devices. The simulation results show the efficacy of the operational approach for scheduling ESEs and SLDs. It also assures the maximum use of locally installed PV energy and high energy consumer satisfaction.

## 7 Thesis Summary and Future Challenges

This study conceptualizes the future of smart homes and introduces a new terminology for Intelligent Home Area Power Networks (HAPN). The work leverages the capabilities of innovative energy generation and flexible load demands through a home communication network, serving as a showcase of the Internet of Things (IoT) within the domain of HAPN. A model-based optimal operation and design algorithm for Photovoltaic (PV) based Microgrids (MGs) is developed, taking into account critical factors such as battery lifetime and grid blackout concerns. A comprehensive generic model for the proposed MGs is introduced, encompassing all operational constraints of MG components. This work highlights the key intelligent features of smart homes that incorporate smart energy generation with flexible load demands and emphasizes the efficacy of power flow strategies in Home Area Power Networks by integrating cost-effective hybrid AC/DC grid configurations and energy storage components.”

The widespread adoption of new technologies and the growing use of electrical appliances in daily life have resulted in a significant surge in energy consumption across all sectors. Currently, conventional power sources such as fossil fuels or coal-fired power plants dominate energy production. However, due to the escalating costs of fuel and the pressing issue of pollution, there is a growing global trend towards cleaner, more affordable, and readily available natural renewable energy sources such as solar and wind. The increasing demand for energy and the desire for cost-effective and clean electricity have fueled the popularity of Photovoltaic (PV) and Electric Vehicle (EV) systems. However, the inconsistent PV power output, the variability of consumer load demands, and the limitations of EV storage pose significant challenges to the stability of power networks. To overcome the issues, a predictive intelligent energy management system (iEMS) is presented in this book. It forecasts seasonal PV power and utilizes real-life consumer load needs while observing the limitations of EV storage and the utility grid. The iEMS uses a day-ahead linear programming based mixed-integer expert system to schedule multiple power sources connected to HAPN. One essential element of the current power system paradigm is the capacity to regulate load demand rather than just increasing generation to meet ever-rising consumption. Hence the scheduling phenomenon of iEMS also includes control of several load demands, such as smart load devices, which are power elastic and time elastic appliances.

In this thesis, the work is divided into two main parts. One part deals with the modelling of various components of the power systems. It includes the detailed mathematical modelling of solar energy generation, diesel engine power production, efficient grid topology, energy storage devices, various energy-hungry devices, grid price modelling, and cost-optimal optimization problems. Whereas, the other part illustrates the case-studies examples of various optimization problems. These problems include the multi-time study of energy distribution by diverse energy resources in a HAPN. The Integrated Energy Management System (iEMS) employs a rule-based mixed-integer dynamic algorithm with a receding horizon approach to determine cost-effective scheduling decisions in advance. As a result, it decreases

spontaneous consumer energy expenditures by employing the cheapest available energy source at any given instant while ensuring high customer comfort and boosting HAPN self-sufficiency. As an illustration, this study describes a rolling horizon-based time-triggered scheduling and distributed coordinated control approach for power sharing in a Hybrid AC/DC Home Area Power Network (HAPN). A unique three-layered multi-time scale Home Energy Management System (HEMS) is proposed, which includes a secondary scheduler that delivers optimal cost scheduling decisions for various dispatchable energy supply entities through a Mixed Integer Linear Programming (MILP) based technique.

While in the last example, the author explored the flexibilities in the consumers' energy demands and optimized the functionalities of home appliances to reduce the overall cost of utilized energy. The goal of all the above examples was to find the most cost-effective optimal decision vectors for home integrated energy supply entities and smart load devices throughout the day. Furthermore, to establish a realistic outcome of the results, this work includes the efficiency parameters of various energy components, including HAPN grid topologies and the energy storage device (ESDs) degradation models. The phenomena of storage life-cycle degradation were also seen to boost the battery's total practical utility. Whereas, the comparison of several HAPN architectural scenarios demonstrated the influence of losses on overall energy costs. Furthermore, the proposed framework was expanded to include optimization of consumer satisfaction and  $CO_2$  footprints. The suggested "min-max" multi-objective optimization problem was based on an optimal approach to reducing cumulative power costs, maximizing self-sufficiency, and increasing consumer happiness.

In general this thesis utilizes a hierarchical control framework for optimal cost scheduling and real-time control of energy entities. Where, the authors have demonstrated that the signals were transferred to the device level controller using a wireless communication strategy after the scheduling. The signals receive at the local central controller are utilized as a reference value for the power electronics operation of the target physical device. Additive noise and limited bandwidth restrictions affect wirelessly disseminate decision signals to local device level management. However, the robust control technique, which employes proportional and integral control, ensure that those reference signals are tracked well. Furthermore, whenever signal loss or power imbalance exists, a distributed coordinated control successfully perform power-sharing by autonomously balancing the imbalance using an auxiliary grid reserve power source. The proposed model's predictive (MP-iEMS) capabilities are proven by incorporating real-life yearly data sets for households, EV driving patterns, and EV battery (dis)charging patterns. Furthermore, the MP-iEMS Scheme shows that by adding dynamic energy pricing, overall energy demands are entirely supplied by energy from the cheapest power source.

The simulation results from the case-study examples demonstrate the success of the proposed operational approach for scheduling Energy Supply Entities (ESEs) and Smart Load Devices (SLDs) based on the lowest cost option. It also assures a high use of locally installed PV energy and a high level of satisfaction among energy consumers. The simulation results compare energy suppliers' penetration levels and utilization variables on a daily, monthly, and annual basis. In addition, the system's battery life-cycle degradation model calculates a daily, monthly, and yearly capacity loss percentage. It shows that by using the proposed MP-iEMS technique,

one reduces the cost of energy up to 13% as compared to conventional optimal techniques for the whole year. The total energy utilization is also less because of the reduced losses during energy transformation from DC to AC and vice versa. Using MP-iEMS, the utilization of optimal storage capacity of the EV battery is achieved with around 23% reduced (dis)charging rates, and with battery deep discharges up to 50% of capacity. While the conventional algorithms maintains the battery deep discharge at up to 73%, which reduces the shelf life of the storage. Similarly, as compared to standard rule-based optimization procedures, the proposed MP-iEMS lowers annual storage capacity loss owing to material deterioration by 0.013%.

## 7.1 Future Prospective

While this thesis has addressed various issues in the realm of smart power networks, further research is necessary to enhance the design and operation of Home Area Power Networks (HAPNs). The following constitutes the potential avenues for future investigation in this field:

- This work has the potential to be advanced towards a multi-agent control system at the microgrid level, wherein a consortium of Home Area Power Networks (HAPNs) collectively make decisions aimed at optimizing cost efficiency.
- The communication model could be altered to provide hybrid time/event-triggered communication systems for offline scheduling and online robust control mechanisms.
- The existing HAPN model might be improved to accommodate a range of energy storage devices such as super capacitors and the innovative batteries.
- Further research into the ageing mechanisms of the storage units might benefit intricate methods with dynamic load behaviour.
- Estimated energy storage system parameters can be incorporated into the operational plan to appropriately estimate the energy storage system's lifespan.
- The suggested operation strategy can be expanded to account for voltage and frequency limits at the primary grid connection point. Furthermore power electronics based control can be enhanced and modified for hybrid control operations under grid stress mode.
- The proposed operating system can be modified for implementation on embedded devices such as Internet of Things (IoT) and microcontrollers. Additionally, the optimal design approach may be adapted to incorporate a graphical user interface for ease of use and operation.

# Bibliography

- [1] *Meteonorm Irradiation Data*.
- [2] Optimization Toolbox Documentation- MathWorks Benelux. [Online; accessed 2022-07-13].
- [3] Epexspot market data intraday auction, December 2018.
- [4] Modawy Adam Ali Abdalla, Wang Min, and Omer Abbaker Ahmed Mohammed. Two-stage energy management strategy of ev and pv integrated smart home to minimize electricity cost and flatten power load profile. *Energies*, 13(23), 2020.
- [5] Yisah Y Adajah, Sadiq Thomas, Mohammed S Haruna, and Sikiru O Anaza. Distributed generation (dg): A review. In *2021 1st International Conference on Multidisciplinary Engineering and Applied Science (ICMEAS)*, pages 1–5. IEEE, 2021.
- [6] Temitope Adefarati, Numbi Bubele Papy, Miriam Thopil, and Henerica Tazvinga. Non-renewable distributed generation technologies: A review. *Handbook of distributed generation*, pages 69–105, 2017.
- [7] Ayaz Ahmad. *Smart grid as a solution for renewable and efficient energy*. IGI global, 2016.
- [8] A. Ahmadi, A. E. Nezhad, and B. Hredzak. Security-constrained unit commitment in presence of lithium-ion battery storage units using information-gap decision theory. *IEEE Transactions on Industrial Informatics*, 15(1):148–157, Jan 2019.
- [9] Ijaz Ahmed, Muhammad Rehan, Abdul Basit, and Keum-Shik Hong. Greenhouse gases emission reduction for electric power generation sector by efficient dispatching of thermal plants integrated with renewable systems. *Scientific Reports*, 12(1):1–21, 2022.
- [10] M. A. Ahmed, A. M. Eltamaly, M. A. Alotaibi, A. I. Alolah, and Y. Kim. Wireless network architecture for cyber physical wind energy system. *IEEE Access*, 8:40180–40197, 2020.
- [11] Maytham S. Ahmed, Azah Mohamed, Tamer Khatib, Hussain Shareef, Raad Z. Homod, and Jamal Abd Ali. Real time optimal schedule controller for home energy management system using new binary backtracking search algorithm. *Energy and Buildings*, 138:215 – 227, 2017.
- [12] N. Ahmed, M. Levorato, and G. P. Li. Residential consumer-centric demand side management. *IEEE Transactions on Smart Grid*, 9(5):4513–4524, Sep. 2018.

- 
- [13] Baris Aksanli and Tajana Simunic Rosing. Human behavior aware energy management in residential cyber-physical systems. *IEEE Transactions on Emerging Topics in Computing*, 8(1):45–57, jan 2020.
- [14] I. Al-Anbagi, M. Erol-Kantarci, and H. T. Mouftah. A low latency data transmission scheme for smart grid condition monitoring applications. In *2012 IEEE Electrical Power and Energy Conference*, pages 20–25, Oct 2012.
- [15] Ayman Al-Quraan and Muhannad Al-Qaisi. Modelling, design and control of a standalone hybrid pv-wind micro-grid system. *Energies*, 14(16), 2021.
- [16] Abdelrahman O Ali, Mohamed R Elmarghany, Mohamed M Abdelsalam, Mohamed Nabil Sabry, and Ahmed M Hamed. Closed-loop home energy management system with renewable energy sources in a smart grid: A comprehensive review. *Journal of Energy Storage*, 50:104609, 2022.
- [17] Asfand Yar Ali, Akhtar Hussain, Ju-Won Baek, and Hak-Man Kim. Optimal operation of networked microgrids for enhancing resilience using mobile electric vehicles. *Energies*, 14(1), 2021.
- [18] Mohamed G Moh Almihat, Mohamed Tariq Kahn, and Ali M Almaktoof. An overview of renewable energy utilization and developments: Challenges and opportunities worldwide. *African Journal of Advanced Pure and Applied Sciences (AJAPAS)*, pages 1–16, 2022.
- [19] Mansour Alramlawi and Pu Li. Design optimization of a residential pv-battery microgrid with a detailed battery lifetime estimation model. *IEEE Transactions on Industry Applications*, 56(2):2020–2030, 2020.
- [20] O. Alrumayh and K. Bhattacharya. Flexibility of residential loads for demand response provisions in smart grid. *IEEE Transactions on Smart Grid*, pages 1–1, 2019.
- [21] Khalid Mhmoud Alzubi, Wesam Salah Alaloul, and Abdul Hannan Qureshi. Technology requirements for cyber physical systems implementation in construction. In *Cyber-Physical Systems in the Construction Sector*, pages 39–59. CRC Press, 2022.
- [22] Aya Amer, Khaled Shaban, Ahmed Gaouda, and Ahmed Massoud. Home energy management system embedded with a multi-objective demand response optimization model to benefit customers and operators. *Energies*, 14(2):257, 2021.
- [23] S Massoud Amin and Bruce F Wollenberg. Toward a smart grid: power delivery for the 21st century. *IEEE power and energy magazine*, 3(5):34–41, 2005.
- [24] A. Andreotti, G. Carpinelli, F. Mottola, D. Proto, and A. Russo. Decision theory criteria for the planning of distributed energy storage systems in the presence of uncertainties. *IEEE Access*, 6:62136–62151, 2018.

- [25] Florin Babota. Increase energy efficiency and comfort in homes by incorporating passive solar design features. *Bulletin of the Polytechnic Institute of Jassy, CONSTRUCTIONS. ARCHITECTURE Section*, 60:175–186, 09 2014.
- [26] Manjulata Badi, Shekarappa G Swetha, Sheila Mahapatra, and Saurav Raj. A architectural approach to smart grid technology. *Smart Grids and Microgrids: Technology Evolution*, pages 295–323, 2022.
- [27] Adamantios Bampoulas and Athanasios Karlis. Real-time energy storage management system of a nanogrid integrating photovoltaics and v2g operation. *The Journal of Engineering*, 2020(1):32–40, jan 2020.
- [28] Amar Kumar Barik, Smriti Jaiswal, and Dulal Chandra Das. Recent trends and development in hybrid microgrid: a review on energy resource planning and control. *International Journal of Sustainable Energy*, 41(4):308–322, 2022.
- [29] C Dennis Barley and C Byron Winn. Optimal dispatch strategy in remote hybrid power systems. *Solar Energy*, 58(4-6):165–179, 1996.
- [30] Daniel Betancur, Luis F. Duarte, Jesús Revollo, Carlos Restrepo, Andrés E. Díez, Idi A. Isaac, Gabriel J. López, and Jorge W. González. Methodology to evaluate the impact of electric vehicles on electrical networks using monte carlo. *Energies*, 14(5), 2021.
- [31] Bishnu Bhattarai, Laurentiu Marinovici, Francis Tuffner, Kevin Schneider, Xiaoyuan Fan, Frederick Rutz, and Gowtham Kandaperumal. Prototypical communication systems for electrical distribution system analysis: Design basis and exemplification through co-simulation. *IET Smart Grid*, 2022.
- [32] Danilo Iglesias Brandao, Rhonei Patric dos Santos, Waner Silva, Thiago R. De Oliveira, and Pedro Francisco Donoso-Garcia. Model-free energy management system for hybrid AC/DC microgrids. *IEEE Transactions on Industrial Electronics*, pages 1–1, 2020.
- [33] Deutscher Bundestag. Gesetz zur einföhrung von ausschreibungen für strom aus erneuerbaren energien und zu weiteren änderungen des rechts der erneuerbaren energien. URL: <https://dipbt.bundestag.de/dip21/brd/2016/0355-16.pdf>. Accessed, 23:2017, 2016.
- [34] Li Cao, Zhengzong Wang, and Yinggao Yue. Analysis and prospect of the application of wireless sensor networks in ubiquitous power internet of things. *Computational Intelligence and Neuroscience*, 2022, 2022.
- [35] Fernando V. Cerna, Mahdi Pourakbari-Kasmaei, Luizalba S. S. Pinheiro, Ehsan Naderi, Matti Lehtonen, and Javier Contreras. Intelligent energy management in a prosumer community considering the load factor enhancement. *Energies*, 14(12), 2021.
- [36] Pengcheng Chen, Li Yu, and Dan Zhang. Event-triggered sliding mode control of power systems with communication delay and sensor faults. *IEEE Transactions on Circuits and Systems I: Regular Papers*, 68(2):797–807, feb 2021.

- 
- [37] Xiangping Chen, Wenping Cao, Qilong Zhang, Shubo Hu, and Jing Zhang. Artificial intelligence-aided model predictive control for a grid-tied wind-hydrogen-fuel cell system. *IEEE Access*, 8:92418–92430, 2020.
- [38] Wei-Yu Chiu, Jui-Ting Hsieh, and Chia-Ming Chen. Pareto optimal demand response based on energy costs and load factor in smart grid. *IEEE Transactions on Industrial Informatics*, 16(3):1811–1822, mar 2020.
- [39] Sunetra Chowdhury, Shyama P Chowdhury, and Peter Crossley. *Microgrids and active distribution networks*. 2022.
- [40] Commission for Energy Regulation. CER Smart Metering Project-Electricity Customer Behaviour Trial, 2009-2010,1st Edition. Irish Social Science Data Archive. SN: 0012-00, "https://www.ucd.ie/issda/data/commissionforenergyregulationcer/". 2021.
- [41] David Feldman, Vignesh Ramasamy,Ran Fu, Ashwin Ramdas, Jal Desai, Robert Margolis. U.s. solar photovoltaic systemand energy storage costbenchmark: Q1 2020, 2020.
- [42] X. Dong, Z. Yuying, and J. Tong. Planning-operation co-optimization model of active distribution network with energy storage considering the lifetime of batteries. *IEEE Access*, 6:59822–59832, 2018.
- [43] I. Duggal and B. Venkatesh. Short-term scheduling of thermal generators and battery storage with depth of discharge-based cost model. *IEEE Transactions on Power Systems*, 30(4):2110–2118, July 2015.
- [44] Chelsie Dundas and Caisheng Wang. Urban microgrids: A review and applications in postindustrial detroit area. In *2018 IEEE Power Energy Society General Meeting (PESGM)*, pages 1–5, 2018.
- [45] EA Technology. My Electric Avenue, "https://eatechnology.com/americas/resources/projects/my-electric-avenue-data-download/", 2021.
- [46] F. Elghitani and E. El-Saadany. Smoothing net load demand variations using residential demand management. *IEEE Transactions on Industrial Informatics*, 15(1):390–398, Jan 2019.
- [47] ed. 2018. Elizondo, L.R. Solar energy: Integration of photovoltaic systems in microgrids — tu delft online. *Delft University ofTechnology (TU Delft)*, 2022.
- [48] Mohamed M. Elmeligy, Mostafa F. Shaaban, Ahmed Azab, Maher A. Azzouz, and Mohamed Mokhtar. A mobile energy storage unit serving multiple ev charging stations. *Energies*, 14(10), 2021.
- [49] ENTSO-E. Transparency Platform, "https://transparency.entsoe.eu/". 2021.
- [50] Oon Erixno, Nasrudin Abd Rahim, Farah Ramadhani, and Noriah Nor Adzman. Energy management of renewable energy-based combined heat and power systems: A review. *Sustainable Energy Technologies and Assessments*, 51:101944, 2022.



- [51] European Commission. European Commission, "https://energy.ec.europa.eu/topics/markets-and-consumers/smart-grids-and-meters\_en", 2022.
- [52] European Commission, Joint Research Centre. PVGIS - Photovoltaic Geographical Information System, "https://re.jrc.ec.europa.eu/pvg\_tools/en/tools.html", 2021.
- [53] Bassam Fattouh. *The drivers of oil prices: the usefulness and limitations of non-structural model, the demand-supply framework and informal approaches*. 2007.
- [54] Yuming Feng, Wei Zhang, Jiang Xiong, and Huaqing Li. Distributed event-triggered communication scheme for economic dispatch problem in power system with uncoordinated step-sizes. *IEEE Access*, 8:43466–43475, 2020.
- [55] Ana Fernández-Guillamón, Eduard Muljadi, and Angel Molina-García. Frequency control studies: A review of power system, conventional and renewable generation unit modeling. *Electric Power Systems Research*, 211:108191, 2022.
- [56] P. Fortenbacher, J. L. Mathieu, and G. Andersson. Modeling and optimal operation of distributed battery storage in low voltage grids. *IEEE Transactions on Power Systems*, 32(6):4340–4350, Nov 2017.
- [57] Maria C. Fotopoulou, Panagiotis Drosatos, Stefanos Petridis, Dimitrios Rakopoulos, Fotis Stergiopoulos, and Nikolaos Nikolopoulos. Model predictive control for the energy management in a district of buildings equipped with building integrated photovoltaic systems and batteries. *Energies*, 14(12), 2021.
- [58] Cornelia A Fjelkestam Frederiksen and Zuansi Cai. Novel machine learning approach for solar photovoltaic energy output forecast using extra-terrestrial solar irradiance. *Applied Energy*, 306:118152, 2022.
- [59] Vasilis M Fthenakis and Paul A Lynn. *Electricity from sunlight: photovoltaic-systems integration and sustainability*. John Wiley & Sons, 2018.
- [60] A Gayathri, V Rukkumani, V Manimegalai, and P Pandiyan. A comprehensive review on energy storage systems. *Smart Electrical Grid System*, pages 211–251.
- [61] Xiaohua Ge, Qing-Long Han, Lei Ding, Yu-Long Wang, and Xian-Ming Zhang. Dynamic event-triggered distributed coordination control and its applications: A survey of trends and techniques. *IEEE Transactions on Systems, Man, and Cybernetics: Systems*, 50(9):3112–3125, sep 2020.
- [62] Clark W Gellings. *The smart grid: enabling energy efficiency and demand response*. River Publishers, 2020.
- [63] Mohammad Gholami, Sajjad Fattaheian-Dehkordi, Hesam Mazaheri, and Ali Abbaspour Tehrani-Fard. *Active Distribution Management System*, chapter 7, pages 125–143. John Wiley Sons, Ltd, 2021.

- 
- [64] Vivien Glönkler, Benedikt Reick, Ralf Stetter, Markus Till, and Markus Pfeil. A contribution to sustainable product development using the example of battery electric vehicles. *Sustainability*, 14(7):3729, 2022.
- [65] C. Gray, R. Ayre, K. Hinton, and L. Campbell. Smart is not free: Energy consumption of consumer home automation systems. *IEEE Transactions on Consumer Electronics*, 66(1):87–95, Feb 2020.
- [66] Clifford Hansen, Daniel Riley, Chris Deline, Fatima Toor, and Joshua Stein. A detailed performance model for bifacial pv modules. Technical report, 2017.
- [67] H. Hao, D. Wu, J. Lian, and T. Yang. Optimal coordination of building loads and energy storage for power grid and end user services. *IEEE Transactions on Smart Grid*, 9(5):4335–4345, Sep. 2018.
- [68] P. J. Hart, R. H. Lasseter, and T. M. Jahns. Coherency identification and aggregation in grid-forming droop-controlled inverter networks. *IEEE Transactions on Industry Applications*, 55(3):2219–2231, May 2019.
- [69] Li He, Yong Li, Josep M. Guerrero, and Yijia Cao. A comprehensive inertial control strategy for hybrid AC/DC microgrid with distributed generations. *IEEE Transactions on Smart Grid*, 11(2):1737–1747, mar 2020.
- [70] M. Hijjo and G. Frey. Stochastic optimization framework for scheduling isolated microgrids. In *2018 19th IEEE Mediterranean Electrotechnical Conference (MELECON)*, pages 149–154, May 2018.
- [71] Ali Hooshmand, Babak Asghari, and Ratnesh Sharma. A power management system for planned & unplanned grid electricity outages. In *2015 IEEE PES Innovative Smart Grid Technologies Latin America (ISGT LATAM)*, pages 382–386. IEEE, 2015.
- [72] Nicklas Hösl and Tijs Teulings. Open ev data, "https://github.com/chargeprice/open-ev-data". 2021.
- [73] Vahid Hosseinnezhad, Miadreza Shafie-Khah, Pierluigi Siano, and Joao P. S. Catalao. An optimal home energy management paradigm with an adaptive neuro-fuzzy regulation. *IEEE Access*, 8:19614–19628, 2020.
- [74] H. O. R. Howlader, M. M. Sediqi, A. M. Ibrahim, and T. Senjyu. Optimal thermal unit commitment for solving duck curve problem by introducing csp, psh and demand response. *IEEE Access*, 6:4834–4844, 2018.
- [75] Jian Hu, Hongwen He, Zhongbao Wei, and Yang Li. Disturbance-immune and aging-robust internal short circuit diagnostic for lithium-ion battery. *IEEE Transactions on Industrial Electronics*, 69(2):1988–1999, Feb 2022.
- [76] B. Hussain, Q. U. Hasan, N. Javaid, M. Guizani, A. Almogren, and A. Alamri. An innovative heuristic algorithm for iot-enabled smart homes for developing countries. *IEEE Access*, 6:15550–15575, 2018.

- [77] Independent Electricity System Operator. Independent Electricity System Operator, "https://www.ieso.ca/en/learn/ontario-power-system/a-smarter-grid", 2022.
- [78] Mohammad Jafari, Zahra Malekjamshidi, Jianguo Zhu, and Mohammad-Hassan Khooban. A novel predictive fuzzy logic-based energy management system for grid-connected and off-grid operation of residential smart micro-grids. *IEEE Journal of Emerging and Selected Topics in Power Electronics*, 8(2):1391–1404, jun 2020.
- [79] N. Javaid, G. Hafeez, S. Iqbal, N. Alrajeh, M. S. Alabed, and M. Guizani. Energy efficient integration of renewable energy sources in the smart grid for demand side management. *IEEE Access*, 6:77077–77096, 2018.
- [80] D. P. Jenkins, J. Fletcher, and D. Kane. Lifetime prediction and sizing of lead-acid batteries for microgeneration storage applications. *IET Renewable Power Generation*, 2(3):191–200, Sep. 2008.
- [81] Y. Jia, Z. Mi, Y. Yu, Z. Song, and C. Sun. A bilevel model for optimal bidding and offering of flexible load aggregator in day-ahead energy and reserve markets. *IEEE Access*, 6:67799–67808, 2018.
- [82] Xing Jin, Ashish Vora, Vaidehi Hoshing, Tridib Saha, Gregory Shaver, R Edwin García, Oleg Wasynczuk, and Subbarao Varigonda. Physically-based reduced-order capacity loss model for graphite anodes in li-ion battery cells. *Journal of Power Sources*, 342:750–761, 2017.
- [83] Anish Jindal, Bharat Singh Bhambhu, Mukesh Singh, Neeraj Kumar, and Kshirasagar Naik. A heuristic-based appliance scheduling scheme for smart homes. *IEEE Transactions on Industrial Informatics*, 16(5):3242–3255, may 2020.
- [84] Dharmaraj Kanakadhurga and Natarajan Prabakaran. Demand side management in microgrid: A critical review of key issues and recent trends. *Renewable and Sustainable Energy Reviews*, 156:111915, 2022.
- [85] S. Kazmi, N. Javaid, M. J. Mughal, M. Akbar, S. H. Ahmed, and N. Alrajeh. Towards optimization of metaheuristic algorithms for iot enabled smart homes targeting balanced demand and supply of energy. *IEEE Access*, 7:24267–24281, 2019.
- [86] A. Khalid, N. Javaid, M. Guizani, M. Alhussein, K. Aurangzeb, and M. Ilahi. Towards dynamic coordination among home appliances using multi-objective energy optimization for demand side management in smart buildings. *IEEE Access*, 6:19509–19529, 2018.
- [87] Saad Ullah Khan, Khawaja Khalid Mehmood, Zunaib Maqsood Haider, Muhammad Kashif Rafique, Muhammad Omer Khan, and Chul-Hwan Kim. Coordination of multiple electric vehicle aggregators for peak shaving and valley filling in distribution feeders. *Energies*, 14(2), 2021.

- 
- [88] Xue Kong, Hongye Wang, Nan Li, and Hailin Mu. Multi-objective optimal allocation and performance evaluation for energy storage in energy systems. *Energy*, 253:124061, 2022.
- [89] Jingang Lai, Xiaoqing Lu, Antonello Monti, and Rik W. De Doncker. Event-driven distributed active and reactive power dispatch for CCVSI-based distributed generators in AC microgrids. *IEEE Transactions on Industry Applications*, 56(3):3125–3136, may 2020.
- [90] Jingang Lai, Xiaoqing Lu, Xinghuo Yu, and Antonello Monti. Stochastic distributed secondary control for AC microgrids via event-triggered communication. *IEEE Transactions on Smart Grid*, 11(4):2746–2759, jul 2020.
- [91] Jingang Lai, Xiaoqing Lu, Xinghuo Yu, Antonello Monti, and Hong Zhou. Distributed voltage regulation for cyber-physical microgrids with coupling delays and slow switching topologies. *IEEE Transactions on Systems, Man, and Cybernetics: Systems*, 50(1):100–110, jan 2020.
- [92] Jingang Lai, Xiaoqing Lu, Xinghuo Yu, Wei Yao, Jinyu Wen, and Shijie Cheng. Distributed multi-DER cooperative control for master-slave-organized microgrid networks with limited communication bandwidth. *IEEE Transactions on Industrial Informatics*, 15(6):3443–3456, jun 2019.
- [93] Robert H Lasseter. Microgrids. In *2002 IEEE power engineering society winter meeting. Conference proceedings (Cat. No. 02CH37309)*, volume 1, pages 305–308. IEEE, 2002.
- [94] Chao Li, Shihong Miao, Di Zhang, and Lixing Li. A two-stage reactive power optimization strategy for AC/DC hybrid distribution network. In *2020 5th Asia Conference on Power and Electrical Engineering (ACPEE)*. IEEE, jun 2020.
- [95] S. Li, J. Yang, W. Song, and A. Chen. A real-time electricity scheduling for residential home energy management. *IEEE Internet of Things Journal*, 6(2):2602–2611, April 2019.
- [96] T. Li and M. Dong. Residential energy storage management with bidirectional energy control. *IEEE Transactions on Smart Grid*, 10(4):3596–3611, July 2019.
- [97] Jian-Tang Liao, Hao-Wei Huang, Hong-Tzer Yang, and Desheng Li. Decentralized v2g/g2v scheduling of ev charging stations by considering the conversion efficiency of bidirectional chargers. *Energies*, 14(4), 2021.
- [98] S. Linsenmayer, B. W. Carabelli, S. Wildhagen, K. Rothermel, and F. Allgower. Controller and triggering mechanism co-design for control over time-slotted networks. *IEEE Transactions on Control of Network Systems*, pages 1–1, 2020.
- [99] K. Liu, C. Wang, W. Wang, Y. Chen, and H. Wu. Linear power flow calculation of distribution networks with distributed generation. *IEEE Access*, 7:44686–44695, 2019.

- [100] Shichao Liu, Wensheng Luo, and Ligang Wu. Co-design of distributed model-based control and event-triggering scheme for load frequency regulation in smart grids. *IEEE Transactions on Systems, Man, and Cybernetics: Systems*, 50(9):3311–3319, sep 2020.
- [101] Y. Liu, L. Xiao, and G. Yao. Pricingbased demand response for a smart home with various types of household appliances considering customer satisfaction. *IEEE Access*, pages 1–1, 2019.
- [102] Xiaoqing Lu, Jingang Lai, Xinghuo Yu, Yaonan Wang, and Josep M. Guerrero. Distributed coordination of islanded microgrid clusters using a two-layer intermittent communication network. *IEEE Transactions on Industrial Informatics*, 14(9):3956–3969, sep 2018.
- [103] Xiaoqing Lu, Xinghuo Yu, Jingang Lai, Josep M. Guerrero, and Hong Zhou. Distributed secondary voltage and frequency control for islanded microgrids with uncertain communication links. *IEEE Transactions on Industrial Informatics*, 13(2):448–460, apr 2017.
- [104] F. Luo, W. Kong, G. Ranzi, and Z. Y. Dong. Optimal home energy management system with demand charge tariff and appliance operational dependencies. *IEEE Transactions on Smart Grid*, pages 1–1, 2019.
- [105] F. Luo, W. Kong, G. Ranzi, and Z. Y. Dong. Optimal home energy management system with demand charge tariff and appliance operational dependencies. *IEEE Transactions on Smart Grid*, 11(1):4–14, Jan 2020.
- [106] Xinxin Lv, Yonghui Sun, Yi Wang, and Venkata Dinavahi. Adaptive event-triggered load frequency control of multi-area power systems under networked environment via sliding mode control. *IEEE Access*, 8:86585–86594, 2020.
- [107] G. Ma, Z. Cai, P. Xie, P. Liu, S. Xiang, Y. Sun, C. Guo, and G. Dai. A bi-level capacity optimization of an isolated microgrid with load demand management considering load and renewable generation uncertainties. *IEEE Access*, 7:83074–83087, 2019.
- [108] Magdi S Mahmoud and M Fouad. *Control and optimization of distributed generation systems*. Springer, 2015.
- [109] K. Mahmud, M. J. Hossain, and G. E. Town. Peak-load reduction by coordinated response of photovoltaics, battery storage, and electric vehicles. *IEEE Access*, 6:29353–29365, 2018.
- [110] Sanamehreen Malik, Binal Modi, and Divyesh Mangrolia. Grid integration of distributed generation: Issues and challenges. In *2022 International Conference for Advancement in Technology (ICONAT)*, pages 1–6. IEEE, 2022.
- [111] M. Manbachi and M. Ordóñez. Intelligent agent-based energy management system for islanded ac–dc microgrids. *IEEE Transactions on Industrial Informatics*, 16(7):4603–4614, July 2020.
- [112] G Masson and I Kaizuka. Trends in photovoltaic applications, international energy agency. 2019.

- 
- [113] MATLAB. *version 9.9 (R2020b)*. The MathWorks Inc., Natick, Massachusetts, 2020.
- [114] D. M. Minhas and G. Frey. Optimal scheduling of energy supply entities in home area power network. In *2019 6th International Conference on Control, Decision and Information Technologies (CoDIT)*, pages 732–737, April 2019.
- [115] D. M. Minhas and G. Frey. Modeling and optimizing energy supply and demand in home area power network (hapn). *IEEE Access*, 8:2052–2072, 2020.
- [116] D. M. Minhas and G. Frey. Two-stage multi-time scale energy management control framework for home area power network. In *2020 IEEE International Conference on Environment and Electrical Engineering and 2020 IEEE Industrial and Commercial Power Systems Europe (EEEIC / I CPS Europe)*, pages 1–6, June 2020.
- [117] D. M. Minhas, R. R. Khalid, and G. Frey. Activation of electrical loads under electricity price uncertainty. In *2017 IEEE International Conference on Smart Energy Grid Engineering (SEGE)*, pages 373–378, Aug 2017.
- [118] D. M. Minhas, R. R. Khalid, and G. Frey. Activation of electrical loads under electricity price uncertainty. In *2017 IEEE International Conference on Smart Energy Grid Engineering (SEGE)*, pages 373–378, Aug 2017.
- [119] D. M. Minhas, R. R. Khalid, and G. Frey. Real-time power balancing in photovoltaic-integrated smart micro-grid. In *IECON 2017 - 43rd Annual Conference of the IEEE Industrial Electronics Society*, pages 7469–7474, Oct 2017.
- [120] D. M. Minhas, R. R. Khalid, and G. Frey. Short term load forecasting using hybrid adaptive fuzzy neural system: The performance evaluation. In *2017 IEEE PES PowerAfrica*, pages 468–473, June 2017.
- [121] Daud Mustafa Minhas and Georg Frey. Optimal scheduling of energy supply entities in home area power network. In *2019 6th International Conference on Control, Decision and Information Technologies (CoDIT)*. IEEE, apr 2019.
- [122] Daud Mustafa Minhas and Georg Frey. Stochastic optimization scheme to schedule energy supply and demands in an islanded microgrid. In *IECON 2020 The 46th Annual Conference of the IEEE Industrial Electronics Society*, pages 1704–1709. IEEE, 2020.
- [123] Daud Mustafa Minhas and Georg Frey. Rolling horizon based time-triggered distributed control for ac/dc home area power network. *IEEE Transactions on Industry Applications*, 57(4):4021–4032, July 2021.
- [124] Daud Mustafa Minhas and Sajjad Hussain. Efficient control strategies to optimize electricity cost and consumer satisfaction. In *Smart Grid as a Solution for Renewable and Efficient Energy*, pages 69–96. IGI Global, 2016.
- [125] Daud Mustafa Minhas, Raja Rehan Khalid, and Georg Frey. Activation of electrical loads under electricity price uncertainty. In *2017 IEEE International Conference on Smart Energy Grid Engineering (SEGE)*, pages 373–378. IEEE, 2017.

- [126] Daud Mustafa Minhas, Raja Rehan Khalid, and Georg Frey. Load control for supply-demand balancing under renewable energy forecasting. In *2017 IEEE Second International Conference on DC Microgrids (ICDCM)*, pages 365–370. IEEE, 2017.
- [127] Daud Mustafa Minhas, Raja Rehan Khalid, and Georg Frey. Real-time power balancing in photovoltaic-integrated smart micro-grid. In *IECON 2017-43rd Annual Conference of the IEEE Industrial Electronics Society*, pages 7469–7474. IEEE, 2017.
- [128] Daud Mustafa Minhas, Raja Rehan Khalid, and Georg Frey. Short term load forecasting using hybrid adaptive fuzzy neural system: The performance evaluation. In *2017 IEEE PES PowerAfrica*, pages 468–473. IEEE, 2017.
- [129] Daud Mustafa Minhas, Raja Rehan Khalid, and Georg Frey. Short term load forecasting using hybrid adaptive fuzzy neural system: The performance evaluation. In *2017 IEEE PES PowerAfrica*. IEEE, jun 2017.
- [130] Daud Mustafa Minhas, Josef Meiers, and Georg Frey. Electric vehicle battery storage concentric intelligent home energy management system using real life data sets. *Energies*, 15(5), 2022.
- [131] Daud Mustafa Minhas, Muhammad Rashad, Sajjad Hussain, and Muhammad Ashraf. Optimal control of power cost and consumer satisfaction using smart grid intelligent energy management system. In *2015 10th Asian Control Conference (ASCC)*, pages 1–6. IEEE, 2015.
- [132] Daud Mustafa Minhas, Muhammad Rashad, Sajjad Hussain, and Muhammad Ashraf. Cost effective bidirectional power transactions for queueing energy requests in smart micro-grids. In *2016 18th Mediterranean Electrotechnical Conference (MELECON)*, pages 1–6. IEEE, 2016.
- [133] S. Moon and J. Lee. Multi-residential demand response scheduling with multi-class appliances in smart grid. *IEEE Transactions on Smart Grid*, 9(4):2518–2528, July 2018.
- [134] Godfrey Gladson Moshi, Alberto Berizzi, Leonardo Taccari, and Castelli Dezza. Optimal planning of hybrid microgrid. 2015.
- [135] C Nagaraj. Reduction of power conversion losses in ac-dc coupled hybrid micro-grid under grid distorted voltage scenario. *Electric Power Systems Research*, 210:108101, 2022.
- [136] Alisher F Narynbaev, Alexey G Vaskov, and Nikolay Yu Mozder. Optimal dispatch of a standalone pv-diesel-battery microgrid using non-commercial minlp solvers. In *2022 International Conference on Industrial Engineering, Applications and Manufacturing (ICIEAM)*, pages 264–270. IEEE, 2022.
- [137] National Institute of Standards and Technology (NIST). National Institute of Standards and Technology (NIST), ”<https://www.nist.gov/ctl/smart-connected-systems-division/smart-grid-group>”, 2022.

- 
- [138] Patrick K Ndwali, Jackson G Njiri, and Evan M Wanjiru. Optimal operation control of microgrid connected photovoltaic-diesel generator backup system under time of use tariff. *Journal of Control, Automation and Electrical Systems*, 31(4):1001–1014, 2020.
- [139] Neon Neue Energieökonomik GmbH. Open power system data, "https://data.open-power-system-data.org/time\_series/", 2021.
- [140] Z. Ni and A. Das. A new incentive-based optimization scheme for residential community with financial trade-offs. *IEEE Access*, 6:57802–57813, 2018.
- [141] Leon Fidele Nishimwe H. and Sung-Guk Yoon. Combined optimal planning and operation of a fast ev-charging station integrated with solar pv and ess. *Energies*, 14(11), 2021.
- [142] Abdul Ghani Olabi, Qaisar Abbas, Ahmed Al Makky, and Mohammad Ali Abdelkareem. Supercapacitors as next generation energy storage devices: Properties and applications. *Energy*, 248:123617, 2022.
- [143] C. Opathella, A. Elkasrawy, A. A. Mohamed, and B. Venkatesh. Optimal scheduling of merchant-owned energy storage systems with multiple ancillary services. *IEEE Open Access Journal of Power and Energy*, 7:31–40, 2020.
- [144] SO Orero and MR Irving. Large scale unit commitment using a hybrid genetic algorithm. *International Journal of Electrical Power & Energy Systems*, 19(1):45–55, 1997.
- [145] Oussama Ouramdane, Elhoussin Elbouchikhi, Yassine Amirat, and Ehsan Sedgh Gooya. Optimal sizing and energy management of microgrids with vehicle-to-grid technology: A critical review and future trends. *Energies*, 14(14), 2021.
- [146] E. M. Pimentão J. P. Sousa P. L. Monteiro, M. Ruiz. Indoor temperature prediction in an iot scenario. *Sensors (Basel, Switzerland)*, 18(11):3610, oct 2018.
- [147] S. Pal and R. Kumar. Electric vehicle scheduling strategy in residential demand response programs with neighbor connection. *IEEE Transactions on Industrial Informatics*, 14(3):980–988, March 2018.
- [148] K. Paridari, A. Parisio, H. Sandberg, and K. H. Johansson. Energy and co2 efficient scheduling of smart appliances in active houses equipped with batteries. In *2014 IEEE International Conference on Automation Science and Engineering (CASE)*, pages 632–639, Aug 2014.
- [149] E. S. Parizy, H. R. Bahrami, and S. Choi. A low complexity and secure demand response technique for peak load reduction. *IEEE Transactions on Smart Grid*, 10(3):3259–3268, May 2019.
- [150] Lorenzo Mario Pastore, Gianluigi Lo Basso, and Livio de Santoli. Can the renewable energy share increase in electricity and gas grids takes out the competitiveness of gas-driven combined heat and power plants for distributed generation? *Energy*, page 124659, 2022.



- [151] Iván Patrao, Emilio Figueres, Gabriel Garcerá, and Raúl González-Medina. Microgrid architectures for low voltage distributed generation. *Renewable and Sustainable Energy Reviews*, 43:415–424, 2015.
- [152] Iván Patrao, Emilio Figueres, Gabriel Garcerá, and Raúl González-Medina. Microgrid architectures for low voltage distributed generation. *Renewable and Sustainable Energy Reviews*, 43:415–424, 2015.
- [153] S. Paul and N. P. Padhy. Resilient scheduling portfolio of residential devices and plug-in electric vehicle by minimizing conditional value at risk. *IEEE Transactions on Industrial Informatics*, 15(3):1566–1578, March 2019.
- [154] Subho Paul and Narayana Prasad Padhy. Real-time bilevel energy management of smart residential apartment building. *IEEE Transactions on Industrial Informatics*, 16(6):3708–3720, jun 2020.
- [155] Jiangkai Peng, Bo Fan, Hao Xu, and Wenxin Liu. Discrete-time self-triggered control of DC microgrids with data dropouts and communication delays. *IEEE Transactions on Smart Grid*, 11(6):4626–4636, nov 2020.
- [156] P. Pérez-Higueras and E.F. Fernández. *High Concentrator Photovoltaics: Fundamentals, Engineering and Power Plants*. Green Energy and Technology. Springer International Publishing, 2016.
- [157] Lolla Phani Raghav, Rangu Seshu Kumar, Dhenuvakonda Koteswara Raju, and Arvind R Singh. Optimal day ahead energy consumption management in grid-connected microgrids. *International Journal of Energy Research*, 46(2):1864–1881, 2022.
- [158] Haifeng Qiu, Wei Gu, Yinliang Xu, and Bo Zhao. Multi-time-scale rolling optimal dispatch for AC/DC hybrid microgrids with day-ahead distributionally robust scheduling. *IEEE Transactions on Sustainable Energy*, 10(4):1653–1663, oct 2019.
- [159] M. H. Rahim, A. Khalid, N. Javaid, M. Alhussein, K. Aurangzeb, and Z. A. Khan. Energy efficient smart buildings using coordination among appliances generating large data. *IEEE Access*, 6:34670–34690, 2018.
- [160] X. Ran and S. Leng. Enhanced robust index model for load scheduling of a home energy local network with a load shifting strategy. *IEEE Access*, 7:19943–19953, 2019.
- [161] X. Ran and K. Liu. Robust scatter index method for the appliances scheduling of home energy local network with user behavior uncertainty. *IEEE Transactions on Industrial Informatics*, 15(7):4129–4139, July 2019.
- [162] Abdul Rauf, Xiaoxing Liu, Waqas Amin, Ilhan Ozturk, Obaid Ur Rehman, and Suleman Sarwar. Energy and ecological sustainability: Challenges and panoramas in belt and road initiative countries. *Sustainability*, 10(8):2743, 2018.

- 
- [163] Kiran H Raut, Asha Shendge, and Jagdish Chaudhari. Recent advancement in battery energy storage system for launch vehicle. In *Planning of Hybrid Renewable Energy Systems, Electric Vehicles and Microgrid*, pages 931–955. Springer, 2022.
- [164] K. Rheinberger. DSM-data, "https://github.com/klaus-rheinberger/DSM-data". *GitHub repository*, 2021.
- [165] Ian Richardson, Murray Thomson, David Infield, and Conor Clifford. Domestic electricity use: A high-resolution energy demand model. *Energy and Buildings*, 42(10):1878 – 1887, 2010.
- [166] Kyung-Sang Ryu, Dae-Jin Kim, Heesang Ko, Chang-Jin Boo, Jongrae Kim, Young-Gyu Jin, and Ho-Chan Kim. Mpc based energy management system for hosting capacity of pvs and customer load with ev in stand-alone microgrids. *Energies*, 14(13), 2021.
- [167] Julia Sachs and Oliver Sawodny. A two-stage model predictive control strategy for economic diesel-pv-battery island microgrid operation in rural areas. *IEEE Transactions on Sustainable Energy*, 7(3):903–913, 2016.
- [168] Christophe Savard, Emiliia Iakovleva, Daniil Ivanchenko, and Anton Rassõlkin. Accessible battery model with aging dependency. *Energies*, 14(12), 2021.
- [169] Sahaj Saxena and Emilia Fridman. Event-triggered load frequency control via switching approach. *IEEE Transactions on Power Systems*, 35(6):4484–4494, nov 2020.
- [170] M. Shafie-Khah and P. Siano. A stochastic home energy management system considering satisfaction cost and response fatigue. *IEEE Transactions on Industrial Informatics*, 14(2):629–638, Feb 2018.
- [171] Md Shafiullah, Shakir D Ahmed, and Fahad A Al-Sulaiman. Grid integration challenges and solution strategies for solar pv systems: A review. *IEEE Access*, 2022.
- [172] Muhammad Shahab, Shaorong Wang, and Abdul Khalique Junejo. Improved control strategy for three-phase microgrid management with electric vehicles using multi objective optimization algorithm. *Energies*, 14(4), 2021.
- [173] H. Shareef, M. S. Ahmed, A. Mohamed, and E. Al Hassan. Review on home energy management system considering demand responses, smart technologies, and intelligent controllers. *IEEE Access*, 6:24498–24509, 2018.
- [174] Danbi Shin, Moses Kang, Hyuna Lee, Seonri Hong, Gihwan Yoon, and Jongbok Baek. Application development and type test for smart inverter based on ieee 1547-2018 utilizing power hils. *Journal of IKEEE*, 26(1):1–9, 2022.
- [175] S. Singh, V. B. Pamshetti, and S. P. Singh. Time horizon-based model predictive volt/var optimization for smart grid enabled cvr in the presence of electric vehicle charging loads. *IEEE Transactions on Industry Applications*, 55(6):5502–5513, Nov 2019.

- [176] S Vikram Singh, Aizad Khursheed, and Zahoor Alam. Wired communication technologies and networks for smart grid—a review. *Cyber Security in Intelligent Computing and Communications*, pages 183–195, 2022.
- [177] K. C. Sou, J. Weimer, H. Sandberg, and K. H. Johansson. Scheduling smart home appliances using mixed integer linear programming. In *2011 50th IEEE Conference on Decision and Control and European Control Conference*, pages 5144–5149, Dec 2011.
- [178] Nathan Subramaniam. Ieee 2.5 beta method unraveled. *Journal of Energy Management Highlights — SCTE*, 1(2):170, October 2016.
- [179] Nurshazlina Suhaimy, Nurul Asyikin Mohamed Radzi, Wan Siti Halimatul Munirah Wan Ahmad, Kaiyisah Hanis Mohd Azmi, and MA Hannan. Current and future communication solutions for smart grids: A review. *IEEE Access*, 2022.
- [180] Pruthiraj Swain and Ashoka Shyamaprasad. Energy storage technologies: Past, present and future. In *ISUW 2019*, pages 179–195. Springer, 2022.
- [181] Abhishek Tiwari and Naran M Pindoriya. Automated demand response in smart distribution grid: a review on metering infrastructure, communication technology and optimization models. *Electric Power Systems Research*, 206:107835, 2022.
- [182] Phi-Hai Trinh and Il-Yop Chung. Optimal control strategy for distributed energy resources in a dc microgrid for energy cost reduction and voltage regulation. *Energies*, 14(4), 2021.
- [183] U.S. Department of Energy. U.S. Department of Energy, ”<https://www.energy.gov/oe/activities/technology-development/grid-modernization-and-smart-grid>”, 2022.
- [184] U.S. Department of Energy, Smart Grid. U.S. Department of Energy, Smart grid, ”[https://www.smartgrid.gov/the\\_smart\\_grid/smart\\_grid.html](https://www.smartgrid.gov/the_smart_grid/smart_grid.html)”, 2022.
- [185] T. S. Ustun, S. M. S. Hussain, and H. Kikusato. Iec 61850-based communication modeling of ev charge-discharge management for maximum pv generation. *IEEE Access*, 7:4219–4231, 2019.
- [186] N. Vazquez, S. S. Yu, T. K. Chau, T. Fernando, and H. H. Iu. A fully decentralized adaptive droop optimization strategy for power loss minimization in microgrids with pv-bess. *IEEE Transactions on Energy Conversion*, 34(1):385–395, March 2019.
- [187] Anjeet Verma, Bhim Singh, Ambrish Chandra, and Kamal Al Haddad. An implementation of solar PV array based multifunctional EV charger. *IEEE Transactions on Industry Applications*, pages 1–1, 2020.
- [188] Aiping Wang, Bingxian Mu, and Yang Shi. Event-triggered consensus control for multiagent systems with time-varying communication and event-detecting delays. *IEEE Transactions on Control Systems Technology*, 27(2):507–515, mar 2019.

- 
- [189] Bo Wang, Xiangsheng Liu, and Yaqi Zhang. Internet of things. In *Internet of Things and BDS Application*, pages 71–127. Springer, 2022.
- [190] Lixing Wang, Zhenning Wu, and Changyong Cao. Integrated optimization of routing and energy management for electric vehicles in delivery scheduling. *Energies*, 14(6), 2021.
- [191] Ruzhu Wang and Xiaoqiang Zhai. *Handbook of energy systems in green buildings*, volume 160. Springer, 2018.
- [192] Evelina Wikner and Torbjörn Thiringer. Extending battery lifetime by avoiding high soc. *Applied Sciences*, 8(10):1825, 2018.
- [193] Ababay Ketema Worku, Delele Worku Ayele, Nigus Gabbiye Habtu, Bimrew Tamrat Admasu, Getu Alemayehu, Biniyam Zemene Taye, and Temesgen Atnafu Yemata. Energy storage technologies; recent advances, challenges, and prospectives. In *Planning of Hybrid Renewable Energy Systems, Electric Vehicles and Microgrid*, pages 125–150. Springer, 2022.
- [194] Jingda Wu, Zhongbao Wei, Weihai Li, Yu Wang, Yunwei Li, and Dirk Uwe Sauer. Battery thermal- and health-constrained energy management for hybrid electric bus based on soft actor-critic drl algorithm. *IEEE Transactions on Industrial Informatics*, 17(6):3751–3761, June 2021.
- [195] Jingda Wu, Zhongbao Wei, Kailong Liu, Zhongyi Quan, and Yunwei Li. Battery-involved energy management for hybrid electric bus based on expert-assistance deep deterministic policy gradient algorithm. *IEEE Transactions on Vehicular Technology*, 69(11):12786–12796, Nov 2020.
- [196] X. Wu, J. He, Y. Xu, J. Lu, N. Lu, and X. Wang. Hierarchical control of residential hvac units for primary frequency regulation. *IEEE Transactions on Smart Grid*, 9(4):3844–3856, July 2018.
- [197] Y. Xia, M. Yu, P. Yang, Y. Peng, and W. Wei. Generation-storage coordination for islanded dc microgrids dominated by pv generators. *IEEE Transactions on Energy Conversion*, 34(1):130–138, March 2019.
- [198] D. Xie, L. Yu, T. Jiang, and Y. Zou. Distributed energy optimization for hvac systems in university campus buildings. *IEEE Access*, 6:59141–59151, 2018.
- [199] Yijing Xie and Zongli Lin. Distributed event-triggered secondary voltage control for microgrids with time delay. *IEEE Transactions on Systems, Man, and Cybernetics: Systems*, 49(8):1582–1591, aug 2019.
- [200] X. Xu, Y. Jia, Y. Xu, Z. Xu, S. Chai, and C. S. Lai. A multi-agent reinforcement learning based data-driven method for home energy management. *IEEE Transactions on Smart Grid*, pages 1–1, 2020.
- [201] Y. Xu and X. Shen. Optimal control based energy management of multiple energy storage systems in a microgrid. *IEEE Access*, 6:32925–32934, 2018.

- [202] Huaicheng Yan, Jiwen Han, Hao Zhang, Xisheng Zhan, and Yueying Wang. Adaptive event-triggered predictive control for finite time microgrid. *IEEE Transactions on Circuits and Systems I: Regular Papers*, 67(3):1035–1044, mar 2020.
- [203] X. Yang, Y. Zhang, H. He, S. Ren, and G. Weng. Real-time demand side management for a microgrid considering uncertainties. *IEEE Transactions on Smart Grid*, 10(3):3401–3414, May 2019.
- [204] Yeong Yoo, Yousef Al-Shawesh, and Alain Tchagang. Coordinated control strategy and validation of vehicle-to-grid for frequency control. *Energies*, 14(9), 2021.
- [205] L. Yu, T. Jiang, and Y. Zou. Online energy management for a sustainable smart home with an hvac load and random occupancy. *IEEE Transactions on Smart Grid*, 10(2):1646–1659, March 2019.
- [206] Fangfei Zhang, Fengji Luo, Zhaoyang Dong, Yanli Liu, and Gianluca Ranzi. Hierarchical energy management scheme for residential communities under grid outage event. *IET Smart Grid*, 3(2):174–181, apr 2020.
- [207] Qiushi Zhang, Jian Zhao, Xiaoyu Wang, Li Tong, Hang Jiang, and Jinhui Zhou. Distribution network hierarchically partitioned optimization considering electric vehicle orderly charging with isolated bidirectional dc-dc converter optimal efficiency model. *Energies*, 14(6), 2021.
- [208] B. Zhao, H. Qiu, R. Qin, X. Zhang, W. Gu, and C. Wang. Robust optimal dispatch of ac/dc hybrid microgrids considering generation and load uncertainties and energy storage loss. *IEEE Transactions on Power Systems*, 33(6):5945–5957, Nov 2018.
- [209] B. Zhao, X. Zhang, J. Chen, C. Wang, and L. Guo. Operation optimization of standalone microgrids considering lifetime characteristics of battery energy storage system. *IEEE Transactions on Sustainable Energy*, 4(4):934–943, Oct 2013.
- [210] C. Zhao, S. Dong, C. Gu, F. Li, Y. Song, and N. P. Padhy. New problem formulation for optimal demand side response in hybrid ac/dc systems. *IEEE Transactions on Smart Grid*, 9(4):3154–3165, July 2018.
- [211] Shuangliang Zhao, Zhiying Song, Leying Qing, Jingmin Zhou, and Chongzhi Qiao. Surface wettability effect on energy density and power density of supercapacitors. *The Journal of Physical Chemistry C*, 2022.
- [212] L. Zhou, Y. Zhang, X. Lin, C. Li, Z. Cai, and P. Yang. Optimal sizing of pv and bess for a smart household considering different price mechanisms. *IEEE Access*, 6:41050–41059, 2018.
- [213] Quan Zhou, Mohammad Shahidehpour, Aleks Paaso, Shay Bahramirad, Ahmed Alabdulwahab, and Abdullah Abusorrah. Distributed control and communication strategies in networked microgrids. *IEEE Communications Surveys & Tutorials*, 22(4):2586–2633, 2020.

- [214] Y. Zhu, D. Zhao, X. Li, and D. Wang. Control-limited adaptive dynamic programming for multi-battery energy storage systems. *IEEE Transactions on Smart Grid*, 10(4):4235–4244, July 2019.
- [215] Siyi Zou, Yali Li, Hanqing Jin, Fandi Ning, Pengpeng Xu, Qinglin Wen, Saifei Pan, Xiong Dan, Wei Li, and Xiaochun Zhou. Highly safe, durable, adaptable, and flexible fuel cell using gel/sponge composite material. *Advanced Energy Materials*, 12(6):2103178, 2022.
- [216] Marta Zurek-Mortka and Jerzy R Szymanski. High-power charging strategies of ev batteries and energy storage. *Smart Charging Solutions for Hybrid and Electric Vehicles*, pages 159–174, 2022.